TNO report | TNO 2019 R100043

Review of worldwide geothermal projects: mechanisms and occurrence of induced seismicity

Date	22 May 2019
Author(s)	L. Buijze, L. van Bijsterveldt, H. Cremer, B. Paap, H. Veldkamp, B. Wassing, J.-D. van Wees, J. ter Heege
Number of pages	257 (incl. appendices)
Sponsor	EBN B.V.
Project name	Review of seismicity in geothermal projects
Project number	060.36021

Since April 1st, 2018, ECN and TNO have joined forces

Preface

Geothermal energy aids in achieving ambitions for the reduction of greenhouse gas emissions by contributing to a more sustainable energy mix. In particular, geothermal energy in the Netherlands can play an important role in providing a sustainable supply for domestic and industrial heat demand. However, just like with any large scale industrial activity, the societal acceptance of geothermal energy as a sustainable energy source depends on the assessment and management of the safety and various risks associated with it. Of particular importance to geothermal energy, a technology requiring operations in the shallow to deep subsurface, is the potential occurrence of earthquakes or induced seismicity. Concerns related to induced seismicity could hamper large scale development of geothermal energy if not properly assessed, evaluated, mitigated and discussed among the various stakeholder groups. This report contributes to the discussion on induced seismicity associated with geothermal operations by providing a compilation of existing knowledge on the mechanisms of induced seismicity, by presenting detailed analysis of selected case studies worldwide, and by reviewing approaches of existing traffic light and monitoring systems. Implications for current and future geothermal projects in the Netherlands are also discussed.

Scope
Safety and responsible development of projects is key in geothermal energy production as much as in any other type of industrial or subsurface activity. Different stakeholders in geothermal energy require a detailed scientific knowledge base on induced seismicity associated with geothermal projects to:

(1) evaluate the development of geothermal projects close to district heating networks in local communities, close to greenhouse farms, or close to industry with heat demand;
(2) define safe boundary conditions for geothermal operations including requirements for monitoring and data gathering during the different phases of a geothermal project; and
(3) receive and maintain a social license to operate for the geothermal sector.

Accordingly, any knowledge base on seismicity associated with drilling, stimulation, and production in geothermal projects needs to be state-of-the-art and reflect current international practices. Such a knowledge base is essential for a quantitative assessment of seismogenic potential associated with geothermal projects. In the Netherlands, induced seismicity is at the forefront of attention due to induced seismicity associated with onshore gas production. In addition, an extensive analysis of the relevance and applicability of case studies worldwide as potential analogs for geothermal projects in the Netherlands is not yet publicly available.

Project
This report is the result of a scientific review carried out in the period September 2018 to January 2019 in collaboration with EBN. EBN is a state-owned company executing parts of the climate and energy policy of the Ministry of Economic Affairs and Climate Policy. One of EBN's key activities is the development, deployment and sharing of knowledge on geological energy sources, including oil and gas and sustainable

energy resources. EBN has an ambition to contribute to the safe development of sustainable energy alternatives to fossil fuels[1].

This report significantly extends the knowledge base on induced seismicity associated with geothermal operations, and as such, contributes to a safer and more responsible development of future geothermal projects in the Netherlands. In particular, the review focusses on the following questions:

(1) What is the probability of induced and triggered seismicity in geothermal projects as a consequence of drilling, stimulation, production or injection?

(2) What could be the associated seismogenic potential for geothermal projects?

(3) What is required to enable quantification and mitigation of seismicity?

The study focusses on reviewing international practices, knowledge and case studies relevant for understanding induced seismicity and assessing seismogenic potential associated with geothermal operations. An inventory was made of mechanisms, publicly available data and field cases relevant to induced seismicity during geothermal operations. The case studies are primarily geothermal projects of various sorts, targeting different types of reservoir, depths and basins and tectonic regimes in the world. Other field cases e.g., waste water injection in connection with shale gas production, are briefly reviewed as well. The literature and data review is used to assess which international geothermal projects, both with or without seismicity, are relevant for induced seismicity in geothermal projects in the Netherlands and which factors essentially control the seismogenic potential of geothermal targets. The study also includes a basic review of currently existing monitoring systems and best practices for designing traffic light systems for geothermal projects. Analysis of seismogenic potential and seismic risk for geothermal operations is discussed within the larger framework of subsurface activities and possibilities for mitigation of induced seismicity are addressed. Although many studies on seismicity in geothermal projects are incorporated in the review and analysis, this report does not claim to be a comprehensive assessment of all published studies and data potentially relevant for induced seismicity.

Reading guide
The report aims to provide value to readers with different levels of background in seismicity associated with geothermal operations. It offers both an in depth analysis of data and case studies as well as a more easily accessible synthesis including implications for geothermal projects in the Netherlands. The report is structured into three main sections:

(1) A "technical expert" section describing (i) mechanisms of induced seismicity (chapter 2), (ii) a synthesis of the review of 40 case studies (chapter 3), (iii) the current status of geothermal energy in the Netherlands (chapter 4), and (iv) a basic review of traffic light and monitoring systems for geothermal sites (chapter 5).

---

[1] See, for example, report "*Masterplan Aardwarmte in Nederland. Een brede basis voor duurzame warmtevoorziening*" Platform Geothermie, DAGO, Warmtenetwerk Voor de energietransitie, EBN (May 2018, in Dutch). www.ebn.nl (accessed December 2018)

(2) A "synthesis" section with (i) a synthesis of results with implications for geothermal projects in the Netherlands (chapter 6) and (ii) the conclusions (chapter 7).

(3) An "appendix with data review" section including (i) detailed data and information of all case studies assessed (Appendix A) and (ii) of other subsurface activities relevant for induced seismicity (Appendix B).

Executive summary

The ambition to increase current geothermal heat production to 50 PJ per year (~175 doublets) in 2030 requires accelerated development of different geothermal targets. Induced seismicity is a key issue for geothermal projects worldwide where its occurrence has caused significant delays in development, and, in some cases damage of buildings and infrastructure. It also has particular focus of attention in the Netherlands due to frequent occurrence of seismicity associated with gas production. In this study, an extensive review was conducted of the occurrence of induced seismicity in case studies including geothermal and other types of projects involving relevant subsurface operations. The review served as a basis to (1) review mechanisms of induced seismicity, (2) identify key parameters affecting the occurrence of induced seismicity in geothermal projects, (3) perform a light review of seismic monitoring and traffic light systems, (4) summarize the current status of geothermal energy development and geothermal targets in the Netherlands, and (5) discuss implications for the likelihood of inducing felt seismicity (i.e. the seismogenic potential) of geothermal projects in the Netherlands.

The main conclusions are:

- Interaction of direct pressure, poroelastic and thermoelastic mechanisms mainly control stress changes in and around geothermal reservoirs and at faults, and thereby control the occurrence of induced seismicity.

- The seismogenic potential is generally low for porous sandstone targets as evidenced by lack of felt seismicity for similar geothermal play and system types in comparable basins and site-specific geological and operational factors. A medium seismogenic potential is attributed to the fractured or karstified carbonate targets affected by active tectonics in the Roer Valley Graben as evidenced by recent occurrence of seismicity associated with geothermal operations in that play at the Balmatt geothermal site near Mol in Belgium. Seismicity also occurred near the Californië geothermal sites in the southeastern part of the Netherlands, and potential causal relation between seismicity and operations are under investigation.

- Seismogenic potential may vary depending on location and local settings, i.e. seismogenic potential may increase from low to medium for deeper, more competent targets in particular if hydraulic connection to deeper (basement) rocks or large critically stressed faults are present, and/or if reservoir stimulation by fluid injection is attempted.

- The seismogenic potential should be assessed by upfront subsurface characterization including acquisition of (3D) seismics and mapping of geological structures to obtain a better model of the subsurface near geothermal projects. This effort can lower seismic risks if geothermal systems and operations are designed and optimized to avoid critically-stressed faults or hydrological connection to deeper basement (preventive measures). Implementation of traffic light systems can help lowering seismic risks for targets with elevated seismogenic potential (control measures).

- Seismic monitoring over long timescales covering a baseline period, the project lifetime and a post-production period is required to demonstrate unequivocal causal relations between seismicity and geothermal operations.

Despite low to medium seismogenic potential for the geothermal targets in the Netherlands, felt seismicity associated with geothermal operations cannot be excluded, even if mitigation measures are implemented. Absolute guarantees that felt seismicity will be absent cannot be given due to uncertainties in geology and interaction of operations with that geology, in particular considering the uncertainty of locations and stress changes at faults. Seismogenic potential is generally low for current porous sandstone targets in the Netherlands compared to cases worldwide. It is unlikely that felt seismicity will occur for these targets. The seismogenic potential is medium for current fractured or karstified sedimentary targets in the Roer Valley Graben, and potentially also for future deeper sedimentary targets that are not yet explored. For these targets, felt seismicity may be expected in some cases with the number and magnitude of seismic events depending on the site specific geology, the type of operations and operational parameters. Mitigation measures such as local seismic monitoring combined with traffic light systems can be successful approaches to reduce seismic risks in these cases.

Contents

1 Introduction

1.1 Background

In the Netherlands, geothermal energy is considered to be capable of making a considerable contribution to a more sustainable energy mix, required to achieve ambitions for reduction of greenhouse gas emissions. In particular, geothermal energy can play an important role in providing a sustainable supply of domestic and industrial heat (e.g., for greenhouse farms). Following the current Coalition Agreement and subsequent statements of the Minister of Economic Affairs[2], an ambition was recently outlined[1] to increase current heat production of 3 PJ per year (17 doublets) in 2017 to 50 PJ per year (~175 doublets) in 2030, and to more than 200 PJ per year in 2050 (~700 doublets) (Figure 1-1).
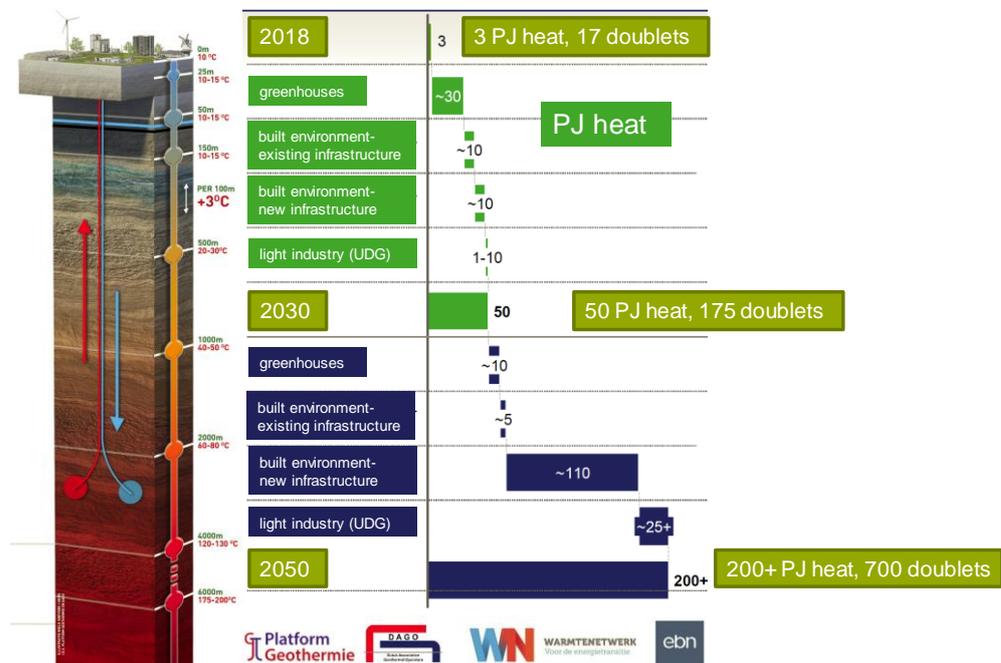
Figure 1-1   Ambition for development of geothermal energy in the Netherlands as outlined in the "Masterplan Geothermal Energy in the Netherlands"[1] (from EBN 2018, Copyright EBN, reproduced with permission).

This ambition requires a significant acceleration of geothermal energy production, which involves developing a broad variety of geothermal target formations, including targets that are more challenging to develop. As a consequence, issues with subsurface spatial planning and the interaction of different subsurface activities (e.g., geothermal energy, gas production or salt mining) will gain importance. An accelerated development of geothermal energy also needs to be accompanied by adequate management of risks that can affect the health, safety and environment (HSE) in local communities. Risks are inevitably associated with industrial activities, and need to be assessed by considering both the likelihood and impacts of incidents.

[2]Regeerakkoord 2017-2021 *"Vertrouwen in de toekomst"* by VVD, CDA, D66 en ChristenUnie (10/10/2017), and subsequent *Kamerbrief over geothermie* by the Minister of Economic Affairs and Climate (08/02/2018). www.rijksoverheid.nl (in Dutch, accessed December 2018).

HSE risks associated with subsurface operations have gained increasing attention over the last decade, and proper assessment, handling and mitigation of risks are required to maintain risks at a level that is acceptable for local populations. Seismic risks are determined by the occurrence and impacts of earthquakes and can be caused by subsurface operations ("induced seismicity"). Within the context of this study, the occurrence of induced seismicity that causes damage to surface infrastructure may be viewed as an example of an incident. The risk associated with this incidents is then determined by the likelihood of inducing seismicity with magnitudes high enough to cause surface damage as well as the severity of damage. Seismic risks are of particular concern considering the direct impact on local communities in terms of potential structural damage as well as public perception of subsurface resource development.

Induced seismicity is a main concern for geothermal projects worldwide and its occurrence has caused damage at surface infrastructure in some cases, and significant delays in development or even ceased operations in certain regions. Notable examples of induced seismicity that has been associated with geothermal projects include projects in (1) Soultz-sous-Forêts, France (maximum reported magnitude[3] M2.9 in 2003, appendix A.1.5), (2) Basel, Switzerland (M3.4 in 2006, appendix A.1.1), (3) Sankt Gallen, Switzerland (M3.5 in 2013, appendix A.2.4), and (4) Pohang, South Korea (M5.4 in 2017, appendix A.7). These examples have received much attention from the general public, regulators, operators and scientists. These and other examples have been used to study controlling mechanisms and key factors determining induced seismicity (Deichmann et al., 2014; Dorbath et al., 2009; Kim, Kwang-Hee et al., 2018; Moeck, Inga et al., 2015). In addition, the examples have been used to screen geothermal projects or assess seismic risks associated with geothermal operations (Baisch, S. et al., 2016). In the Netherlands, most geothermal operations have taken place without recorded seismicity. The main concerns are with geothermal projects targeting Dinantian carbonate formations in the Roer Valley Graben in the southeastern part of the Netherlands, an area that is also known for the occurrence of natural seismicity. Seismicity has been recorded near the Californië projects in the Netherlands and the Balmatt project in Belgium that target the Dinantian carbonate formation. Unequivocal causal relations between geothermal operations and seismicity have not (yet) been established for the geothermal projects near Californië in the Netherlands.

The occurrence of induced seismicity is determined by a combination of site-specific (e.g., geological) and operational (e.g., stimulation) factors (Candela et al., 2018). Most examples of felt seismicity[3] associated with geothermal projects occurred in geological settings that are very different from settings in the Netherlands, in particular concerning play and rock types, target depths and tectonic regimes. Some operational factors can be varied (within limits) to minimize seismicity (e.g., injection volumes for reservoir stimulation). Many site-specific factors can only be taken into account in the design of geothermal projects (e.g., avoiding pore pressure changes in large critically-stressed faults). It is therefore the subject of discussion to what extent findings can be extrapolated outside the regions where geothermal projects induced seismicity.

---

[3]If not specified M denotes maximum reported magnitude quoted in the literature in this report. M > 2 is chosen as a threshold for felt seismicity (see in section 1.2 on earthquake magnitude scales and definition of felt seismicity).

Induced seismicity has particular focus of attention in the Netherlands due to the frequent occurrence of seismicity associated with depletion of gas, in particular for the Groningen gas field in the North of the Netherlands (Figure 1-2, Appendix B.3).
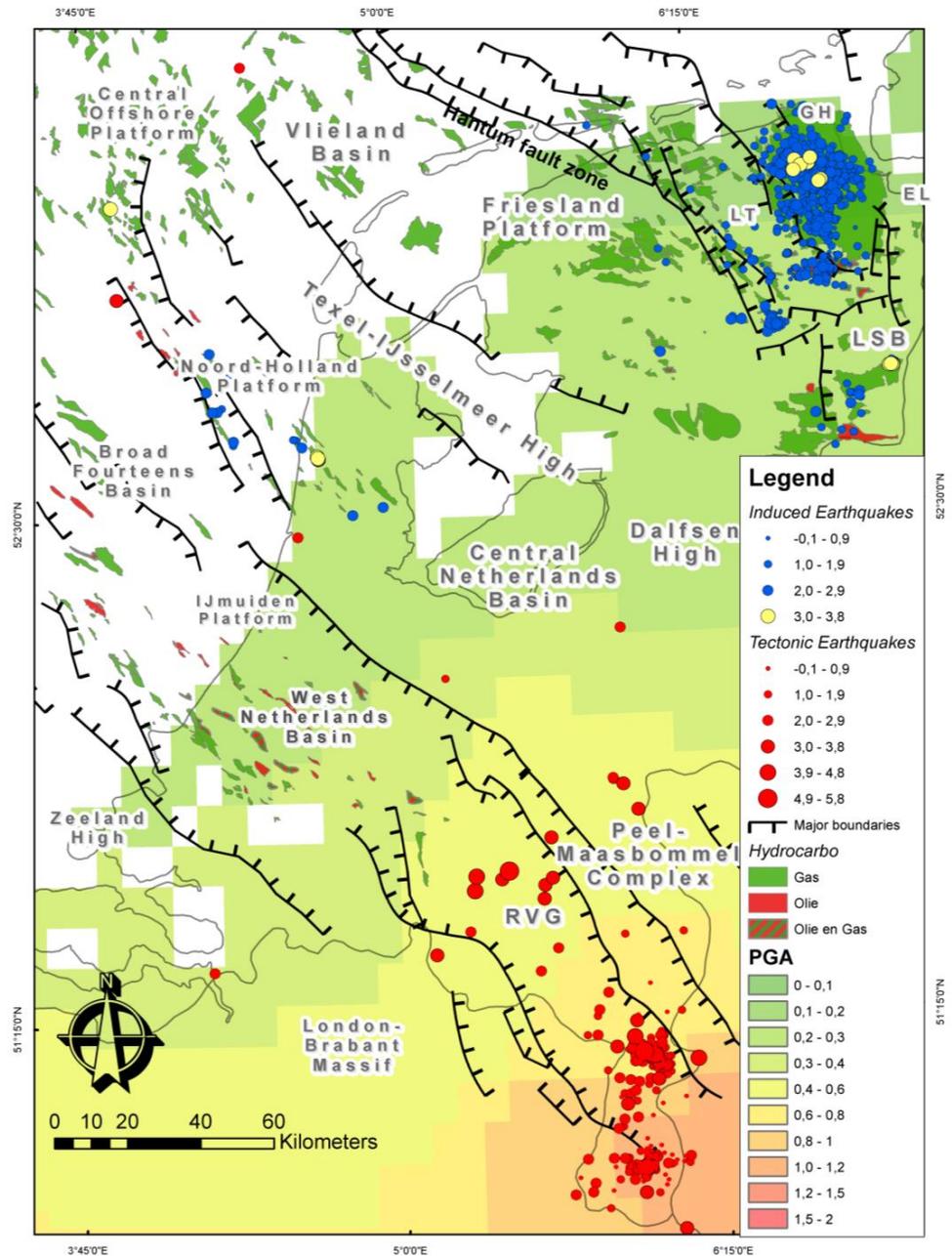
Figure 1-2   Overview of main induced and natural (tectonic) earthquakes in the Netherlands, superimposed on a map indicating the main structural basins, platforms and (fault) boundaries (thick black lines), and contours of peak ground acceleration (PGA) associated with natural seismicity (green to red shades). PGA (ms−2) with 10% chance of exceedance in 50 years (data from Giardini (1999) Recent seismicity in the vicinity of the Californië geothermal projects is not indicated given the unsure relation between operations and seismicity (map produced by TNO).

It is important to emphasize that the main mechanism responsible for depletion-induced seismicity (i.e. mainly differential compaction of porous sandstone reservoirs) differs from the main mechanisms responsible for induced seismicity associated with geothermal operations (i.e. a combination of direct pressure, poroelastic and thermoelastic effects, see section 2 for details). Differences in mechanisms, scale of activities and effects in the subsurface result in different characteristics of depletion-induced seismicity compared to seismicity associated with geothermal operations, and comparison of seismic risks is not straightforward. Nevertheless, the occurrence of depletion-induced seismicity is also important for the development of geothermal energy, mainly because (1) it plays a crucial role in public perceptions of subsurface operations for development of energy resources, and (2) the effects of gas depletion and geothermal operations may interact[4]. Interaction between natural seismicity and geothermal operations may play a role in areas that are more prone to natural seismicity, such as the southeast of the Netherlands[4] (Figure 1-2). Important research questions for development of geothermal projects are how to best assess overall seismic risks given these interacting activities and processes, and how these risks can be practically handled to ensure safety for local populations, and considered in the public debate between different stakeholders.

1.2 Geothermal plays & systems in brief

Geothermal plays are characterized by a specific geological setting that includes a heat source, heat migration pathway, heat/fluid storage capacity (reservoir), and the potential for economic recovery of the heat (Moeck, Inga S., 2014). Geothermal play types are characterized by geological factors such as rock types of target formations and depth. Heat sources can be heat flow from deeper parts in the Earth, or elevated heat flow from local geological structures such as igneous intrusions (i.e. plutons). Temperatures of geothermal reservoirs can be controlled by conduction- or convection-dominated heat transfer depending on regionally geological settings. While conduction in rocks is mainly controlled by temperature difference and thermal conductivity, convection relies on fluid flow. High enthalpy geothermal plays generally refer to high temperature, convection-dominated geothermal systems that occur in geological settings with active tectonics or volcanism. Low enthalpy geothermal plays generally refer to low to moderate temperature, conduction-dominated geothermal systems that occur in passive play tectonics settings. Geothermal play types can be developed with different well configurations (e.g., single well, doublets, triplets) connected to a larger operational infrastructure for heat extraction or electricity production.

Different geothermal systems can exploit the geothermal resources within plays. Geothermal fields (hydrothermal field) are the oldest geothermal systems, situated in convection-dominated settings. These fields are usually fractured, high temperature (>200 °C) reservoirs at shallow depth (~3 km up to the surface) and can be classified as vapor-dominated or water-dominated fields. Well-known examples include The Geysers (USA), and Larderello (Italy). Since the early 1900's hot water from these fields was used for heating (direct-use) and the first commercial production of electricity was achieved in 1926 at Larderello. The fields can be extensive (>10km) and contain numerous wells. Initially the fields only produced steam and/or water.

---

[4] Note the discussion on exploration permits for a geothermal project in Groningen (see *Advies aan minister over opsporingsvergunning aardwarmte Groningen*, 02/10/2017) and on the Californië projects (6/8/2018 and 21/01/2019), accessed December 2018, www.sodm.nl, in Dutch.

From the 1970s reinjection of cooled water for waste water injection and/or pressure maintenance became common practice (cf. Appendix A.12).

The Hot-Dry Rock HDR concept was proposed in the early 1970s by Los Alamos National Laboratory to exploit deeper formations for electricity. HDR targets hot, impermeable rocks at depth (often granite), and consists of two wells which are connected by hydraulic fracturing (e.g. Jung, 2013). The concept of Enhanced or Engineered Geothermal Systems (EGS) was introduced in 1977 by the Camborne School of Mines. For EGS, the permeability of natural fracture networks between two wells is stimulated by high pressure fluid injection that mainly involves shearing of natural fractures as opposed to tensile fracturing in HDR. Since the 1980's a number of pilot-EGS projects have been conducted, and the first commercial plants are operational (Lu, 2018).

Another type of geothermal systems are low to moderate temperature (30 - 150°C) systems in permeable sedimentary aquifers at relatively shallow depth (1 – 4 km). Typically, water is circulated between two wells (a doublet) at low pressures. Temperatures can be high enough for electricity generation (e.g. near München) but are mostly suitable for direct use of heat, for example in district heating. These systems are common in the North German Basin and Paris Basin. All geothermal systems in the Netherlands are of this system type.

1.3 Seismicity in brief

Induced seismicity refers to earthquakes that are caused by anthropogenic activities. Earthquakes caused by natural (tectonic) processes are referred to as natural seismicity (Giardini et al., 1999). In some cases, so-called triggered seismicity is distinguished from induced seismicity. A distinction between triggered and induced seismicity may be made on the basis of stress release on faults due to earthquakes (McGarr et al., 2002). For induced seismicity, the stress released due to earthquakes is comparable to the stress change introduced to the system by anthropogenic activities. For triggered seismicity the stress release can be much larger due to the additional release of natural stresses build up by tectonic processes. The difference between induced and triggered seismicity is therefore mainly in the stress state of faults prior to activities and the changes to that stress state caused by the activities (Candela et al., 2018). For induced seismicity anthropogenic activities affect the stress state at faults to an extent that they become seismically active. For triggered seismicity only small perturbations of the stress state at critically stressed faults are required to cause fault reactivation and seismic slip. In practice, it is difficult to distinguish induced seismicity from natural or triggered seismicity as the analysis of the natural stress state at faults and the effect of anthropogenic activities on that stress state are subject to considerable uncertainty. In addition, natural stresses and stress changes induced by anthropogenic activities is relieved by aseismic deformation. The relative contribution of aseismic stress release is rarely quantifiable, hampering clear relations between induced stress changes and stress release due to earthquakes. A combination of (baseline) seismic monitoring and site-specific geomechanical modelling is critical to understanding relations between induced, triggered and natural seismicity.

In this report, the likelihood of generating (felt) seismicity ("seismogenic potential") for different geothermal plays and operations is assessed on the basis of a case study review and analysis of mechanisms and key parameters or factors controlling

induced seismicity. When dealing with induced seismicity, it is important to distinguish seismogenic potential, and seismic hazard from seismic risk. Seismogenic potential is used to indicate the likelihood that geothermal operations generate (felt) seismicity. Seismic hazard is defined as the probability that specific ground motion (usually expressed as Peak Ground Acceleration, PGA, or Peak Ground Velocity, PGV) occurs in an area over a certain timespan (Giardini et al., 2013). Seismic risks are determined by the likelihood that seismicity with a certain frequency of occurrence (or number of events) and magnitude occurs as well as the impacts of the earthquakes. Accordingly, seismic risk accounts for the effect of seismicity, and therefore is also dependent on factors such as population density. Seismogenic potential, seismic hazard and seismic risks all critically depend on local conditions.

The most important and widely quoted characteristics of seismicity are earthquake magnitudes. Earthquake magnitudes (*M*) are often expressed using a local magnitude scale (*M*$_L$, (Richter, 1935; Gutenberg & Richter, 1956), a magnitude scale based on short-period arrivals of body (compressional or P-) waves (*m*$_b$, (Gutenberg & Richter, 1956) or using a moment magnitude scale (*M*$_w$, (Hanks & Kanamori, 1979). Besides earthquake magnitudes, the number of seismic events is important in determining seismic risks. Seismicity generally shows a characteristic relation between the number and magnitude of earthquakes with fewer larger magnitude earthquakes than smaller magnitude ones (Gutenberg & Richter, 1956). In many cases reported in the literature the magnitude scale is not specified or not considered relevant, and differences between scales are often assumed to be minor. In this report, magnitude scales reported in literature are taken at face value and used interchangeably without attempts to compensate for differences in seismic monitoring networks and geological settings that may affect seismic wave attenuation. If magnitudes are quoted without subscript for a site (e.g., *M*3.4 for Basel), the magnitude scale is unspecified and quoted magnitude indicate the maximum reported magnitudes of (a series of) seismic events.

Whereas most inventories of induced seismicity focus on earthquake magnitudes (McGarr, 2002; Davies et al., 2013), ground motions (PGA, PGV) resulting from earthquakes determine the damage at the Earth's surface and are better measures of the effects at the surface. PGA and PGV are not solely dependent on magnitude, but also depend on wave dampening/amplification in the (shallow) subsurface (including soil), the depth of the hypocentre and the distance from the epicenter. Ground motions associated with most induced seismicity are only detectable by dedicated sensor networks at the surface or in monitoring wells (Bohnhoff et al., 2018). For "felt" seismicity, ground motions can be felt by people at the surface and can even cause structural damage (Ellsworth, 2013). As the effect of induced seismicity at the surface strongly depends on site-specific factors, there is not a unique definition of felt seismicity in terms of seismic magnitude as derived from instrumental measurement. Intensity scales, such as the European Macroseismic Scale (EMS), use a classification of the severity of ground shaking based on observed effects in a limited area (e.g., EMS-98, Grünthal (1998)). Observed effects include the behavior of people and animals, shaking or falling of objects, and damage to buildings (Table 1-1). Intensity scales are based on observed effects at the surface, and are not always reported in studies of induced seismicity (cf. Appendix A, Appendix B). Earthquake magnitudes as derived from instrumental measurement are generally available and are therefore used to define felt seismicity, although critical threshold magnitude for felt seismicity can vary between regions. Based on existing data, magnitude of completeness of regional seismic networks and current practices,

a threshold magnitude (M) of 2 was taken in this study to distinguish felt seismicity from seismicity that is only detectable by seismic networks (see also Evans et al., 2012). While a threshold of $M2$ may be considered low for many regions worldwide, frequent events with $M > 2$ have been problematic for subsurface operations in the Netherlands (van Thienen-Visser & Breunese, 2015). An $M2$ event would be associated with a maximum EMS-98 intensity III-IV in the N. Netherlands (Crook et al., 1998), although the cumulative effect of multiple $M2$ events may yield higher intensities. Zang et al. (2014) report a similar relation between seismic magnitude and EMS intensity for the Landau (M_w 2.6) and Soultz-sous-Forêts (M_w 2.7) events.

EMS-98 intensity degrees	Observed effects		
	Effects on humans	Effects on objects and on nature	Damage to buildings
I (Not felt)	Not felt	No effect	No damage
II (Scarcely felt)	Felt at isolated instances (<1%) at receptive indoor positions	No effect	No damage
III (Weak)	Felt indoors by few	Hanging objects swing slightly	No damage
IV (Largely observed)	Felt indoors by many, outdoor by very few	Hanging objects swing, furniture shakes, woodwork creaks	No damage
V (Strong)	Felt indoor by most, outdoor by few	Hanging objects swing, doors & windows swing open or shut	Slight damage, no structural damage
VI (slightly damaging)	Felt by most indoors and by many outdoors	Small objects may fall and furniture may be shifted	Mostly slight damage, some building types with structural damage
VII (Damaging)	Most people frightened, difficult to stand (upper floors)	Furniture is shifted, many objects fall from shelves	Slight to heavy damage, depending on building type
VIII (Heavily damaging)	Many people find it difficult to stand, even outdoors	Furniture overturned, objects fall to the ground	Moderate to destructive damage, depending on building type
IX (Destructive)	General panic, people may be forcibly thrown to the ground	Many monuments fall or are twisted, waves seen on soft soil	Some building types destroyed, others moderate to severe damage
X (Very destructive)	-	-	Many building types destroyed or with moderate to severe damage
XI (Devastating)	-	-	Most building types destroyed or with severe damage
XII (Completely devastating)	-	-	Maximum conceivable effects (all buildings are destroyed)

Table 1-1 The European Macroseismic Scale (EMS-98) with classification of intensity (I-XII) and observed effects on humans, objects, nature and buildings based on description of Grünthal (1998).

Naturally occurring seismicity plays an important role in assessing felt seismicity and critical threshold magnitudes. In areas prone to natural seismicity, elevated ground motions due to subsurface operations can be detected only as deviations from long-term background motions. Induced seismicity may then only be considered problematic if operations lead to a considerable increase in frequency and magnitude of seismic events compared to natural baseline seismicity. Accordingly, seismogenic potential, seismic hazards and seismic risks for a specific area are determined by the combined effects of natural and induced seismicity. Induced seismicity particularly affects public perceptions regarding safety and impacts of subsurface operations in areas with absent or low levels of natural (baseline) seismicity.

1.4 Methodology

In this project, an extensive review of the occurrence of induced seismicity in case studies was conducted that includes geothermal projects as well as other types of projects with relevant subsurface operations. The review analyses (as much as possible) the mechanisms, factors, occurrence, frequency and magnitudes of induced seismicity as reported in publicly available literature. It serves as a basis to (1) analyse mechanisms of induced seismicity, (2) identify key parameters affecting the occurrence of induced seismicity in geothermal systems, (3) perform a light review of seismic monitoring and traffic light systems, (4) summarize the current

status of geothermal energy development and geothermal targets in the Netherlands, and (5) discuss implications for geothermal projects in the Netherlands.

Implications for geothermal projects in the Netherlands are discussed in terms of seismogenic potential (cf. section 6.5) of different geothermal plays. The following plays are distinguished on the basis of (potential) differences in seismogenic potential (cf. section 4.1): (1) Jurassic/Cretaceous permeable porous sandstone reservoirs that are currently the main geothermal target, (2) Triassic and Permian tight or permeable porous sandstone reservoirs, (3) Dinantian fractured or karstified carbonate reservoirs in the southeastern part of the Netherlands affected by active tectonics in the Roer Valley Graben (labelled RVG Dinantian carbonates), (4) Dinantian fractured or karstified carbonate reservoirs in the central (including southwestern part) and northern parts of the Netherlands not affected by active tectonics in the Roer Valley Graben (labelled CNNNLD Dinantian carbonates, cf. Figure 3-2, currently not targeted but under investigation[5]), (5) deeper (Devonian) sedimentary reservoirs (currently not targeted but under consideration as deep targets).

Analysis of the seismogenic potential for these plays is based on the following criteria:

1) the current presence or absence of seismicity in the plays
2) the presence or absence of felt seismicity as reported for case studies in basins with analogue geological settings in Europe, and
3) the effect of key factors on seismogenic potential as determined from the review of mechanisms and observations in case studies (cf. section 3.2).

A qualitative ranking (low, medium or high) of seismogenic potential is determined on the basis of these analyses (Table 1-2). An overall low seismogenic potential is assigned to a play if no seismicity is reported in the Netherlands or in analogue cases and key factors for the play indicate low seismogenic potential. A low seismogenic potential is meant to indicate that induced seismicity is unlikely to occur. An overall medium seismogenic potential is assigned to a play if seismicity has occurred in the Netherlands as well as in analogue cases, and key factors for the play indicate a medium seismogenic potential.

Seismogenic potential of play	Occurrence seismicity in play	Occurrence of seismicity in analogue cases	Effect of key factors (cf. Table 3-2)
Low	Absent	Absent	Low
Medium	Present	Present	Medium
High	Present	Present	High

Table 1-2　Criteria for ranking (low, medium, high) of seismogenic potential for the 5 geothermal plays distinguished in the Netherlands.

For geothermal plays in the Netherlands, a medium seismogenic potential is meant to indicate that induced seismicity may be expected in some cases with the number and magnitude of seismic events depending on the site-specific geology, type of operations, operational parameters and mitigation measures. A high seismogenic

---

[5]Ultradeep Scan Dinantian project (www.ebn.nl).

potential is assigned to a play if seismicity has occurred in the Netherlands as well as in analogue cases, and key factors for the play indicate a high seismogenic potential. For geothermal plays in the Netherlands, a high seismogenic potential is meant to indicate that induced seismicity may be expected in many cases and mitigation measures are needed to control the number and magnitude of seismic events. The seismogenic potential of current geothermal plays is specific for the Netherlands. The classification can be different for geothermal plays in other regions worldwide. As analysis of seismic risk requires assessment of the effects of seismicity, it requires a much more extensive analysis than possible in this review including surface conditions and effects (e.g., damage to infrastructure, costs, health & safety). Therefore, seismogenic potential rather than seismic risks were analysed in this study.

2 Mechanisms of induced seismicity

During subsurface operations there are changes in subsurface pressures, temperatures, mass and volumes. These changes cause the in-situ stress to change, and can lead to fault failure and seismicity. In this section, the mechanisms of stress changes causing induced seismicity are described. Examples of where these mechanisms were observed/inferred are presented, including not only geothermal systems, but also other activities where the mechanism was relevant. Note that in this chapter only a brief description is given of the most important aspects that are relevant for discussion on mechanisms of induced seismicity within the context of this study. More detailed information on basic geomechanics theory can be found, for example, in e.g. Jaeger (2007) and Fjaer (2008).
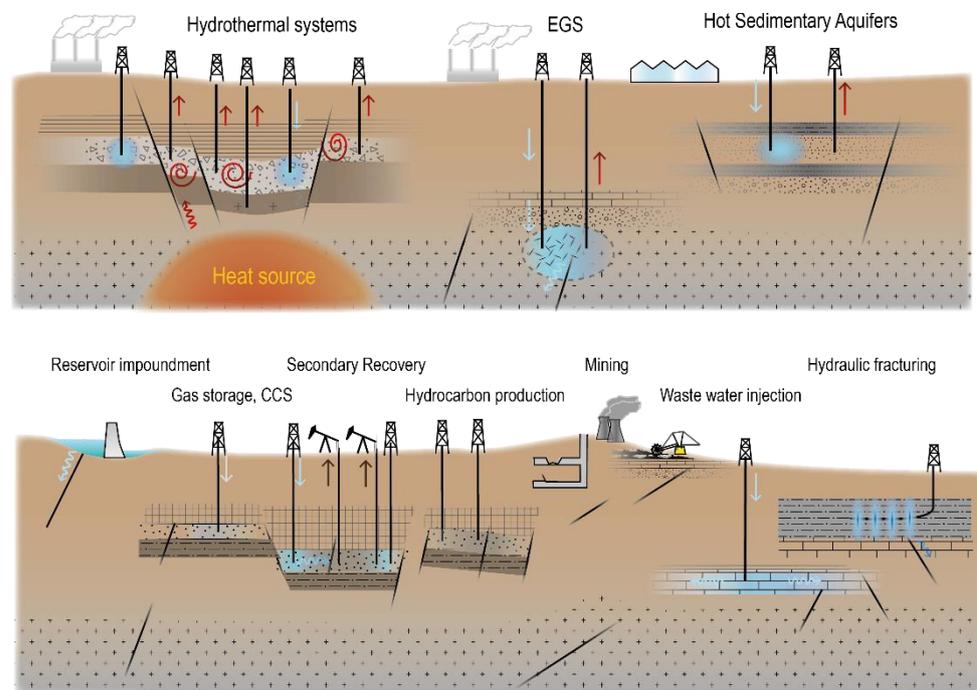
Figure 2-1   Overview of anthropogenic activities that may lead to fault reactivation and induced seismicity. Top: Operations that are (also) performed for the development of geothermal systems. Bottom: Other types of operations (Figure produced by TNO).

2.1 Stresses in the subsurface and at faults

Plate tectonic forces and crustal deformation control the regional stress field in the subsurface. The stress state in the subsurface and at faults can be described by three principal total stresses (S_1, S_2, S_3). Effective stresses (σ') are determined by total stress (S) and pore fluid pressure (P_f), i.e. $\sigma' = S - \alpha P_f$, with α indicating Biot's coefficient. Biot's coefficient determines the relative contribution of σ' that is carried by the fluid compared to that carried by the solid framework in porous rocks. Effective stresses control conditions of fault reactivation. Local effective stresses result in an effective normal stress (or "clamping force", σ_n'), and in a shear stress (τ) driving slip along faults. Important factors determining the stress state at faults are differential stress (i.e. the difference between the maximum S_1 and minimum S_3 principal stress,

$\Delta S = S_1 - S_3 = \sigma_1' - \sigma_3'$). In an isotropic stress state the three principal stresses are equal ($S_1 = S_2 = S_3$) and conditions are not favorable for fault slip. For increasing differential stress (i.e. an anisotropic stress state, $S_1 \neq S_2 \neq S_3$), faults may become critically stressed and seismic slip along faults becomes more favorable. Under most subsurface conditions, the stress state is anisotropic. In the Netherlands, in most situations the vertical stress is the maximum principal stress ($S_1 = S_v$), the intermediate principal stress is the largest horizontal stress ($S_2 = S_{Hmax}$) and the minimum principal stress is the smallest horizontal stress ($S_3 = S_{hmin}$). This stress state promotes normal faulting.

2.2 Induced fault reactivation and the Mohr-Coulomb failure criterion

The stress state of a rock mass or fault is determined by the regional tectonic stress field. In areas with active tectonics, the stress state may be closer to a state where the rock mass starts to fracture or faults starts to slip compared to areas with passive tectonics. Anthropogenic activities in the subsurface alter the state of stress, as a result of changes in e.g. pore pressure and temperature. When in the altered stress state the failure strength of the rock mass or of a fault is exceeded, faults or fracture may initiate or fault slip may occur. Failure of faults and rocks is potentially seismic. To understand the occurrence of induced seismicity it is important to assess the potential for failure. In the upper crust where most anthropogenic activities are located mainly brittle failure occurs. The brittle strength of intact rocks can be described by various failure criteria (Fjaer et al., 2008). The most commonly used criterion for compressive stresses is the Mohr–Coulomb criterion, where the failure strength increases linearly with stress (Figure 2-2a).

In terms of effective normal stress σ_n' and shear stress τ_f the Mohr-Coulomb criterion is given as

$$\tau_f = C + \sigma_n'\tan\varphi = C + \sigma_n'\mu \qquad \text{2-1}$$

where C is the cohesion, φ is the friction angle, and μ is the friction coefficient (i.e. the slope of the failure line). For intact rock the friction coefficient equals the internal friction coefficient μ_i. In the Mohr diagram, failure is indicated when the failure line is tangent to the circle representing the local stress state (Figure 2-2a). At initiation of failure, the most critically stressed fault has angle θ between σ_1 and the pole of the fault plane (indicated by angle 2θ in the Mohr diagram). Shearing (or mode II fracturing) will occur along the fault or fracture with this orientation when the criterion is reached. In Figure 2-2a, the Mohr–Coulomb criterion is combined with the Griffith failure criterion in the tensional regime

$$\tau_f^2 = 4\left(T_0^2 - \sigma_n`T_0\right) \qquad \text{2-2}$$

where T_0 is the tensile strength. Tensile opening (or mode I fracturing) may occur when the smallest effective stress σ_3' is tensional, e.g. as a result of high pore pressure. Mixed – mode behaviour (e.g. dilational shearing) may also occur at low stresses.
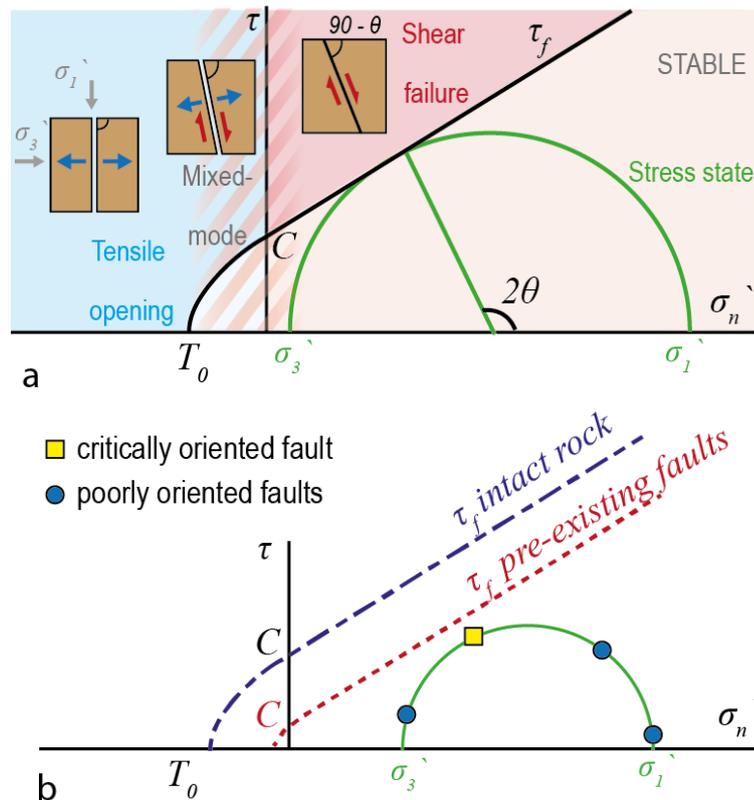
Figure 2-2   Mohr diagrams in 2D with failure criteria and example stress state. a) Mohr diagram with a composite Griffith – Coulomb failure envelope for intact rock (black line), with tensile strength T_0 and cohesion C. The stress state at shear failure on a fault plane with θ (angle w.r.t. σ_3 orientation) is drawn (green semi-circle). Different failure modes (tensile, compressive shear, mixed mode) are illustrated. b) Mohr diagram with failure lines for intact rocks and pre-existing faults. An example stress state is given (green semi-circle) with three different fault orientations relatively far from failure (blue dots) and one fault orientation relatively close to failure (yellow square). It means the fault with the orientation relatively close to failure (yellow square) is more likely to reactivate, slip and generate seismicity (Figure produced by TNO).

The Earth's subsurface is cross-cut by faults and fractures, which form pre-existing planes of weakness. Failure on these fault planes will occur at lower stresses than for intact rock, since the cohesion is usually much lower (Figure 2-2b). Hence, pre-existing faults and fractures may be dominant in accommodating deformation of rocks. As they represent discontinuities in rocks that may otherwise act as homogeneous elastic permeable media, faults and fractures are also prone to stress concentrations and may act as permeable fluid conduits accommodating pressure diffusion. The reactivation of (pre-existing) faults is also commonly described by Mohr – Coulomb failure (Equation 2-1), with μ then denoting the friction coefficient of the fault instead of the internal friction coefficient. The stress required for fault reactivation depends on the initial stress and the friction coefficient and the cohesion, but also on the orientation of the pre-existing faults in the stress field. Some fault orientations may be critical, whereas faults with other orientations may be far from failure (Figure 2-2b).
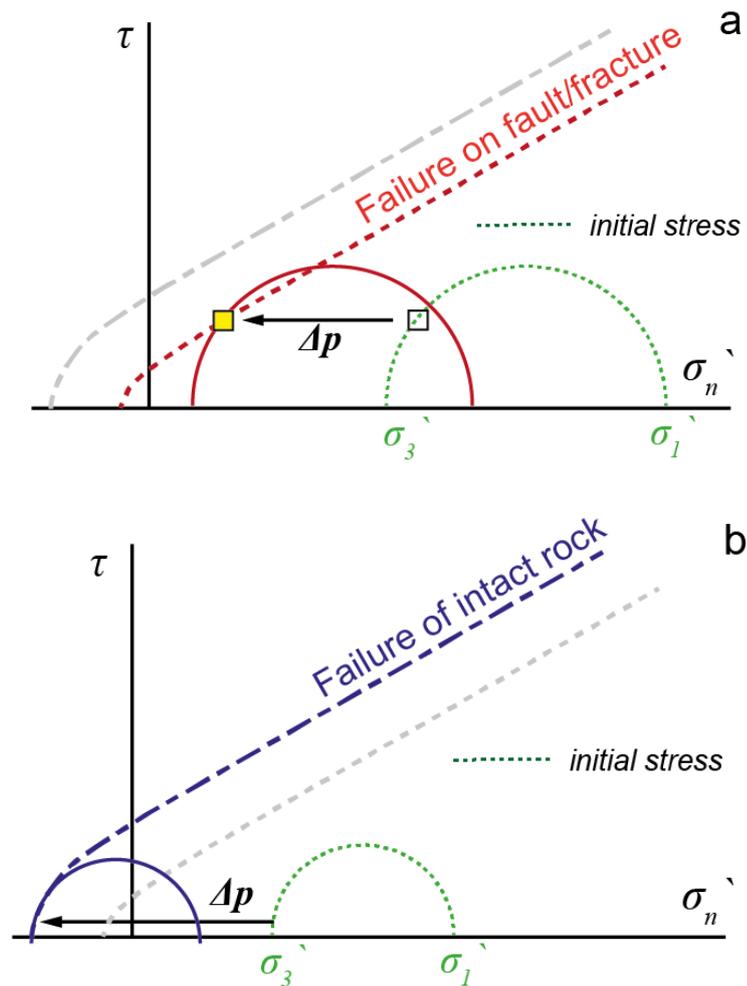
Figure 2-3   Effect of fluid increases on fault stress and reactivation. a) Pressure increase Δp causes shear failure on a pre-existing fault with a near-optimal orientation in the stress field. b) Pressure increase Δp larger than σ_3 causes tensile failure (Figure produced by TNO).

The (2D) Mohr-Coulomb failure criterion is useful because of straightforward application, and is commonly applied to determine the stress state at faults and conditions for fault reactivation. However, it has some limitations as it relies on differential stress ($\Delta\sigma = \sigma_1 - \sigma_3$) to analyze rock failure, thereby neglecting the intermediate principle stress (σ_2). The intermediate principle stress is known to affect the failure criterion of rock, in particular for anisotropic rocks (e.g., layered sediments) in an anisotropic stress field (Labuz & Zang, 2012; Mogi, 1971). Some experimental studies have calibrated 3D failure criteria that accounts for the effects of σ_1, σ_2, σ_3 by applying true triaxial stress states in experimental setups (Chang, C. & Haimson, 2012). Parameters describing 3D failure criteria such as the Mogi criterion can be related to the parameters describing the 2D Mohr-Coulomb failure criterion (Al-Ajmi and Zimmerman, 2005). The effect of applying a 3D failure criterion based on true triaxial experiments to analyze failure around a doublet system that is stimulated using waterfrac was determined for the geothermal project at Groβ Schönebeck (cf. appendix A.3.1, Blöcher et al., 2018). Such analysis may provide valuable insight on

the relation between spatiotemporal stress changes and induced seismicity, but requires detailed field scale numerical modelling in combination with accurate data.

It is clear that pre-existing faults and fractures are of paramount importance for induced seismicity. Seismological evidence suggests that in many cases induced seismicity occurred on pre-existing faults, as the hypocenters of relocated seismic events line up on distinct planes or are located on mapped fault planes (e.g., Figure 2-4). Depending on the initial fault stress small changes in stress may be sufficient for fault reactivation.

2.3　The effect of rock properties on stress changes

The mechanical properties of rocks determine how rocks deform under stress changes as well as how stress changes are spatially and temporarily distributed in rock formations. If rocks are uniform and behave elastically, the distribution of stress changes is also uniform within the rock mass. Elastic rock deformation can be described by elastic parameters such as Young's modulus and Poisson's ratio. In determining poroelasticity and thermoelasticity of rocks, it is generally assumed that deformation is entirely elastic. The elastic response of porous rocks to pore pressure changes depends on the stress carried by the framework of grains compared to the stress carried by the pore fluid, which can be described using Biot's coefficient (α, cf. section 2.1). The relation between total and effective stresses (and hence Biot's coefficient) is determined by rock properties. If mechanical rock properties are such that locally brittle deformation (e.g., fracturing or pore collapse) occurs, rock deformation is (partly) inelastic and deformation is often localized along failure planes or zones of weakness resulting in an inhomogeneous distribution of stress. Failure of porous rocks is best described using effective stresses with α = 1 (following Terzaghi's definition, Fjaer et al., 2008). The type of failure criterium and failure conditions are determined by rock properties. In case rock failure can be described by the Mohr-Coulomb criterion, failure conditions can be described using cohesion and friction coefficient or angle (cf. Eq. 2-1). The mechanical rock properties thus determine the relative contribution of elastic and inelastic deformation. Due to the inhomogeneous distribution of stress and localized deformation, the effect of brittle deformation in the reservoir on the stress state at faults is difficult to determine. For example, local stress paths will be different if brittle deformation occurs, and accurate assessment of the spatial distribution of stress requires numerical models.

Besides elastic and inelastic brittle deformation, some rocks show time-dependent deformation (i.e. creep) under differential stress. Creep is particularly important for rocks such as claystones, shales and rocksalt, and can locally relieve differential stress by aseismic deformation, resulting in a (more) isotropic stress state. Creep of rock formations is of importance for induced seismicity as it affects the transfer of stress between formations. For example, mechanically decoupling between a geothermal reservoir and deeper basement rocks due to the presence of creeping formations can be beneficial as the stress state of the basement rocks is not transferred to the geothermal reservoir.

In this report, rock competency is used to qualitatively indicate the resistance of rocks to deformation. More competent (stiffer) rocks have a higher resistance to deformation than less competent rocks. Alternatively, for similar strain, more competent rocks exhibit a larger increase in stress than less competent rocks. Together with the local stress field, mechanical rock properties determine changes in

local stress state following anthropogenic activities as well as the failure behavior of rock formations and faults (Figure 2-2). For example, critical conditions for fault reactivation and characteristics of seismic or aseismic fault slip are affected by rock properties.

The distribution of fluid pressure and associated stress changes during subsurface operations is determined by flow properties such as permeability. Flow properties determine the sealing capacity of rocks or faults, and hence fluid flow in the rock matrix, or along and across faults and fractures. For example, pressure build up around sealing faults can result in high effective stresses and a critical stress state of faults. Formations with a high sealing capacity are generally not suitable as geothermal reservoirs, but can act as top, lateral or bottom seals if situated around reservoirs resulting in hydraulic decoupling of reservoirs and surrounding formations. Hydraulic sealing or decoupling is important for induced seismicity as it reduces direct pressure effects (i.e. reduction in effective stress) at faults outside the reservoir (for example, hydraulic decoupling between the reservoir and critically stressed basement faults can lower the seismogenic potential although poroelastic effects remain important).

Rock properties also determine thermoelasticity in rocks undergoing temperature changes (for example cooling at injection wells). In particular, thermoelastic effects are controlled by the combination of thermal expansion coefficient and elastic parameters. Temperatures of geothermal reservoirs can be controlled by conduction- or convection-dominated heat transfer depending on regional geological settings. While conduction in rocks is mainly controlled by temperature difference and thermal conductivity, convection relies on fluid flow and is thereby dependent on flow properties such as permeability.

Fluid flow and temperature changes may result in chemical reactions between fluids and rock matrix or fault rock. Such reactions may alter mechanical, hydrological and thermal properties of rocks, and thereby affect (re-)distribution of stress, fault reactivation and induced seismicity. Examples include clay swelling causing permeability reduction and water weakening of fault rock promoting fault reactivation.

Accordingly, the local stress state as well as the stress state at faults and potential fault reactivation and induced seismicity following anthropogenic activities are affected by the interplay of different rock properties. The different mechanisms of stress changes leading to fault reactivation and induced seismicity are discussed in the following sections.

2.4 Pore pressure changes and poroelastic stressing

Changes in subsurface pore pressure are a common consequence of many subsurface activities. Changes in fluid pressure affect both the effective stresses in the bulk rock mass and in faults and fractures, and can lead to induced seismicity if the failure criterion on those faults is exceeded. Different subsurface activities target distinct rock formations with different types of operations, and hence the effect of pressure changes on stress and on how seismicity can be induced are different. In the following sections a number of different pressure-related mechanisms for inducing (micro)seismicity are presented.

2.4.1   *Pressure increases in faults and the role of pressure diffusion*

Pre-existing fractures and faults are ubiquitous in the subsurface, and an increase in pressure in those faults can cause seismicity. An initial effective normal stress and shear stress act on fault planes as a result of tectonic stresses. Stress on the fault plane may be less or more critical, depending on the fault's orientation in the stress field and the magnitude of the initial stresses (Figure 2-2). An increase in pressure in the fault due to e.g. fluid injection reduces the effective normal stress on the fault. This is represented by a shift of the Mohr circle to the left – i.e. the fault is brought closer to failure (Figure 2-3a). When the fault is reactivated rapid shear motion can occur which generates seismic waves.

The hydraulic properties of the rock, fractures and faults control the fluid flow and pressure diffusion, and affect the evolution of induced seismicity. As fluid is injected locally the elevated pressure diffuses away from the injection well as a function of time, raising pressures over a larger area and potentially inducing seismic events further away from the source. When injection occurs in a relatively impermeable but fractured rock mass, the fractures dominate fluid flow and diffusion. For porous rocks the matrix is more important in controlling the fluid flow and diffusion. The pressure distribution depends on the rock type targeted in the various activities, as well as on the operational parameters. For reservoir stimulation by fluid injection performed in the geothermal project near Basel (cf. appendix A.1.1), Zang et al. (2014) suggest a change in fracture type from mode I close to the injection well (near-field) to mode II further away from the well (far-field). This change is interpreted as a transition of hydraulic tensile fractures near well to hydro-shear at locations far from the well.

Relevancy for geothermal: Direct pressure effects play an important role in Enhanced Geothermal Systems (EGS) and reinjection in geothermal fields. An EGS is often situated in fractured granite (e.g. Basel, Soultz-sous-Forêts), requiring high pressure stimulation to reactivate fractures and faults to enhance the permeability (Figure 2-4). For several types of injection operations including stimulation at the Soultz-sous-Forêts geothermal site, the spatiotemporal evolution of the recorded microseismicity showed that the distance of events from the well increased as the square root of time, indicative of diffusion (Parotidis et al., 2004; Shapiro & Dinske, 2009). Pressure diffusion is a time-dependent process, and hence may cause seismicity to occur even after the injection operations are terminated. Post-injection seismicity was for example observed in Basel (appendix A.1.1). Reinjection in geothermal fields also locally increases the pore pressure potentially causing seismicity around the injection well, e.g. in Larderello geothermal field (appendix A.10). In low/medium-enthalpy doublets in permeable formations the injection pressures are generally lower (~1 MPa), but seismicity can still occur if a hydraulic connection exists with critically stressed faults. This was for example observed for some sites in the Molasse Basin (appendix A.2).
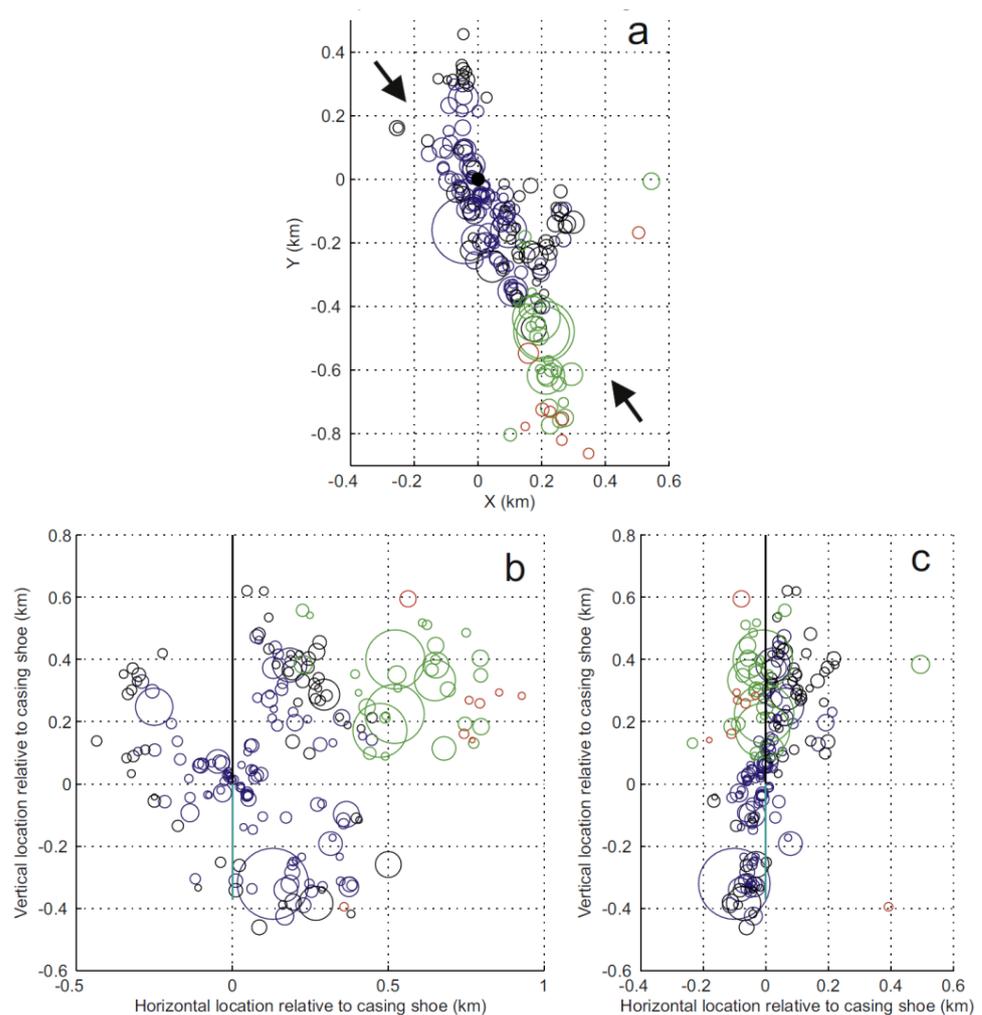
Figure 2-4 Location of seismic events at the Basel 1 EGS. Darkblue: events recorded during stimulation from 2 to 8 December 2006, black: 9 to 31 December 2006, green: 1 January to 30 November 2007, red: eight events in 2010, 2012, 2013. The area of the circles is proportional to the seismic moment of the event, assuming a stress drop of 10 MPa (i.e. the largest circle at -0.2 to -0.3 km depth represents the M_L 3.4 mainshock of December 8th, 2006). The borehole is indicated with the black line, and the open hole section with a light blue line. Arrows indicate the maximum horizontal stress (From Deichmann et al., 2014, Copyright Elsevier, reproduced with permission).

Relevancy for other activities: Pore pressure increase as a mechanism for inducing seismic events was first proposed for the Rocky Mountain Arsenal waste water injection site in Denver (Evans, D., M., 1966; Healy et al., 1968). Diffusion of pressure through permeable faults near the wells to greater depths likely induced the events. In fact, in many cases seismicity induced by wastewater seems to occur mainly in the crystalline basement, below the targeted formation for injection, e.g. in Oklahoma (Keranen, K. M. et al., 2014), Youngstown, Ohio (Kim, Won-Young, 2013), and the Raton Basin (Rubinstein et al., 2014). Note that the estimated changes in pressure at the hypocentre location are often small (0.1 – 0.01 MPa), indicating that the reactivated faults were close to failure.

Contrary to fluid circulation during geothermal operations, waste water injection causes fluid volume in the reservoir to be raised dramatically over time which causes progressive pressure increase and associated changes in stress state in the formation and at faults, even at distance from the injection well. Therefore, the high earthquake magnitudes associated with waste water injection are not representative for geothermal operations, although valuable insights in mechanisms of induced seismicity can be obtain by studying waste water injection.

Other activities where pressure increases play a role are shale gas hydraulic fracturing in Canada (see section 2.4.2, appendix B.1), other large-scale wastewater injection in the United States (appendix B.2), reinjection during secondary recovery of hydrocarbons (appendix B.4), reservoir impoundment (appendix B.6) and reflooding of abandoned mines. Pressure decreases on the other hand occur when fluid or hydrocarbons are extracted from the subsurface, such as during hydrocarbon depletion and steam production from geothermal fields. Also lowering of the water table during mining decreases the pore pressure.

2.4.2   *Tensile fracturing due to high injection pressures*

During some operations the injection pressure can become very high, and the minimum horizontal stress close to the wellbore can become tensile. In this case, not only shear (mode II) faulting but also dilatant shear or tensile (mode I) fracturing may occur – i.e. hydraulic fracturing (Figure 2-3a). A hydraulic fracture opens in the direction of the minimum horizontal stress and propagates in the direction of the maximum horizontal stress (Figure 2-3b). Fracture opening enhances the permeability and improves hydrocarbon or fluid transport. Dilatant shear fracturing can also occur on pre-existing faults and fractures oriented parallel or close to the direction of maximum horizontal stress when injection pressures are high, or the in-situ stresses are low. Where the pressures are lower (e.g. further away from the injection well) and stresses are compressive, faults and fractures are predominantly reactivated in shear, as discussed in the previous section. The different faulting mechanisms (tensile, mixed-mode, shear) occur together, as shown from microseismicity recorded during hydraulic fracturing (Busetti et al., 2014) and EGS stimulations (Zhao et al., 2014). Larger magnitude events far from the wellbore are however usually predominantly shear events (Cuenot et al., 2006; Urbancic & Zinno, 1998; Zhao et al., 2014). Tensile events likely still represent a significant portion of the (subseismic) deformation process during hydraulic fracturing, although they may not always be recorded. In addition, slow shear slip events on misoriented faults contributes to deformation but is generally unrecorded (Das & Zoback, 2013).

Relevancy for geothermal systems: Hydraulic fracturing was performed in a number of geothermal test sites in the North German Basin, to enhance the permeability of tight sandstones. During these fracturing tests only very low magnitude events M<0 were recorded. Reservoir stimulation by fluid injection can result in tensile (hydraulic) fracturing, in case the minimum horizontal stress (or fracturing pressure) is exceeded, and in shear fracturing of existing natural fractures which can occur at lower pressures (cf. Figure 2-3). Besides shear fracturing, tensile fracturing also plays a role during EGS stimulation. Events with a large tensile component were observed in e.g. the Basel stimulation, even though the pore pressure likely did not exceed the minimum stress (Zhao et al., 2014). Tensile fracturing is important for permeability increase in porous sedimentary reservoirs, but will likely not lead to large seismic events as these are mostly related to shear slip along faults.

Relevancy for other activities: Hydraulic fracturing is extensively used for the production of gas from tight sandstones or shales (appendix B.1).

2.4.3   Poroelastic stressing

In the previous sections the direct effect of fluid pressure on faults and fractures was discussed. However, the rock matrix affected by a pressure change will also experience a volumetric strain (i.e. volume changes due to reservoir contraction or expansion). This volume change causes a change in stress within the rock mass itself controlled by pore pressure changes, and in the surrounding rock formations – i.e. poroelastic stressing. The vertical contraction (for pressure decrease) or expansion (for pressure increase) is (partly) accommodated as subsidence or upheave at the surface (Geertsma, 1966; Segall, P. et al., 1994). Horizontal contraction or expansion is resisted by the surrounding rock, and the horizontal stress in the reservoir changes (Figure 2-5).
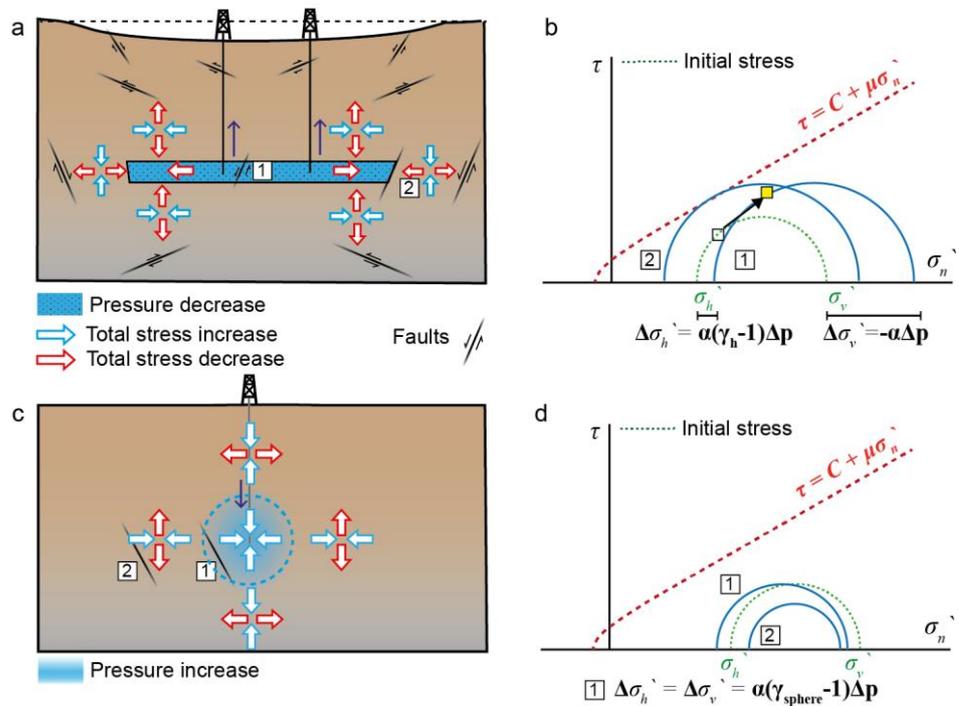
Figure 2-5   Illustration of poroelastic stressing in and around a laterally extensive depleting gas field. a) Total stress changes in and around a depleting gas field or a geothermal field undergoing net depletion. b) Mohr circle diagram of stress changes within (1) and just beside (2) a laterally extensive depleting reservoir in a normal faulting regime. c) Total stress changes for injection leading to pressure increase in a near-spherical volume. d) Mohr circle diagram of stress change within (1) and just outside (2) the boundary of the spherical pressure front (Figure produced by TNO).

For a laterally extensive reservoir (zero lateral strain, uniaxial compaction) that deform elastically, the change in total horizontal stress $\Delta\sigma_h$ with depletion Δp is given by (e.g. Hettema et al., 2000).

$$\Delta\sigma_h = \alpha\gamma_u\Delta p = \alpha\frac{1-2\nu}{1-\nu}\Delta p \qquad\qquad 2\text{-}3$$

where α is Biot's coefficient ($0 < \alpha < 1$), and γ_u is the uniaxial stress path parameter, which is a function of Poisson's ratio ν. For example, for a Poisson's ratio of 0.2 and a Biot coefficient of 1, a decrease in pressure of 1 MPa will result in a decrease in total horizontal stress of 0.75 MPa, and an increase in effective horizontal stress of 0.25 MPa. The total vertical stress change is 0 and the effective vertical stress change equals $\alpha\Delta p$ = 1 MPa. Hence, the effect of pressure decrease is an increase in differential stress – i.e. a larger size of the Mohr circle (case 1 in Figure 2-5b). These stress changes are resulting from elastic deformation only, and differ from the effective stress for failure (Figure 2-3). Nevertheless, the stress increase can cause fault reactivation, even though the effective stresses became more compressive due to pressure decrease. With lower Poisson's ratio the slope of the stress path and the reactivation potential increase. The effect of pressure on stress and stress path is also affected by Biot's coefficient, which depends on the reservoir porosity. For high porosities it may be close to 1 but for lower porosities and a stiff rock matrix it may be much smaller, reducing the effect of pressure changes on the reservoir stress. Accordingly, the magnitude of poroelastic stress changes depend on the pressure change, the elastic properties of the rock mass and the geometry of the rock mass experiencing a pressure.

Relevancy for geothermal systems: Poroelastic stressing is expected to play a role in geothermal systems where pressure is decreased (e.g. producing geothermal fields) or increased (e.g. stimulation in an EGS). Poroelastic stressing was identified as the most likely mechanism controlling subsidence observed above the Geysers geothermal field, in favour of thermoelastic contraction (eg. Mossop & Segall, 1997). During fluid injections in an EGS, poroelasticity may cause a more compressive stress (expansion of the rock due to the injected volume), which stabilizes certain fault geometries (e.g. normal faults to the side of the injector), thereby counteracting the effect of the direct pressure increase (Figure 2-5). Direct pressure effects are expected to dominate nearby the well, but poroelastic effects may reach further and destabilize certain fault geometries (Segall, P. & Lu, 2015). Note that poroelastic effects in geothermal systems usually occur in conjunction with thermoelastic effects.

Relevancy for other activities: Poroelastic stressing was suggested as an important mechanisms for the induced seismicity observed in and around producing gas fields. This includes the Lacq field (Segall, P., 1989; Segall, P. et al., 1994), but also the Groningen field and other gasfields in the Netherlands (Van Wees et al., 2014). Depletion of a hydrocarbon reservoir causes contraction of the reservoir. The vertical contraction (i.e. reservoir compaction) is (partly) accommodated as subsidence at the surface (Geertsma, 1966; Segall, P. et al., 1994). Horizontal contraction is resisted by the surrounding rock, and the horizontal stress in the reservoir decreases (Figure 2-5a). Poroelastic stresses can be strongly enhanced by the local reservoir geometry, such as an anticlinal structure or offset faults (Buijze et al., 2017; Mulders, 2003; Orlic & Wassing, 2013). The Groningen reservoir in the Netherlands is one example where poroelastic stress changes play an important role

in seismicity driven by reservoir compaction (appendix B.3). The depletion of the reservoir causes the stresses outside the reservoir to change as well. Laterally, outside the reservoir, horizontal stress decreases in response to lateral contraction of the reservoir (Orlic & Wassing, 2012; Segall, P. & Fitzgerald, 1998). Conversely, above the reservoir, horizontal stress becomes more compressive as the reservoir contracts laterally (Figure 2-5a). Stress arching causes a lateral increase in vertical stress outside the reservoir, and a decrease above the reservoir (Orlic & Wassing, 2012). The stress changes promote thrust faulting above and below the reservoir, and normal faulting at the sides of the reservoir. Note however that the poroelastic stress changes decay rapidly with distance from the reservoir. Poroelastic stress changes of 0.2 MPa are for example estimated around the Lacq field after a pressure decrease of 50 MPa (Segall, P. et al., 1994). Despite small poroelastic stress changes, seismicity may be induced on critically stressed faults. Stress concentration on faults by reservoir compaction may play a role in inducing seismicity in the Lacq field. Additionally, shallow faulting related to the subsidence bowl above a hydrocarbon field can cause seismicity, as seen in the Wilmington oil field where significant shallow seismic events occurred (Yerkes & Castle, 1976).

Poroelastic stressing is also important during fluid injection. The direct pressure effect on faults may be larger, but poroelastic stresses may reach further (Segall, P. & Lu, 2015). Poroelastic stressing can affect faults that are hydraulically isolated and do not themselves experience a pressure change. For example, this effect is important during waste water injection (Chang, K. W. & Segall, 2016). Poroelastic stressing may be responsible for the earthquake swarm that occurred during hydraulic fracturing operations near Crooked Lake in 2013 (Schultz et al., 2015). Seismic events of M_w up to 3.2 were recorded during and following hydraulic fracturing of the Duvernay formation near Crooked Lake, Alberta Canada, at distances up to 4 km from the well. Modeling showed that these events occurred in a region of increased stress due to poroelastic stressing, suggesting poroelastic stress may have contributed to inducing the events (Deng et al., 2016). Modeling of CO_2 injection into a layered faulted system also showed poroelastic stress to promote shear faulting outside of the area affected by CO_2 injection (Rutqvist, J. et al., 2008). Note that again the poroelastic stress changes outside the volume affected by the water or CO_2 injections are likely small and can only reactive faults that are already close to failure, emphasizing the influence of faults and the in-situ stress field on induced seismicity.

2.5 Temperature changes and thermoelastic stressing

Anthropogenic activities may result in a temperature change in the subsurface, which leads to a shrinking (cooling) or expansion (heating) of the rock mass. These effects cause stress changes – i.e. thermoelastic stressing. Thermoelastic stressing works in a similar way as poroelastic stressing. The volume change due to temperature changes results in stress changes inside as well as outside of the rock volume. The magnitude of thermoelastic stress can be large and comparable to pressure changes.

The relative magnitude of stress changes resulting from temperature changes with respect to pore pressure changes is given by (Segall, P. & Fitzgerald, 1998)

$$\frac{\sigma_{ij}^{\text{thermo}}}{\sigma_{ij}^{\text{poro}}} = \frac{K\lambda\Delta T}{\alpha\Delta P}$$

2-4

where K is the bulk modulus ($K = E / 3(1 - v)$), λ is the linear thermal expansion coefficient, and α is Biot's coefficient. Cooling of 5°C of a laterally extensive reservoir with a bulk modulus of 20 GPa and a thermal expansion coefficient of 10^{-5} °C^{-1} would for example cause compaction and subsidence, as well a reduction in horizontal stress of 1 MPa (Figure 2-6b).
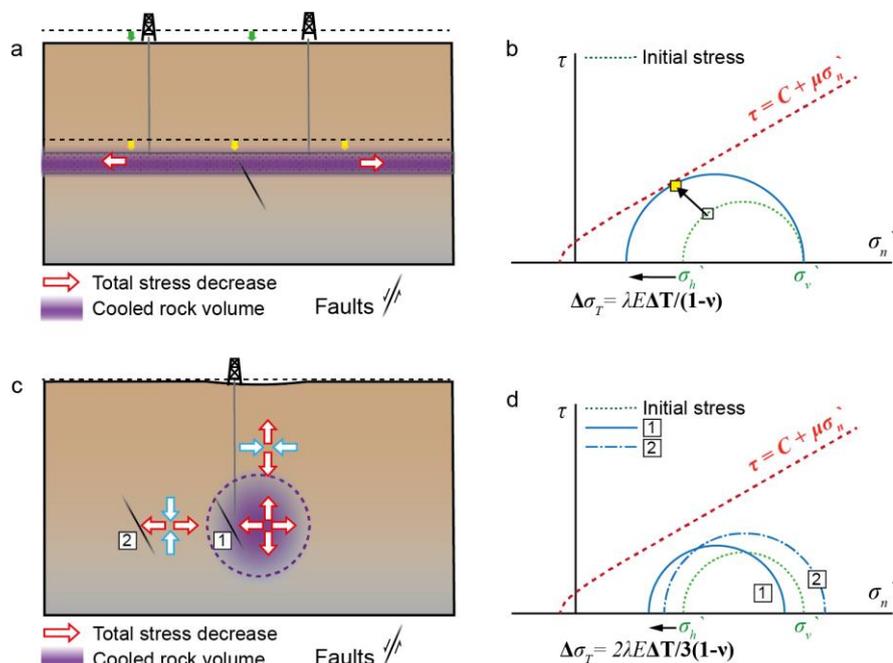
Figure 2-6   Illustration of thermoelastic stressing inside and outside a cooled rock volume. a) Laterally extensive reservoir which is cooled and undergoing uniaxial compaction as the reservoir rock contracts. The horizontal stress decreases. b) Mohr circle of stress change within the laterally extensive reservoir. Example stress path on a fault is shown. c) Cooling of a near-spherical volume. d) Stress change within (1) and just outside (2) the boundary of the cooled spherical volume (Figure produced by TNO).

In a normal faulting regime, the consequence is an increase in differential stress, which may cause fault reactivation (Figure 2-6b). In the vicinity of a wellbore injecting cold fluids, the thermal stress changes may be much larger, and can exceed the pore pressure changes.

Relevancy for geothermal systems: Temperature changes and thermoelastic stressing play an important role in geothermal systems. In producing high-enthalpy geothermal fields hot water/steam is extracted and cold water is reinjected to extract more heat from the rock mass. The temperatures of the reinjected fluids may be >200 °C lower than the temperature of the geothermal reservoir, such as observed at The Geysers and Larderello sites (Batini, F. et al., 1985; Martínez‐Garzón et al., 2014). Also hydraulic stimulations and circulations in medium enthalpy systems are

performed with fluids that are 100 – 200 °C colder than the rock mass (e.g. the systems in the Upper Rhine Graben, (Baillieux et al., 2013). The temperature difference of injected water in low-enthalpy geothermal doublets is smaller, 30 – 70 °C (section 4). Over time (10 – 30 years, depending on design of operations and local geological setting) these temperature changes cool the rock mass to the extent that a temperature decrease is observed in the production well, and eventually cold water breakthrough occurs in the geothermal doublet. For all these temperature changes the thermal stresses in the vicinity of the wellbore (<100 m) can be significant and lead to tensile failure, but the stresses decrease rapidly with distance (Koh et al., 2011). Note that besides thermoelastic stressing geothermal operations also simultaneously cause pore pressure changes and poroelastic stressing (section 2.4). These three processes may act on different timescales, and may amplify or counteract one other. For example, the injection of cold water causes a stress increase due to poroelasticity, a stress reduction due to direct pressure increase, and a stress reduction due to thermoelasticity. The processes are fully coupled (e.g. thermal shrinking of the rock reduces the pressure) and cannot simply be determined by linear superposition. In addition, inelastic deformation (e.g., plasticity) may occur that critically affects the local stress state (cf. section 2.3). It is challenging to separate the relative influence of pore pressure and temperature effects on seismicity.

In the Geysers geothermal field the relative effects of pressure and temperature changes on subsidence during the field's early extraction phase were evaluated (Mossop & Segall, 1997). The authors concluded that the amount of reservoir contraction resulting from the reservoir cooling of 5.3°C estimated for the field cannot explain the observed subsidence. A pressure drop of 2 MPa in the field could explain the subsidence. Temperature changes and thermoelastic stressing may have strong local effects, and lead to microseismicity. Thermal effects likely generated microseismic events near EGS wells in The Geysers field, whereas pressure effects reach further and may cause seismic events further away (Figure 2-7, (Martínez‐Garzón et al., 2014). Thermal effects may become more important with time (Ghassemi & Zhou, 2011). Thermal fracturing is sometimes used intentionally to enhance the geothermal reservoir injectivity (e.g. Rittershoffen) and generates microseismicity (Baujard, C. et al., 2017).
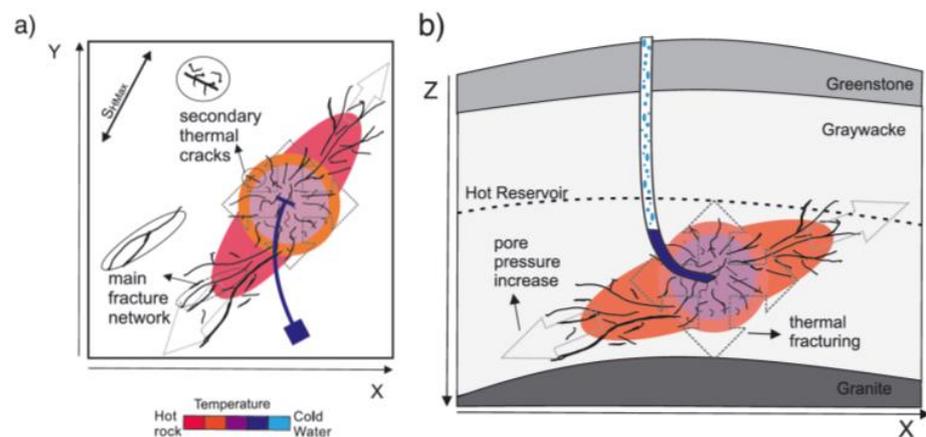
Figure 2-7   Schematic drawing of the extent of pressure and temperature changes around an EGS within the Geysers geothermal field (From Martínez-Garzón et al., 2014, Copyright American Geophysical Union, reproduced with permission).

Relevancy for other activities: Thermal effects are also expected during CO_2 injection, as CO_2 is injected at low temperatures (Goodarzi 2015). Also for gas injection in gas storage reservoirs cooling is expected, which may lead to stress changes on nearby faults (Orlic & Wassing, 2013). In both cases the effects are likely confined to the vicinity of the injection well.

2.6　Chemical alterations of fault and/or rock strength

Fluid injection may lead to water-weakening of fault or reservoir rock. Altering the pore fluid composition or adding gases or acids to the subsurface can cause chemical reactions between fluids and rock matrix or fault rock. For example, the mechanical properties of clay minerals may be altered, dissolution and precipation of quartz may change the rock strength, and feldspars may react if in contact with CO_2-rich fluids. These chemical reactions may promote seismic behavior by altering fault rock properties – i.e. lower the fault cohesion and/or friction (Figure 2-8). The effects of chemical reactions on fault cohesion and friction are determined by a complex interplay between rock composition, microstructure, and rock properties such as porosity.
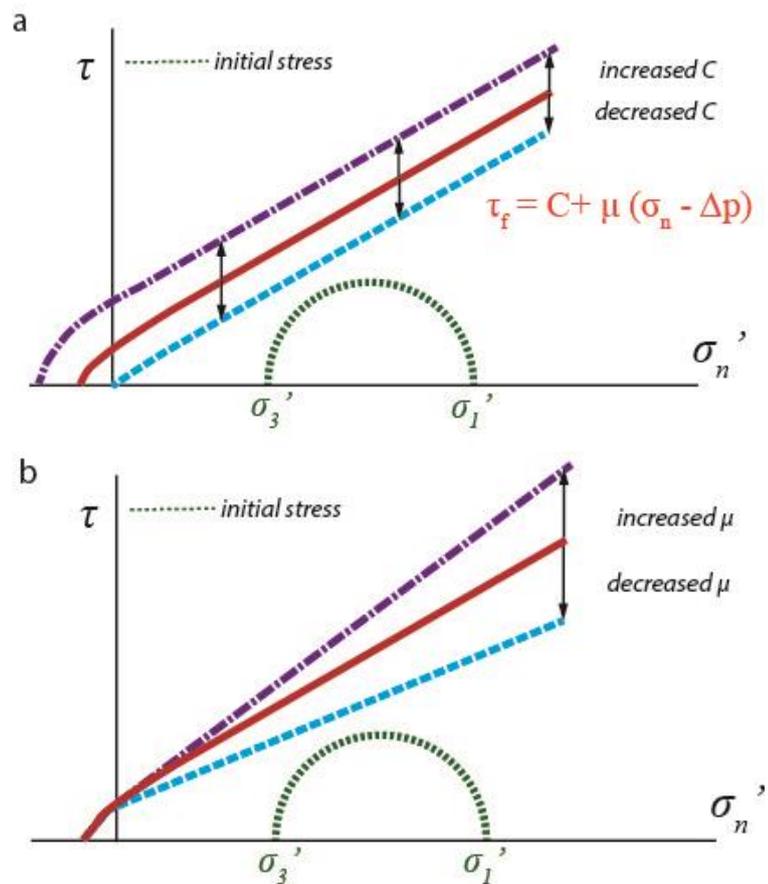
Figure 2-8　Mohr circles showing the effect of a) changes in fault cohesion and b) changes in fault friction which may be the result of chemical alteration, for example due to fluid injection or acid stimulation (Figure produced by TNO).

Relevancy for geothermal systems: Acid stimulations are often conducted to enhance the near-well injectivity. In Soultz some events were recorded during the chemical stimulation (Nami et al., 2008). The causal relationship between chemical effects, pore pressure changes, and temperature changes and the seismicity are however unclear and subject to ongoing research.

Relevancy for other activities: Stress-dependent corrosion reactions occur in silicate rocks in the presence of water and may weaken the rock (Suckale, 2009). Stress corrosion and water-weakening of the reservoir trapping faults is suggested as a potential mechanism for induced seismicity in the Fashing Field, Texas, US (Davis, Scott D. et al., 1995). Water-weakening of faults was also hypothesized as a potential cause of induced seismicity during water injection into the depleting gas field Weststellingerwerf Field, The Netherlands (Bois et al., 2013). It is challenging to pinpoint the causal effects as poroelastic stressing and pressure effects occur simultaneously. Dissolution of carbonate has been suggested as a mechanism for induced events in karstified limestone formations below impounded reservoirs (Chen & Talwani, 1998). For the Monticello reservoir a decrease in friction of clay-filled faults as a result of water was suggested as a contributory mechanism for seismic events (Talwani & Acree, 1984).

2.7 Static and dynamic triggering

Seismic or aseismic fault slip will reduce the average shear stress on the slipping fault itself, but redistribute the stress to the region around the fault. Some regions will become more critically stressed, and others less stressed. The stress change on a particular fault orientation is typically expressed as the Coulomb stress change

$$\Delta CFS = \Delta\tau - \ \Delta\sigma_n\mu \qquad\qquad 2\text{-}5$$

where $\Delta\tau$, $\Delta\sigma_n$ indicate the difference in shear and normal stress, respectively, and μ indicates the friction coefficient. A positive value of Coulomb stress change (ΔCFS) indicates that a fault orientation has become more critical, and a negative value indicates that a fault has become more stable. After one or more induced events have occurred, other seismic events can be triggered in the additional areas of positive Coulomb stress. The stress changes for static triggering are usually low.

Relevancy for geothermal systems: Static stress triggering can play a role for induced seismicity in geothermal systems, mainly for fluid injection into the basement that can induce numerous events. For example, the interaction between earthquakes (static stress transfer) around Basel likely contributed significantly to the evolution of the seismic cloud (Catalli et al., 2013). In Soultz-sous-Forêts a minor contribution from the Coulomb stress triggering mechanism to the total number of events was observed (Schoenball et al., 2012)

Relevancy for other activities: A positive correlation was found between areas of positive Coulomb stress (>0.05 MPa) and mining-induced events in the Rudna mine (Orlecka-Sikora, 2010). Static stress triggering may have promoted the M_w 5.7 seismic event that followed an M_w 5.0 event near the waste water injection wells in the Wilzetta oil field, Prague, Oklahoma (Sumy et al., 2014).

2.8 Drilling-induced seismicity

Pressure perturbations related to losses of drilling fluids can potentially reactivate critically stressed faults. Pressure perturbations due to drilling can potentially interact with existing perturbations in areas with multiple types of subsurface operations that are currently active at the same time or have been active in the past.

Relevancy for geothermal systems: The occurrence of seismicity during drilling activities for geothermal operations at sites like Hellisheidi in Iceland and during pumping of mud to regain well control at St Gallen, Switzerland indicate that pressure perturbations related to losses of drilling fluids during drilling for geothermal systems can potentially reactivate critically stressed faults. Julian et al. (2010) reported induced seismicity related to mud losses in the Coso geothermal field in eastern California in March 2005.

Relevancy for other activities: In the Netherlands, at least one case of drilling-induced seismicity has been reported. In 2009, a series of 41 small seismic events with magnitudes up to M 1.4 was recorded near Midlaren by the seismic monitoring network of KNMI over a period of one month (Dost et al., 2012). Based on its spatial and temporal correlation with mud losses during drilling activities nearby, this swarm of small seismic events has been related to the loss of drilling fluids approximately 5 km away from the epicenter locations, and is generally characterized as 'drilling-induced seismicity'. For two other sites, the relation between mud-losses during drilling operations and recorded seismicity has been investigated but not demonstrated (Anna-Paulowna and Castricum aan Zee). On June 23rd, 2015, two seismic events of magnitude M_L 1.5 and M_L 2.3 were recorded by the national seismic monitoring network of KNMI, in vicinity of the town of Anna Paulowna, Noord-Holland. The seismic events have been localized within a distance of approximately 5 km of the producing Slootdorp gas field. In the month preceding the earthquakes, multiple mud losses were reported during drilling of production well in the Slootdorp gas field, but it is unknown whether the mud losses are the source of these earthquakes. In the period from October 22nd to end November 2013, 6 earthquakes with magnitudes M_L 1.4 to M_L 2.5 were recorded by the national seismic monitoring network of KNMI, in close vicinity of the Castricum-Zee gas field, Noord-Holland. In the 5 to 3 months preceding the earthquakes, mud losses have been reported during drilling of a production well near Heemskerk, some 6 km's to the south-east of the earthquake locations but again it is unknown if the mud losses are the source of these earthquakes. Considering the spatial and temporal correlation between the mud losses during drilling and the seismic events, the question has been raised whether the seismic events could potentially be 'drilling-induced'[6]. Due to the large uncertainties in the locations of the seismic events related to the sparse seismic monitoring network, the limited availability of subsurface data, and the vicinity of the hypocenters to gas fields with a history of production (and associated stress changes), no unequivocal causal relation between the drilling activities and seismicity has been established.

---

[6]More information can be found in TNO reports TNO 2016 R11209 and TNO 2016 R11210 (www.sodm.nl).

2.9   Stress concentrations due to the local geometry and geology

As mentioned, the presence of optimally oriented pre-existing faults plays a major role in the occurrence of large magnitude induced seismic events. However, there are other geometrical and geological aspects that can affect the stress changes and fault reactivation potential. All of the stress changes described in the previous sections can be enhanced by specific reservoir geometry or local geology. For depleting gas fields differential compaction along offset faults can for example strongly concentrate the poroelastic stresses and promote fault reactivation (Mulders, 2003; Orlic & Wassing, 2013; Pennington et al., 1986; Wassing et al., 2017). Also differential subsidence between mined and unmined regions may concentrate the stress in overburden formations (Hasegawa et al., 1989). Stresses may also concentrate in competent rock formations and lead to the failure of these formations. Mining-induced events focused e.g. in quartzite near a gold mine in South Africa (McGarr, 1975), or in more competent sandstone layers near a coal mine in Germany (Fritschen, 2010).

2.10 Other mechanisms leading to induced seismicity

Loading or unloading by the addition or removal of fluid or rock mass near the Earth's surface and mining-induced stresses related to excavation of rock may induce seismic events. As these mechanisms have not been associated with geothermal operations or have limited relevance for geothermal operations, they are described in Appendix B, together with case studies of other types of subsurface operations that may lead to induced seismicity.

2.11 Summary of mechanisms relevant for geothermal systems

The review in this section shows there are several mechanisms that can cause fault reactivation and induced seismicity. In many cases these mechanisms operate simultaneously. For geothermal systems, pore pressure changes in faults (direct pressure effects), poroelastic stressing, and thermoelastic stressing are the most important. Pore pressure changes and poroelastic stressing have an immediate effect on faults and fractures close to the wellbore, as evidenced by seismicity starting within hours of an injection. The effect of pore pressure changes are most important if reservoir stimulation by fluid injection (hydraulic fracturing) is performed. It is less important, but still relevant if doublet operations are restricted to fluid circulation. Diffusion of pore pressure may result in fault reactivation more than a kilometer from the injection well, and cause fault reactivation after injection has ceased. For reservoir stimulation by fluid injection (hydraulic fracturing), increase in pore pressure may result in tensile (mode I), shear (mode II) or mixed mode fracturing, depending on the distribution of pore pressure and stress changes as well as geological factors such as rock properties or structures. Thermoelastic stresses develop more slowly, and remain more confined to the injection well. The magnitude of thermoelastic stress can however be significant, and may even lead to thermal fracturing. Coupled pressure- and temperature-dependent processes lead to induced seismicity, i.e. the combination of direct pressure effects, poroelastic stressing and thermoelastic stressing determine stress changes and thereby induced seismicity. For example, combined hydraulic and thermal fracturing may lead to a growing fracture that ultimately creates a pathway for fluids to larger natural faults causing felt seismicity. In most cases where felt seismicity was recorded the stress required for fault failure

and seismicity appears to be low (< 1 MPa) emphasizing the role of pre-existing critically stressed faults (Keranen et al., 2013; Candela et al., 2018).

In the Netherlands, a lot of emphasis is on induced seismicity associated with gas production from the Groningen gas field (cf. appendix B.3). In this case, the inferred mechanisms leading to a long history (~30 years) of induced seismicity including multiple felt events are poroelastic stressing and differential compaction of reservoir compartments juxtaposed along faults with offset. Although poroelastic stressing also plays a role in geothermal systems, the combination of depletion of large volume of gas, progressive differential compaction and poroelastic stressing is not comparable to geothermal systems. In particular, conventional geothermal systems in the Netherlands are based on fluid circulation and an (approximate) overall balance of fluid volume in the reservoir (cf. section 6). Accordingly, reservoir compaction is not significant in these conventional geothermal systems. The driving mechanisms of induced seismicity differ between gas production and geothermal systems, and thereby characteristics of induced seismicity (e.g., spatiotemporal distribution, number, frequency and magnitudes) will be different.

3 Synthesis of case study review

In the previous section it was described how pressure, temperature changes and volume changes can induce seismic events in geothermal systems and in other subsurface resources. The role of critically stressed faults was also evident from the described examples. To determine additional factors influencing the (lack of) occurrence of felt induced events, a case study review was performed. This review focused on geothermal systems, including those associated with felt seismicity, but also those for which no or only very small induced events were observed. Cases were included according to the following criteria:

1) Well-known examples where felt induced seismicity was observed in a geothermal system. These include for example Basel and Pohang.
2) Geothermal systems in tectonic and geological settings comparable to The Netherlands, including a number of cases in The Netherlands. These include geothermal systems with and without associated induced seismicity.
3) Geothermal systems used predominantly for electricity and district/building heating.

For each case study the tectonic setting and local geology, wellbore design, operational parameters, occurrence (or lack of) induced events, and interpretations are described (Appendix A). A total of 40 cases were included; most of these are in northwest Europe, but there are also a number in the USA, Asia, and Oceania (Figure 3-1).

Figure 3-1   Locations of geothermal case studies considered in the review (Map produced by TNO).

In addition, other well-known examples where felt induced seismicity was observed for subsurface operations other than used in geothermal systems are briefly described (Appendix B). These non-geothermal cases are often referred to in literature or news articles. Examples include hydraulic fracturing for hydrocarbon production and waste water injection, conventional hydrocarbon production, and

secondary recovery where direct pressure and poroelastic mechanisms also play a role, as well as reservoir impoundment and mining that are included for reference to differences in seismic magnitudes associated with anthropogenic operations.

Here, the general findings of the case study review are summarized. For each geothermal play the regional geology, geothermal systems, operational activities and the occurrence of induced seismicity are described (section 3.1). In section 3.2, the key parameters related to the occurrence of induced seismicity in geothermal systems are listed. These are also placed in the broader perspective of induced seismicity in non-geothermal activities.

3.1 Summary of case studies

The geothermal case studies are grouped according to their specific geothermal region or sedimentary basin. Within a geothermal play, the tectonic setting and the geology are largely similar. This similarity allows for a concise summary of the geothermal systems within one region as well as for a straightforward comparison to geothermal plays in the Netherlands (section 6). The geothermal plays are characterized according to the classification given in Moeck (2014), which is based on the geological controls on the thermal regime, heat flow and hydrogeology. A distinction is made between convection-dominated systems and conduction-dominated systems. Conduction and convection refer to heat transfer mechanisms in a structural geological context, not during geothermal operations. Convection-dominated systems are high enthalpy regions where active plate tectonic processes or active magmatism or volcanism occur, and include:

- Volcanic Field Type (VFT) plays, which are found near magmatic arcs, mid-oceanic ridges, and other active volcanic areas,
- Plutonic Type (PT) plays, which are related to young orogens and post-orogenic collapse, and
- Extensional Domain Type (EDT) plays, which are situated in metamorphic core complexes, back-arc extension, pull-apart basins and intracontinental rifts.

Fluid flow and convective heat flow in these regions is dominated by fractures and faults. These active tectonic regions usually also have a relatively high natural seismicity rate.

Conduction-dominated systems on the other hand are found in passive plate-tectonic regions. Thermal gradients are near-normal and governed mainly by conduction. Conduction-dominated plays include:

- Intracratonic Basin Type (IBT) plays, which are inactive intracratonic rift basins or passive margin basins,
- Orogenic Belt Type (OBT) plays, which are situated in fold-and-thrust belts and foreland basins, and
- Basement Type (BT) plays, which are related to intrusions or heat-producing element regions.

The IBT and OBT plays include permeable sedimentary aquifers where fluid flow is governed mainly by matrix permeability and/or fault zones, whereas BT systems are typically in fractured low permeability rock (e.g., granite). Natural seismicity in these regions is usually much lower than in the convection-dominated systems.
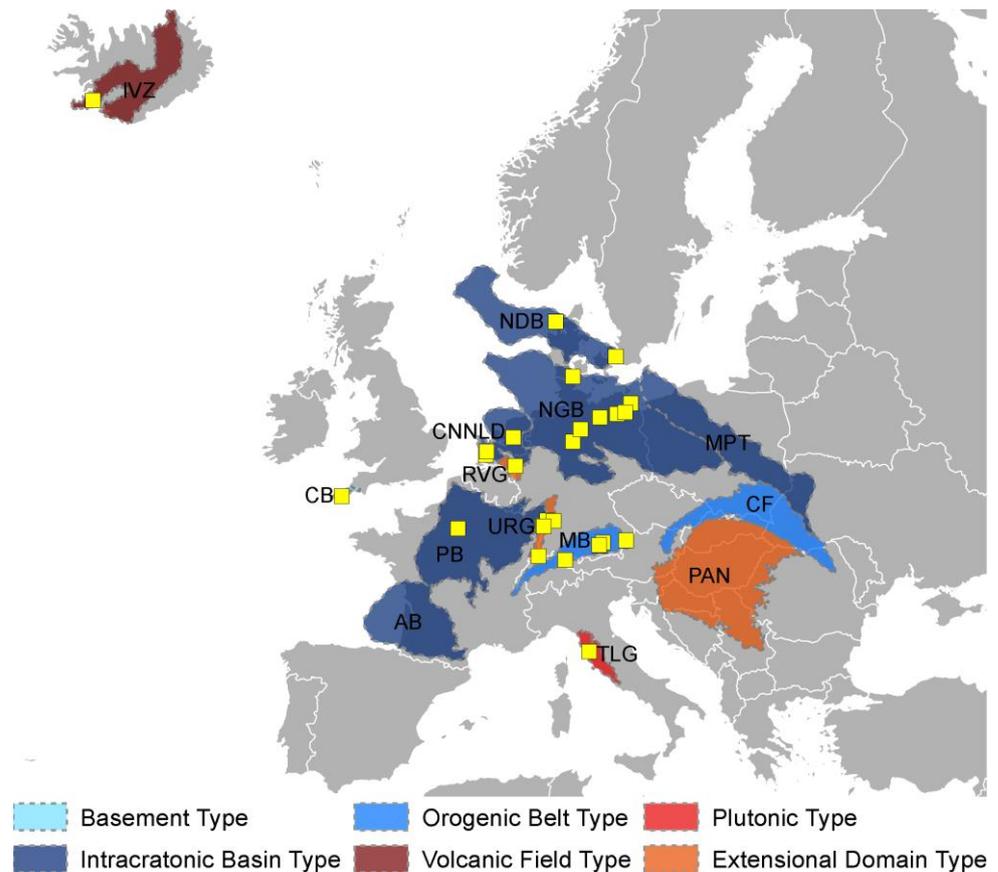
Figure 3-2   Main geothermal areas in Europe with selected sites considered in the case study review..The areas are colored according the geothermal play types defined by Moeck (2014). Case studies included in the review were located in AB: Acquitane Basin, CB: Cornubian Batholith, CF: Carpathian Mountains and Foreland, CNNNLD: central and north Netherlands, IVZ: Icelandic Volcanic Zones, MB: Molasse basin, MPT: Mid-Polish Trough, NDB: Norwegian – Danish Basin, NGB: North German Basin, PAN: Pannonian Basin, PB: Paris Basin, RVG: Roer Valley Graben, TLG: Tuscan-Lazio Geothermal region, URG: Upper Rhine Graben (Map produced by TNO).

In Europe the cases studies considered in the review belong to five different geothermal plays (Figure 3-2). Basement type plays (Cooper Basin,) are not distinguished for the European plays, i.e. the plays are better characterized by the five plays shown in Figure 3-2. In another review of induced seismicity associated with geothermal operations igneous/metamorphic reservoirs were distinguished from sedimentary reservoirs (Evans et al., 2012).

In addition, three system types are defined:
- geothermal field or hydrothermal system (HS): porous or permeable geothermal reservoir in convection-dominated settings
- EGS or petrothermal systems (EGS): impermeable geothermal targets which require stimulation before flow can be achieved between wells. These can be both in conduction-dominated (tectonically quiet) or convection-dominated (tectonically active) settings.
- Hot sedimentary aquifers (HSA): porous or permeable sedimentary formations in conduction-dominated settings

Basin/geothermal area	Type[1]	PGA[2] (ms^{-2})	T (ºC)	Rock type	Depth (km)	Fluid flow[3]	Stimulation[4]	System type[5]	# of sites	sites with M > 2.0 (M_{max})
North German Basin	IBT	0.22	45 – 170	sandstone	2 – 4	POR FRA	CIR, CS some HF	HSA	7	none reported
Upper Rhine Graben	EDT	0.85	130 - 200	granite sandstone	2 – 5	FRA	CIR,HS, CS	EGS, HS	6	5 (M_L 3.4)
Molasse Basin	OBT	0.72	80 – 150	carbonate	2 – 4.3	FRA	CIR some CS	HSA	27	3 (M_L 3.5)
Paris Basin	IBT	0.48	50 – 90	carbonate	1.5 – 2.5	FRA	CIR, some CS	HSA	35	none reported
Norwegian Danish Basin	IBT	0.24	40 – 80	sandstone	1 – 3	POR	CIR	HSA	2	none reported
Cooper Basin	BT		240 – 280	granite	4 – 5	FRA	HS	EGS	3	2 (M_L 3.7)
Great Basin	EDT	1.9	100 – 300	carbonates andesite	1 – 3.5	FRA	CIR, HS	HS, EGS	>25	2 (M 4.4)
Geysers	PT	7.5	250 – 400	metamorphic various	< 2.5	FRA	none, HS	HS, EGS	1	1 (M 5.0)
Tuscan-Lazio	PT	1.5	200 – 300	carbonates	< 3.5	FRA	CIR, some HS	HS	5	3 (M 4.5)
West Netherlands Basin	IBT	0.3	60 – 90	sandstones	1.5 – 2.7	POR	CIR	HSA	10	none reported
Iceland Volcanic Zones	VFT	5.1	150 - 450	volcanic	1 - 2	POR/FRA	CIR, some HS	HS	>25	5 (M 4.0)
Salton Sea	EDT	6.9	250 – 370	sandstones, various	1 – 2.5	FRA/POR	some HS	HS	1	1 (M_w 5.1)
Taupo Volcanic Zone	VFT	4.3	250 – 350	volcanics	1 – 3	POR/FRA	CIR	HS	19	4 (M_L 3.5)
Pohang Basin	EDT	0.3	140	granodiorite	4.2	FRA	CIR	EGS	1	1 (M_w 5.5)

Table 3-1   Summary of geothermal plays considered in the case study review. 1: Type of geothermal play according to Moeck (2014) with IBT = Intracontinental Basin, OBT = Orogenic Belt Type, BT = Basement Type, VFT = Volcanic Field Type, PT = Plutonic Type, and EDT = Extensional Domain Type. 2: PGA taken from GSHAP seismic hazard map in ms^{-2} with a 10% chance of exceedance in 50 years (Giardini et al., 1999). The PGA value was averaged over the basin area , 3: POR = matrix-dominated flow, FRA = fracture-dominated flow, 4: CIR = circulation (no stimulation), CS = chemical stimulation, HS = hydraulic stimulation. 5: System types: HS: hydrothermal systems or geothermal fields (porous permeable reservoirs in tectonically active regions), HSA: hot sedimentary aquifers (porous/permeable aquifers in tectonically quiet regions), and EGS (or petrothermal systems): target formations that need to be stimulated before flow can be achieved. M > 2 is chosen as a threshold for felt seismicity (cf. section 1.3) (Table produced by TNO).

The current classification is based on thermal regime, heat flow and hydrogeology rather than rock type. Three of the geothermal plays in Europe are intracratonic plays; the North German Basin, the Norwegian-Danish Basin, and the Paris Basin. These basins are tectonically inactive, and have relatively low temperature gradients. The Molasse Basin is an orogenic belt type play situated in the foreland of the Alps. The Upper Rhine graben is an active rift system and falls under the Extensional Domain type plays. Two high enthalpy areas are also considered; the Icelandic volcanic zones, and the Tuscan-Latium geothermal region. Geothermal plays in the Netherlands are mainly of intracratonic basin type in regions that are not tectonically active, apart from the Roer Valley Graben.

In addition to European plays, several geothermal plays in the USA, New Zealand, Cooper Basin, and Pohang in South Korea were considered in the review (Figure 3-1). The review of (Evans, K. F. et al., 2012) includes some additional geothermal projects and areas in Europe, also covering areas in Poland and Lithuania.
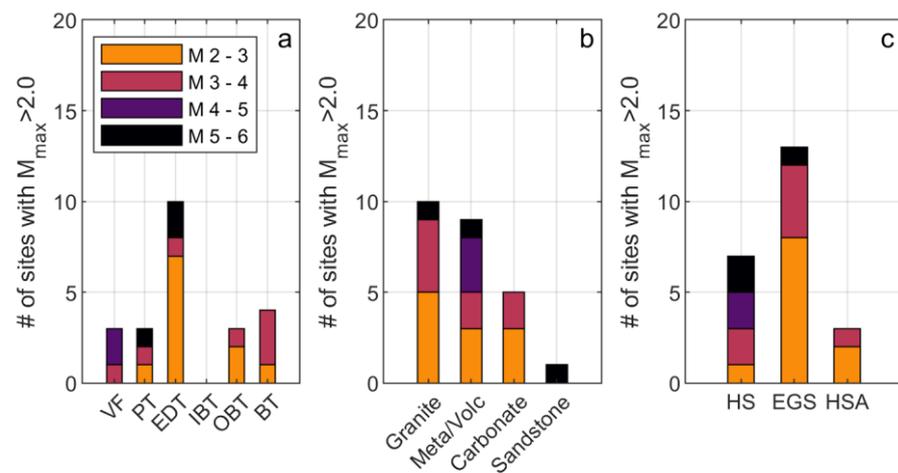
Figure 3-3   Occurrence of felt seismicity for various play types (a), rock types (b), and system types (c). VF: volcanic field type, PT: plutonic type, EDT: extensional domain type, IBT: intracratonic basin type, OBR: orogenic belt type, BT: basement type. System type HS; geothermal field (hydrothermal system), EGS (Enhanced Geothermal System), HSA: hot sedimentary aquifers (Figure produced by TNO).

Most induced events were observed in convection-dominated plays, and geothermal field or EGS systems (Figure 3-3). This is reflected in the rock types related to induced seismicity, which are typically granitic, metamorphic, or volcanic targets. Hot sedimentary aquifers (HSA) on the other hand generated less events, and of smaller magnitude (maximum magnitude was 3.5 at Sankt Gallen).

In the following section, the main observations by geothermal play are summarized (see also Table 3-1 for an overview).

3.1.1   North German Basin (Germany, Denmark)

The North German Basin is a Permian rift basin (intracratonic basin type) covering the north of Germany (Figure 3-4, appendix A.3). It is filled with several kilometers of Mesozoic and Cenozoic sediments. The main geothermal target formations are sandstone aquifers from the Lower Jurassic Lias, the Upper Triassic Keuper

(including the Rhaetian formation). These are low-enthalpy geothermal targets, with geothermal systems at depths of 1 – 2.5 km and temperatures of 45 – 100 °C. The heat is used mainly for district heating. The porosity and permeability of the Jurassic sandstones and the Keuper sandstones can be very high in particular in the northeastern parts of the basin, as in Neustadt-Glewe where a porosity of 25% was measured at 2.5 km depth (appendix A.3.5). No stimulation techniques (apart from an incidental acid stimulation to clean the well) are required, and high flow rates can be obtained at low injection pressures.

The deeper lower Triassic Middle Bundsandstein was targeted by two geothermal research projects in the west of the basin, at a depth of 4.1 km and a temperature of 150 – 170 °C. Reservoir stimulation was required in order to increase permeability. Hydraulic fracturing was conducted in the two wells (see appendix A.3.2, A.3.3).

The older Permian Rotliegend sediments and volcanics are also a potential geothermal target, and geothermal operations have been conducted for research purposes. The Permian rocks are tight and require hydraulic fracturing to increase the permeability, which was tested in the Gross Schönebeck research well (appendix A.3.1).

Induced seismicity: No felt seismicity has been observed in the 6 investigated geothermal case studies, even though sensitive monitoring systems were in place during the hydraulic fracturing experiments. For example, at the Horstberg and Hannover geothermal sites, microseismic monitoring was performed using borehole and surface seismic sensors which can detect down to M -0.5. Stimulation at the Gross Schönebeck research site was also monitored using borehole seismometers. At the other sites no monitoring was in place, but no events were reported by the public.
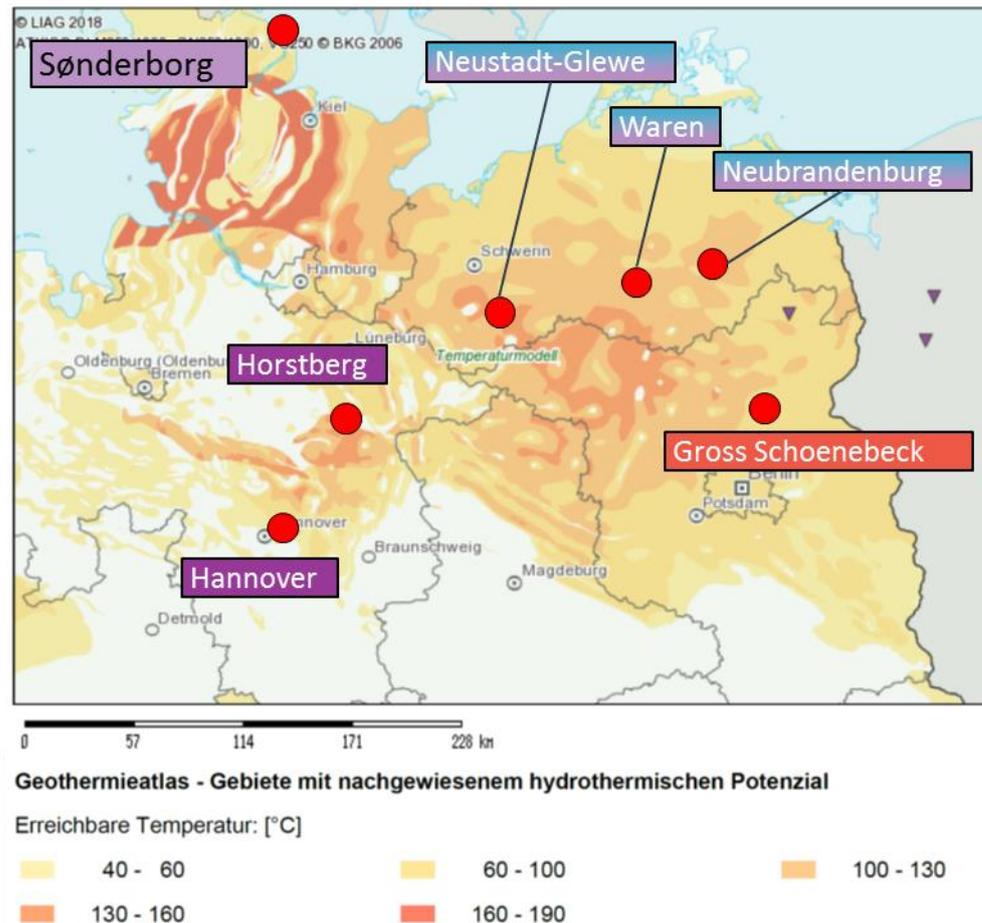
Figure 3-4   North German Basin and geothermal sites incorporated in the case study review (Appendix A.3). Map source: www.geotis.de.

3.1.2   Upper Rhine Graben (Germany, France, Switzerland)

The Upper Rhine Graben is a 300 km long active rift system on the border of France and Germany (Figure 3-5, appendix A.1). It trends NNE-SSW, from Basel in the south to Frankfurt in the north. The graben is seismically active, with frequent small events and occasional moderate sized events. High temperature gradients exist in the area. A number of medium to high enthalpy geothermal power plants have been installed in the graben. These plants target the fractured granitic basement at 3.5 – 5 km deep with temperature of 160 - 200 °C (e.g. Soultz-sous-Forêts, Basel), and/or the fractured Triassic-Carboniferous sediments overlying the basement at depth of 2.5 – 3.5 km deep with temperatures of 100 – 150 °C (e.g., Bruchsal, appendix A.1.2). Because of the low permeability of these rocks, stimulation of the pre-existing fracture network is often required. This is typically achieved through the injection of 1,000 – 100,000 m^3 of water.

Induced seismicity: Seismicity was monitored in most geothermal systems. At a number of sites (5 out of 8 investigated case studies) felt events were induced, with the largest event in Basel (M 3.4). At other locations earthquake magnitudes were smaller, but still felt by the local population with M_L 2.9 in Soultz-sous-Forêts, M_L 2.7 in Landau, and M_L 2.4 in Insheim. At Rittershoffen, close to Soultz-sous-Forêts, lower magnitude events up to M_L 1.6 were induced, indicating how seismicity can be site specific.
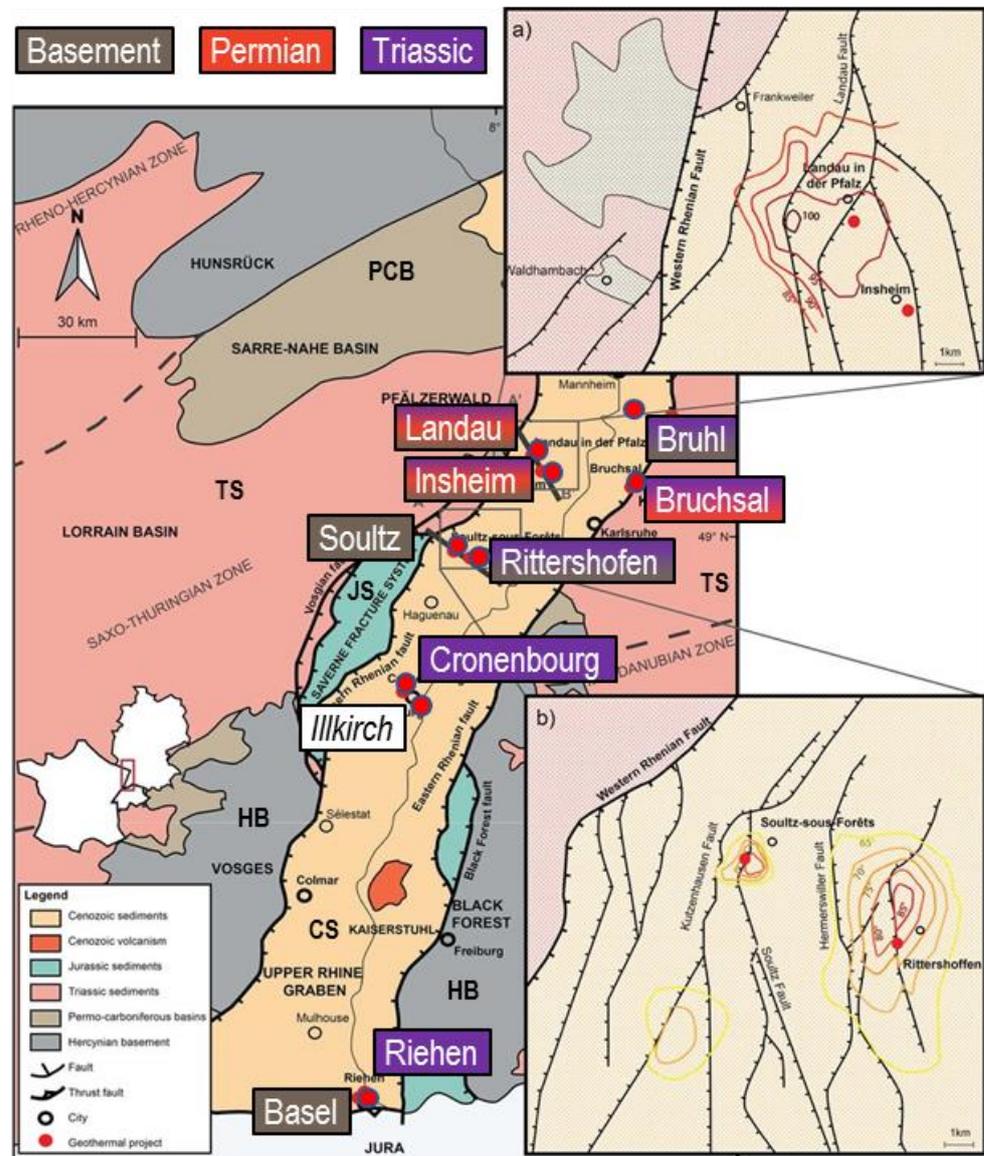
Figure 3-5 Upper Rhine Graben and geothermal plants. Illkirch is not yet operational. Modified from Vidal et al. (2018), Copyright Elsevier, published under a Creative Commons License.

3.1.3   Molasse Basin (Germany, Austria, Switzerland)

The Molasse Basin is a foreland basin north of the Alps, stretching from Switzerland in the west to Austria in the east (Figure 3-6, appendix A.2). The Variscan basement (made of gneisses and granites) and overlying Mesozoic sediments were flexed by the Alpine orogeny, creating a marine foredeep. The marine foredeep was filled with younger molasse sediments which increase in thickness towards the Alps in the south, exceeding 4 km at the southern margin. The geothermal target formation in the Molasse Basin is the karstified Upper Jurassic Malm limestones. Near München the Malm lies at a depth of 3 km, and has a thickness of over 600 m, with temperatures of 85 – 130 °C. Here the Malm directly overlies the Variscan basement. Further to the west Middle Jurassic and Triassic sediments are found below the Malm and above the basement, and local Permo-Carboniferous grabens filled with

siliciclastic sediments are present in the basement – e.g. at Sankt Gallen (appendix A.2.4). The karstified Malm has a high permeability, and therefore hydraulic stimulation is not required. Fluids are typically circulated between two wells at low injection pressures (< 2 MPa). Faults are sometimes targeted with a well doublet because of their high permeability – e.g. at Unterhaching (appendix A.2.5).
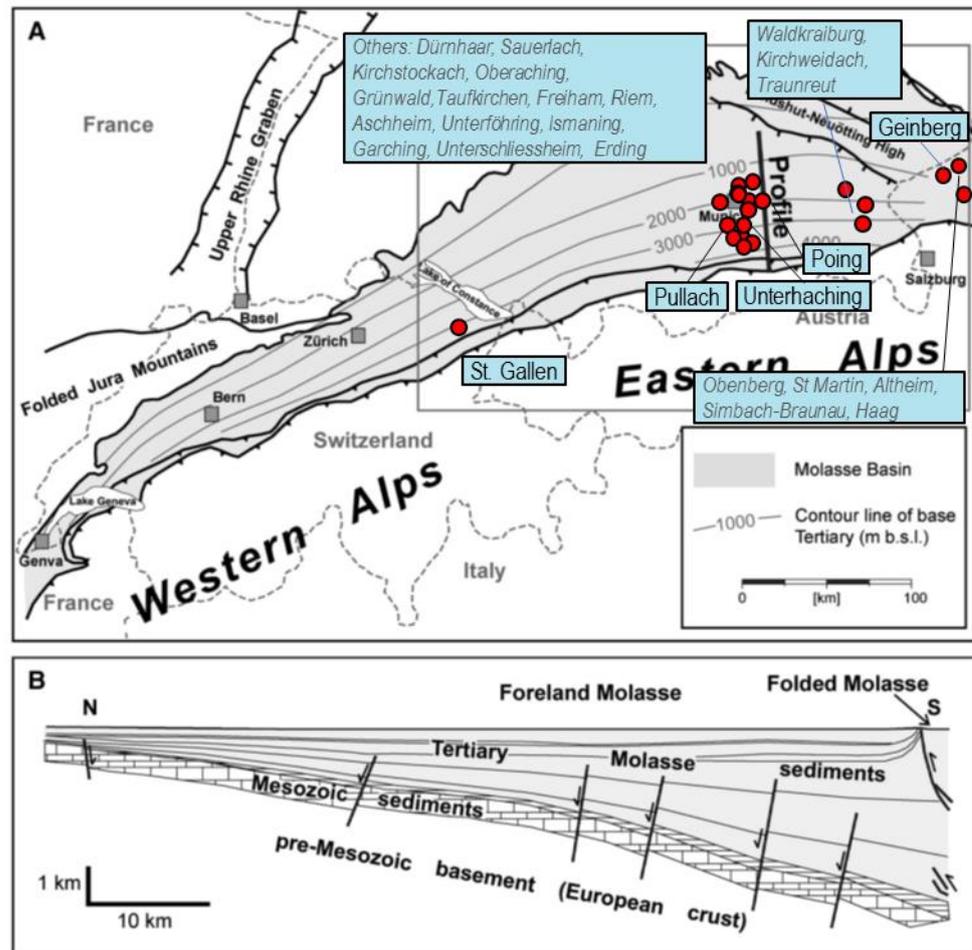
Figure 3-6   Molasse Basin and geothermal systems. a) Top view of the MolasseBasin and the depth of the Tertiary molasse sediments. Active geothermal systems are indicated by red circles (see geotis.de), with the systems that are described in the Appendix in black, and other systems in italic gray text. b) north-south cross-section of the Molasse basin east of Munich, showing the Mesozoic carbonate sediments. The Mesozoic sediments are largely constituted of the Malm carbonates which are the target formation for geothermal exploration (From Reinecker et al., 2010, Copyright Elsevier, reproduced with permission).

Induced Seismicity: No events have been reported for 24 geothermal systems. 3 out of 27 investigated geothermal sites in the Molasse Basin are associated with felt induced events. The most well-known example is Sankt Gallen in Switzerland, where a M_L 3.5 was recorded (appendix A.2.4). The event occurred during well control operations to suppress the inflow of gas into the well. Other felt events of M_L 2.4 and M_L 2.1 were recorded in Unterhaching (appendix A.2.5) and Poing (appendix A.2.2), two geothermal doublets near Munich. Both these events occurred during circulation between the two wells. In Unterhaching felt seismicity was observed within a few

months of the start of circulation and is interpreted to be due to re-injection of cold water that caused repeated rupture of part of a NE-SW trending fault that is favorably oriented for reactivation (Megies & Wassermann, 2014). In Poing the first felt events were recorded after 5 years of circulation, and likely due to reactivation of critically stressed faults near the wells as pore pressure and thermally-induced stress changes were likely very small.

3.1.4   Paris Basin

The Paris Basin is a Permo-Triassic sedimentary basin which covers the northern part of France (Figure 3-7, appendix A.4). The total sediment thickness is up to 3 km in the centre. The basin is tectonically inactive, and natural seismicity levels are very low. The prime geothermal target in the Paris Basin are the Middle Jurassic Dogger carbonate rocks. The Dogger is found at 1.5 – 2 km depth, with temperatures between 55 and 85 °C. The most productive layers in the Dogger strata are permeable Bathonian oolitic reef deposits and Comblanchian shelf sediments with a net thickness of 15 - 25 m, which is 10% of the total thickness of the Dogger. The average porosity of the production layers is 15% and the permeability is 1-10 Darcy. The fluid flow is generally matrix controlled, although in some units fracturing and dissolution has increased the porosity and fluid flow may therefore locally be fracture-controlled. The Dogger is underlain by Lower Jurassic shales, Triassic sands and shales, which are underlain by the granitic basement. Between 1970 and 1985 more than 100 geothermal wells were drilled in the Paris Basin, mainly used for district heating. Of the 55 doublets 34 are still operational, without any thermal decline (Lopez et al., 2010). Because of the high permeability hydraulic stimulation is not necessary and circulation can occur at low injection pressures (< 1 MPa). However, chemical stimulation is sometimes used to improve the injectivity, circulating several 1000's m^3 water and acid between the two wells at pressures up to 2.5 MPa (Ungemach et al., 2005).
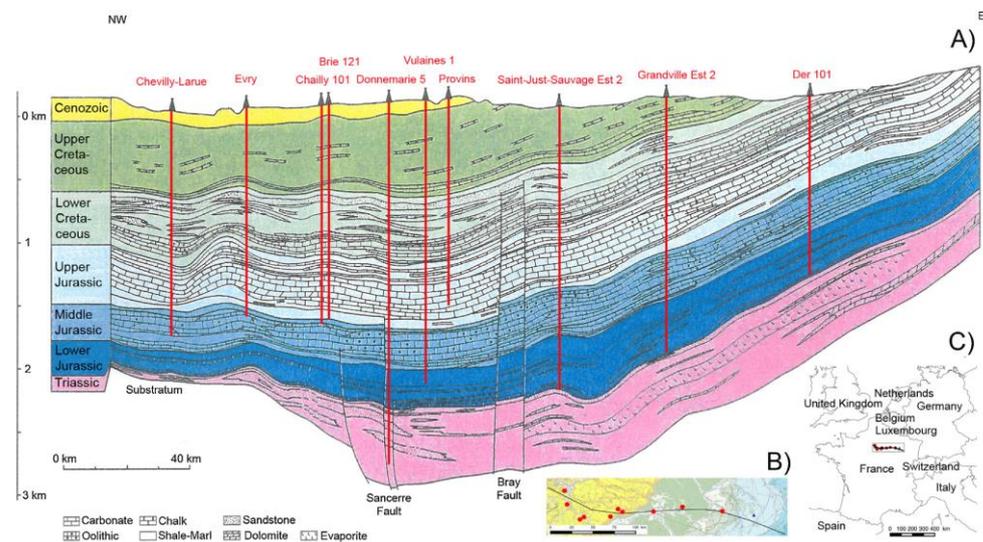
Figure 3-7 Stratigraphic cross-section of the Paris Basin from west to east (From Dentzer et al., 2016, Copyright Elsevier, reproduced with permission).

Induced seismicity: No (felt) induced events have been reported for any of the doublets in the Paris Basin (this study indicated 35 operational systems). No site-specific monitoring is in place.

3.1.5   Norwegian-Danish Basin

The Norwegian Danish Basin (Figure 3-8, appendix A.5) formed in the Permo-Carboniferous, and is an intracratonic basin similar to the North German Basin. The thickness of the sedimentary cover ranges from 1 – 2 km in the south to 9 km in the north of the basin. The main geothermal targets are the Upper Triassic Gassum (Rhaetian in Germany) and the Lower Triassic Bundsandstein. The Gassum is found in the middle and north of Denmark at depths up to 3 km (Figure 3-8), and the Bundsandstein is predominantly found in the south and middle of Denmark. Two geothermal plants are operative; Thisted (1984) and Margretheholm (2005) near Copenhagen (appendix A.5.1, A.5.2). Thisted targets the Gassum sandstone at 1.2 km depth, which has a porosity of 26%. The Margretheholm plant targets the Bundsandstein at 2.5 km depth, which is directly overlying the granitic basement. Reservoir temperatures are 45 °C and 73 °C respectively.

Induced seismicity: No (felt) induced events have been reported for the 2 investigated case studies of geothermal plants. No site-specific monitoring is in place.
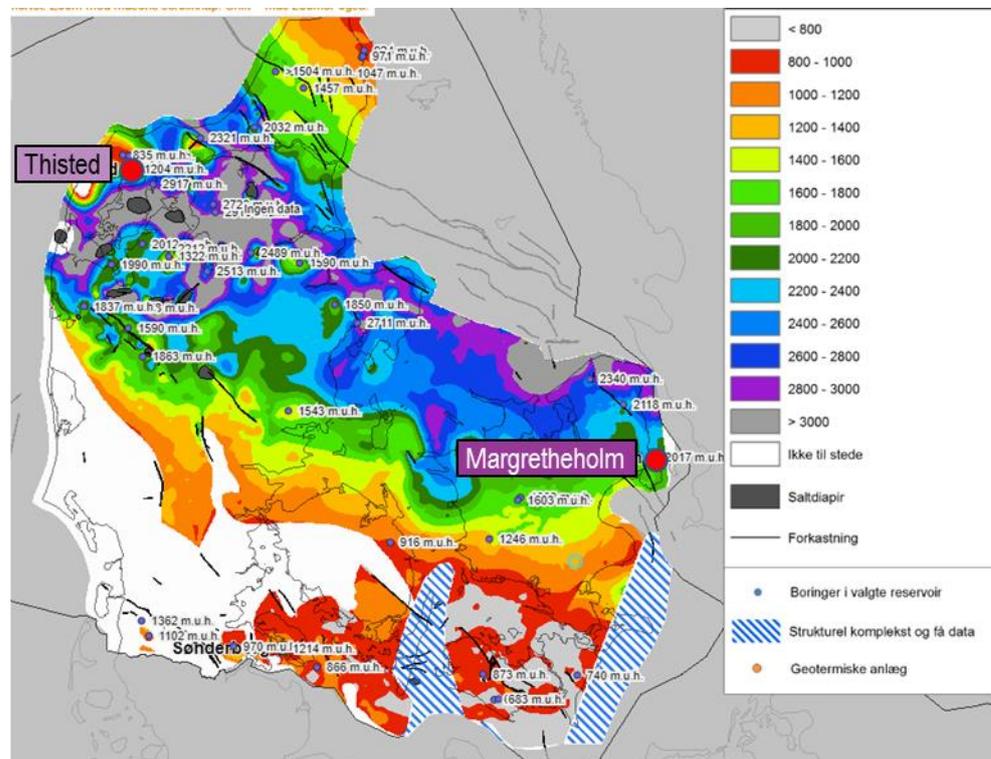
Figure 3-8   Norwegian-Danish Basin and the top depth of the Bundsandstein. The two geothermal plants Thisted and Margretheholm are shown. Colors indicate the depth of the Bundsandstein. Map from http://data.geus.dk.

3.1.6   Other geothermal systems in crystalline rocks

Other relevant examples of geothermal systems in the world (mainly HDR or EGS, cf. section 1.2) that target crystalline basement rocks include the Cooper Basin (appendix A.9), Rosemanowes (appendix A.6), and Pohang (appendix A.7) sites. These lie at depths between 3 and 5 km with temperatures of 250, 95, and 140 °C, respectively. All were stimulated to enhance the permeability.

Induced seismicity: Thousands of events were recorded by the local monitoring systems at the three sites. The largest magnitude of M 5.4 was recorded at Pohang, making this the largest event associated with geothermal operations thus far. In Habanero in the Cooper Basin (appendix A.9) magnitudes ranged up to 3.7, but in Rosemanowes the largest event had a magnitude of 1.9 (appendix A.6).

3.1.7   Convection dominated geothermal fields

Several convection-dominated systems were evaluated in the case study review, including volcanic fields in Iceland, USA, New Zealand and Italy. These fields are high-enthalpy systems in sedimentary or volcanic rocks with temperatures up to 350 °C. Fluid flow is mostly dominated by the fractures. These geothermal regions are often characterized by high natural seismic activity and high tectonic loading rates. Steam, water or a mixture of both are produced from these fields. Since the 1960's cooled water is reinjected into the geothermal fields to maintain the reservoir pressures. Occasionally wells are stimulated like in an EGS.

Induced seismicity: Many of the convection-dominated geothermal systems show seismicity, but not always of large magnitude. The largest magnitudes included in the case study review is a M 5.1 near Salton Sea, U.S.A (Appendix A.13), and a M_w 5.0 in The Geysers (Appendix A.12). It has been suggested that fluid extraction in the Cerro Prieto Geothermal Field in Mexico contributed to triggering even larger magnitude earthquakes in the region, but evidence on distinguishing between natural and triggered events is not conclusive (Glowacka & Nava, 1996; Trugman et al., 2016). The largest magnitude recorded in Iceland is a M 4.0 in the Hellisheidi field (Appendix A.8); other fields in Iceland have not generated seismicity exceeding M 3.0. In the Taupo geothermal area (New Zealand) there are many geothermal fields, e.g. Rotokawa (Appendix A.15), but induced seismic magnitudes have not exceeded M 3.2. Also in the Great Basin, USA, magnitudes have remained low e.g. Desert Peak (A.14).

Many of the geothermal fields are in tectonically active regions. In such situations it may be challenging or even impossible to distinguish induced seismicity from natural seismicity. For some fields there is a very clear correlation between operational parameters and seismicity (e.g. The Geysers, Rotokawa), whereas for others (e.g. Salton Sea) the correlation is not as strong and it is difficult to identify how events are related to the geothermal field.

3.2 Key parameters affecting felt induced seismicity in geothermal systems

The geothermal plays discussed in the previous section showed a difference in potential for induced seismicity associated with geothermal systems. Felt seismicity was frequently observed in some of the plays, such as in the Upper Rhine Graben, and in some of the high-enthalpy volcanic fields (Table 3-1). Occasional felt events were recorded in the Molasse Basin, whereas for the North German Basin, Paris Basin and West Netherlands Basin no felt seismicity was reported. Seismicity is linked to the local geology and hydrogeology of the geothermal plays, and to the operational procedures required to exploit the geothermal potential. Each play is related to specific rock formations that are targeted for geothermal exploration (e.g., granites, sandstones, carbonates). These rock formations may lie at different depths and have different in-situ temperature. Granites for example are usually found at greater depth and are warmer, which makes them suitable for the production of electricity. Porous sandstones are usually found at shallower depth and are cooler, hence they are mainly used for district or space heating. The rock types exhibit certain

porosities and permeabilities, which generally decreases with depth. The hydrogeology determines whether stimulations are required; for example tight fractured granites or cemented sandstones need to be stimulated before productive flow can be established between the wells. In this section we summarize the relationship between geological and operational factors and the occurrence and maximum reported magnitudes of seismicity in the different geothermal plays.
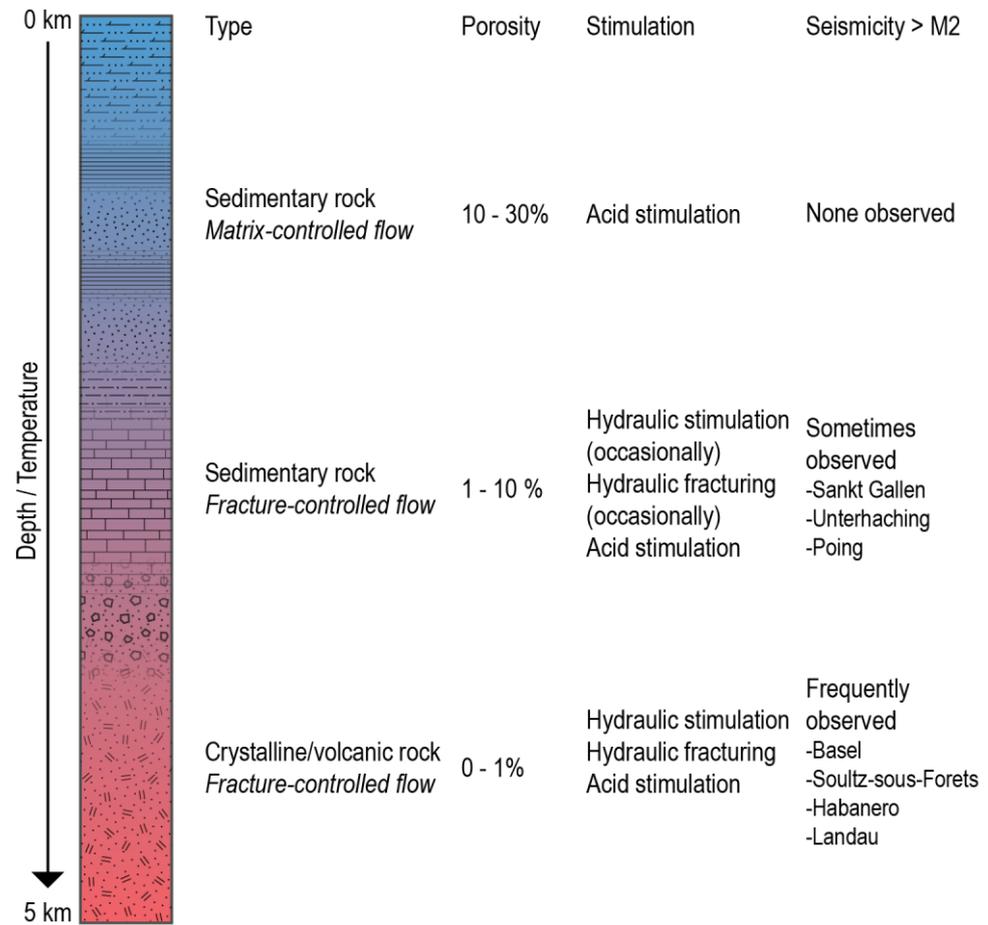
Figure 3-9   Summary of case study review. Three different types of geothermal plays (example for conduction-dominated geothermal settings) (Figure produced by TNO).

Based on the case study review three main types of geothermal target formation are recognized (Figure 3-9):

1) High porosity and permeability sedimentary rocks with the matrix controlling the flow. These include the sites in the North German Basin targeting the Keuper, the Dogger in the Paris Basin, and the geothermal sites in the Netherlands (appendix A.11) excluding the Californië geothermal projects (appendix A.11.4).

2) Tighter cemented or fractured sedimentary rocks with flow predominantly controlled by the (natural or induced) fractures. These include for example the Malm carbonates in the Molasse Basin (appendix A.2), the tight Triassic and Permian sandstones in the Upper Rhine Graben (appendix A.1), and the Californië geothermal projects (appendix A.11.4).

3) Fractured crystalline or volcanic rocks with flow controlled by the fracture system. Stimulation is usually required to enhance the permeability (section 2.4.2).

These three rock types are related to depth, with porous aquifers found at shallow depth (1 – 2.5 km), and the tighter rocks and crystalline rocks at greater depths (3 – 5 km). For convection-dominated systems the depth at which the hot fractured volcanic/igneous/metamorphic rocks are found is usually smaller, e.g. the Geysers is exploited at depths up to 2.5 km with temperatures exceeding 300 °C (Martínez ‑ Garzón et al., 2014).

For these three main types of geothermal target formations the occurrence of felt seismic events (here defined as M > 2) is evaluated against a number of geological and operational key factors:

- Rock type and porosity
- Operational parameters ΔP, ΔV, ΔT, flow rate
- Natural seismic hazard & tectonic loading rate
- Depth, distance to basement

The case studies in this review indicate that most felt events occurred in systems that target low porosity rock where fluid flow is dominated by the fractures and faults (Figure 3-10). Case studies include well-known deep EGS projects like Soultz-sous-Forêts (appendix A.1.5), Basel (appendix A.1.1), and Pohang (appendix A.7) as well as shallower convection-dominated volcanic fields with case studies such as The Geysers (appendix A.12), Larderello (appendix A.10) and Hellisheiði (appendix A.8).

On the other hand, porous sandstone aquifers which do not require stimulation have not been associated with felt seismicity. Case studies include several sites in the North German Basin (appendix A.3), Norwegian-Danish Basin (appendix A.5), and the Netherlands (appendix A.11). Also, the tighter sandstones of the North German Basin which were hydraulically fractured did not produce significant induced events (see #1 in Figure 3-10). The presence of salt may have contributed to a lower seismogenic potential at these sites as it often contributes to a more stable state of stress (i.e. a lower differential stress). Carbonates have a wide spread in porosity due to their variability in facies. The Dogger carbonates in the Paris Basin (appendix A.4) contain porous oolites, and flow is dominated by the matrix (#4 in Figure 3-10). The Malm carbonates of the Molasse basin (appendix A.2) on the other hand are karstified limestones and dolomites with flow dominated by the factures and karst (#5 in Figure 3-10). In general, the seismogenic potential increases with decreasing porosity and when fluid flow is controlled by fractures. The porosity is linked to rock type, and often to depth and temperature. However, other factors also affect the seismogenic potential, including the site-specific state of stress, and presence and orientation of faults. In fact, the presence of large fault zones (mapped or hidden) may be critical in controlling seismogenic potential, regardless of the type of target formation. For example, the presence of critically-stressed faults may account for some of the variation of magnitudes in granite or carbonate reservoirs. Despite the fact that potential presence of faults is not explicitly accounted for in Figure 3-10, it does indicate a clear distinction in seismogenic potential for different types of geothermal targets. Although this information is useful to analyse the seismogenic potential of geothermal targets, other factors such as the proximity of projects to faults and stress

state of faults should be included in site-specific analysis of seismogenic potential for individual geothermal projects.
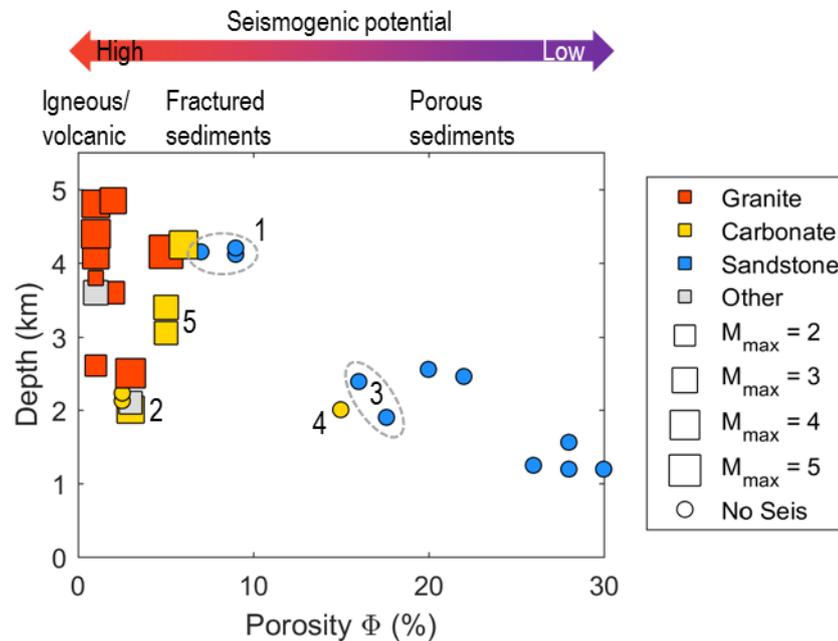
Figure 3-10   Porosity of the geothermal target formation versus geothermal system depth, for the geothermal case studies discussed in Appendix A. The color of the markers is indicative of the rock type of the geothermal target. Squares indicate where seismicity with M>2 occurred with the symbol size showing the maximum observed magnitude. Circles are used for sites where no seismicity was observed/recorded (M<2). Numbers indicate: 1) Tight sandstones in the North German Basin; Horstberg, Hannover, and Gross Schönebeck, 2) volcanic fields which have a relatively shallow depth (Húsmúli, Larderello), 3) geothermal doublets in the Netherlands (Honselerdijk, Koekoekspolder), and 4) average value for 35 sites in the Paris Basin, 5) Molasse Basin (Poing, Unterhaching) (Figure produced by TNO).

It is challenging to determine unique correlations between geological and operational parameters, and seismogenic potential because factors are interrelated and many factors together contribute to the occurrence of felt seismicity. It is not possible to uniquely correlate individual factors to seismogenic potential. However, rough trends or bounds between maximum observed earthquake magnitudes and operational or geological parameters can sometimes be discerned. The following analysis attempts to established such trends or bounds but the interaction of different factors should be taken into account when applying these findings to assess the seismogenic potential for projects, sites or regions.

Another important aspect is that seismic magnitudes are not homogenized with respect to local variations in magnitude of completeness of seismic monitoring networks, moment magnitudes, and site-specific attenuation, cf. section 5.2, (Edwards & Douglas, 2014).

The operational parameters are largely determined by the geothermal play type and geothermal system type (e.g. volcanic field, EGS, regular doublet). The geothermal systems used for district and space heating in sandstone and carbonate plays require low reinjection pressures to maintain circulation (ΔV ~0) at flow rates 20 – 120 l/s

(Figure 3-11). For most of these sites no seismic events are reported. The larger seismic magnitudes mostly occurred in hot, tight, igneous rock that require reservoir stimulation by fluid injection at pressures exceeding 10 MPa (Figure 3-11a).
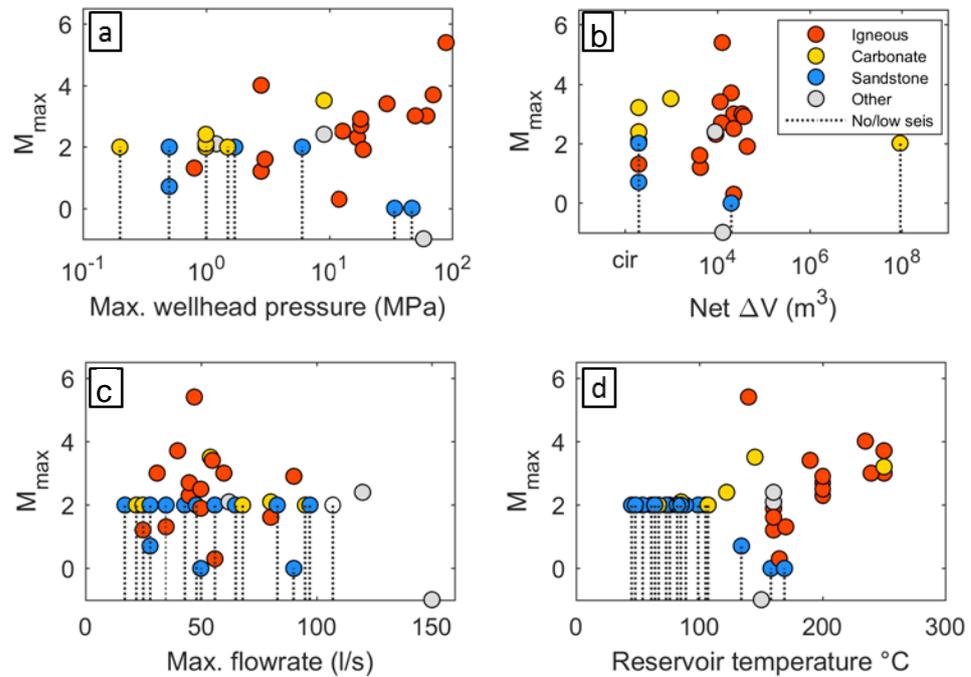
Figure 3-11   Operational parameters and geothermal reservoir temperature versus observed seismicity for the geothermal case studies. Dotted lines indicate cases where no seismicity was reported or recordedand indicate a range of possible magnitudes that may have been missed. The upper limit of this range is determined by the magnitude of completeness of the monitoring system, or in absence of a monitoring system, the approximate threshold for events to be felt at the srufurface M 2.0. a) Maximum (re)Injection pressures at the wellhead, b) injected fluid volume. cir (on x-axis) indicates ciriculation of fluid (ΔV=0), c) maximum flowrates, d) geothermal reservoir temperature (Figure produced by TNO).

The largest event of M 5.4 occurred at the Pohang EGS. Crystalline reservoir rocks were stimulated with injection pressures upt to 89 MPa. Two months after the last stimulation, a M5.4 earthquake occurred. For smaller injection pressures of 1 to several MPa felt seismicity can also occur. One example is reinjection at 2.8 MPa injection pressure near Húsmúli in the Hellisheiði geothermal field, which led to an earthquake swarm with a maximum observed magnitude of M 4.0 (appendix A.8). No clear trend is observed between the event magnitude and the net injected volume or the flow rate (Figure 3-11b, c). Note that the volume range investigated in the case study review is relatively small. Also note that felt seismicity can occur during circulation only under low injection pressure, as illustrated by the M 2.7 observed at the Unterhaching doublet (appendix A.2.5). The trend between reservoir temperature and maximum observed seismic magnitude shows that nearly all events with M > 2 have occurred in the medium- and high-enthalpy fractured reservoirs with T > 100 °C (Figure 3-11d). Hence, trends show increasing maximum observed seismic magnitude with injection pressure above 10 MPa and with reservoir temperature above 100°C. Other trends between operational parameters and maximum observed seismic magnitude are not conclusive.

Important geological parameters are the geothermal play type, tectonic loading and depth of activity or proximity to basement. Again, geological factors interact with operational factors in determining seismogenic potential or maximum observed seismic magnitude. The convection-dominated systems are generally located in tectonically active regions, and the conduction-dominated systems in tectonically inactive areas. To investigate the effect of the tectonic loading rate on induced seismicity the maximum observed magnitudes are shown against the strain rate magnitude (Kreemer et al., 2014) and the natural seismic hazard, which is given in Peak Ground Acceleration (PGA) with a 10% chance of exceedance in 50 years (Giardini et al., 1999). The largest events with M > 4.5 often occur in regions of high tectonic loading and high natural seismicity (Figure 3-12). These include for example the Geysers and Salton Sea geothermal fields in California. However, the Pohang EGS with M 5.4 is situated in a region that is relatively inactive tectonically with low strains and low natural seismicity rates. A number of large tectonic earthquakes up to M 7 did occur in the Pohang Basin, which shows that even in areas with low tectonic strains, being classified as areas of low seismic hazard, large magnitude earthquakes can occur. Accordingly, strain magnitude or natural seismic hazard are not good indicators for maximum observed seismic magnitude. Evans et al. (2012) also found a complex relation between maximum observed seismic magnitude and PGA, and suggest that for igneous rock all felt events (M_L>2) occurred at sites where PGA exceeds 0.8 m/s^2 (~0.8g with g=9.81 m/s^2 the acceleration due to Earth's gravity). The recent M 5.4 Pohang event does not follow that apparent trend. Also, M_{max} close to or above 2 (e.g., Unterhaching) occurs at lower PGA in both igneous and sedimentary rock types. The M 5.4 Pohang event is an outlier in most of the plots with higher seismic magnitude than expected from trends. The potential relation between the hydraulic stimulations at the Pohang EGS site and the occurrence of the M_w 5.4 event have been extensively investigated by different research teams (Grigoli et al., 2018; Kim, Kwang-Hee et al., 2018). Recent research has indicated that EGS activities at the Pohang site induced earthquakes on a previously unmapped fault, which triggered the mainshock. Once triggered the earthquake grew to a magnitude M5.4 event through the release of tectonic strain (ORAC, 2019). Other examples of relatively large magnitudes in tectonically inactive areas include a M 3.7 in Habanero, Cooper Basin (appendix A.9). These observations imply that the state of stress may be sufficient to generate significant felt events, even if tectonic loading rates are low, and natural seismic hazard and loading rate are not a good proxy for the occurrence of induced seismicity. Effects of seismic wave attenuation in the sediment cover also plays a role in site-specific relations between seismicity and PGA.
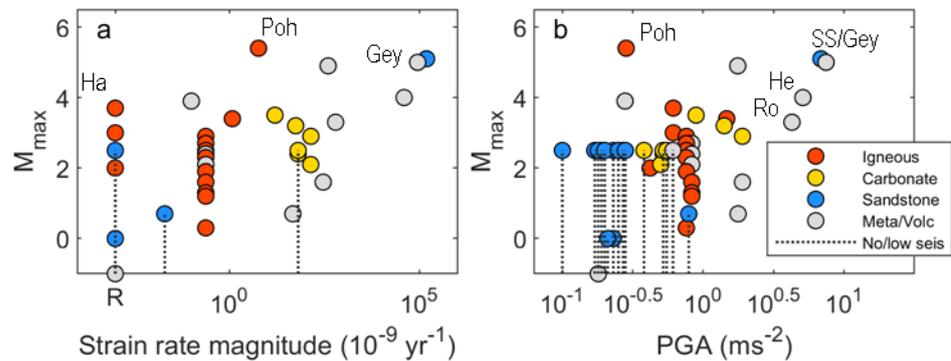
Figure 3-12　Tectonic loading rate and natural seismic hazard against induced seismic event magnitudes in geothermal systems. a) Second invariant of the strain rate tensor from the Global Strain Rate Model (Kreemer et al., 2014) b) Natural seismic hazard defined as Peak Ground Acceleration (PGA) with a 10% chance of exceedance in 50 years (Giardini et al., 1999). Labels indicate geothermal sites: Gey-The Geysirs (U.S.A.), Ha-Habanero (Cooper Basin, Australia), He-Hellisheiði (Iceland), Poh-Pohang (S. Korea), Ro- Rotokawa (New Zealand), SS- Salton Sea (U.S.A.). For legend symbols see Figure 3-11 (Figure produced by TNO).

At depth, stresses are higher and rocks are tighter and more competent, which may lead to larger seismic events. For operations shallower than 2 km (mostly porous sandstone aquifers) no felt events have been reported (Figure 3-13). For a number of operations at depths of 2 – 3 km relatively large events have been reported, up to M 5.1. All of these occurred in convection-dominated systems (dashed oval in Figure 3-13a), including the Geysers, Salton Sea, Hellisheiði and Larderello.
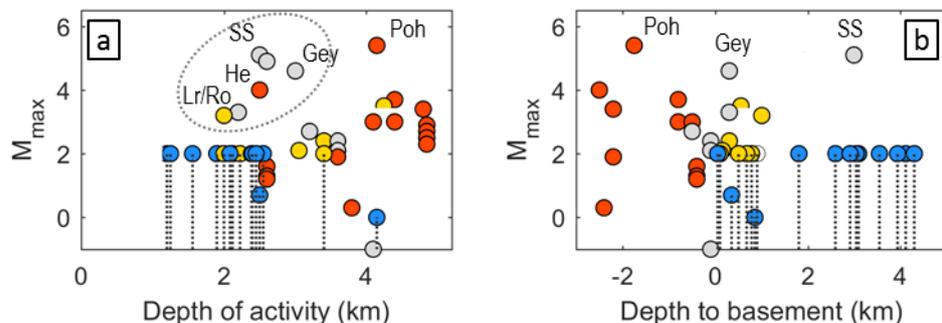
Figure 3-13　Depth of the geothermal target formation and distance to basement against induced seismic event magnitudes. a) Depth of the geothermal operation, usually the maximum depth of the injection borehole. b) Distance from the geothermal system to the crystalline basement (values below zero indicate wells target depths below the top of the basement). Labels indicate geothermal sites: Gey-The Geysirs (U.S.A.), He-Hellisheiði (Iceland), Lr- Larderello (Italy), Poh-Pohang (S. Korea), Ro- Rotokawa (New Zealand), SS- Salton Sea (U.S.A.). For legend symbols see Figure 3-11 (Figure produced by TNO).

For conduction-dominated systems no seismicity of M > 2 was observed deeper than 3 km. At depths larger than 3 km felt seismicity is more common, with M generally smaller than 4. One exception is the Pohang stimulation which triggered a M 5.4. Many of the conduction-dominated systems operate relatively far from the basement

(Figure 3-13b). A hydraulic connection to the basement such as seen in Unterhaching, Sankt Gallen and Insheim increases the potential to induce seismicity at depth.

Several other important factors have been identified in the case study review:

- The presence of (large) faults in the vicinity of the injection well is favourable for reservoir permeability, but can also lead to larger seismic events. First, large fault zones can form hydraulic conduits for pressure diffusion and transmit pressure changes (far) away from the well (section 2.4). This effect increases the likelihood of reactivating a critically stressed fault patch. Of particular importance is hydraulic connectivity to the basement; it is often observed that if pressure changes can be transmitted to the basement felt events can be generated. Examples include the Insheim, Unterhaching, and Sankt Gallen cases. Second, large faults can host larger seismic events, in particular if they are critically stressed. Such faults can be reactivated for small stress or pressure changes, as was indicated for all stressing mechanisms that were discussed in the previous section. Some geothermal systems deliberately target large fault zones because of high permeability in the fault damage zone (Moeck, 2014; Zang et al., 2014). Pressure increase in the fault zone is a particular concern considering the seismogenic potential of these systems (Figure 2-3a). However, injection into faults does not necessarily lead to felt seismicity as was also indicated in the review by Evans et al. (2014).
- A large differential stress leads to more critically stressed faults (i.e. larger Mohr circles in Figure 2-1. Conversely, a more isotropic stress state leads to more stable faults. At Horstberg, for example, no seismic events were recorded during hydraulic fracturing, despite a sensitive monitoring system. It means induced seismicity associated with hydraulic fracturing was below the detection threshold at Horstberg. The state of stress at this location was found to be near-isotropic due to the proximity of salt domes.
- More competent rocks (the reservoir rock itself, or overlying/underlying formations) can build up more stress than creeping rock types and fail in a more brittle manner. The relationship between rock type and induced seismicity is complex, but most of the events observed in the case study review seem to occur in competent rocks like granites and carbonates (Figure 3-10).
- When the target formation is underlain and/or overlain by rock types that seal and creep (claystones, shales, rocksalt), a hydraulic connection is less likely, and stress may be less critical as the creeping formations can cause decoupling of the stresses from those deeper in the crust (see also Evans et al., 2014).
- Geothermal area is related to the scale of the geothermal system. It is large for volcanic fields compared to sedimentary targets. Induced seismicity is more prominent in geothermal systems that cover a large area.

These findings are in agreement with other review studies that analyse induced seismicity (Evans, K. F. et al., 2012; Zang et al., 2014) and/or provide guidelines (Baisch, S. et al., 2016; Wiemer et al., 2017).

Key factors	Geothermal rock type		
	Porous sediments	Fractured sediments	Igneous/ volcanics
Operational parameters (rock/play type specific)			
Pressure difference (ΔP)	low	low – high[1]	EGS – high VF – low – high
Net injected volume (ΔV)[2]	low	low	EGS – med VF – high
Temperature difference (ΔT)	med[3]	med	high
Geological parameters (rock/play type specific)			
Geothermal area	small	small	EGS: small VF: large
Competency of rock	low – med	med - high	med – high
Differential stress	low – med	med	high
Hydraulic connection to depth	low	med	N/A
Reservoir depth	low - med	low - med	EGS: high VF: low
Geological parameters (relevant for each rock/play type)			
Distance to large (critically stressed) faults[4]			
Distance to competent underburden[4]			

Table 3-2   Key factors against different geothermal rock types. Colours indicate the seismogenic potential (green, yellow, orange and red indicate low, medium, medium to high and high seismogenic potential, respectively). The text in coloured cells indicate typical ranking of values for each parameter (low, medium, high) derived from comparison between different geothermal systems (note that values may vary between individual projects). [1]ΔP may be low or high depending on the permeability. [2]Net injected volume in the reservoir (injected minus produced fluid volumes). [3]Temperature differences in shallow porous sediments may still be > 50 °C. [4]The presence of large faults and competent underburden are always important factors in determining the seismogenic potential, regardless of geothermal system or rock type. The distance between wells and faults or underburden is a critical factor that is not rock/play type specific (and therefore colours indicate medium to high seismogenic potential, but differentiation of ranking between the different geothermal rock types is given) (Table produced by TNO).

The relevance of the different factors is summarized for the three different types of geothermal targets (Table 3-2). The colours indicate seismogenic potential (i.e. green colours indicate a low seismogenic potential, and red a high seismogenic potential or likelihood of inducing seismicity). The ranking of seismogenic potential is qualitative and based on the findings in the case study review. The classification low, medium, high is analogous to the ranking of seismogenic potential for the Netherlands (cf. section 1.4). For example, doublet systems targeting porous and permeable sediments (such as the porous sandstone targets in the Netherlands) are based on circulation of fluids without reservoir stimulation. Pressure and net volume changes for these systems are generally low, the geothermal area (usually the doublet spacing in sedimentary systems) is small, and rock competency is low. Also the porous, shallow formations are often hydraulically isolated from deeper basement rocks as they are overlain or underlain by shales and siltstones. Case studies show that the seismogenic potential of these systems is also low (green), in particular if temperature changes are low, and if large optimally oriented faults and competent underburden

are not present. However, if the formations are underlain/overlain by competent formations (e.g. a porous formation overlying a granitic basement such as in Margretheholm), the seismogenic potential can be larger as stresses and pressure changes can be transferred to the surrounding, competent formations. On the other hand, EGS targeting igneous or volcanic rocks are often based on production of high enthalpy fluids from stimulated reservoirs. Pressure, volume and temperature changes for these systems are generally high. Case studies show that the seismogenic potential of these systems is high, in particular if large optimally oriented faults are present that connect the target to deeper competent rocks at depth. Distance to large optimally oriented faults and competent underburden need particular consideration as targets may have elevated seismogenic potential if such distances are small, regardless of the rock type.

3.3 Key parameters observed for other activities and comparison to geothermal operations

For geothermal systems included in the current review, no clear correlation was observed between the induced magnitudes and the injected volume (Figure 3-11). If injected volumes of other activities, such as hydraulic fracturing and waste water injection, are included, a trend of increasing maximum reported magnitude with injected volume is observed (Figure 3-14) (Foulger et al., 2018). The extended dataset can be used to define an upper limit for earthquake magnitudes. McGarr (2014) derived a theoretical relation describing an upper limit for earthquake magnitude based on injected volume, pore pressure changes, and seimic moment. Although some injection operations resulted in earthquake magnitudes that exceed those predicted by the relation, it does capture the rough trend between injection volumes and maximum observed earthquake magnitudes indicated by the data. Many earthquake magnitudes are well below those predicted by the relation that could be caused by aseismic deformation or limited poro-elastic response to injection. Accordingly, the relation and data trends are only relevant as an upper limit for earthquake magnitudes. They should be applied with caution as outliers exist with earthquake magnitudes that far exceed values predicted by the relation (e.g., Pohang, cf. Figure 3-11, appendix A.7). In general, it suggests that maximum earthquake magnitudes increase with injected volumes, which may be relevant for projects where high volume hydraulic fracturing is considered.
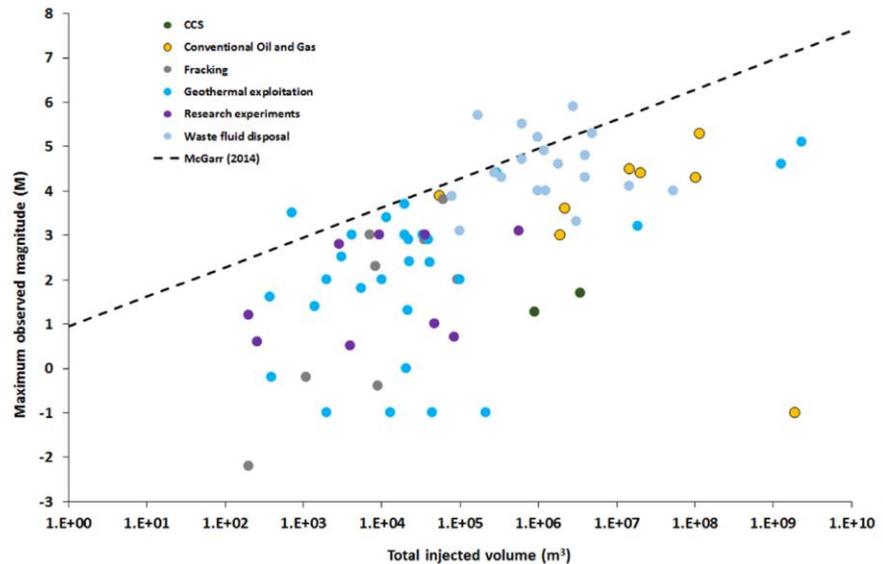
Figure 3-14   Injected volume versus maximum reported magnitude for different activities. (Foulger et al., 2018, Copyright Elsevier, published under a Creative Commons License.

The findings in the case study review are in agreement with other review studies that analyse induced seismicity (Evans, K. F. et al., 2012; Zang et al., 2014). In particular (1) effects of short term fluid injection operations (e.g., EGS stimulations) are different from long term fluid injection operations (e.g., waste fluid disposal), (2) injection into fractured reservoirs should be separated from injection into fault zones when considering seismogenic potential, and (3) the state of stress at target depth is crucial in determining the seismogenic potential of geothermal reservoirs.

3.4   Summary of key observations from the review of case studies

- Low-enthalpy geothermal systems in sedimentary aquifers with matrix-controlled flow have a low potential to induce felt seismic events. The net injected volumes and injection pressures are generally low and the formations are often hydraulically isolated. So far no seismic events have been observed in such plays.
- Medium- to high-enthalpy systems in sedimentary formations with fracture-controlled flow may occasionally produce felt seismic events. A hydraulic connection (e.g., through permeable faults) to deeper, more competent rocks such as crystalline basement increases the potential to induce felt events.
- Medium- to high-enthalpy systems targeting crystalline rocks usually generate a large number of seismic events, both during stimulation and, to a lesser extent, during fluid circulation. The events frequently reach magnitudes that can be felt at the surface.
- For conduction-dominated geothermal plays, the potential for inducing felt seismicity increases with increasing target depth and (related) decreasing matrix porosity. The local hydrogeology is an important factor.
- Production and reinjection in convection-dominated high-enthalpy geothermal fields with volcanic rocks in tectonically active regions occasionally generate felt seismicity and have induced relatively large events (typically M>4).

- Natural seismic hazard (as indicated by PGA taken from GSHAP seismic hazard map in ms^{-2} with a 10% chance of exceedance in 50 years) and tectonic loading are not good indicators for the occurrence of induced events. Induced seismicity with typically M > 3.5 (geothermal) and M > 5 (waste water injection) has been observed in tectonically inactive regions (low PGA). The state of stress may be critical despite slow tectonic loading rates.
- For the geothermal case studies investigated in this review no clear relation of event magnitude and injected volume was observed. If the range of volume or scale of activity is increased by including other geothermal cases and activities, maximum reported magnitudes tend to increase with volume change and the scale of the activity.

4 Current and future targets for geothermal energy in the Netherlands

4.1 Current status of geothermal energy in the Netherlands

Compared to oil & gas activities or other countries worldwide, extraction of geothermal energy is a relatively new source of energy in the Netherlands. The first deep[7] geothermal well was drilled in 1986 in Asten. The well targeted a number of Tertiary aquifers. The drilling did not result in the establishment of an operational doublet. The next geothermal exploration well was then drilled in 2006 in Bleiswijk. This well was successful, as were all subsequent wells in the area. As of January 1st 2018, 14 operational geothermal systems out of a total of 19 systems that were developed or drilled[8]. Figure 4-1 shows the locations of those systems.

4.2 Geothermal target formations in the Netherlands

The aquifers that are targeted for geothermal energy production are largely the same as those that have been explored for oil and gas exploration for many decades (Table 4-1). The West Netherlands Basin in the southwest of the Netherlands has been the most important play for geothermal exploration. Here, rocks of Jurassic and Cretaceous age offer the best geothermal potential (appendix A.11.2, A.11.3). In the northeast of the Netherlands, rocks of Permian (Rotliegend) age are targeted (appendix A.11.1). All aquifers that are currently developed consist of porous sandstones, with the exception of the Lower Carboniferous Zeeland Formation aquifer, which consists of limestones (appendix A.11.4). All doublets produce from target aquifers that are buried between ~1000 and ~3000 meters deep. The Trias Westland project drilled to Triassic sandstones at ~4 km depth, but the sandstones were too tight to be developed and operations are now in the shallower Lower Cretaceous sandstones.

As of January 1st 2018[8], 11 doublets have been drilled to reservoirs of Jurassic and Cretaceous age, 5 to reservoirs of Rotliegend (Permian) age, 2 to reservoirs of Dinantian (Early Carboniferous) age and 1 to a reservoir of Triassic age. The Heerlen Mine Water project is a special case: warm water is being produced from an old coal mine in rocks of Carboniferous age. Exploration efforts mostly focus on development of conventional doublets targeting permeable aquifers with favourable flow properties of Rotliegend, Triassic, Jurassic/Cretaceous and Tertiairy age (Brussel Sand formation). Research programs look into possibilities of developing other (deeper) targets such as Dinantian carbonates[5].

---

[7]No clear depth definition of 'deep geothermal' exists. Here we adopt the Mining Law definition of more than 500 meters below surface. The 35 geothermal wells that were drilled between 2006 and 2017 reached TVD depth between 1600 and 3100 meters below surface.
[8]The annual report 'Natural resources and geothermal energy in the Netherlands' reports the official status of geothermal projects as of January 1st, 2018, including the number of geothermal wells drilled and the produced power (Ministry of Economic Affairs and Climate Policy, 2018). Analysis performed within the framework of this project suggest 15 operational systems out of 23 systems that were developed or drilled (see text, cf. Table 6-1) but the number of new and suspended or terminated projects need to be officially confirmed in the 2019 annual report (cf. www.nlog.nl).
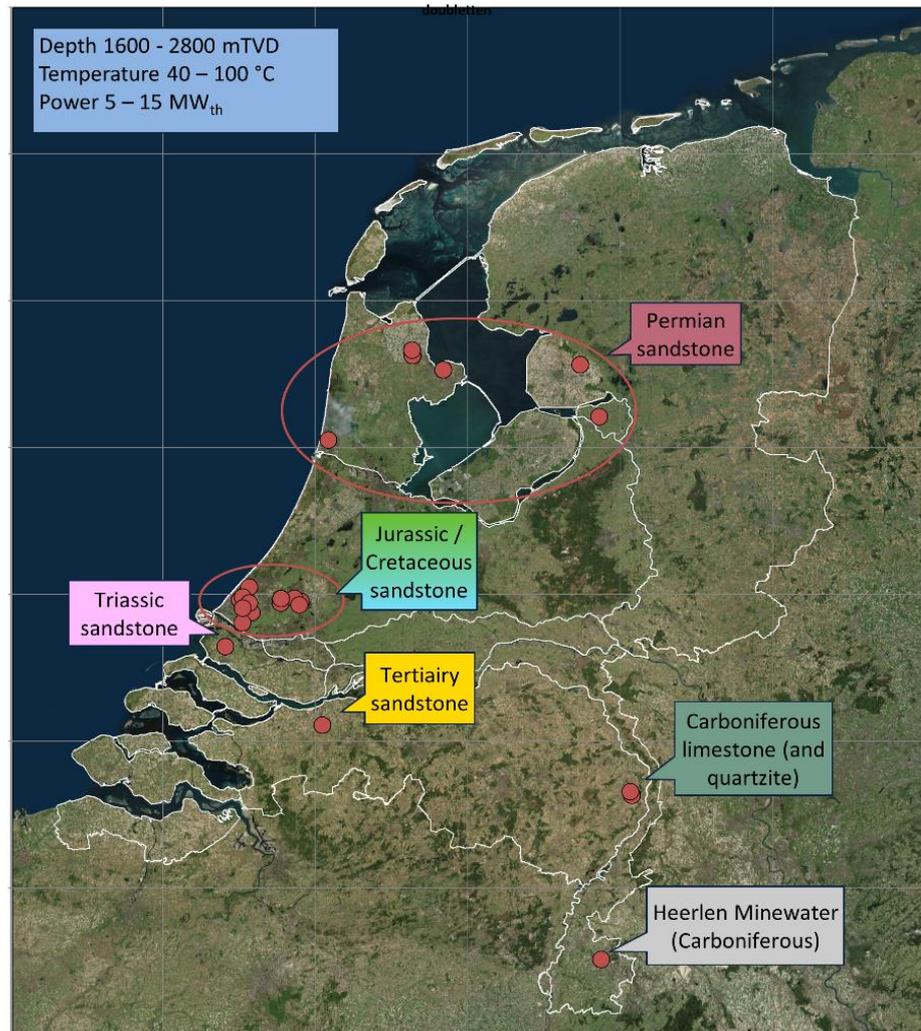
Figure 4-1   Location of geothermal systems in the Netherlands with labels indicating different plays (play distinction based on age and rock type). Status Januray 1st 2018[8] (Source: www.nlog.nl, TNO).

The production temperatures of deeper doublets that are currently operational are between ~65 and ~100 °C, the injection temperatures between ~20 and ~45 °C. The shallower Zevenbergen doublet, which was drilled in 2018 to the Tertiairy Brussel Sand at ~1 km depth has a lower production temperature (~30°C). The maximum flow rates range between 80 and 390 m³/hr (maximum of monthly average). All active doublets are used for heating greenhouses. The only doublet that was drilled with the aim of supplying heat to a city heating network in the Hague, has been suspended. A greenhouse doublet in Pijnacker also supplies heat to a small number of houses. The average power produced per doublet has increased over the last decade, mainly due to increased drilling depth (and therefore higher production temperature) and increased flow rate due to larger casing diameters. In 2016, the average power per doublet was 14-16 MW_{th} and the cumulative installed capacity of doublets was ~130 MW_{th}.

Age	Name	Geothermal targets
Tertiairy	**Lower North Sea Group**	**unconsolidated sediments of the Middle & Lower North Sea Group**
Cretaceous	**Rijnland Group**	**sandstones of the Vlieland Sandstone Formation**
Jurassic	**Schieland Group**	**sandstones of the Nieuwerkerk Formation (Alblasserdam Member & Delft Sandstone Member)**
Triassic	**Triassic Supergroup**	**Sandstones of the Main Buntsandstein Formation (Nederweert Sandstone Member, Volpriehausen Formation, Detfurth Formation & Hardegsen Formation)**
Permian	Permian Zechstein Supergroup	Zechstein carbonates
Permian	**Permian Rotliegend Supergroup**	**porous sandstones of the Slochteren Formation**
Carboniferous	**Carboniferous Limestone Group**	**Dinantian karstified or fractured limestones (Zeeland Formation)**
Devonian	Devonian (and older) Supergroup	deep tight and/or fractured sedimentary rocks (not drilled), e.g. Condroz Sandstone

Table 4-1   Main lithostratigraphic units and (generalized) age. The units displayed in bold contain formations that are geothermal targets (see appendix A.11 for details). The Devonian targets are not drilled (currently little information is available on these targets in the Netherlands) (Table produced by TNO).

Within the framework of the "Masterplan Geothermal Energy in the Netherlands"[1], EBN suggests future development of geothermal energy in the Netherlands will focus on extending development of (1) present Devonian, Permian (Rotliegend Slochteren Fm.), Trias (Main Buntsandstein Fm.) and Lower Cretaceous sandstone targets, and (2) present Dinantian and future Devonian and Zechstein carbonate targets (Figure 4-2).

For the current analysis of seismogenic potential, the different targets in the Netherlands are grouped in 5 current and potential future geothermal plays following the criteria outlined in section 1.4 (cf. Table 1-2). The five plays and operational or drilled systems[8] are: (1) Jurassic/Cretaceous permeable porous sandstone reservoirs (9 systems currently producing out of a total of 13 systems drilled, mainly in the southwestern part of the Netherlands), (2) Triassic (1 system currently producing out of a total of 2 systems drilled[9], in the southwestern part of the Netherlands) and Permian (5 systems currently producing out of a total of 6 systems drilled, mainly in the north of the Netherlands) tight or permeable porous sandstone reservoirs, (3) Dinantian fractured or karstified carbonate reservoirs in the southeastern part of the Netherlands affected by active tectonics in the Roer Valley Graben (labelled RVG Dinantian carbonates, 2 systems, currently not producing), (4) Dinantian fractured or karstified carbonate reservoirs in the central (including southwestern part) and northern parts of the Netherlands away from the Roer Valley Graben (labelled CNNNLD Dinantian carbonates, currently not targeted but under investigation, see also Lipsey et al., 2016; TerHeege et al., 2018), (5) deeper

---

[9]The Vierpolders VPD-GT and Trias Westland NLW-GT projects drilled to the Triassic sandstones but the latter is currently producing from the Cretaceous Delft Sandstone Member.

(Devonian) sedimentary reservoirs (currently not targeted but under consideration as deep targets, distribution and properties are largely unknown).

Sandstone reservoirs:
- Lower Cretaceous Sandstone **(present)**
- Triassic (Main Buntsandstein) **(present)**
- Rotliegend (Slochteren Sst) **(present)**
- Devonian (Condroz Sst) **(present)**

Carbonate reservoirs:
- Zechstein carbonates
- Dinantian carbonates (**present**, UDG[5])
- Devonian carbonates

Production from basement rocks is not envisaged

Depth: 500-6000 m
Temperature: 30-180°C

Stimulation techniques:
- Chemical methods
- Thermal methods (due to injection?)
- Radial drilling or jetting (research)
- Hydraulic fracturing (last resort)

Figure 4-2 Present and future geothermal targets in the Netherlands (From EBN, with permission).

5   Traffic light and monitoring systems for geothermal sites

Risk assessment is an integral part of management and control protocols for induced seismicity that aim at mitigating seismic risks (Mignan et al., 2017). Risk assessment in turn relies on analysis of seismic hazard, and thereby on the availability of processed seismic monitoring data. Monitoring data can be used to continuously update risk assessments techniques during production activities, and therefore provide essential information on changing conditions affecting seismic risks.

Assessment of seismic risks of a geothermal project generally requires: (1) Knowledge on seismogenic potential and seismic hazard for specific operational parameters and geological setting (cf. section 3), (2) effects of induced seismicity on ground motions (PGA, PGV) and damage at the surface, (3) preventive barriers (e.g., operational parameters, locations) for seismic hazards that change the likelihood of induced seismicity, (4) control barriers that change the impacts of induced seismicity (e.g., traffic light systems). This section gives an overview of studies presenting protocols and techniques for monitoring seismicity. These protocols can reduce seismic risks during geothermal operations by increasing the control barriers with an emphasis on traffic light systems. Furthermore, we discuss relevant studies where recommendations for seismic monitoring of induced seismicity are presented. We mainly consider studies in a geothermal setting, or that are otherwise of direct relevance to geothermal sites. Brief specification of the availability and type of traffic light system and monitoring network per case is given in Appendix A. This includes threshold levels of traffic light systems if reported in report or literature.

5.1   Traffic light systems for geothermal sites

Traffic light systems (TLS) are an integral part of protocols for hazard and risk management and mitigation (Bommer et al., 2006; Ellsworth, 2013; Hirschberg et al., 2015; Majer et al., 2012). In cases with frequent occurrence of seismicity (e.g., Soultz-sous-Forêts in France, appendix A.1.5), there may be an increase in earthquake magnitude during geothermal operations as well as post-operational seismicity which should be considered when defining threshold values for traffic light systems. In these cases, a distinction can be made between traditional traffic light systems and adaptive traffic light systems. Traditional traffic light systems are based on decision variables (e.g., seismic magnitudes) and on threshold value above which actions must be taken (based on expert judgement and regulations). Adaptive traffic light systems evaluate whether an earthquake magnitude threshold behaves conform a specific risk-based safety standard or norm. In adaptive traffic light systems, the magnitude threshold can be updated in real-time based on temporal probabilistic forecasting of the induced seismicity rate as a function of known injection flow profile (Mignan et al., 2018; Mignan et al., 2017). Table 5-1 shows an overview of the availability of traffic light systems for the geothermal cases considered in this report, including the used threshold levels if applicable. This overview shows that traffic light systems have been used only in a few cases.

Site	Country	M_min	M_max	Depth activity	Mag_scale	Rocktype	Mon_type	TLS	TLS_cutoff (mm/s; ML)
Gross Schoenebeck water-frac	DEU	-2	-1	4.1	Mw	Volcaniclast	SSBDB	Yes	Not traceable
Gross Schoenebeck 4120 gel	DEU	-2	-9999	4.12	Mw	Sandstone	SSBDB	Yes	Not traceable
Basel[1]	FRA	0.5	3.4	4.8	ML	Granite	SSBDB	Yes	[0.5, 2.0, 5.0];[2.3, 2.9]
Habanero 1 2003	AUS	-	3.7	4.4	ML	Granite	SBDB	Yes	Not traceable
Habanero 1 2005	AUS	-1	3	4.4	ML	Granite	SBDB	Yes	Not traceable
Habanero 4 2012	AUS	-1.6	3	4.1	ML	Granite	SSBDB	Yes	Not traceable
Insheim production	DEU	0.4	2.1	3.6	ML	Multiple	SSB	Yes	PGV: [0.5, 1, 3, 5, 10]
Insheim stimulation	DEU	-0.4	2.4	3.6	ML	Multiple	SSB	Yes	PGV: [0.5, 1, 3, 5, 10]
Sankt Gallen[2]	CHE	0	3.5	4.25	ML	Carbonate	SSB	Yes	ML=1.6 (yellow)
Pohang (PX-1 + PX-2)	KOR	-	5.4	4.15	Mw	Granodiorite	SSB	Yes	PGV: [0.8, 5, 10, 20]; Ml: [1.0, 1.4, 1.7, 2.0]

Table 5-1   Table summarizing the characteristics of traffic light systems that were in use at geothermal operations. This table was extracted from the case overview in Appendix A (-9999 indicates that no data was available). Abbreviations for monitoring types: SSB=local surface and shallow boreholes, SSBDB=local surface, shallow borehole and deep borehole network, SBDB=local shallow surface and deep borehole network. [1,2] Examples of traffic light systems that triggered shut-in of operations following exceedance of critical thresholds in earthquake magnitude (Table produced by TNO).

Examples of traffic light systems that triggered operational decisions include the Basel (cf. appendix A.1.1) and Sankt Gallen (cf. appendix A.2.4) projects. At Basel, production was stopped after an event of M_L=2.6 occurred accompanied by an

increasing seismicity rate. Aftershocks occurred after shut-in up to M_L=3.4. At Sankt Gallen, injection needed to continue to control a gas kick in the well despite that the yellow status of the TLS after M_L=1.6 occurred, indicating that activities should be ceased. Later on the same day an M_L=3.5 occurred.

5.1.1 *Traditional traffic light systems*

Traditional traffic light systems (TLS) were first proposed by Bommer et al. (2006) for the 'Berlin' geothermal project in El Salvador, and the scheme for this system is depicted in Figure 5-1. The approach of Bommer et al. (2006) has been applied for instance for the EGS projects in Basel (Häring et al., 2008) and Pohang (Kim, Kwang-Il et al., 2018), and for the hydrothermal project in Sankt Gallen (Edwards et al., 2015). The traffic light systems were based on a combination of public response, calculated local magnitude and measured PGV as shown in Figure 5-1 (Hirschberg et al., 2015). The motivation was that peak ground acceleration is poorly correlated with damage, whereas the peak ground velocity (PGV) is a more stable parameter (Bommer et al., 2006). If either of the three threshold criteria are exceeded the TLS status changes. The chosen levels for PGV depend on the geological conditions and local regulations and criteria set for ground motions. For Basel threshold criteria were mainly based on expert judgement, where a four stage action plan (green, yellow, amber and red) was followed depending on the chosen threshold criteria. For the case of Pohang, the protocol for induced seismicity associated with EGS was followed as published by the department of energy of the United States (Majer et al., 2012).
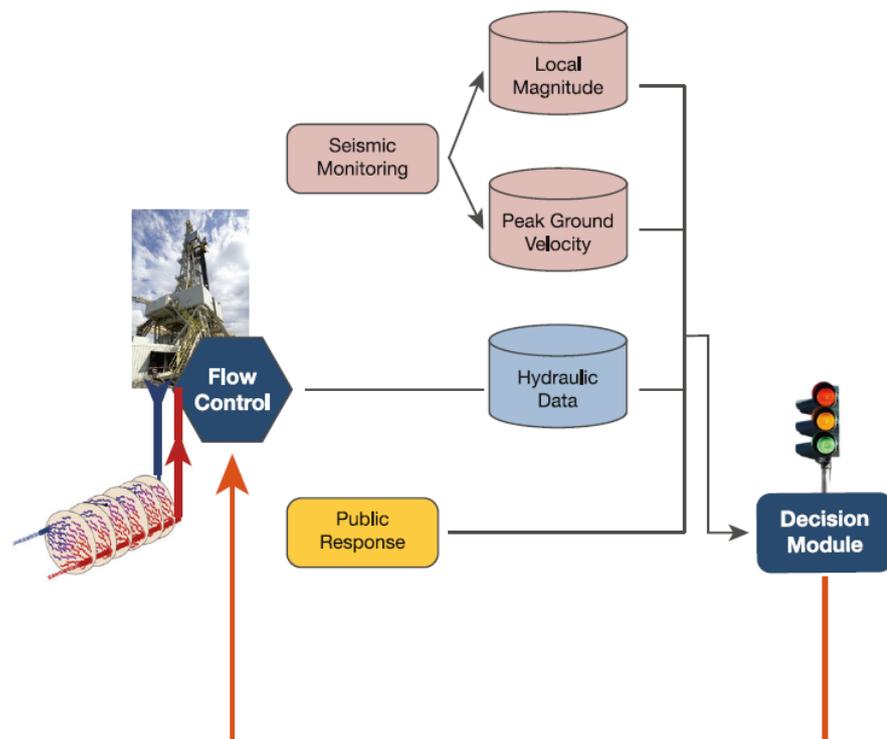
Figure 5-1 Traditional traffic light system (From Hirschberg et al., 2015, Figure 126a, Copyright vdf Hochschulverlag, published under a Creative Commons License).

When defining threshold values in TLS, both the effect of earthquakes on damage of constructions as well as the public perception of vibrations should be considered. This is illustrated in Figure 5-2 showing limits for cosmetic damage to prevent damage to plaster and dry wall as recommended by the U.S. Bureau of Mines, together with human perception limits (Rutqvist, Jonny et al., 2014). The damage limits were based on a study of monitoring data of structural damage due to blasts (Siskind et al., 1980). The shown human perception limits were proposed by the U.S. Army Engineering (USACE, 1972) and were considered as well for ground-vibration induced pile driving and associated EGS developments (Athanasopoulos & Pekelis, 2000; Bommer et al., 2006). Figure 5-2 shows that in the frequency range of 1-100 Hz, people have a greater perception to vibrations with increasing frequencies, while structural damage decreases with increasing frequency. It should be noted however that the defined perception levels were based on steady-state sinusoidal vibrations and not on short event characteristics for earthquakes, and thus are not fully representative for earthquakes (Rutqvist, Jonny et al., 2014). Because the damage to constructions caused by vibrations is closely related to the frequency content (Nicholls et al., 1971), criteria are often subdivided per frequency level (Kim, Kwang-Il et al., 2018). This practice is followed in some countries, such as the United States, Germany and England.
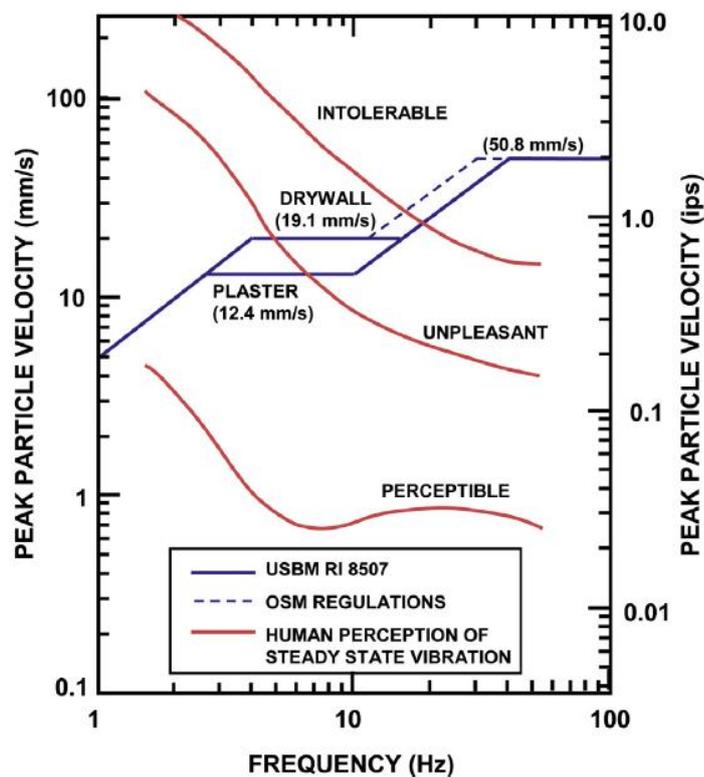
Figure 5-2   Limits for cosmetic damage in plaster stucco and drywall recommended by USBM (blue curves), and human-perception limits (red) for blast vibration (USACE, 1972). From: (Rutqvist et al., 2014, Copyrght Elsevier, published under a Creative Commons License).

5.1.2   *Adaptive traffic light systems*

More recently adaptive traffic light systems (ATLS) were developed, that contain a predictive component instead of being just reactive like the traditional traffic light system (Goertz-Allmann & Wiemer, 2012; Hirschberg et al., 2015; Mignan et al.,

2018; Mignan et al., 2017). ATLS aim at including geomechanical modeling and probabilistic forecasts on predicted seismicity based on a range of key parameters. Key parameters can include observed seismicity, magnitude, current and planned pressure levels, permeability and Coulomb stress changes (Hirschberg et al., 2015). The forecast is made within a probabilistic framework, which accounts for uncertainties related to the description of physical processes, as well as the random variability within those processes. Predictions of seismicity are updated automatically and in real-time based on continuously recorded data. Mignan et al. (2017) show that a relatively simple statistical seismicity forecasting model used within an ATLS, already makes predictions with a close match to data. In this case data consisted of induced seismicity rate sequences observed in fluid injection experiments from six enhanced geothermal systems. In addition, a safety criterion is defined which is a probability of exceedance with respect to different safety specifications. The criterion relies on earthquake magnitude, injection volumes and model parameters describing the underground characteristics.

With respect to seismicity forecasting, a general distinction between statistical, physics-based and hybrid models can be made. Although statistical models are computational efficient, they have limitations. The main limitation is that they account for the physical processes that underlie induced seismicity only to a limited degree. Physics based models on the other hand are more comprehensive and account for (thermo-) hydromechanical processes. This mechanistic basis makes these models more accurate as forecasting models compared to statistical models. However, they are computational intensive due to their complexity, and therefore difficult to run in real-time. Also, model parametrization requires more effort in physics-based models, where parameters are often poorly constrained. Hybrid models combine both aspects of statistical and physical models using flow models together with stochastic models (Bachmann et al., 2012; Goertz-Allmann & Wiemer, 2012; Hirschberg et al., 2015).

Although ATLS have not been demonstrated in real-time mode yet, it is a promising approach for mitigating seismicity during geothermal operations. They are likely to be more robust and sophisticated compared to traditional TLS. However, ATLS systems do require a more intensive monitoring effort compared to traditional TLS, and a considerable seismicity rate (i.e. frequent occurrence of (micro-)seismicity). In those cases, monitoring can provide accurate information on fluid migration, preferential fault reactivation, and 3-D distribution of the frequency-magnitude distribution of seismicity (Edwards et al., 2015). A challenge for ATLS is that larger magnitude events may not always be preceded by a (series of) smaller events. In these cases application of ATLS to mitigate the occurrence of larger events may not be possible. For geothermal operations in the Netherlands the ATLS may therefore not be directly applicable, as continued operations after the occurrence of a vast amount of seismic events (such as observed in Basel and St. Gallen) will not likely be accepted, in particular if felt seismicity is part of the seismic catalogue.
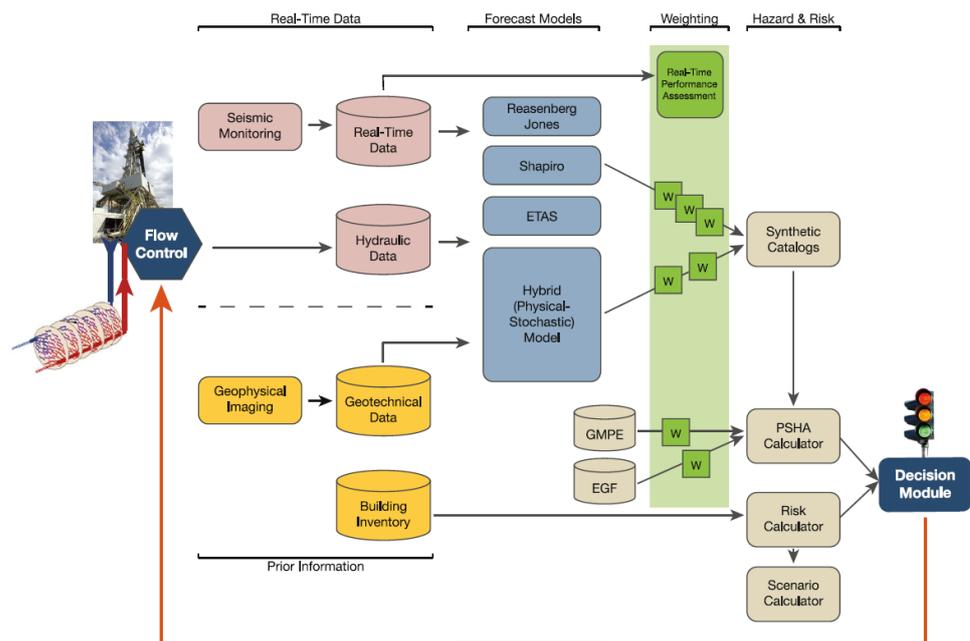
Figure 5-3   Adaptive traffic light system (From Hirschberg et al., 2015, Figure 126b, Copyright vdf Hochschulverlag, published under a Creative Commons License).

5.1.3   *Other considerations and outlook for the Netherlands*

Given the large concern about induced seismicity in the Netherlands, it is likely that any geothermal project where elevated seismogenic potential is identified will require a TLS during operations. Geomechanical modeling and (probabilistic) forecasts on seismicity will need to be performed upfront to assess seismogenic potential and determine TLS threshold levels. Although notoriously difficult to assess, an important consideration in these TLS are forecasts of the maximum earthquake magnitude, and thresholds required to minimize the occurrence of potentially damaging earthquakes. The chosen threshold levels defined within TLS or ATLS can be a matter of debate. When traffic light systems are set conservatively it is less likely that potentially damaging earthquakes occur. This means that interruption thresholds are set lower and production is therefore interrupted earlier. On the other hand, more conservative traffic light systems will have an impact on the commercial success rate of the projects (Wiemer et al., 2017). In addition, threshold values for PGV and magnitude are likely to be set more conservatively in densely populated areas, such as in the Netherlands, compared to sparsely populated areas. A disadvantage of using only PGV is that there is not a unique relation between PGV and macroseismic intensity e.g., EMS-98 (Edwards & Douglas, 2014; Grünthal, 1998), and that observed PGV values can be very location specific due to local site amplification. Therefore, when using traffic light systems, the strength of ground shaking may be better represented by a combination of more complex parameters, such as PGV together with the magnitude, duration and energy content of the earthquake. Another factor that should be considered is the frequency of occurrence with respect to human perception, where the public tolerance will likely decay with an increase of the number of perceptible (felt) seismic events (Bommer et al., 2006). Public perceptions are critical factors that need to be considered to maintain a license to operate.

Outside of the geothermal context addressed in this study, the Groningen gas production site is one of the few sites in the Netherlands, where a protocol is defined

to mitigate seismic risks. It prescribes when and how measures should be taken to mitigate depletion-induced seismicity (NAM, 2017), and includes a TLS. This TLS relies on the signal parameters; peak ground acceleration (PGA), activity rate, earthquake density, peak ground velocity (PGV) and damage state. Besides the "baseline" status with continuous monitoring of seismic activity, the TLS distinguishes three stages (green, amber and red), each with critical levels for the signal parameters and specific measures (Table 5-2). The stages are translated to different response levels (NAM, 2017) ranging from a watchfulness/alertness level (green) requiring analysis to identify trends or developments, a signal/preparation level (amber) requiring preparation of (regional) measures that can be implemented within several weeks, to an intervention level (red) requiring immediate measures in the system (on field scale if required).

Signal parameter	Measurement	Status Traffic Light System Groningen		
		Green	Amber	Red
Activity rate	# events M $\geq$ 1.5 per year	15	20	25
Earthquake density	# events M $\geq$ 1.0 per km^2 per year	0.17	0.25	0.4
PGA	g (maximum, during last M $\geq$ 2.0 event)	0.05	0.08	0.1
PGV	mm/s (calculated, during last M $\geq$ 2.0 event)	5	50	80

Table 5-2   Signal parameters, critical threshold values for activity rate, earthquake density, peak ground acceleration (PGA) and peak ground velocity (PGV) for different stages of the traffic light system at the Groningen gas production site (Source: NAM, 2017).

Although gas production is markedly different compared to geothermal operations, the definition of thresholds in the Groningen TLS can serve as a reference (not an example) for anticipated geothermal projects in the Netherlands. Data relating seismicity to structural damage at the Groningen site may be useful to consider in determining threshold criteria in TLS for geothermal projects. An important consideration is the relation between structural damage and the cumulative effect of successive earthquakes during gas depletion. Also, the mechanisms driving induced seismicity are different, i.e. (differential) compaction due to cumulative gas extraction as opposed to a combination of direct pressure, poroelastic and thermoelastic effects during circulation of fluids (cf. section 2.4.3).

In any case, the design of future TLS for geothermal operations in the Netherlands will likely aim at avoiding earthquakes with magnitudes that can lead to damage at the surface. Current practice is to implement measures such as modification of operations or (temporary) shut-in if felt seismicity occurs (see for example the current status of geothermal projects near Californië, cf. appendix A.11.4).

With respect to geothermal operations in the Netherlands, Baisch et al. (2016) differentiate between low, medium and high hazard areas, where they follow guidelines for seismic hazard assessment for natural gas fields (SODM, 2016). In the case of a low seismic hazard scenario (Baisch, S. et al., 2016) they propose that no traffic light system should be installed. In case of medium seismic hazard real-time monitoring in combination with a traffic light system should be required for the entire lifetime of the geothermal system or limited to specific project phases. In case of high

seismic hazard (Baisch, S. et al., 2016) recommend that real-time monitoring in combination with a traffic light system is required for the entire lifetime of a geothermal system.

The effectiveness of TLS still differs from case to case in geothermal plays, which is illustrated by the case study review in Appendix A. For instance, at the EGS site in Basel, stimulation was stopped after an earthquake of M_L=2.7 occurred and the seismicity rate became unacceptably high. Note that seismicity rate was formally not a factor in the TLS for the Basel project, and the status red was formally not reached as it was set to M_L=2.9. Still, after shut-in of the injection well a total of three earthquakes with $2.5 < M_L < 3.4$ occurred. Such rise in earthquake magnitude over time during injection is observed in other cases as well, and should be accounted for in the design of TLS. In general, a TLS can be considered as a method to reduce seismic risk, but does not provide absolute guarantees that earthquake magnitudes will stay below a specific threshold value. This notion is supported by observations of induced seismicity related to gas production that may show relatively high magnitude earthquakes without precursors of smaller magnitude events, e.g., seismicity near the Bergermeer gas (storage) field (Orlic & Wassing, 2013). TLS should be regarded as a control measure that reduces the likelihood of induced seismicity and thereby seismic risks rather than a measure that guarantees that seismic events will not exceed certain magnitude thresholds.

5.2   Monitoring networks at geothermal sites

In general, the completeness of earthquake catalogue data relies on the availability of accurate monitoring data, such that relevant earthquake characteristics can be determined accurately. Typical parameters that should result from data analysis are the earthquake's origin, timing, location, magnitude and focal mechanism. Throughout literature there is a general consensus regarding monitoring recommendations at geothermal sites, which is summarized in Table 5-3.

5.2.1   *Purpose of seismic monitoring*
The design of a seismic monitoring network should be guided by the required sensitivity and earthquake location accuracy. Site-specific geology and reservoir characteristics should be considered in the design of seismic monitoring networks. The local threshold (i.e. magnitude of completeness and detection limit for surface ground motion) and location accuracy of a seismic monitoring network is determined by the number of stations, their spatial distribution (both at the surface and with depth), the instrument types used, and the local geology.

The accuracy of the earthquake locations depends both on the network design, as well as the accuracy and detail of the underlying geological model. In particular, an accurate velocity model is needed, preferably with both compressional (P-) and shear (S-) wave data. The quality of the velocity model critically determines the horizontal and vertical (depth) resolution. For examples, the recent seismic event close to the Californië geothermal site (cf. appendix A.11.4) has large uncertainty in depth, mainly because the local S- wave velocity structure is not well known.

	Aspect	Guideline
Data quality	Perception threshold in 5-40 Hz	0,3 mm/s, M~1[(1)]
	Detection threshold in 5-40 Hz	0,02-0,03 mm/s, M~0[(1)]
	Maximum noise amplitude	2 µm/s, vertical component in range 5-40 Hz
	Number of components	3
	Eigenfrequency	≤ 4.5 Hz
	Sampling frequency	≥ 100 Hz
	Robustness	Accuracies should be achievable for 99 % of time
Spatio-temporal coverage	Baseline monitoring	6-12 months
	Post-production monitoring	Until restabilization of reservoir
	Spatial network coverage	Cover subsurface volume that is at least twice the size of the reservoir volume
	Density and placement of sensors	Guided by network design study. Minimum of 5-8 stations for typical geothermal project[2].
	Sensor depth	Depending on required detection threshold; specific combinations of surface/borehole and/or downhole sensors
Event characterization	Event location error, horizontal (95% confidence level)[3]	+/-500 m
	Event location error, vertical (95% confidence level)[3]	+/-2000 m
	Focal mechanism	Should be determined for M>2. Especially relevant during production or when operational strategy changes
Data policy	Data storage	Continuous recorded and stored, ≥ 24 bit recording system, standardized data format
	Data access	Should be directly available to monitoring authority, real-time data access and (near) real-time processing
	Data status	Public available when seismicity exceeds anticipated levels[4]

Table 5-3   Table summarizing guidelines for different aspects of monitoring networks (Baisch, S. et al., 2016; Bohnhoff et al., 2018; Kraaijpoel et al., 2013; Majer, E. et al., 2012). Annotations: [1]Depending on hypocenter and geology. [2]A typical geothermal project is defined by Majer et al. (2012) as 1 or 2 injection wells and several production wells, in an area with a maximum diameter of 5 km. [3]In general, hypocenter location methods using root mean square algorithms do not take into account systematic errors in crustal velocity models. [4]It is considered beneficial for public engagement to make all recorded data publicly available rather than only data that exceeds anticipated levels in order to provide a more comprehensive view on monitoring efforts and seismic risks (Table produced by TNO).

The relation between the cumulative number and magnitude of earthquakes is described by the Gutenberg-Richter law (Richter, 1935). Relatively weak seismic events (i.e. low magnitude of completeness) are important to detect since they can precede the occurrence of a rarer, larger magnitude event, and also enable more detail regarding fault structure, seismicity rates, failure mechanisms and stress

conditions (Majer, E. et al., 2012). To support seismic network design, seismic simulations can be valuable to calculate expected spatio-temporal variations of the earthquake wavefield, accounting for site-specific geology. From this an optimum sensor network configuration can be determined (Miller et al., 1998).

This implies that at the start of a geothermal project, a detailed subsurface characterization phase should be conducted. Subsurface characterization may include acquisition of new 2D and/or 3D seismic data, depending on the availability and coverage of prior data. These acquisition campaigns should aim at accurately imaging the target reservoir, and its overlying and underlying formations, as well as faults. The existing regional velocity model can be refined with the velocity model derived from the newly acquired seismic data. Additional data sources that can be used for velocity building are available well log data, downhole calibration shots and vertical seismic profiling, although they are of limited use in determination of the seismic properties of formations at larger scale. An accurate (preferably 3D) velocity model is important because errors in the velocity models map into earthquake locations as systematic errors and thus cannot be reduced by methods such as root mean square residual minimization or averaging algorithms for determination of hypocenter locations. Increased accuracy of source location estimation is important to tie earthquake recordings to specific faults, thereby providing valuable insight in potential causal relations between operations and seismicity.

To accurately translate observed peak ground velocities to earthquake magnitude values and vice versa, the local attenuation should be known, which is determined by the site-specific geology and can be measured with a strong-motion sensor. In this respect, regional attenuation relationships often require modification to be applicable for local monitoring networks. This means that the range of validity of attenuation relationship needs to be extended downwards to lower epicentral distances (Edwards et al., 2015).

5.2.2 *Guidelines for seismic monitoring*

Various literature sources provide monitoring recommendations specifically for geothermal sites (Baisch, S. et al., 2016; Bohnhoff et al., 2018; Kraaijpoel et al., 2013; Majer, E. et al., 2012), as summarized in Table 5-3. This section summarizes some relevant monitoring aspects of these selected sources.

Three operational stages are distinguished for spatio-temporal coverage, i.e. baseline, production, post-production. Assessment of the optimum duration of seismic monitoring often requires site-specific analysis of geological setting and seismic hazard before commencing geothermal operations. Within the protocol for addressing induced seismicity associated with EGS, Majer et al. (2012) recommend that the acquired seismic monitoring data should cover the baseline period as well as the production and post-production period. Here, the baseline period is the period prior to drilling and operations when the reservoir is in its natural state. Baseline monitoring is crucial to identify contrasts between seismicity observed during the production- and the baseline period. For geothermal projects, lower magnitude thresholds should be typically detected to identify active seismic zones prior to operations (typically magnitudes below M1.0, Majer, E. et al., 2012). Existing regional networks are often not sensitive enough to detect these events. They should be densified with additional stations in the area of the planned project from the start of the baseline monitoring period. Alternatively, an additional dedicated local network

can be deployed. A baseline period of 6-12 months is generally recommended (Bohnhoff et al., 2018; Majer, E. et al., 2012).

When considering a typical sized geothermal project, with the injection and production wells located in an area of maximum 5 km diameter, Majer et al. (2012) recommend that a minimum of 8 three-component stations should be distributed over the area. For larger sites more stations are required to acquire analyzed results with sufficient accuracy. Baisch et al. (2012; 2016) recommend a minimum of five three-component stations positioned at the surface. More specific technical specifications for monitoring networks at geothermal sites are made by Kraaijpoel et al. (2013), who propose specifications for instrument characteristics and data quality (e.g. noise levels, frequency response), spatio-temporal coverage and data policy.

More extensive monitoring efforts are considered by Bohnhoff et al. (2018), who propose placement of sensors at the surface, in shallow boreholes or downhole in deeper boreholes, depending on the operational stage and resolution of recorded seismicity (Figure 5-4).

Type	Usable bandwidth	Instrument OD	Sensor cost	Relative sensor + deployment cost			Step 1	Step 2	Step 3
				surface	posthole	deep well	suggested deployment		
BB ●	40 s - 20 Hz	~250 mm	high	moderate	moderate		~ 4 @ 1 m		
1 Hz ● ●	4 s - 100 Hz	~200 mm	moderate	low	low	high	~ 2 @ 30 m	~ 6 @ 30 m	
4.5 Hz ● ● ●	1-500 Hz	70 mm	Low	low	low	moderate	~ 1 @ 300 m	~ 4 @ 300 m	~ 12 @ 300 m
15 Hz VSP ●—●—	4-2000 Hz	50 mm	lowest			high	< 3000 m VSP array		
4.5 Hz SET ●	1-500 Hz	70 mm	Low		moderate	high	~ 36 @ 100 m buried SET array		

Network detection, location, source parameters versus depth
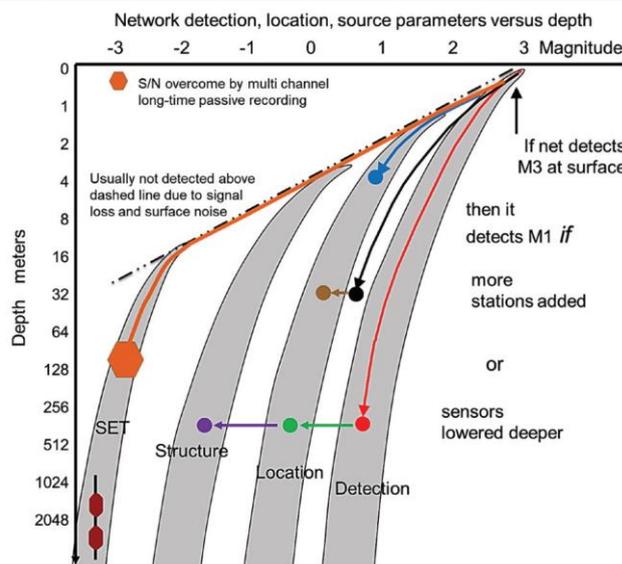
Figure 5-4   Common instruments, deployments, relative costs and seismic magnitude detection limits for different monitoring systems. Deployment of the systems is considered in a notional stepwise development plan for seismic monitoring of a 5 x 5 km target area covering a resource at a depth of ~1.5-2 km (From Bohnhoff et al., 2018 (First Break, 36, 59-65, Copyright M. Bohnhoff et al., reproduced with permission).

Bohnhoff et al. (2018) distinguish three project phases, i.e. (1) Phase I (pre-drilling phase) dedicated to establishing baseline seismicity and (approximate) locations of seismic events, (2) phase II (drilling, completion & stimulation phase) dedicated to

short term monitoring of reservoir (stimulation) operations, and (3) phase III (production and post-production phase) dedicated to long term passive monitoring for hazardous earthquakes. Within each phase different steps are defined that deploy monitoring systems with different characteristic data quality and deployment costs. There is a general trade-off between the data quality of the acquired data (i.e. signal to noise ratio) and the instrument type and its placement depth, which is shown in Figure 5-5 (Bohnhoff et al., 2018). It shows that data with a higher signal to noise ratio can be acquired, by installing instruments with a higher frequency response at a larger depth. Signal to noise ratio is greatly enhanced for borehole sensor arrays compared to surface arrays. Implementation of borehole sensor arrays therefore greatly reduces the magnitude of completeness of seismicity. Data on seismicity recorded with surface networks may be extremely noisy, for example due to ground vibrations caused by pumps required for hydraulic fracturing.

In practice it will be a cost-benefit decision which number and combinations of instrument types are installed at specific depths at a geothermal site. Such an approach could be considered for geothermal sites, and may include a value of information analysis . Benefits can be related to reduced seismic risks and safety and/or related to the economic success of geothermal projects.
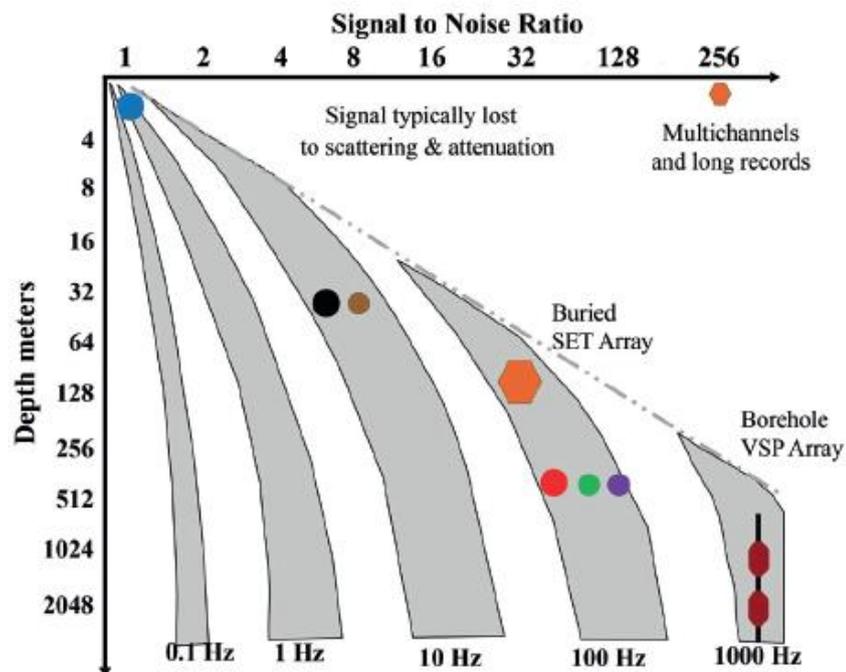
Figure 5-5   Relation between signal to noise ratio and instrument type and instrument burial depth. Blue dot: broadband seismometer. Black and brown dots: 1Hz geophone. Orange dot: 4.5 Hz seismic emission tomography sensors. Red, green and purple dots: 4.5 Hz geophones. Dark-red dots: 15 Hz VSP instruments (Adopted from Bohnhoff et al., 2018, First Break, 36, 59-65, Copyright M. Bohnhoff et al., reproduced with permission).

5.2.3   *Novel monitoring systems and data-processing techniques*
More recently various case studies have demonstrated the added value of using distributed acoustic sensing systems (DAS) within seismic monitoring networks, as well as low-cost sensors. These systems could provide additional information within a network of standardized seismometers. DAS fiberoptic cables are relatively low-

cost and can be deployed outside of the casing of the wells of a geothermal doublet. Along the fiberoptic cable strain rate measurements can be conducted at a very dense interval down to 1 m. Adequate SNR levels can be reached provided a good coupling can be realized with the cement and the surrounding medium. Low-cost sensors, such as micro-electromechanical systems accelerometers (MEMS), can play a role in public participation and perception. For instance, Stanford initiated the quake-catcher network, which is a low-cost strong motion seismic network consisting of MEMS placed in domestic buildings throughout the world. Similarly, at the Groningen site a low-cost sensor network consisting of sensors attached to internet-connected computers of a few hundred sensors was placed in domestic buildings to facilitate public participation in seismic monitoring. Although low-cost sensors have lower SNR levels, are less robust compared to standardized seismometers, and are often deployed at extremely noisy sites, they might help in acquiring additional data in uncovered areas in between seismometers and thereby densifying the spatial coverage. By optimizing placement in terms of spatial distribution and coupling of many low-cost sensors, their performance can be maximized. Issues with low-cost sensors placed in domestic houses are that they are generally only suitable to measure low frequency ground motions, and that domestic noise is high during the day and low during the night yielding data that is only useful for part of the 24-hr day/night cycle.

Furthermore, the recent development of machine learning techniques for seismic event characterization can play a complimentary role to the existing processing techniques in earthquake analysis (Holtzman et al., 2018; Ross et al., 2018). It is likely that much progress will be achieved in developing cost-effective approaches to reservoir seismic monitoring and seismic data processing. Machine learning techniques are especially efficient in analyzing large datasets and in identifying spatio-temporal trends that help improving the accuracy of reservoir seismic monitoring.

6 Synthesis of results and implications for geothermal projects in the Netherlands

This section provides a brief overview of the results from the review of international practices, knowledge and case studies relevant for induced seismicity associated with geothermal operations. It particularly focusses on the implications for safe and responsible development of geothermal projects in the Netherlands. This section is included as an easily accessible synthesis with implications for potential seismicity associated with geothermal projects in the Netherlands. It provides a brief overview linked to the more in depth analysis in the previous sections.

6.1 Key mechanisms of induced seismicity for geothermal projects in the Netherlands

Mechanisms of induced seismicity have been analyzed in detail for different subsurface operations (section 2). In this section, the key mechanisms are summarized, and implications for geothermal projects in the Netherlands are discussed. Induced seismicity may be associated with geothermal (or other subsurface) operations if the operations change the stress state of faults so that they become critically stressed, (re-)activate and accommodate seismic slip.

There is a clear difference between stimulated and non-stimulated reservoirs. For reservoir stimulation by fluid injection (i.e. tensile hydraulic fracturing or shear fracturing, cf. section 2.4), reservoir pressures are temporarily raised to values above the minimum principal stress. Therefore, the effect of pressure-dependent mechanisms leading to induced seismicity will increase during stimulation. This effect is observed in many case studies with reservoir stimulation (cf. section 3.1). Reservoir stimulation by fluid injection is currently not performed for conventional geothermal systems in the Netherlands.

For conventional geothermal systems in the Netherlands the most important mechanisms that change the stress state at faults in and around the reservoir, and that may lead to induced seismicity are:

1) **Direct pressure effects** (cf. section 2.4.1): Local changes in reservoir fluid pressure during doublet operation affect the effective normal stress on faults (Figure 6-1). If poroelastic effects are minor, injection of fluids at the injector reduces the effective normal stress resulting in a stress state where fault reactivation and associated induced seismicity is more favorable (Figure 2-3a). At the producer, effective normal stress is increased under this assumption, resulting in a stress state where fault reactivation and associated induced seismicity is less favorable (Figure 2-5b).

2) **Poroelastic stressing** (cf. section 2.4.3): Local changes in reservoir fluid volume during doublet operation cause pressure changes and elastic deformation of the reservoir (Figure 2-5). Extraction of formation fluids around the producer causes local reservoir contraction, while fluid injection around the injector causes local reservoir expansion. Poroelastic stressing affects the stress state at faults, and thereby may induce fault reactivation and seismic slip (Figure 2-5b).

3) **Thermoelastic stressing** (cf. section 2.5): Doublet operation causes a decrease of reservoir fluid temperature, in particular at the injector (Figure 6-1). Cooling of

the reservoir results in elastic deformation (contraction) of the reservoir. Thermoelastic stresses affect the stress state at faults, and thereby may induce fault reactivation and seismic slip (Figure 2-6).

These mechanisms do not act independently but interact in a non-linear manner. The combination of direct pressure, poroelastic and thermoelastic effects determine the local stress state in the reservoir and at faults. The flow properties of target formations are different for different geothermal play types. As flow properties control the pressure and temperature distribution in the reservoir, direct pressure, poroelastic and thermoelastic effects vary between different play and rock types. Geomechanical properties also vary between different rock types, and thereby the response to stress changes (cf. section 2.3). Accordingly, differences in characteristics and occurrence of induced seismicity may be expected.
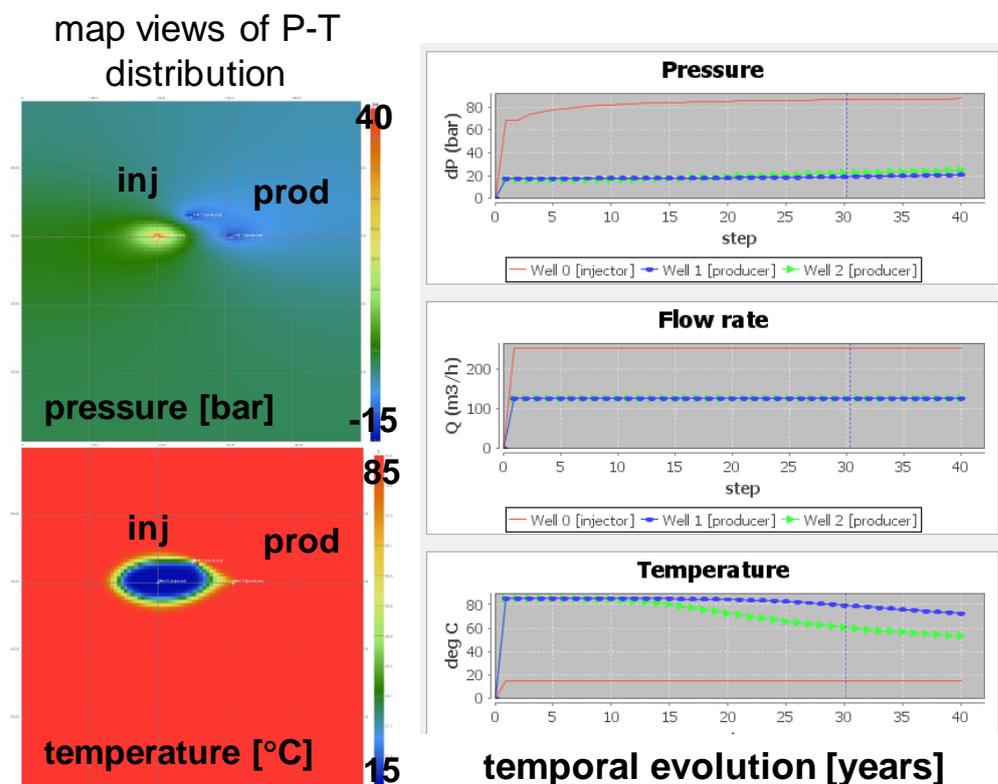
Figure 6-1　　Spatiotemporal distribution of pressure and temperature for a hypothetical geothermal system consisting of a single injector (inj) and two producers (prod). Note that the geothermal system and reservoir has typical features for systems in the Netherlands. However, horizontal reservoir permeability is anisotropic in this examples (e.g., due to fracture populations), resulting in an oval shaped pressure and temperature front in the reservoir, and different pressure and temperature interference at the two producers towards the end of operations (apparent after ~12 years of operation) (Figure produced by TNO).

Variations in fluid volume are generally local and minor for geothermal doublets, for example compared to extraction of gas. Therefore, **reservoir compaction mechanisms** responsible for induced seismicity around some gas fields in the Netherlands are of minor importance for geothermal operations (cf. section 2 and appendix B.3). It is often mentioned that induced seismicity is unlikely to occur during

doublet operation given an overall balance of fluid volume in the reservoir. However, local variations in fluid pressures occur during fluid circulation, i.e. fluid pressures are elevated around injectors and lowered around producers during circulation (Figure 6-1). Reservoir temperatures are also lowered around the injector, and in and around the entire reservoir over the lifetime of geothermal projects. If faults are located near areas with changing pressure and temperature (i.e. the pressure and temperature fronts around the wells), they can become critically stressed, reactivate and cause induced seismicity. In particular faults that are favorably oriented for reactivation may slip seismically. The relative magnitude of local variations in pressure and temperature depends on factors such as reservoir permeability.

Although **reservoir stimulation by fluid injection** is currently not performed for conventional geothermal systems in the Netherlands, it may be considered for future geothermal targets. This type of stimulation involves permeability enhancement by shear or tensile fracturing of reservoir rock (cf. section 2.4.2). During hydraulic fracturing, local reservoir pore pressures are increased to the fracturing pressure of the target formation for a limited period of time. The effect on reservoir fluid pressure near the injector is significantly larger than for conventional operation of doublets, and depends on injected fluid volumes. Total injected fluid volume can differ dramatically, depending on the scale of fracturing (i.e. compare injected volumes for stimulation of geothermal reservoirs in Appendix A to stimulation of gas shales in B.1.1). Therefore, the direct pressure and poroelastic effects described above are amplified, depending on the scale of fracturing. The resulting stress state is generally more favorable for fault reactivation and associated induced seismicity (Figure 2-3). **Acid stimulation** relies on chemical reactions (mineral dissolution) between injection fluid and reservoir rock rather than on pore pressure effects. Acid stimulation can change direct pressure and poroelastic effects due to changes in permeability and elastic properties of reservoir rock, but the effects are generally more local (near well) compared to reservoir stimulation by fluid injection and effects on the occurrence of induced seismicity are likely minor.

6.2 Spatial and temporal distribution of induced seismicity for geothermal systems in the Netherlands

The direct pressure, poroelastic and thermoelastic effects on local stress states during operation of conventional geothermal systems can be analyzed to assess the probability of reactivating local faults, and thereby determine the most likely locations and timing of seismic events should induced seismicity occur. The locations and timing of seismic events can be related to analysis of spatial and temporal distribution of pressure, temperature and stress changes during geothermal operations. The analysis only considers this relation and does not attempt to relate stress drops or energy dissipation of multiple events to the induced stress changes. Therefore, it does not encompass a probabilistic analysis of the number of events within a certain timeframe (Dost et al., 2017). As mentioned, local variation in pore fluid pressure and temperature occur during fluid circulation despite an approximate overall balance of injected and produced fluid volumes (Figure 6-1). At the injector there is a local pressure increase and temperature decrease on relatively short timescales after the onset of fluid circulation. At the producer, there is a local pressure decrease on relatively short timescales, and a temperature decrease on relatively long timescales due to progressive reservoir cooling after the onset of fluid circulation. Eventually, fluid circulation may lead to cold water breakthrough at the end of the lifetime of geothermal projects. In the reservoir, away from the injector and producer,

temperature is also decreasing on relatively long timescales. The spatial and temporal pressure and temperature distribution in the reservoir are dependent on factors such as flow rate and reservoir permeability. Outside the reservoir, stress states can be affected by pore pressure diffusion on relatively long timescales and poroelastic effects on relatively short timescales (cf. Figure 2-5). Temperature changes outside the reservoir are generally more local on relative timescales for geothermal operations, but stress changes outside the reservoir may be affected by thermoelastic stressing due to the finite cooled volume (cf. Figure 2-6c, d).

A pressure increase results in a direct pressure effect lowering the effective normal stress (cf. Figure 2-3) and a poroelastic effect due to reservoir expansion (cf. Figure 2-5). A temperature decrease results in a thermoelastic effect due to reservoir contraction (cf. Figure 2-6). If faults are present in the vicinity of the injector, these effects may alter their stress state so that they become critically stressed and prone to inducing seismicity (cf. Figure 2-6b). Accordingly, seismicity in the vicinity of the injector may occur on relatively short timescales after the onset of fluid circulation. Seismicity in the vicinity of the producer may occur on relatively short timescales due to poroelastic effects (cf. Figure 2-5b), and on relatively long timescales due to thermoelastic effects (cf. Figure 2-6b). These findings stress the need for long term seismic monitoring during the entire lifetime of geothermal operations. In practice it may be challenging to mitigate seismicity occurring after years of operation as thermoelastic effects and (possibly) pore pressure diffusion have been taken place over long timescales. However, long term seismic monitoring can provide valuable insight into relations between subsurface perturbations and seismicity due to doublet operation that aid understanding and assessment for other geothermal projects. Also, information of the source and location of seismic events aid assessments of possible interaction between doublets and other subsurface activities.

6.3 Key factors affecting induced seismicity for geothermal projects in the Netherlands

The key parameters influencing induced seismicity in geothermal systems have been analyzed on the basis of case studies worldwide (section 3.2, Table 3-2). In this section, key factors are summarized. Implications are also discussed, focusing on the importance for geothermal systems in the Netherlands and on the potential for inducing felt seismicity (M > 2).

Geothermal play & system type: Geothermal plays are characterized by a specific geological setting that includes a heat source, heat migration pathway, heat/fluid storage capacity (reservoir), and the potential for economic recovery of the heat (Moeck (2014) cf. section 1.2). Relevant geothermal play types have been classified based on factors such as target rock type, depth and operational characteristics (section 3.2, Figure 3-9 to Figure 3-13). Geothermal systems exploit the geothermal resources within plays. Geothermal fields (hydrothermal fields), Hot-Dry Rock (HDR) and Enhanced or Engineered Geothermal Systems (EGS), and low to moderate temperature (30 - 150°C) permeable sedimentary aquifers are distinguished as geothermal system types. The design and operational characteristics can be different for different geothermal play and system types.

Geothermal plays can be convection-dominated in areas that are characterized by high enthalpy geothermal reservoirs, active tectonic processes and high surface heat flow (e.g., Iceland, appendix A.8). Well configurations in this play may be based on

single producing well or multiple producing and injection wells, and can be used for both electricity generation or district heating (e.g., an Enhanced Geothermal System or EGS). Conduction-dominated geothermal plays are characterized by low enthalpy geothermal reservoirs, by little or no tectonic activity and by low surface heat flow. Well configurations in this play are usually doublet systems or systems with multiple wells to produce hot water for district heating or industrial demand of heat, and wells to re-inject cooled water for circulation.

Three main types of geothermal target formation have been distinguished within different play types: (1) High porosity sedimentary rocks with the matrix controlling the flow (e.g., sites in the North German Basin targeting the Keuper, the Dogger in the Paris Basin, and some of the geothermal sites in the Netherlands, (2) tighter cemented or fractured sedimentary rocks with flow predominantly controlled by the (natural or induced) fractures (e.g., the Malm carbonates in the Molasse Basin and the tight Triassic and Permian sandstones in the Upper Rhine Graben, and (3) fractured crystalline or volcanic rocks with flow controlled by the fracture system where stimulation is usually required to enhance the permeability (e.g., the Geysers in the U.S.A.). Temperatures of geothermal reservoirs can be controlled by conduction- or convection-dominated heat transfer depending on regionally geological settings.

In the near future, porous sandstones will likely dominate new geothermal targets in the Netherlands. Accelerated development of geothermal projects may drive development towards hotter, tighter and more competent sandstone reservoirs or fractured sedimentary formations. Large temperature contrasts and high rock competence may lead to more prominent thermoelastic effects on the stress state at faults and in the reservoir. Higher rock competence in itself can also make the rocks more prone to seismicity. Crystalline (basement) rocks have currently not been encountered in wells and depth of crystalline basement is largely unknown in the Netherlands. Crystalline rocks may only become relevant targets if geothermal development becomes feasible at depths far beyond that of current oil & gas reservoirs.

Well configurations in the Netherlands are mostly doublets, consisting of an injection well (injector) and a producing well (producer). Most systems consist of two wells although some systems with more injectors or producers have been operational (Figure 6-1, section 4.1). The main principle of a doublet is that heat is produced by circulation of hot formation fluids from a reservoir (aquifer) via the producer to surface infrastructure, and back to the reservoir via the injector. The surface infrastructure includes a heat exchanger that transfers heat from the circulating formation fluid to a separated heat network. A doublet system with injectors and producers accessing an aquifer is approximately a closed system, i.e. fluids produced are injected again. As mass may be locally removed by scaling (i.e. precipitation of solids) in wells or different parts of the reservoir, local mass balance is only approximately maintained in the reservoir during fluid circulation. Although scaling has minor influence on total fluid mass in the reservoir (i.e. reducing dissolved matter), it may affect reservoir permeability and thereby injectivity at the injector, productivity at the producer and overall pressure distribution in the reservoir. Operation of *conventional geothermal systems* in the Netherlands generally does *not* involve reservoir permeability stimulation by fluid injection ("hydraulic fracturing"). Reservoir permeability enhancement by acid stimulation to increase well injectivity or productivity is more common.

<u>**Geological factors affecting the occurrence of induced seismicity**</u>: Case studies show that most geothermal systems with felt seismicity operate in **play types** characterized by low porosity formations with flow dominated in fractures or faults (e.g., fractured sedimentary or crystalline rocks, Figure 3-9, Figure 3-10). No felt seismicity has been associated with conventional (conduction-dominated) geothermal systems targeting porous sandstone aquifers that do not require stimulation of reservoir permeability. Of the three main geothermal plays or classes of target rock types identified (section 3.2, Figure 3-9, Figure 3-10), two are most relevant for the Netherlands: (i) high porosity sedimentary rock with flow controlled by matrix porosity (e.g., the Permian to Cretaceous sandstone targets) and (ii) tighter cemented or fractured sedimentary rocks with flow controlled by fractures (e.g., the Dinantian carbonate targets). All geothermal plays in the Netherlands are conduction-dominated. There is some indication for the occurrence of temperature anomalies associated with convection (Lipsey et al., 2016), but the contribution of convection is not comparable to that in convection-dominated geothermal plays in areas with active tectonics and high heat flow.

The **depth** of target formations affects **reservoir pressure** and **temperature** as well as the mechanical (**rock competency**) and **flow** (porosity and permeability) properties of rocks. For operations at depths shallower than 2 km felt seismicity is not observed in the investigated case studies. For conduction dominated geothermal systems no felt seismicity was observed for depths below 3 km. Except for the Californië geothermal projects that target fractured or karstified carbonates (appendix A.11.4), all current geothermal systems in the Netherlands target porous sandstones at depths of 1.0-3.0 km.

Reservoir temperature mainly impacts the thermoelastic effect as geothermal operations may result in a larger temperature drop and associated reservoir contraction for higher reservoir temperatures. Case studies show that felt seismicity is usually associated with medium- and high-enthalpy fractured reservoirs (T > 100°C). Currently, reservoir temperatures for conventional geothermal systems in the Netherlands are between 65 and 100 °C.

Rock competency affects stress buildup in formations, i.e. more competent rocks (e.g., granites or some carbonate rocks) can build up more stress and fail in a more brittle manner compared to creeping rock types (cf. section 2.3). The relationship between rock type and induced seismicity is complex, but most of the seismicity observed in the case study review seems to occur in competent rocks. Rock competency of the sedimentary formations that are geothermal targets in the Netherlands is likely much lower than that of crystalline rocks that are more prone to felt seismicity. For the porous sandstone targets in the Netherlands, rock competency may be low for unconsolidated Jurassic and Cretaceous targets, and higher for consolidated and cemented Triassic and Permian targets.

Geothermal area (i.e. the area accessed by geothermal operations) can be large for volcanic fields compared to sedimentary targets, but volcanic fields do not occur in the Netherlands so this factor is of limited importance. Doublet spacing can be considered as an indication of geothermal area for conventional geothermal systems in the Netherlands. For such systems, effects may only be relevant if a number of systems target the same geothermal reservoir. The **presence of large faults** may be most critical for the geothermal targets in the Netherlands, in particular if they are

active, critically stressed, and/or optimally oriented in the present stress field. Fault zones and fracture populations may be beneficial for reservoir permeability and flow rates, but large faults are also prone to inducing felt seismicity. As mentioned, local pressure and temperature variations caused by doublet operation may lead to induced seismicity, in particular if large faults are present near injectors. For the porous sandstone targets in the Netherlands, faults can be present as relatively large reservoir-bounding faults or can intersect parts of the reservoir. For the fractured carbonate targets, faults and fractures are more widespread throughout the reservoir. While large faults may be mapped using seismic data, limits in resolution of seismic data may prevent detection of smaller faults that can still generate felt seismicity if reactivated (Figure 6-2).
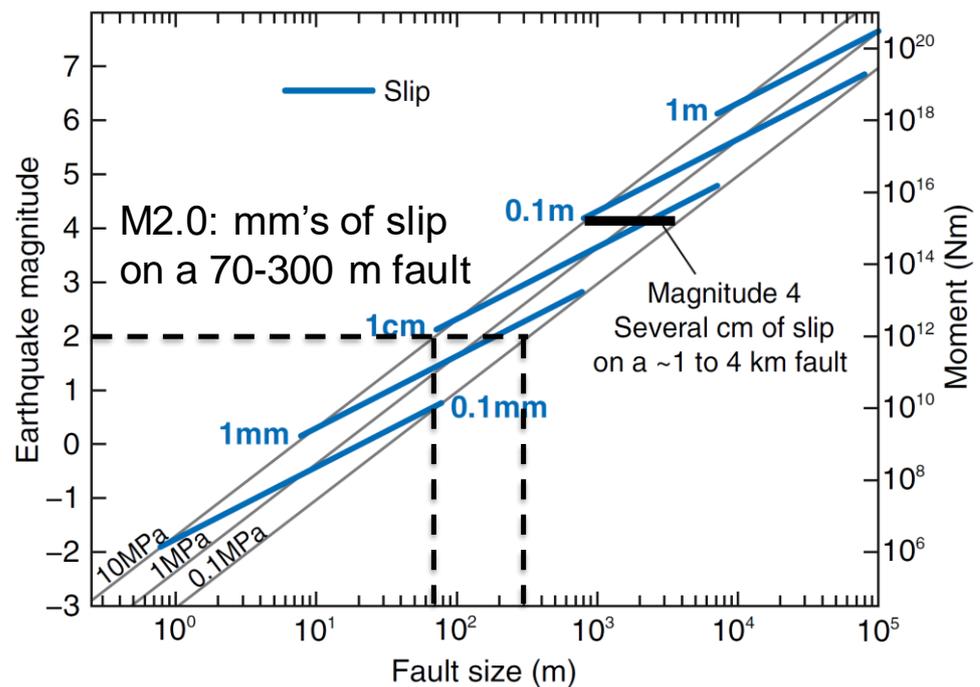
Figure 6-2   Relation between reactivated fault size and earthquake magnitudes (left axis) or seismic moments (right axis). Faults that can potentially generate M 2 earthquakes may not be mapped before commencement of operations due to limitations of the resolution of seismic surveys in terms of fault sizes (> 300 meter resolution is common for standard approaches) (From Zoback and Gorelick, 2012 (PNAS 109: 10164-10168), Copyright Zoback and Gorelick, published under a Creative Commons License).

In general, large **differential stress** promotes fault reactivation and induced seismicity as faults tend to be more critically stressed compared to faults in a more isotropic stress state. Stress regimes in tectonically active regions (for example close to mountain belts) may be prone to generating larger differential stresses, although local stress state may not follow regional trends. Different tectonic stresses may be expected for the southeast of the Netherlands (maybe extending into the West Netherlands Basin) compared to other parts of the Netherlands. The prevailing stress regime in most tectonically inactive regions in the Netherlands promotes normal faulting ($S_v>S_{Hmax}>S_{hmin}$), although anthropogenic operations may lead to reverse faulting (Wiprut & Zoback, 2000). Geothermal operations in regions prone to inducing felt seismicity can have prevailing stress regimes that (also) promote reverse

($S_{Hmax}>S_{hmin}>S_v$) or strike slip ($S_{Hmax}>S_v>S_{hmin}$) faulting. Fault properties as well as occurrence of induced seismicity are known to change with faulting regime. For example, the fault zone architecture of strike slip faults may differ from normal faults (Moeck, 2014). Accordingly, the combination of large faults, fault properties and structure, stress regime and differential stress determines the likelihood of felt seismicity.

As pore fluid pressure controls the effective stress, **hydraulic connection to depth** is important for the occurrence of felt seismicity, in particular if the stress state of large faults in crystalline basement rocks is altered. Case studies show that large fault zones may act as fluid conduits that may extend pressure diffusion and poroelastic pressure changes to locations far away from the wells, and increase the likelihood of reactivating a critically stressed fault patch (cf. section 2.2). Besides hydraulic connection, mechanical decoupling between geothermal targets and crystalline basement is important (cf. section 2.3). Creeping formations (e.g., claystones, shales or rocksalt) have a tendency to release stress aseismically as well as hydraulically seal formations, i.e. geothermal targets that are underlain by such formations are less prone to generating felt seismicity. In Netherlands, the exact depth of crystalline basement is largely unknown, but it is likely located at much greater depth than most geothermal targets. Moreover, a likely thick sedimentary sequence between the geothermal targets and crystalline basement in the Netherlands probably hydraulically seals and mechanically decouples target formations from basement rocks.

Operational factors affecting the occurrence of induced seismicity: Case studies show that felt seismicity is usually associated with large **reservoir pressure increase** due to fluid injection (typically above 10 MPa wellhead injection pressure for igneous rocks, Figure 3-11a). Such injection pressure is usually only achieved during reservoir stimulation by fluid injection. Such stimulation is currently not performed for conventional geothermal systems in the Netherlands. Induced seismicity has been observed during fluid circulation at low wellhead pressures in fractured carbonate formations in the Molasse Basin (appendix A.2), which may be relevant to some extent for the Californië geothermal projects. For fluid circulation during doublet operation, maximum reservoir pressure change is related to factors such as reservoir permeability, fluid composition and flow rate, i.e. maximum reservoir pressure change may be higher for tighter reservoirs. Reservoir pressure increase due to geothermal operations mainly impacts the direct pressure effect as it reduces the effective normal ("clamping") stress on faults (cf. section 2.4.1), and the poroelastic effect as it increases reservoir expansion (cf. section 2.4.3). Case studies show no clear correlation between the occurrence of felt seismicity and **net injected volume or flow rate** for the range of injected volumes (Figure 3-11b, c). If the analysis is extended to include other subsurface operations that involve much larger range of net injected volumes (e.g., waste water disposal), maximum earthquake magnitudes are observed to increase with injected volume (Figure 3-14). Net injected volume and flow rate impact the direct pressure, poroelastic and thermoelastic effects as they affect the pressure and temperature distribution in the reservoir. The conventional geothermal systems in the Netherlands exhibit maximum flow rates of 80-390 m³/hr (approximately 20-120 l/s) and rely on fluid circulation with an overall net injected volume of zero. It should be emphasized that fluid volumes may vary locally during operations. For these conditions, net injected volume and flow rate do not seem to exert a major influence on the occurrence of induced seismicity. If hydraulic fracturing is considered in the future to develop geothermal systems in

tighter formations, larger maximum reservoir pressure changes and net injected volume may become feasible.

It should be emphasized that the occurrence of felt seismicity is controlled by the interaction of geological and operational factors. For example, reservoir characteristics as well as injection pressure determine the pressure and temperature distribution in the reservoir and thereby the potential occurrence of induced seismicity. Analysis of factors separately is useful to identify trends and to assess their relative importance for the occurrence of felt seismicity. However, a fundamental problem is that causal relations may be difficult to establish as different factors are changing simultaneously from one geothermal project to another. All factors are **site- or project-specific**, and should be jointly analyzed to assess the likelihood of inducing felt seismicity. The interaction of site-specific factors makes it difficult to uniquely **rank or score the different factors** in terms of relevance for determining the occurrence of induced seismicity and quantify seismogenic potential. A decision tree for different levels of seismic hazard and risk assessment that includes a scoring of parameters has been suggested in a framework for seismic hazard assessment in geothermal projects (Baisch, S. et al., 2016). In general, most studies agree that the most critical factors for induced seismicity are (1) local stress state with higher seismogenic potential for areas where the stress state is close to rock strength or close to a critical stress state for fault reactivation, (2) presence of faults at critical orientations with respect to the stress field, (3) reservoir-specific relations between pore pressure changes due to injection and stress changes with higher seismogenic potential for low permeability or fractured reservoirs (in particular if reservoir stimulation by fluid injection is performed), (4) the spatial distribution of pressure and stress controlled by the local geology with higher seismogenic potential for situations where large areas are affected by pore pressure changes and if hydraulic connection with critically-stressed faults or underburden (basement rocks) is established.

6.4 Issues with monitoring seismicity for geothermal projects in the Netherlands

A light review of traffic light and monitoring systems for geothermal sites was performed (section 5). Current practices for implementing traffic light systems and characteristics of monitoring networks are described. In this section, some issues with monitoring seismicity for geothermal projects in the Netherlands are addressed. Seismic monitoring is crucial for understanding and mitigating the occurrence of induced seismicity. Induced seismicity can be used to monitor subsurface processes if they result in seismic slip along faults or fractures, thereby providing a better understanding of the effect of geothermal operations in the subsurface. Critical are limits in resolution of different seismic monitoring networks (Bohnhoff et al., 2018). The magnitude detection limit of earthquakes (**magnitude of completeness**) is dependent on the type and design of monitoring networks. The completeness-of-detection magnitude limit is much smaller than the location-completeness magnitude limit, i.e. the magnitude of earthquakes that can be detected is lower than magnitudes required to determine hypocenter locations (Figure 6-3; B. Dost 2018, pers. comm.). The southwestern part of the Netherlands is an exception with a magnitude of completeness of approximately M2.0. It means that felt seismicity as defined in this study (M > 2.0) can be detected using the regional seismic monitoring networks, but accurate hypocenter locations are difficult to determine. When considering public perception or damage to surface infrastructure, peak ground velocity (PGV) is a better indicator than earthquake magnitude. PGV levels that are acceptable from a public

perception point of view may be lower in areas prone to enhanced ground motions due to seismic waves (a PGV of 0.3 mm/s, corresponding to approximately M~0, is often taken as a threshold for public perception, section 5.2.2).
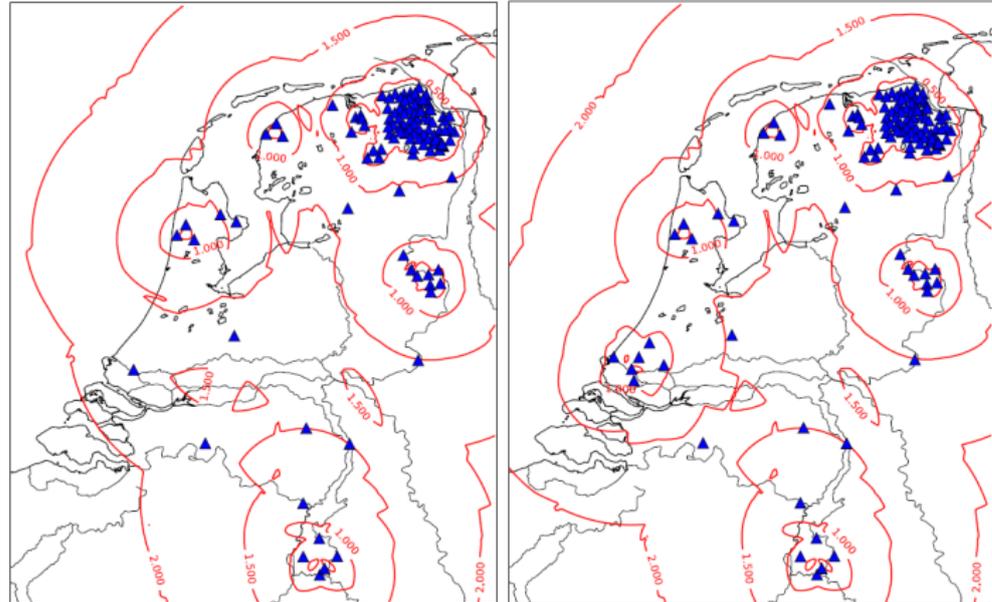
Figure 6-3   Location magnitude threshold for the Netherlands based on all available seismic stations in operation. Red contours indicate   magnitude thresholds. Left figure : situation in January, 2019. Right figure: situation after foreseen installation of a borehole network in southwest of the Netherlands (From B. Dost, KNMI, pers. comm. by e-mail).

Claims of **causal relations** between seismicity and subsurface operations are usually based on **temporal and spatial relations**. Evidence for causal relations is most convincing if observed seismicity can be explained by models that forecast the spatiotemporal distribution of stress changes and reactivation of faults that have been mapped upfront using passive seismic data. The spatiotemporal relation between seismicity and injection operations for reservoir stimulation may be more clear than for fluid circulation. If progressive subsurface stress changes occur over relatively long timescales (e.g., for fluid circulation or due to pressure diffusion), temporal relations may be complex with seismicity occurring months or years after the onset of geothermal operations. Regional seismic monitoring networks are not suitable to locate earthquake hypocenters with the degree of accuracy required to investigate spatial relations between seismicity and specific subsurface operations. Local seismic monitoring seismic monitoring networks can provide more site-specific data on seismicity with lower magnitude threshold and higher accuracy of hypocenter locations (see for example monitoring of the Californië or Balmatt geothermal projects, cf. appendix A.11.4). Dedicated monitoring networks that are specifically designed to perform **reservoir seismic monitoring** can have much lower detection levels (M < -2.0), and horizontal (<2000 meter) and vertical (<500 meter) error in event locations (cf. section 5.2). Dedicated seismic monitoring may be required to investigate adequately possible causal relations between seismicity and subsurface operations in areas prone to natural seismicity or areas with different subsurface operations that potentially interact. However, networks capable of reservoir seismic monitoring are expensive.

Subsurface data and knowledge, in particular of the **regional velocity model**, are critical for the assessment of spatial relations between seismicity and operations (section 5.2.1). Parts of the Netherlands lack accurate data of shear wave velocity which limits accurate assessment of seismic source locations. For example, accurate data on shear wave velocity can significantly improve source location assessment of the seismicity that occurred in the vicinity of the Californië geothermal projects. Additional seismic data at specific frequency, or data from dipole sonic well logs, downhole calibration shots and vertical seismic profiling can be used to more accurately assess earthquake hypocenters, and thereby a better assessment of potential causal correlations between seismicity and geothermal operations can be made.

Baseline monitoring of (natural) seismicity need to be considered in establishing causal relations between seismicity and subsurface operations. It is therefore recommended that seismic monitoring covers a baseline period (typically 6-12 months), the period of geothermal operations, and a post-production period (section 5.2). For operations in areas prone to natural seismicity, causal relations may only be convincingly demonstrated if there are data on both the induced and natural seismicity, and if both types of seismicity can be distinguished. For operations in areas with different (past) subsurface operations that potentially interact, it may be very difficult to convincingly link seismicity to individual operations. Geomechanical modelling of the relative contribution of different operations may aid in establishing causal relations between seismicity and subsurface operations.

6.5 Seismogenic potential for geothermal projects in the Netherlands

The analysis of mechanisms, key factors and case studies of seismicity in geothermal projects allow the likelihood of induced seismicity ("**seismogenic potential**") for geothermal projects in the Netherlands to be assessed. Seismic risks are determined by the seismogenic potential as well as the impacts of induced seismicity (cf. section 1.3). Seismic risk analysis requires additional site specific examination of seismic wave attenuation and site response (e.g., application of ground motion prediction equations) as well as surface conditions and effects (e.g., potential damage to infrastructure, costs, health & safety, Grünthal, 1998). Therefore, seismic risks are not determined in this study. It should be emphasized that both seismogenic potential and seismic risks critically depend on local conditions. Therefore, assessment of seismogenic potential and seismic risks for individual projects should be based on site-specific analysis.

Here, a qualitative assessment of seismogenic potential for 5 current and potential future geothermal plays in the Netherlands is made following the criteria outlined in section 1.4 (Table 6-1; cf. Table 1-2; section 4.2). The five plays are: (1) Jurassic/Cretaceous permeable porous sandstone reservoirs, mainly in the southwestern part of the Netherlands, (2) Triassic and Permian tight or permeable porous sandstone reservoirs, in the southwestern part and northern part of the Netherlands, respectively, (3) Dinantian fractured or karstified carbonate reservoirs in the southeastern part of the Netherlands affected by active tectonics in the Roer Valley Graben (labelled RVG Dinantian carbonates), (4) Dinantian fractured or karstified carbonate reservoirs in the central (including southwestern part) and northern parts of the Netherlands away from the Roer Valley Graben (labelled CNNNLD Dinantian carbonates, e.g. in the area near Luttelgeest in the northern part

of the Netherlands), (5) deeper (Devonian) sedimentary reservoirs (e.g., Devonian Condroz Sandstone).

In the Netherlands, no seismicity has been associated with geothermal operations in porous sandstone reservoirs (Permian and Triassic, and Jurassic/Cretaceous plays, section A.11). Seismicity occurred in the vicinity of the Californië geothermal projects targeting Dinantian fractured/karstified carbonate reservoirs in the Roer Valley Graben (RVG Dinantian carbonates, Table 6-1, cf. appendix A.11.4), but an unequivocal causal relation between geothermal operations and seismicity has not (yet) been established. However, geothermal operations were put on hold and no geothermal operations in fractured/karstified carbonate reservoirs are currently active. The Balmatt geothermal project in Belgium targets the same formation, and induced seismicity has been recorded (appendix A.11.4). The other plays have not yet been targeted by geothermal operations.

The review of case studies shows that geothermal projects targeting porous sandstones in the North German Basin (appendix A.3) and Danish Norwegian Basin (appendix A.5) are good analogues for the porous sandstone plays in the Netherlands. Target rock types are similar porous sandstones with flow controlled by matrix porosity, some of which are Permian Rotliegend or Triassic Bundsandstein formations. Geological settings are intracratonic basins with crystalline basement at large depth and large vertical separation between geothermal reservoir and basement. Geothermal plays include low enthalpy reservoirs at 1.5-2.5 km depth with reservoir temperatures of 60-125°C. Although geothermal operations have been active for more than 30 year in some cases, no felt seismicity has been observed. The Molasse Basin is a reasonable analogue for the fractured/karstified carbonate plays because targets are fractured carbonate rocks with flow controlled by fractures or karst structures (low matrix porosity). However, targets are Dinantian carbonates in the Netherlands and Malm carbonates in the Molasse Basin. Other differences are that the Molasse Basin is a foreland basin with the basement close to the geothermal target, that the stress state is likely different, that some projects specifically target faults for permeability, and that the targets are low to medium enthalpy reservoirs at 2.0-3.5 km depth with reservoir temperatures of 70-150°C (e.g., Sankt Gallen, cf. appendix A.2.4). Felt seismicity (M > 2) is reported for 3 out of 27 projects that were reviewed for the Molasse Basin. For the other plays, no good analogues were found (mainly because formation properties and flow regimes are uncertain).

The review of key mechanisms and factors for induced seismicity (sections 2, 3.2) indicates that mechanisms for fluid circulation in low enthalpy, conduction-dominated geothermal targets are not likely to lead to felt seismicity. For porous sandstone targets in the Netherlands all factors indicate a low to medium seismogenic potential (Table 3-2). Projects may only exhibit medium seismogenic potential for the more deeper, more competent, and potentially tight Triassic and Permian sandstone targets if operations cause large changes in reservoir temperature or interact with large optimally oriented faults (in particular if the faults cause hydraulic connection with deeper crustal levels) or with other subsurface operations (e.g., gas depletion), or if reservoir stimulation is performed to develop tight sandstone reservoirs. For the RVG Dinantian carbonate targets in the Netherlands some factors indicate a medium seismogenic potential, including larger reservoir pressure changes, higher competency of rocks, and interaction with natural faults that are potentially critically stressed. Limited information is available for the CNNNLD Dinantian carbonate targets, and the seismogenic potential critically depends on site-specific settings.

They may exhibit a low seismogenic potential if operations are restricted to fluid circulation and if interaction with natural faults can be prevented. If flow is dominated by fractures, interaction with natural faults may increase the seismogenic potential to medium. Pore pressure diffusion may occur over larger distances in these targets compared to porous reservoir targets. The regional tectonic setting in the southeastern part of the Netherlands with known occurrence of natural earthquakes, some of which were reported to occur at fairly shallow depth, suggests a higher seismogenic potential for the RVG Dinantian carbonate targets than for the CNNNLD Dinantian carbonate targets and porous sandstone targets in the west and north of the Netherlands. The seismogenic potential for the CNNNLD Dinantian carbonate targets is therefore likely lower than (best case) or equal to (worst case) that of the RVG Dinantian carbonate targets, hence low to medium. Almost no information is available for the deeper (Devonian) sedimentary targets, and seismogenic potential will critically depend on flow behaviour (likely fracture-dominated flow) and location of these targets (i.e. higher seismogenic potential may be expected for locations in or close to the Roer Valley Graben compared to other parts of the Netherlands). The larger depth of these targets suggest a higher (medium) seismogenic potential compared to the overlying targets.

Accordingly, observations of induced seismicity in current plays and analogue basin in combination with analysis of key factors for induced seismicity indicate (ranked according to increasing seismogenic potential, Table 6-1) (1) an overall low seismogenic potential for Jurassic/Cretaceous sandstones, (2) an overall low-medium seismogenic potential for the Triassic/Permian sandstones (mainly depending on rock competency, reservoir temperature, presence of critically stressed faults, level of reservoir stimulation and potential interaction with other subsurface operations), (3) an overall low-medium seismogenic potential for the (RVG and CNNNLD) Dinantian carbonates depending on location and local settings (mainly influence of active tectonics in the Roer Valley Graben), and (4) a medium but very uncertain seismogenic potential for deeper (Devonian) sedimentary targets (mainly due to increasing seismogenic potential with depth). The seismogenic potential of Triassic/Permian sandstone targets is likely lower than that of the CNNNLD Dinantian carbonate targets if flow in the carbonates is dominated by fractures. In general, the seismogenic potential of future plays (Devonian, Dinantian or other plays) consisting of tighter sandstone reservoirs or fractured sedimentary formations is largely unknown, in particular in areas other than the Roer Valley Graben in the southeastern part of the Netherlands. Deeper targets close to the Roer Valley Graben are likely to have medium seismogenic potential, comparable or higher than the RVG Dinantian carbonate geothermal play, although this picture may change when more experience with developing these plays is gained. More insight into the seismogenic potential of these future plays will be gained by conducting a (research) program that include the drilling of wells and injection tests.

A low seismogenic potential basically means that felt seismicity is unlikely to occur, although it cannot be excluded. As a general rule, felt seismic events cannot be excluded, mainly due to uncertainties of the presence, stress state and properties of faults, and due to potential interaction with other subsurface operations such as gas production. For targets with a medium seismogenic potential, mitigation measures for induced seismicity may be required such as implementing a traffic light system for operations (Baisch, S. et al., 2016). If such a traffic light system is properly designed (cf. section 5), the probability of felt events can be reduced and the occurrence of a

longer time period with multiple felt events is unlikely as exemplified by the experience with the Californië geothermal projects.

Although this *play-based* qualitative ranking of seismogenic potential is too general to directly apply to individual projects within the plays (i.e. site-specific analysis is still required to determine a *project-based* ranking), it helps in determining optimum strategies to accelerate development of geothermal energy in the Netherlands. Within a portfolio of geothermal projects in the Netherlands, it can be used to assist in determining the optimum order or priority of project development and in de-risking of portfolio development by differentiating in mitigation measures between targets.

Geothermal play	# systems producing/ total (NL)	Seismicity occurred in play?	Analogues (similarity, cause)	Seismicity analogue case	Effect of key factors	Seismogenic potential
Jurassic/Cretaceous sandstones	11	No	North German & Danish Norwegian basins (good)	0/8	Low	Low
Permian/Triassic sandstones	6	No	North German & Danish Norwegian basins (good)	0/8	Low-medium	Low-medium
RVG Dinantian carbonates	2	Yes (Californië[1], Balmatt)	Molasse Basin (reasonable, basement)	3/27	Medium	Medium
CNNNLD Dinantian carbonates	-	-	-	-	Low-medium	Low-medium
Deeper (Devonian) sedimentary targets	-	-	-	-	Medium	Medium (uncertain)

Table 6-1   Seismogenic potential for the 5 geothermal plays distinguished in the Netherlands (Table produced by TNO). [1]Causal relation between operations and seismicity under investigation.

Besides the likelihood of induced seismicity or seismogenic potential, analysis of **seismic risk** includes assessment of the effects. The occurrence of seismicity in the vicinity of the Californië geothermal projects targeting fractured/karstified carbonates has led to a stop of operations. Other factors that may increase seismic risk by increasing the effect of seismicity are surface conditions such as the presence of vulnerable infrastructure, and the vicinity of other subsurface operations such as extraction of natural gas. For example, drilling-induced seismicity has been observed near Midlaren in 2009 (section 0). Although drilling was conducted for production of natural gas in these cases, drilling of geothermal wells in the vicinity of gas reservoirs may lead to increased seismic risk. In general, geothermal operations in the vicinity of operations for production of natural gas may have elevated seismic risk due to interaction of subsurface processes.

Besides technical factors that determine seismic risk, **social factors** are equally or even more important for the future of geothermal projects. The development of geothermal energy in Europe was seriously hampered by the occurrence of the *M*3.4 and *M*3.5 earthquakes in Basel and Sankt Gallen in Switzerland. Recently, the *M*5.4 earthquake in Pohang, South Korea has intensified discussion on seismic risks associated with geothermal operations. Although occurring in markedly different geological settings compared to the Netherlands, **public perceptions** of geothermal energy development are affected. Although felt seismicity is most critical in affecting

public perceptions, efforts to detect induced seismicity with lower magnitudes greatly helps to understand mechanisms leading to felt seismicity and to provide a more robust knowledge base in the public debate. In the Netherlands, the occurrence of induced seismicity associated with subsurface operations has particular focus of attention mainly due to frequent occurrence of seismicity associated with depletion of gas in the Groningen gas field in the North of the Netherlands. Although mechanisms of induced seismicity are different for gas depletion compared to geothermal energy extraction, public perceptions affect both operations. Accordingly, seismic risks need to be properly managed and mitigated in order to ensure safe operations so that geothermal projects will be positively perceived by the public and maintain a long term **social license to operate**.

6.6 Mitigation measures for seismic risks

Preventive and control measures can be implemented to mitigate seismic risks, for example in a bow-tie approach to analyse seismic risks (de Waal et al., 2017). Preventive measures mainly reduce the probability that an incident occurs, while control measures mainly mitigate the effects of incidents. For seismic risks associated with geothermal operations, important preventive measures are (1) to **improve or optimize the design of operations**, (2) to **characterize the subsurface** focussing on the presence of optimally oriented faults and modelling the spatiotemporal distribution of stress changes and potential reactivation of mapped faults, and (3) to perform baseline monitoring of seismicity long (typically 6-12 months) before the start of operations. The most important control measure is the implementation of a **traffic light system** to modify or terminate operations when seismicity exceeds a certain pre-defined threshold (cf. section 5.1).

Considering the key factors affecting induced seismicity, optimized design of geothermal operations may focus on reducing the **maximum pressure increase** in the reservoir and on planning wells away from large fault structures. If reservoir stimulation by fluid injection is considered, **limiting net injected volume** and/or performing **cyclic stimulation** (Hofmann et al., 2018). **Seismic surveys** may be used to characterize the subsurface in terms of the lateral extent of geothermal reservoir and location of large faults before the start of operations. It should be emphasized that seismic resolution is an important issue as faults may be too small to be detected using seismic data but large enough to cause felt seismicity (Figure 6-2).

Traffic light systems can be considered as an integral part of protocols for seismic hazard and risk management and mitigation in cases of elevated seismic risks (section 5.1). The design of the traffic light system is critical with thresholds that are based on a mechanistic understanding of seismicity and that account for seismicity after shut-in of operations. It is crucial to define beforehand (1) what acceptable thresholds of maximum observed seismic magnitude or peak ground velocity or acceleration are, (2) what measures need to be performed if thresholds are exceeded, (3) what criteria are used to evaluate the success of the traffic light system, and (4) what and when modifications will be performed if performance of the traffic light system is not acceptable. There also needs to be consideration of the fact that the largest induced earthquakes may occur after the traffic light systems enforces shut-in of operations. Thresholds based on ground motion indicators (in particular peak ground velocity) are generally preferred above thresholds based on seismic magnitudes as ground motions determine the effects of seismicity at the surface. If

reservoir stimulation by fluid injection is considered, it is important to consider that research suggests that maximum earthquake magnitudes during operations occur after steep pressure gradients following shut-in or flow back of wells (Häring et al., 2008; Hofmann et al., 2018). Technical as well as public perception criteria need to be considered to maintain a social license to operate. In any case, thresholds for traffic light systems should acknowledge site-specific factors such as seismic wave propagation in the (shallow) subsurface and population density. In the Netherlands it is currently unlikely that geothermal operations would be allowed to continue following felt seismicity. It may be considered to specifically design traffic light systems as to avoid damage at the surface. Adaptive traffic light systems that update the thresholds in real-time based on temporal forecasting of induced seismicity may only be relevant if reservoir seismic monitoring systems are operational and seismic magnitudes remain far below that of damaging seismicity.

7 Conclusions

The research conducted in this project on "*Seismicity in geothermal projects*" focussed on reviewing international practice, knowledge and case studies relevant for understanding induced seismicity and assessing the seismogenic potential of geothermal operations.

The main research activity was an extensive review of the occurrence of induced seismicity in case studies including geothermal and other types of project involving relevant subsurface operations. The review served as a basis to (1) review mechanisms of induced seismicity, (2) identify key parameters affecting the occurrence of induced seismicity in geothermal systems, (3) perform a light review of seismic monitoring and traffic light systems, (4) summarize the current status of geothermal energy development and geothermal targets in the Netherlands, and (5) discuss implications for geothermal projects in the Netherlands.

The research allows the following conclusions to be made:

- For conventional geothermal systems that are based on fluid circulation for heat production, **key mechanisms that determine stress changes in and around the reservoir and potential of induced seismicity are direct pressure effects on effective normal stress, poroelastic stressing due to pressure-dependent reservoir expansion or contraction, and thermoelastic stressing due to temperature-dependent reservoir contraction**.
  The location and timing of seismic events are determined by the interplay of direct pressure, poroelastic and thermoelastic effects with most prominent effect exerted by direct pressure effects in fault zones. Direct pressure and poroelastic effects occur on relatively short timescales, while thermoelastic effects caused by progressive cooling may occur on relatively long timescales. As poroelastic and thermoelastic effects can occur without hydrological connection, seismicity can occur both inside and outside the reservoir (Figure 2-5; Figure 2-6). The mechanisms interact in a non-linear manner, depending on site-specific geological and operational factors. Operational factors (e.g., injection rates) can be varied to minimize induced seismicity, but only to a limited extent. Geological factors such as the presence, geometry and stress state of faults, and interaction with these factors by operations are critical. Faults that are favourably oriented for reactivation and seismic slip need to be present for induced seismicity to occur, and site-specific analysis is required to fully assess these factors. If reservoir stimulation by fluid injection (hydraulic fracturing) is considered, the direct pressure and poroelastic effects become more prominent and likelihood of inducing seismicity may increase, in particular near the injector (section 6.1-6.2). Overall, the likelihood of inducing felt seismicity is relatively low for conventional geothermal systems based on fluid circulation relying on matrix porosity without reservoir stimulation, and the occurrence of seismic events likely will be absent for such systems.

- The review of case studies worldwide showed that **geological settings in the North German Basin and Danish-Norwegian Basin are good analogues for the (Permian to Jurassic/Cretaceous) porous sandstone geothermal targets in the Netherlands. Geological settings in the Molasse Basin are reasonable**

analogues for (Dinantian) fractured or karstified carbonate and deeper geothermal targets in the Roer Valley Graben, but differ in the proximity of basement rocks with critically stressed faults.

Felt seismicity is not observed for geothermal projects in the North German Basin and Danish-Norwegian Basin. Low competency for Cretaceous sandstones compared to higher competency for Permian sandstones may play a role as well as porosity and permeability (e.g., some Triassic sandstones are tight). Felt seismicity is observed in some (3 out of 27) geothermal projects in the Molasse Basin. While geothermal targets and geothermal systems have similar characteristics in the Molasse Basin, the type of basin, vicinity of crystalline basement to targets, reservoir temperatures and stress regimes are different (section 3.1). The geothermal projects of the Paris Basin mainly target mid-Jurassic (Dogger) carbonate rocks. No seismicity has been reported for > 40 years of geothermal operations in the Paris Basin, but matrix-dominated rather than fracture-dominated flow occurs in the carbonate rocks. Therefore, the Paris Basin systems are not a very good analogue for the Dinantian fractured or karstified carbonate geothermal targets in the Roer Valley Graben, but may be relevant analogues for the Dinantian carbonate targets away from the Roer Valley Graben.

• **Key factors that affect the occurrence of felt seismicity are site-specific; the combination of geological and operational factors is important. Analysis of seismogenic potential and seismic risks of individual geothermal projects should be site-specific. Most influence is exerted by the type of geothermal play, system and target lithology. Geological factors such as the presence, geometry, state of stress of faults and hydraulic connection to basement and large faults are critical in all plays, in particular interaction of these geological factors with operational factors such as injection pressure, flow rate and temperature.**

The relative importance of different factors have been analysed on the basis of case studies worldwide. Most cases of induced seismicity occurred in geothermal play or rock types that are not targeted in the Netherlands, i.e. most prone to felt seismicity are cases of medium- to high-enthalpy systems targeting crystalline or volcanic rocks with reservoir stimulation by fluid injection performed. Geological and operational factors are not independent but interact in controlling induced seismicity (section 6.3). Faults are always relevant, not only if they are active or critically stressed faults prior to operations, but also if they are not critically stressed prior to operations as stress changes caused by operation may change the stress state and reactivate faults.

• **The main issues with monitoring seismicity are related to the resolution of seismic monitoring networks, necessity to monitor over long timescales covering a baseline period, the project lifetime and a post-production period, and difficulty in demonstrating unequivocal causal relations between seismicity and geothermal operations due to lack of subsurface data.**

The resolution of seismic monitoring networks and accuracy of local velocity models are critical, in particular concerning errors in vertical location of earthquakes. Natural seismicity and interaction of different subsurface operations also hamper demonstration of unequivocal relations between seismicity and geothermal operations (section 6.4).

- **Seismogenic potential is (1) low for the Jurassic/Cretaceous sandstone targets, (2) low-medium for the Triassic/Permian sandstone targets, (3) low-medium for the Dinantian carbonate targets in the Netherlands (depending on location and local settings, mainly active tectonics in the Roer Valley Graben), and (4) medium but very uncertain for deeper (Devonian) sedimentary targets.**
  Assessment of seismogenic potential is based on (section 6.5, Table 6-1):

  (1) Current absence of seismicity for the porous sandstone targets and occurrence of seismicity in the vicinity of the Dinantian carbonate targets (Californië, Balmatt). It should be noted that causal relations between seismicity and geothermal operations have not (yet) been established for the Dinantian carbonates targeted by the Californië geothermal projects.
  (2) The review of case studies that shows long term (> 30 years) geothermal operations without induced seismicity in geological settings that are analogous to the settings for the porous sandstone targets (North German Basin and Norwegian-Danish Basin) and some induced seismicity in settings that are reasonable analogous Dinantian carbonate targets (Molasse Basin).
  (3) The review of key mechanisms and factors for induced seismicity indicates low seismogenic potential for geothermal projects that involve fluid circulation in low enthalpy sedimentary reservoirs without reservoir stimulation by fluid injection. The seismogenic potential may increase if operations cause large changes in reservoir temperature or interact with large critically stressed, optimally oriented faults, or if reservoir stimulation is performed.
  (4) If sedimentary formations that are deeper than current targets are considered as future targets in the Netherlands, the seismogenic potential of the underburden ("basement") may play an increasingly important role.

This project provides a play-based qualitative ranking of seismogenic potential. It is too general to directly apply to individual projects within the plays (i.e. site-specific analysis is still required to determine a project-based assessment). As proper mitigation measures can lower seismic risk, ranking of seismogenic potential alone should not be used to disregard entire plays.

- **The most important measures to mitigate seismic risks are upfront optimization of geothermal operations and reservoir characterization efforts (preventive measures), and seismic monitoring before, during and after the geothermal operations with implementation of traffic light systems (control measures).**
  Reservoir characterization should focus on the presence and stress state of optimally oriented faults, in combination with modelling of the spatiotemporal distribution of stress changes and potential reactivation of mapped faults. Optimization of geothermal operations may focus on reducing the maximum pressure changes near faults and on planning wells away from large fault structures. The design of the traffic light system is critical, in particular concerning the definition and type of thresholds of maximum observed seismic magnitude or ground motions that trigger actions for modification or shut-in of operations. Technical as well as public perception criteria need to be considered to maintain a social license to operate. Site-specific geological and operational factors or surface conditions may lead to different thresholds at different locations (section 6.6).

- **Despite low to medium seismogenic potential for the geothermal targets in the Netherlands, <u>felt seismicity</u> associated with geothermal operations cannot be excluded, even if mitigation measures are implemented.**
  Seismogenic potential is generally low for current targets (in particular porous sandstone targets) in the Netherlands compared to cases worldwide where felt seismicity occurred. However, there can be no absolute guarantee that felt seismicity will not occur given the many unknowns associated with geology and interaction of operations with that geology, in particular considering the uncertainty of locations and stress changes at faults. Risk mitigation measures such as upfront reservoir characterization, geomechanical modelling, installation of state-of-the art seismic monitoring, and implementation of traffic light systems can all help to reduce seismic risks (section 6.6).

8   Suggestions for future research

The research conducted in this project focussed on reviewing case studies relevant for understanding induced seismicity and assessing the seismogenic potential of geothermal targets. Literature on case studies of geothermal projects with induced seismicity worldwide is so extensive that additional case studies or data certainly exist where future or more in depth analysis would be valuable and informative. Focussing on preventive measures to mitigate seismic hazard and risks for geothermal projects in the Netherlands, five main areas of research can be identified where additional research can help to lower seismic hazard and risks by reducing seismogenic potential of geothermal plays:

- **Subsurface characterization:** Better characterization of geological formations and faults including the mechanical properties and stress state. Further work on the quantification of factors affecting induced seismicity and assessing their interrelation would greatly help forecasts of seismogenic potential and develop mitigation measures for seismic hazard and risk. This study would in particular focus on areas that were previously not targeted for hydrocarbon exploration and on Carboniferous and Devonian rocks about which little is known.

- **Monitoring of induced seismicity**: Some issues were identified in the discussion on the current limitations of seismic monitoring and desirable standards for geothermal projects. Future research should focus on (1) acquiring better regional velocity models to improve the accuracy of earthquake hypocentre locations and focal mechanisms, (2) establishing criteria or guidelines for understanding causal relations between seismicity and geothermal operations, (3) applying novel seismic monitoring approaches (e.g., Distributed Acoustic Sensing, cf. section 5.2.3), and (4) implementing new (automated, real time) seismic processing methods (e.g., template matching processing methods to improve detection resolution without additional seismic stations, Cochran, 2018; Pena-Castro, 2018, and machine learning techniques for seismic event characterization, Holtzman et al., 2018; Ross et al., 2018). Another crucial aspect is how monitoring results are managed by different stakeholders in geothermal projects. Most importantly, it can help (1) the general public and local communities to understand uncertainties that are inherent in monitoring and mitigating seismicity, (2) regulatory agencies to impose guidelines on handling seismic hazard and risks, and (3) operators to outline internal procedures for managing seismic hazard and risks.

- **Validated modelling of induced seismicity**: Many modelling approaches exist that have not been addressed in this report. Geomechanical modelling of the effect of geothermal operations in the subsurface can aid in probabilistic forecasts of induced seismicity (upfront), in defining thresholds and measures for traffic light systems, or in establishing causal relations between seismicity and operations. Of particular interest for the Netherlands is future research that focusses on (1) deciphering the relative contribution of pressure (direct pressure and poroelastic) and temperature (thermoelastic) effects of doublet operation on subsurface stresses and induced seismicity, and (2) incorporation of subsurface data (e.g., location and stress state of faults) in modelling workflows. Additionally, seismic wave propagation modeling can help to improve the design of monitoring networks by accounting for lateral variations in site response, and inverting

observed ground motions to source mechanisms. Model validation using monitoring data is a crucial aspect.

- **<u>Optimizing the design of geothermal systems and operations</u>:** Flow and temperature have been the main factors influencing the design of geothermal systems and operations. Given the potential influence of induced seismicity on future development of geothermal energy in the Netherlands, reducing seismic hazards and risks may be equally important. Future research should focus on developing dual objective optimization workflows that optimize operations for minimum seismicity as well as maximum flow and heat extraction. Recent dual objective optimization approaches applied to gas production (e.g., ter Heege et al., 2018) can be adapted to fluid circulation in doublet operations. Modelling of the interference between different subsurface operations can be included in such optimization approach.

- **<u>Conduct a field experiment</u>**: Targets with elevated seismogenic potential (mainly the fractured or karstified Dinantian carbonate or deeper targets in the southeastern part of the Netherlands) are currently difficult to develop due to induced seismicity, but may host significant geothermal potential. A field experiment consisting of a conventional doublet with state-of-the-art seismic monitoring and traffic light system can provide valuable insight in safe development of these targets. Long term seismic monitoring can provide insight into reservoir behaviour and include background seismicity if started prior to operations. The field experiment could include hydraulic (tensile and shear) stimulation with limited injection volume and pressure if closely monitored. Although much more costly than the previous suggestions for future research and probably challenging considering public perceptions, such field experiment can provide valuable insight and data on mechanisms of induced seismicity required to gain confidence in development of these targets.

9   References

Agemar, T., Weber, J., & Schulz, R. (2014). Deep Geothermal Energy Production in Germany. *Energies, 7* (7), 4397-4416.

Agemar, T., Alten, J., Ganz, B., Kuder, J., K\uhne, K., Schumacher, S., & Schulz, R. (2014). The Geothermal Information System for Germany - GeotIS. *Zeitschrift Der Deutschen Gesellschaft Für Geowissenschaften (ZDGG), 165* (2), 129-144.

Agustsson, K., Kristjansdottir, S., Flovenz, O., & Gudmundsson, O. (2015). Induced seismic activity during drilling of injection wells at the Hellisheidi power plant, SW Iceland. *Proceedings World Geothermal Congress 2015, Melbourne, Australia, 19 - 25 April.*

Ahorner, L., & Sobisch, H. -. (1988). Ein untertägiges Überwachungssystem im Kalibergwerk Hattdorf zur Langzeiterfassung von seismischen Ereignissen im Werra-Kaligebiet. *Kali Und Steinsalz, 10* (2), 38-49.

Allis, R. G. (1982). Mechanisms of induced seismicity at the Geysers geothermal reservoir, California. *Geophysical Research Letters, 9* (2), 629.

Arabasz, W. J., & Pechmann, J. C. (2001). Seismic characterization of coal-mining seismicity in Utah for CTBT monitoring. *Lawrence Livermore National Laboratory Internal Report UCRL-CR-143772,*

Athanasopoulos, G., & Pekelis, P. (2000). Ground vibrations from sheetpile driving in urban environment: Measurements, analysis and effects on buildings and occupants. *Soil Dynamics and Earthquake Engineering, 19* , 371-387.

Atkinson, G. M., Eaton, D. W., Ghofrani, H., Walker, D., Cheadle, B., Schultz, R., Shcherbakov, R., Tiampo, K., Gu, J., & Harrington, R. M. (2016). Hydraulic Fracturing and Seismicity in the Western Canada Sedimentary Basin. *Seismological Research Letters, 87* (3), 631-647.

Bachmann, C. E., Wiemer, S., Goertz-Allmann, B., & Woessner, J. (2012). Influence of pore-pressure on the event-size distribution of induced earthquakes. *Geophysical Research Letters, 39* (9), L09302.

Bachmann, G. H., Müller, M., & Weggen, K. (1987). Evolution of the Molasse Basin (Germany, Switzerland). *Tectonophysics, 137* (1), 77-92.

Baillieux, P., Schill, E., Edel, J., & Mauri, G. (2013). Localization of temperature anomalies in the Upper Rhine Graben: insights from geophysics and neotectonic activity. *International Geology Review, 55* (14), 1744-1762.

Baisch, S., Fritschen, R., Groos, J., Kraft, T., Plenefisch, T., Plenkers, K., Ritter, J., Wassermann, J. (2012). Position des FKPE e.V. zur Induzierten Seismizität. *FKPE Arbeitsgruppe "Induzierte Seismizität".*

Baisch, S., Koch, C., Stang, H., Pittens, B., Drijver, B., & Buik, N. (2016). Defining the framework for seismic hazard assessment in geothermal projects V0.1. *Technical Report , Report No. 161005, Bad Bergzabern, Germany: prepared for KennisAgenda Aardwarmte.*

Baisch, S., Vörös, R., Weidler, R., & Wyborn, D. (2009). Investigation of Fault Mechanisms during Geothermal Reservoir Stimulation Experiments in the Cooper Basin, Australia. *Bulletin of the Seismological Society of America, 99* (1), 148.

Baisch, S., Weidler, R., Voros, R., Wyborn, D., & Graaf, L. d. (2006). Induced Seismicity during the Stimulation of a Geothermal HFR Reservoir in the Cooper Basin, Australia. *Bulletin of the Seismological Society of America, 96* (6), 2242.

Baisch, S., Rothert, E., Stang, H., Vörös, R., Koch, C., & McMahon, A. (2015). Continued Geothermal Reservoir Stimulation Experiments in the Cooper Basin (Australia). *Bulletin of the Seismological Society of America, 105* (1), 198-209.

Bao, X., & Eaton, D. W. (2016). Fault activation by hydraulic fracturing in western Canada. *Science, 354* (6318), 1406-1409.

Batchelor, A. (1982). Stimulation of a hot dry rock geothermal reservoir in the Cornubian granite, England. *Proceedings Eight Workshop Geothermal Reservoir Engineering December 14 - 16, 1982.*

Batchelor, A., Baria, R., & Hearn, K. (1983). Monitoring the effects of hydraulic stimulation by microseismic event location: a case study. *SPE Annual Technical Conference and Exhibition, 1983.*

Batini, F., Console, R., & Luongo, G. (1985). Seismological study of Larderello—Travale geothermal area. *Geothermics, 14* (2-3), 255-272.

Batini, F., Brogi, A., Lazzarotto, A., Liotta, D., & Pandeli, E. (2003). Geological features of Larderello-Travale and Mt. Amiata geothermal areas (southern Tuscany, Italy). *Episodes, 26* (3), 239-244.

Baujard, C., Genter, A., Dalmais, E., Maurer, V., Hehn, R., Rosillette, R., Vidal, J., & Schmittbuhl, J. (2017). Hydrothermal characterization of wells GRT-1 and GRT-2 in Rittershoffen, France: Implications on the understanding of natural flow systems in the rhine graben. *Geothermics, 65* , 255-268.

Baujard, C., Genter, A., Cuenot, N., Mouchot, J., Maurer, V., Hehn, R., Ravier, G., Seibel, O., & Vidal, J. (2018). Experience learnt from a successful soft stimulation and operational feedback after 2 years of geothermal power and heat production in Rittershoffen and Soutz-sous-Forets plants (Alsace,France). *GRC Transactions, 42.*

Baumann, T., Bartels, J., Lafogler, M., & Wenderoth, F. (2017). Assessment of heat mining and hydrogeochemical reactions with data from a former geothermal injection well in the Malm Aquifer, Bavarian Molasse Basin, Germany. *Geothermics, 66* , 50-60.

Baumgärtner, J., Teza, D., & Wahl, G. (2013). Gewinnung geothermischer Energie durch Entwicklung und Zirkulation eines Störungssystems im Kristallin und deren mikroseismische Überwachung am Beispiel des Geothermieprojektes Insheim. *Schlussbericht , Report No. 0325158, Landau: BESTEC GmbH.*

Benato, S., Hickman, S., Davatzes, N. C., Taron, J., Spielman, P., Elsworth, D., Majer, E. L., & Boyle, K. (2016). Conceptual model and numerical analysis of the Desert Peak EGS project: Reservoir response to the shallow medium flow-rate hydraulic stimulation phase. *Geothermics, 63* , 139-156.

Bischoff, M., Cete, A., Fritschen, R., & Meier, T. (2010). Coal mining induced seismicity in the Ruhr area, Germany. *Pure and Applied Geophysics, 167* (1-2), 63-75.

Bisschops, J. H., Broertjes, J. P., & Dobma, W. (1985). Toelichtingen bij de geologische kaart van Nederland 1: 50.000 blad Eindhoven West.

Blöcher, G., Cacace, M., Jacquey, A. B., Zang, A., Heidbach, O., Hofmann, H., Kluge, C., & Zimmermann, G. (2018). Evaluating Micro-Seismic Events Triggered by Reservoir Operations at the Geothermal Site of Groß Schönebeck (Germany). *Rock Mechanics and Rock Engineering, 51* (10), 3265 - 3279.

Böhm, F., Koch, R., Höferle, R., & Baasch, R. (2010). Der Malm in der Geothermiebohrung Pullach Th2 – Faziesanalyse aus Spülproben (München, S-Deutschland). *Geologische Blätter Für Nordorst-Bayern, 60* (1-4), 17-49.

Bohnhoff, M., Malin, P., Heege, J. t., Deflandre, J., & Sicking, C. (2018). Suggested best practice for seismic monitoring and characterization of non-conventional reservoirs *First Break, 36* (2), 59.

Bois, A., Mohajerani, M., Dousi, N., & Harms, S. (2013). Inducing Earthquake By Injecting Water In A Gas Field: Water-weakening Effect. *SPE Annual Technical Conference and Exhibition, 30 September - 2 October 2013, New Orleans, Louisiana, USA.*

Bommer, J. J., Oates, S., Cepeda, J. M., Lindholm, C., Bird, J., Torres, R., Marroquin, G., & Rivas, J. (2006). Control of hazard due to seismicity induced by a hot fractured rock geothermal project. *Engineering Geology, 83* , 287.

Bourne, S. J., Oates, S. J., van Elk, J., & Doornhof, D. (2014). A seismological model for earthquakes induced by fluid extraction from a subsurface reservoir. *Journal of Geophysical Research: Solid Earth, 119* (12), 8991-9015.

Brodsky, E. E., & Lajoie, L. J. (2013). Anthropogenic seismicity rates and operational parameters at the Salton Sea Geothermal Field. *Science (New York, N.Y.), 341* (6145), 543-546.

Brogi, A., Lazzarotto, A., Liotta, D., & Ranalli, G. (2003). Extensional shear zones as imaged by reflection seismic lines: the Larderello geothermal field (central Italy). *Tectonophysics, 363* (1-2), 127-139.

Buijze, L., van den Bogert, P. A. J., Wassing, B. B. T., Orlic, B., & ten Veen, J. (2017). Fault reactivation mechanisms and dynamic rupture modelling of depletion-induced seismic events in a Rotliegend gas reservoir. *Netherlands Journal of Geosciences, 96* (5), s131-s148.

Busetti, S., Jiao, W., & Reches, Z. (2014). Geomechanics of hydraulic fracturing microseismicity: Part 1. Shear, hybrid, and tensile events. *AAPG Bulletin, 98* (11), 2439-2457.

Candela, T., Wassing, B., ter Heege, J., & Buijze, L. (2018). How earthquakes are induced. *Science, 360* (6389), 598-600.

Cappetti, G., & Stefani, G. (1994). Strategies for sustaining production at Larderello. *Bulletin of the Geothermal Resources Council, 23* (9), 303-306.

Catalli, F., Meier, M., & Wiemer, S. (2013). The role of Coulomb stress changes for injection-induced seismicity: The Basel enhanced geothermal system. *Geophysical Research Letters, 40* (1), 72-77.

Chang, C., & Haimson, B. (2012). A failure criterion for rocks based on true triaxial testing. *The ISRM Suggested Methods for Rock Characterization, Testing and Monitoring: 2007-2014* (pp. 259-262 Springer.

Chang, K. W., & Segall, P. (2016). Injection-induced seismicity on basement faults including poroelastic stressing. *Journal of Geophysical Research: Solid Earth, 121* (4), 2708-2726.

Charléty, J., Cuenot, N., Dorbath, L., Dorbath, C., Haessler, H., & Frogneux, M. (2007). Large earthquakes during hydraulic stimulations at the geothermal site of Soultz-sous-Forêts. *International Journal of Rock Mechanics & Mining Sciences, 44* , 1091.

Chen, L., & Talwani, P. (1998). Reservoir-induced seismicity in China. *Pure and Applied Geophysics, 153* (1), 133-149.

Cook, N. G. W. (1976). Seismicity associated with mining. *Engineering Geology, 10* (2–4), 99-122.

Cornet, F. H., & Burlet, D. (1992). Stress field determinations in France by hydraulic tests in boreholes. *Journal of Geophysical Research: Solid Earth, 97* , 11829-11849.

Crook, Th., Haak, H.W., Dost, B. (1998). Seismisch risico in Noord Nederland. *KNMI publicatie TR-205.*

Cuenot, N., Charléty, J., Haessler, H., & Dorbath, L. (2006). Faulting mechanisms and stress regime at the European HDR site of Soultz-sous-Forêts, France. *Geothermics, 35* , 561.

Das, I., & Zoback, M. (2013). Long-period, long-duration seismic events during hydraulic stimulation of shale and tight-gas reservoirs — Part 1: Waveform characteristics. *Geophysics, 78* (6), KS97-KS108.

Dash, Z.V., & Murphy, H.D. (1981). Summary of hot dry rock geothermal reservoir testing 1978 to 1980. *7th Workshop on Geothermal Reservoir Engineering, Stanford, CA, SGP-TR-55*, 97-102.

Davies, R., Foulger, G., Bindley, A., & Styles, P. (2013). Induced seismicity and hydraulic fracturing for the recovery of hydrocarbons. *Marine and Petroleum Geology, 45* (0), 171-185.

Davis, S. D., & Frohlich, C. (1993). Did (or will) fluid injection cause earthquakes? - criteria for a rational assessment. *Seismological Research Letters, 64* (3-4), 207-224.

Davis, S. D., Nyffenegger, P. A., & Frohlich, C. (1995). The 9 April 1993 earthquake in south-central Texas: Was it induced by fluid withdrawal? *Bulletin of the Seismological Society of America, 85* (6), 1888-1895.

Davis, S. D., & Pennington, W. D. (1989). Induced seismic deformation in the Cogdell oil field of west Texas. *Bulletin of the Seismological Society of America, 79* (5), 1477-1495.

de Waal, J. A., Muntendam-Bos, A. G., & Roest, J. P. A. (2017). From checking deterministic predictions to probabilities, scenarios and control loops for regulatory supervision. *Netherlands Journal of Geosciences, 96* (5), s17-s25.

Deichmann, N., Kraft, T., & Evans, K. F. (2014). Identification of faults activated during the stimulation of the Basel geothermal project from cluster analysis and focal mechanisms of the larger magnitude events. *Geothermics, 52* , 84-97.

Dempsey, D., Kelkar, S., Davatzes, N., Hickman, S., Moos, D., & Zemach, E. (2014). Evaluating the roles of thermoelastic and poroelastic stress changes in the Desert Peak EGS stimulation. *39th Workshop on Geothermal Reservoir Engineering, Stanford, CA, Feb. 24-26.*

Deng, K., Liu, Y., & Harrington, R. M. (2016). Poroelastic stress triggering of the December 2013 Crooked Lake, Alberta, induced seismicity sequence. *Geophysical Research Letters, 43* (16), 8482-8491.

Dentzer, J., Lopez, S., Violette, S., & Bruel, D. (2016). Quantification of the impact of paleoclimates on the deep heat flux of the Paris Basin. *Geothermics, 61* , 35-45.

Diehl, T., Kraft, T., Kissling, E., & Wiemer, S. (2017). The induced earthquake sequence related to the St. Gallen deep geothermal project (Switzerland): Fault reactivation and fluid interactions imaged by microseismicity. *Journal of Geophysical Research: Solid Earth, 122* (9), 7272-7290.

Dorbath, L., Cuenot, N., Genter, A., & Frogneux, M. (2009). Seismic response of the fractured and faulted granite of Soultz-sous-Forêts (France) to 5 km deep massive water injections. *Geophysical Journal International, 2003* , 2004.

Dost, B., Goutbeek, F., Van Eck, T., & Kraaijpoel, D. (2012). Monitoring induced seismicity in the North of the Netherlands: status report 2010. *Scientific Report , Report No. WR 2012-03, De Bilt: Royal Netherlands Meteorological Institute.*

Dost, B., Ruigrok, E., & Spetzler, J. (2017). Development of seismicity and probabilistic hazard assessment for the Groningen gas field. *Netherlands Journal of Geosciences, 96* (5), s235-s245.

Dreger, D. S., Boyd, O. S., Gritto, R., & Taira, T. (2018). Seismic Analysis of Spatio-Temporal Fracture Generation at The Geysers EGS Demonstration Project. *PROCEEDINGS, 43rd Workshop on Geothermal Reservoir Engineering Stanford University, Stanford, California, February 12-14, 2018, SGP-TR-213.*

Edwards, B., & Douglas, J. (2014). Magnitude scaling of induced earthquakes. *Geothermics, 52* , 132-139.

Edwards, B., Kraft, T., Cauzzi, C., Kästli, P., & Wiemer, S. (2015). Seismic monitoring and analysis of deep geothermal projects in St Gallen and Basel, Switzerland. *Geophysical Journal International, 201* (2), 1022-1039.

El Hariri, M., Abercrombie, R. E., Rowe, C. A., & Do Nascimento, A. F. (2010). The role of fluids in triggering earthquakes: observations from reservoir induced seismicity in Brazil. *Geophysical Journal International, 181* (3), 1566-1574.

Ellsworth, W. L. (2013). Injection-Induced Earthquakes. *Science, 341* (6142).

EPA, U. S. (2016). Hydraulic Fracturing for Oil and Gas: Impacts from the Hydraulic Fracturing Water Cycle on Drinking Water Resources in the United States. *Report No. EPA/600/R-16/236Fa, Washington, DC: U.S. EPA (U.S. Environmental Protection Agency), Office of Research and Development.*

Erlström, M., Boldreel, L. O., Lindstrom, S., Kristensen, L., Mathiesen, A., Andersen, M., Kamla, E., & Nielsen, L. (2018). Stratigraphy and geothermal assessment of Mesozoic sandstone reservoirs in the Oresund Basin-exemplified by well data and seismic profiles. *Bulletin of the Geological Society of Denmark, 66* , 123-149.

European Geothermal Energy Council. (2017). 2016 EGEC Geothermal Market Report. *Full report. Sixth edition , European Geothermal Council.*

Evans, D., M. (1966). The Denver area earthquakes and the Rocky Mountain Arsenal disposal well. *Mountain Geologist, 3* (1), 23.

Evans, K. F., Zappone, A., Kraft, T., Deichmann, N., & Moia, F. (2012). A survey of the induced seismic responses to fluid injection in geothermal and CO2 reservoirs in Europe. *Geothermics, 41* (0), 30-54.

Faulds, J. E., Coolbaugh, M. F., Benoit, D., Oppliger, G., Perkins, M., Moeck, I., & Drakos, P. (2010). Structural controls of geothermal activity in the northern Hot Springs Mountains, western Nevada: The tale of three geothermal systems (Brady's, Desert Peak, and Desert Queen). *Geothermal Resources Council Transactions, 34* , 675-683.

Fjaer, E., Holt, R. M., Horsrud, P., Raaen, A. M., & Risnes, R. (2008). *Petroleum related rock mechanics* (2nd Edition ed.) Elsevier.

Foulger, G. R., Wilson, M. P., Gluyas, J. G., Julian, B. R., & Davies, R. J. (2018). Global review of human-induced earthquakes. *Earth-Science Reviews, 178* , 438-514.

Frederiksen, S., Nielsen, S. B., & Balling, N. (2001). A numerical dynamic model for the Norwegian–Danish Basin. *Tectonophysics, 343* (3-4), 165-183.

Fritschen, R. (2010). Mining-Induced Seismicity in the Saarland, Germany. *Pure and Applied Geophysics, 167* (1-2), 77-89.

Gan, W., & Frohlich, C. (2013). Gas injection may have triggered earthquakes in the Cogdell oil field, Texas. *Proceedings of the National Academy of Sciences, 110* (47), 18786-18791.

Garcia, J., Hartline, C., Walters, M., Wright, M., Rutqvist, J., Dobson, P. F., & Jeanne, P. (2016). The Northwest Geysers EGS demonstration project, California: Part 1: characterization and reservoir response to injection. *Geothermics, 63* , 97-119.

Gaucher, E. (2016). Earthquake detection probability within a seismically quiet area: Application to the Bruchsal geothermal field. *Geophysical Prospecting, 64* (2), 268-286.

Gaupp, R., & Okkerman, J. A. (2011). Diagenesis and reservoir quality of rotliegend sandstones in the northern netherlands - a review. In J. Grötsch, & R. Gaupp (Eds.), *The Permian Rotliegend of the Netherlands* (SEPM Special Publication 98 ed., pp. 193 SEPM.

Geertsma, J. (1966). Problems of Rock Mechanics In Petroleum Production Engineering. *1st ISRM Congress. International Society for Rock Mechanics, 1966.*

Geluk, M. (2005). *Stratigraphy and tectonics of Permo-Triassic basins in the Netherlands and surrounding areas.* (PhD, Utrecht university).

Ghassemi, A., & Zhou, X. (2011). A three-dimensional thermo-poroelastic model for fracture response to injection/extraction in enhanced geothermal systems. *Geothermics, 40* (1), 39-49.

Giardini, D., Woessner, J., Danciu, L., Crowley, H., Cotton, F., Gruenthal, G., . . . Rovida, A. (2013). *Seismic hazard harmonization in europe (SHARE): Online data resource.* Retrieved, 2013, from doi:10.12686/SED-00000001-SHARE.

Giardini, D., Grünthal, G., Shedlock, K. M., & Zhang, P. (1999). The GSHAP Global Seismic Hazard Map. *Annals of Geophysics, 42* (6).

Glowacka, E., & Nava, F. A. (1996). Major earthquakes in Mexicali Valley, Mexico, and fluid extraction at Cerro Prieto Geothermal Field. *Bulletin of the Seismological Society of America, 86* (1A), 93-105.

Goebel, T. H. W., Weingarten, M., Chen, X., Haffener, J., & Brodsky, E. E. (2017). The 2016 Mw5.1 Fairview, Oklahoma earthquakes: Evidence for long-range poroelastic triggering at >40 km from fluid disposal wells. *Earth and Planetary Science Letters, 472* , 50-61.

Goertz-Allmann, B., & Wiemer, S. (2012). Geomechanical modeling of induced seismicity source parameters and implications for seismic hazard assessment. *Geophysics, 78* (1), KS25-KS39.

Goldbrunner, J. (1999). Hyrdogeology of deep groundwaters in Austria. *Mitteilungen Der Österreichischen Geologischen Gesellschaft, 92* , 281-294.

Gough, D. I., & Gough, W. I. (1970). Load-induced Earthquakes at Lake Kariba—II. *Geophysical Journal International, 21* (1), 79-101.

Gregersen, S., & Voss, P. (2014). Review of some significant claimed irregularities in Scandinavian postglacial uplift on timescales of tens to thousands of years–earthquakes in Denmark? *Solid Earth, 5* (1), 109-118.

Grigoli, F., Cesca, S., Rinaldi, A. P., Manconi, A., López-Comino, J. A., Clinton, J. F., Westaway, R., Cauzzi, C., Dahm, T., & Wiemer, S. (2018). The November 2017 M_w 5.5 Pohang earthquake: A possible case of induced seismicity in South Korea. *Science, 360* (6392), 1003-1006.

Grimmer, J. C., Ritter, J. R. R., Eisbacher, G. H., & Fielitz, W. (2017). The Late Variscan control on the location and asymmetry of the Upper Rhine Graben. *International Journal of Earth Sciences, 106* (3), 827-853.

Grünthal, G. (1998). *European Macroseismic Scale 1998,* Conseil de l'Europe, Cahier du Centre Europeen de Geodynamique et de Seismologie. Vol. 15, Luxemburg, 99 pp.

Guillocheau, F., Robin, C., Allemand, P., Bourquin, S., Brault, N., Dromart, G., Friedenberg, R., Garcia, J., Gaulier, J., . . . Grandjean, G. (2000). Meso-Cenozoic geodynamic evolution of the Paris Basin: 3D stratigraphic constraints. *Geodinamica Acta, 13* (4), 189-245.

Gunnarsson, G. (2013). Temperature Dependent Injectivity and Induced Seismicity - Managing Reinjection in the Hellisheidi Field, SW-Iceland. *GRC-Transactions, 37.*

Gunnarsson, G., Kristjansson, B. R., Gunnarsson, I., & Juliusson, B. M. (2015). Reinjection into a Fractured Reservoir - Induced Seismicity and Other Challenges in Operating Reinjection wells in the Hellisheidi Field, SW-Iceland. *Proceedings World Geothermal Congress 2015, Melbourne, Australia, 19 - 25 April.*

Gupta, H. K. (2002). A review of recent studies of triggered earthquakes by artificial water reservoirs with special emphasis on earthquakes in Koyna, India. *Earth-Science Reviews, 58* (3–4), 279-310.

Gutenberg, B., & Richter, C. F. (1956). Earthquake magnitude, intensity, energy, and acceleration: (Second paper). *Bulletin of the Seismological Society of America, 46* (2), 105-145.

Hanks, T. C., & Kanamori, H. (1979). A Moment Magnitude Scale. *Journal of Geophysical Research, 84* (85), 2348-2350.

Harding, S. T. (1981). Induced Seismicity Cogdell Canyon Reef Oil Field. *Open File Report , Report No. 81-167, Menlo Park, USA: USGS.*

Häring, M. O., Schanz, U., Ladner, F., & Dyer, B. C. (2008). Characterisation of the Basel 1 enhanced geothermal system. *Geothermics, 37* , 469.

Hasegawa, H. S., Wetmiller, R. J., & Gendzwill, D. J. (1989). Induced seismicity in mines in Canada: An overview. *Pure and Applied Geophysics, 129* (3), 423-453.

Healy, J. H., Rubey, W. W., Griggs, D. T., & Raleigh, C. B. (1968). The Denver Earthquakes. *Science, 161* (3848), 1301-1310.

Henares, S., Bloemsma, M. R., Donselaar, M. E., Mijnlieff, H. F., Redjosentono, A. E., Veldkamp, J. G., & Weltje, G. J. (2014). The role of detrital anhydrite in diagenesis of aeolian sandstones (Upper Rotliegend, The Netherlands): Implications for reservoir-quality prediction. *Sedimentary Geology, 314* , 60.

Herzberger, P., Münch, W., Köbel, T., Bruchmann, U., Schlagermann, P., H., H., . . . Ptak, T. (2010). The geothermal plant Bruchsal. *Proceedings World Geothermal Congress 2010, Bali, Indonesia, 25-29 April 2010.*

Hettema, M. H. H., Schutjens, P. M. T. M., Verboom, B. J. M., & Gussinklo, H. J. (2000). Production-induced compaction of a sandstone reservoir: The strong influence of stress path. *SPE Reservoir Evaluation and Engineering, August.*

Hirschberg, S., Wiemer, S., & Burgherr, P. (2015). *Energy from the earth: Deep geothermal as a resource for the future?.* Zürich: TA-SWISS Study TA/CD 62/2015, vdf Hochschulverlag AG. doi: https://doi.org/10.3929/ethz-a-010277690

Hjuler, M. L., Vosgerau, H., Nielsen, C. M., Frykman, P., Kristensen, L., Mathiesen, A., Bidstrup, T., & Nielsen, L. H. (2014). A multidisciplinary study of a geothermal reservoir below Thisted, Denmark. *Geological Survey of Denmark and Greenland Bulletin, 31* , 51-54.

Hofmann, H., Zimmermann, G., Zang, A., & Min, K. (2018). Cyclic soft stimulation (CSS): a new fluid injection protocol and traffic light system to mitigate seismic risks of hydraulic stimulation treatments. *Geothermal Energy, 6* (1), 27.

Holl, H., & Barton, C. (2015). Habanero Field - Structure and state of stress. *Proceedings World Geothermal Congress 2015, Melbourne, Australia, 19 - 25 April.*

Holtkamp, S., & Brudzinski, M. (2015). Regional detection and monitoring of injection-induced seismicity: Application to the 2010-2012 Youngstown, Ohio seismic sequence. *AAPG Bulletin, 99* (9), 1671-1688.

Holtzman, B. K., Paté, A., Paisley, J., Waldhauser, F., & Repetto, D. (2018). Machine learning reveals cyclic changes in seismic source spectra in Geysers geothermal field. *Science Advances, 4* (5)

Horálek, J., Jechumtálovaá, Z., Dorbath, L., & Šílený, J. (2010). Source mechanisms of micro-earthquakes induced in a fluid injection experiment at the HDR site Soultz-sous-Forêts (Alsace) in 2003 and their temporal and spatial variations. *Geophysical Journal International, 181* , 1547.

Hornbach, M. J., Jones, M., Scales, M., DeShon, H. R., Magnani, M. B., Frohlich, C., Stump, B., Hayward, C., & Layton, M. (2016). Ellenburger wastewater injection and seismicity in North Texas. *Physics of the Earth and Planetary Interiors, 261* , 54-68.

Horton, S. (2012). Disposal of Hydrofracking Waste Fluid by Injection into Subsurface Aquifers Triggers Earthquake Swarm in Central Arkansas with Potential for Damaging Earthquake. *Seismological Research Letters, 83* (2), 250-260.

Houtgast, R. F., & Van Balen, R. T. (2000). Neotectonics of the Roer Valley Rift System, the Netherlands. *Global and Planetary Change, 27* , 131-146.

Jaeger, J. C., Cook, N. G. W., & Zimmerman, R. (2007). *Fundamentals of rock mechanics* (4th ed.) Wiley-Blackwell.

Jeanne, P., Rutqvist, J., Rinaldi, A. P., Dobson, P. F., Walters, M., Hartline, C., & Garcia, J. (2015). Seismic and aseismic deformations and impact on reservoir permeability: The case of EGS stimulation at The Geysers, California, USA. *Journal of Geophysical Research: Solid Earth, 120* (11), 7863-7882.

Julian, B. R., Foulger, G. R., Monastero, F. C., & Bjornstad, S. (2010). Imaging hydraulic fractures in a geothermal reservoir. *Geophysical Research Letters, 37* (7)

Juncu, D., Árnadóttir, T., Geirsson, H., Guðmundsson, G. B., Lund, B., Gunnarsson, G., Hooper, A., Hreinsdóttir, S., & Michalczewska, K. (2018). Injection-induced surface deformation and seismicity at the Hellisheidi geothermal field, Iceland. *Journal of Volcanology and Geothermal Research, in press.*

Jung, R. (2013). EGS—goodbye or back to the future. *ISRM International Conference for Effective and Sustainable Hydraulic Fracturing*

Kabus, F., & Jäntsch, E. (1995). The geothermal heating plant at Waren-Papenberg-Experience and Modernisation. *Proceedings of the World Geothermal Congress, 3, 2227-2232.*

Karytsas, C., Mendrinos, D., & Goldbrunner, J. (2009). Production Monitoring at the Geinberg Geothermal Site. *Energy Sources Part A, 31* (17), 1537-1552.

Keranen, K. M., Weingarten, M., Abers, G. A., Bekins, B. A., & Ge, S. (2014). Sharp increase in central Oklahoma seismicity since 2008 induced by massive wastewater injection. *Science, 320* (6195), 448-451.

Keranen, K. M., Savage, H. M., Abers, G. A., & Cochran, E. S. (2013). Potentially induced earthquakes in Oklahoma, USA: Links between wastewater injection and the 2011 Mw 5.7 earthquake sequence. *Geology, 41* (6), 699-702.

Kim, H., Xie, L., Min, K., Bae, S., & Stephansson, O. (2017). Integrated In Situ Stress Estimation by Hydraulic Fracturing, Borehole Observations and Numerical Analysis at the EXP-1 Borehole in Pohang, Korea. *Rock Mechanics and Rock Engineering, 50* (12), 3141-3155.

Kim, K., Ree, J., Kim, Y., Kim, S., Kang, S. Y., & Seo, W. (2018). Assessing whether the 2017 M_w 5.4 Pohang earthquake in South Korea was an induced event. *Science (New York, N.Y.), 360* (6392), 1007.

Kim, K., Min, K., Kim, K., Choi, J. W., Yoon, K., Yoon, W. S., Yoon, B., Lee, T. J., & Song, Y. (2018). Protocol for induced microseismicity in the first enhanced geothermal systems project in Pohang, Korea. *Renewable and Sustainable Energy Reviews, 91* , 1182-1191.

Kim, W. (2013). Induced seismicity associated with fluid injection into a deep well in Youngstown, Ohio. *Journal of Geophysical Research: Solid Earth, 118* (7), 3506-3518.

King, G. E. (2010). Thirty Years of Gas Shale Fracturing: What Have We Learned?

Klose, C. D. (2007). Geomechanical modeling of the nucleation process of Australia's 1989 M5.6 Newcastle earthquake. *Earth and Planetary Science Letters, 256* (3–4), 547-553.

Koh, J., Roshan, H., & Rahman, S. S. (2011). A numerical study on the long term thermo-poroelastic effects of cold water injection into naturally fractured geothermal reservoirs. *Computers and Geotechnics, 38* (5), 669-682.

Kombrink, H. (2008). *The Carboniferous of the Netherlands and surrounding areas; a basin analysis.* (PhD, Utrecht University). *Geologica Ultraiectina, 294,* 184 pp.

Kombrink, H., Doornenbal, J., Duin, E., Den Dulk, M., ten Veen, J., & Witmans, N. (2012). New insights into the geological structure of the Netherlands; results of a detailed mapping project. *Netherlands Journal of Geosciences, 91* (04), 419-446.

Kraaijpoel, D., Kraft, T., Tramelli, A., De Natale, G., Troise, C., Orazi, M., Jupe, A. (2013). GEISER Deliverable D6.2 - Seismic Monitoring Strategies. *INGV, ETHZ, BRGM, NORSAR, KNMI.*

Kramers, L., Van Wees, J. D., Pluymaekers, M. P. D., Kronimus, A., & Boxem, T. (2012). Direct heat resource assessment and subsurface information systems for geothermal aquifers; the Dutch perspective. *Netherlands Journal of Geosciences, 91* (04), 637-649.

Kreemer, C., Blewitt, G., & Klein, E. C. (2014). A geodetic plate motion and global strain rate model. *Geochemistry, Geophysics, Geosystems, 15* (10), 3849-3889.

Kristensen, L., Hjuler, M. L., Frykman, P., Olivarius, M., Weibel, R., Nielsen, L. H., & Mathiesen, A. (2016). Pre-drilling assessments of average porosity and permeability in the geothermal reservoirs of the Danish area. *Geothermal Energy, 4* (1), 6.

Küperkoch, L., Olbert, K., & Meier, T. (2018). Long-Term Monitoring of Induced Seismicity at the Insheim Geothermal Site, Germany. *Bulletin of the Seismological Society of America, 108* (6), 3668-3683.

Kwiatek, G., Bohnhoff, M., Dresen, G., Schulze, A., Schulte, T., Zimmermann, G., & Huenges, E. (2008). Microseismic event analysis in conjection with stimulation treatments at the geothermal research well GTGRSK4/05 in Groß Schönebeck, Germany. *PROCEEDINGS, Thirty-Third Workshop on Geothermal Reservoir Engineering Stanford University, Stanford, California, January 28-30, 2008 SGP-TR-185.*

Kwiatek, G., Bohnhoff, M., Dresen, G., Schulze, A., Schulte, T., Zimmermann, G., & Huenges, E. (2010). Microseismicity Induced During Fluid-Injection: A Case Study from the Geothermal Site at Groß Schönebeck, North German Basin. *Acta Geophysica, 58* (6), 995.

Labuz, J. F., & Zang, A. (2012). Mohr–Coulomb failure criterion. *Rock Mechanics and Rock Engineering, 45* (6), 975-979.

Lei, X., Huang, D., Su, J., Jiang, G., Wang, X., Wang, H., Guo, X., & Fu, H. (2017). Fault reactivation and earthquakes with magnitudes of up to Mw4. 7 induced by shale-gas hydraulic fracturing in Sichuan Basin, China. *Scientific Reports, 7* (1), 7971.

Lengline, O., Boubacar, M., & Schmittbuhl, J. (2017). Seismicity related to the hydraulic stimulation of GRT1, Rittershoffen, France. *Geophysical Journal International, 208* (3), 1704-1715.

Leydecker, G. (2011). *Erdbebenkatalog für deutschland mit randgebieten für die jahre 800 bis 2008* Schweizerbart.

LIAG. (2012). Geothermische Charakterisierung von karstig-klüftigen Aquiferen im Großraum München - Endbericht. *Endbericht , Report No. 0130392, Hannover: LIAG.*

LIAG. (2018). Untersuchung der Seismizität am Standort des Geothermieprojekts Poing unter Einbeziehung von Strukturgeologie, Geohydraulik, Hydrochemie, Geomechanik und Dublettenbetrieb. *Zusammenfassung , Hannover: LIAG (Leibniz-Institut für Angewandte Geophysik).*

Lipsey, L., Pluymaekers, M., Goldberg, T., van Oversteeg, K., Ghazaryan, L., Cloetingh, S., & van Wees, J. (2016). Numerical modelling of thermal convection in the Luttelgeest carbonate platform, the Netherlands. *Geothermics, 64* , 135-151.

Lopez, S., Hamm, V., Le Brun, M., Schaper, L., Boissier, F., Cotiche, C., & Giuglaris, E. (2010). 40 years of Dogger aquifer management in Ile-de-France, Paris Basin, France. *Geothermics, 39* (4), 339-356.

Lu, S. (2018). A global review of enhanced geothermal system (EGS). *Renewable and Sustainable Energy Reviews, 81* , 2902-2921.

Lutz, S. J., Hickman, S., Davatzes, N., Zemach, E., Drakos, P., & Robertson-Tait, A. (2010). Rock mechanical testing and petrologic analysis in support of well stimulation activities at the Desert Peak Geothermal Field, Nevada. *Proceedings 35th workshop on geothermal reservoir engineering, Stanford University, February 1-3, 2010 SGP-TR-188.*

Mahler, A. (1995). Geothermal Plant in Thisted with absorption heat pump and 10 years operation without corrosion or reinjection problems in sandstone for 15% saline water. *Proceedings World Geothermal Congress, 1995.*

Mahler, A., & Magtengaard, J. (2005). Geothermal Development in Denmark, Country Update 2005. *Proceedings World Geothermal Congress 2005, Antalya, Turkey, 24-29 April 2005.*

Majer, E., Nelson, J., Robertson-tait, A., Savy, J., & Wong, I. (2012). Protocol for addressing induced seismicity associated with enhanced geothermal systems. *Report No. DOE/EE-0662, U.S. Department of energy.*

Majer, E. L., Freeman, K., Johnson, L., Jarpe, S., Nihei, K. T., Hartline, C., Walter, M., & Deniliger, M. (2017). Monitoring the Effect of Injection of Fluids from the Lake County Pipeline on Seismicity at The Geysers, California, Geothermal Field. *Final Report, Lawrence Berkeley National Laboratory, Calpine Corporation, Lake County.*

Martínez-Garzón, P., Kwiatek, G., Sone, H., Bohnhoff, M., Dresen, G., & Hartline, C. (2014). Spatiotemporal changes, faulting regimes, and source parameters of induced seismicity: A case study from The Geysers geothermal field. *Journal of Geophysical Research: Solid Earth, 119* (11), 8378-8396.

Maurer, V., Cuenot, N., Gaucher, E., Grunberg, M., Vergne, J., Wodling, H., Schmittbuhl, J. (2015). Seismic monitoring of the Rittershoffen EGS project (Alsace,France). *Proceedings World Geothermal Congress 2015, Melbourne, Australia, 19 - 25 April.*

Mazurek, M., Hurford, A. J., & Leu, W. (2006). Unravelling the multi-stage burial history of the Swiss Molasse Basin: integration of apatite fission track, vitrinite reflectance and biomarker isomerisation analysis. *Basin Research, 18* (1), 27-50.

McGarr, A. (2002). Case histories of induced and triggered seismicity. In W. H. K. Lee, H. Kanamori, P. C. Jennings & C. Kisslinger (Eds.), *International Handbook of Earthquake and Engineering Seismology* (81A ed., pp. 647.

McGarr, A. (2014). Maximum magnitude earthquakes induced by fluid injection. *Journal of Geophysical Research: Solid Earth, 119* (2), 1008-1019.

McGuire, J. J., Lohman, R. B., Catchings, R. D., Rymer, M. J., & Goldman, M. R. (2015). Relationships among seismic velocity, metamorphism, and seismic and aseismic fault slip in the Salton Sea Geothermal Field region. *Journal of Geophysical Research: Solid Earth, 120* (4), 2600-2615.

Megies, T., & Wassermann, J. (2014). Microseismicity observed at a non-pressure-stimulated geothermal power plant. *Geothermics, 52* , 36-49.

Meixner, J., Schill, E., Gaucher, E., & Kohl, T. (2014). Inferring the in situ stress regime in deep sediments: an example from the Bruchsal geothermal site. *Geothermal Energy, 2* (1).

Meixner, J., Schill, E., Grimmer, J. C., Gaucher, E., Kohl, T., & Klingler, P. (2016). Structural control of geothermal reservoirs in extensional tectonic settings: An example from the Upper Rhine Graben. *Journal of Structural Geology, 82* , 1-15.

Mignan, A., Broccardo, M., Wiemer, S., & Giardini, D. (2018). Autonomous decision-making against induced seismicity in deep fluid injections. *International Symposium on Energy Geotechnics.* In: Ferrari A., Laloui L. (eds) *Energy Geotechnics.* SEG 2018. Springer Series in Geomechanics and Geoengineering. Springer, Cham.

Mignan, A., Broccardo, M., Wiemer, S., & Giardini, D. (2017). Induced seismicity closed-form traffic light system for actuarial decision-making during deep fluid injections. *Scientific Reports, 7* (1), 13607.

Mijnlieff, H. F. (2017). Actualisatie beoordeling gerealiseerd vermogen AARD01008 na hoorzitting (Vierpolders). *Report No. AGE 17-10.015, Utrecht: TNO.*

Mijnlieff, H. F., & Geluk, M. C. (2011). Palaeotopography-governed sediment distribution - a new predictive model for the permian upper rotliegend in the dutch sector of the southern permian basin. In J. Grötsch, & R. Gaupp (Eds.), *The Permian Rotliegend in the Netherlands* (SEPM Special Publication 98 ed., pp. 147-159. Tulsa, Oklahoma: SEPM.

Miller, A. D., Foulger, G., & Julian, B. R. (1998). Non-double-couple earthquakes 2. Observations. *Reviews of Geophysics, 36* (4), 551-568.

Min, K. (2018). Overview of the hydraulic stimulation activities at the Pohang site. *DESTRESS - General Assembly in Glasgow. Mid-Conference, April 5 2018.*

Ministry of Economic Affairs and Climate Policy. (2018). Natural resources and geothermal energy in the Netherlands. Annual review 2017. *Haarlem: Ministry of Economic Affairs and Climate Policy.*

Minkley, W. (2004). Back analysis rockburst volkershausen 1989. In H. Konietzky (Ed.), *Numerical modeling of discrete materials* (pp. 105-112. London: Taylor & Francis Group.

Moeck, I., Bloch, T., Graf, R., Heuberger, S., Kuhn, P., Naef, H., . . . Wolfgramm, M. (2015). The St. Gallen project: development of fault controlled geothermal systems in urban areas. *Proceedings World Geothermal Congress 2015. M*elbourne, Australia, 19-25 April 2015.

Moeck, I., Kwiatek, G., & Zimmermann, G. (2009). Slip tendency analysis, fault reactivation potential and induced seismicity in a deep geothermal reservoir. *Journal of Structural Geology, 31* , 1174.

Moeck, I. S. (2014). Catalog of geothermal play types based on geologic controls. *Renewable and Sustainable Energy Reviews, 37* , 867-882.

Mogi, K. (1971). Fracture and flow of rocks under high triaxial compression. *Journal of Geophysical Research, 76* (5), 1255-1269.

Morris, A. P., Ferrill, D. A., Walter, G. R., Price, A. M., Smart, K. J., Skoumal, R. J., Brudzinski, M. R., & Currie, B. S. (2017). Lessons learned from the Youngstown, Ohio induced earthquake sequence from January 2011 to January 2012. *Journal of Rock Mechanics and Geotechnical Engineering, 9* (5), 783-796.

Mossop, A., & Segall, P. (1997). Subsidence at The Geysers Geothermal Field, N. California from a comparison of GPS and leveling surveys. *Geophysical Research Letters, 24* (14), 1839-1842.

Mulders, F. M. M. (2003). *Modelling of stress development and fault slip in and around a producing gas reservoir.* (Doctoral Thesis, Technical University of Delft).

Nachtmann, W., & Wagner, L. (1987). Mesozoic and Early Tertiary evolution of the Alpine foreland in upper Austria and Salzburg, Austria. *Tectonophysics, 137* (1), 61-76.

NAM. (2013). Technical addendum to the Winningsplan Groningen 2013: Subsidence, induced earthquakes and seismic hazard analysis in the Groningen field. *NAM.*

NAM. (2017). Groningen Meet- en Regelprotocol. *NAM* (www.nam.nl)*.*

Nami, P., Schellschmidt, R., Schindler, M., & Tischner, T. (2008). Chemical stimulation operations for reservoir development of the deep crystalline HDR/EGS system at Soultz-sous-Forêts (france). *Prpceedings, Thirty-Second Workshop on Geothermal Reservoir Engineering Stanford University, Stanford, California, January 28-30, 2008 SGP-TR-185.*

Nicholls, H. R., Johnson, C. F., & Duvall, W. I. (1971). Blasting vibrations and their effects on structures. *Pittsburgh, Pennsylvania: US Department of the Interior Bureau of Mines.*

Obermann, A., Kraft, T., Larose, E., & Wiemer, S. (2015). Potential of ambient seismic noise techniques to monitor the St. Gallen geothermal site (Switzerland). *Journal of Geophysical Research: Solid Earth, 120* (6), 4301-4316.

ORAC (2019). Summary Report of the Korean Government Commission on Relations between the 2017 Pohang Earthquake and EGS Project. The Geological Society of Korea & Korean Government Commission on the Cause of the Pohang Earthquake.

Orlecka-Sikora, B. (2010). The role of static stress transfer in mining induced seismic events occurrence, a case study of the Rudna mine in the Legnica-Glogow Copper District in Poland. *Geophysical Journal International, 182* , 1087.

Orlic, B., & Wassing, B. B. T. (2012). Modeling stress development and fault slip in producing hydrocarbon reservoirs overlain by rock salt caprocks. *46th US Rock Mechanics / Geomechanics Symposium;, Chicago 2012.*

Orlic, B., & Wassing, B. B. T. (2013). A Study of Stress Change and Fault Slip in Producing Gas Reservoirs Overlain by Elastic and Viscoelastic Caprocks. *Rock Mechanics and Rock Engineering, 46* (3), 421-435.

Orzol, J., Jung, R., Jatho, R., Tischner, T., & Kehrer, P. (2005). The GeneSys-Project: extraction of geothermal heat from tight sediments. *Proceedings World Geothermal Congress 2005,* Antalya, Turkey, 24-29 April 2005.

Park, S., Xie, L., Kim, K., Kwon, S., Min, K., Choi, J., Yoon, W., & Song, Y. (2017). First Hydraulic Stimulation in Fractured Geothermal Reservoir in Pohang PX-2 Well. *Procedia Engineering; ISRM European Rock Mechanics Symposium EUROCK 2017, 191* , 829-837.

Parker, R. (1999). The Rosemanowes HDR project 1983 - 1991. *Geothermics, 28* , 603.

Parotidis, M., Shapiro, S. A., & Rothert, E. (2004). Back front of seismicity induced after termination of borehole fluid injection. *Geophysical Research Letters, 31* (L02612).

Pawley, S., Schultz, R., Playter, T., Corlett, H., Shipman, T., Lyster, S., & Hauck, T. (2018). The geological susceptibility of induced earthquakes in the Duvernay play. *Geophysical Research Letters, 45* (4), 1786-1793.

Pechmann, J. C., Walter, W. R., Nava, S. J., & Arabasz, W. J. (1995). The February 3, 1995, ML 5.1 Seismic Event in the Trona Mining District of Southwestern Wyoming. *Seismological Research Letters, 66* (3), 25-34.

Pennington, W. D., Davis, S. D., Carlson, S. M., DuPree, J., & Ewing, T. E. (1986). The evolution of seismic barriers and asperities caused by the depressuring of fault planes in oil and gas fields of South Texas. *Bulletin of the Seismological Society of America, 76* (4), 939-948.

Pluymaekers, M., Kramers, L., Van Wees, J. D., Kronimus, A., Nelskamp, S., Boxem, T., & Bonté, D. (2012). Reservoir characterisation of aquifers for direct heat production: Methodology and screening of the potential reservoirs for the Netherlands. *Netherlands Journal of Geosciences, 91* (04), 621-636.

Reijmer, J. J. G., ten Veen, J. H., Jaarsma, B., & Boots, R. (2017). Seismic stratigraphy of Dinantian carbonates in the southern Netherlands and northern Belgium. *Netherlands Journal of Geosciences, 96* (4), 353-379.

Reinecker, J., Tingay, M., Müller, B., & Heidbach, O. (2010). Present-day stress orientation in the Molasse Basin. *Tectonophysics, 482* (1), 129-138.

Richards, H. G., Parker, R. H., Green, A. S. P., Jones, R. H., Nicholls, J. D. M., Nicol, D. A. C., Randall, M. M., Richards, S., Stewart, R. C., & Willis-Richards, J. (1994). The performance and characteristics of the experimental hot dry rock geothermall reservoir at Rosemanowes, Cornwall. *Geothermics, 23* (2), 73.

Richter, C. F. (1935). An instrumental earthquake magnitude scale. *Bulletin of the Seismological Society of America, 25* (1), 1-32.

Rioseco, E. M., Löhken, J., Schellschmidt, R., & Tischner, T. (2013). 3-D geomechanical modeling of the stress field in the North German basin: case study GeneSys-borehole GT1 in hanover Groß-Buchholz. *Proceedings of the 38th Workshop on Geothermal Reservoir Engineering, Stanford University, Stanford, California, February 11-13,* 2013SGP-TR-198.

Røgen, B., Ditlefsen, C., Vangkilde-Pedersen, T., Nielsen, L. H., & Mahler, A. (2015). Geothermal energy use, 2015 country update for Denmark. *Proceedings world geothermal congress, April 19-24, 2015,* Australia-New Zealand.

Rojas, J., Giot, D., Le Nindre, Y. M., Criaud, A., Fouillac, C., Brach, M., . . . Pauwels, H. (1989). Caractérisation et modélisation du réservoir géothermique du Dogger Bassin Parisien, France   . *Report No. BRGM/RR-30169-FR, Orléans, France: BRGM.*

Ross, Z., Meier, M., Hauksson, E., & Heaton, T. (2018). Generalized Seismic Phase Detection with Deep Learning. *Bulletin of the Seismological Society of America, 108 (5A),* 2894-2901*. (arXiv Preprint arXiv:1809.02880).*

Rubinstein, J. L., Ellsworth, W. L., McGarr, A., & Benz, H. M. (2014). The 2001–present induced earthquake sequence in the Raton Basin of northern New Mexico and southern Colorado. *Bulletin of the Seismological Society of America, 104* (5), 2162-2181.

Rutqvist, J., Dobson, P. F., Garcia, J., Hartline, C., Jeanne, P., Oldenburg, C. M., Vasco, D. W., & Walters, M. (2015). The northwest Geysers EGS demonstration project, California: Pre-stimulation modeling and interpretation of the stimulation. *Mathematical Geosciences, 47* (1), 3-29.

Rutqvist, J., Birkholzer, J. T., & Tsang, C. (2008). Coupled reservoir–geomechanical analysis of the potential for tensile and shear failure associated with CO2 injection in multilayered reservoir–caprock systems. *International Journal of Rock Mechanics and Mining Sciences, 45* (2), 132-143.

Rutqvist, J., Cappa, F., Rinaldi, A. P., & Godano, M. (2014). Modeling of induced seismicity and ground vibrations associated with geologic CO2 storage, and assessing their effects on surface structures and human perception. *International Journal of Greenhouse Gas Control, 24* , 64-77.

Sausse, J., Dezayes, C., Dorbath, L., Genter, A., & Place, J. (2010). 3D model of fracture zones at Soultz-sous-Forêts based on geological data, image logs,

induced microseismicity and vertical seismic profiles. *C.R.Geoscience, 342* , 531.

Scheck, M., & Bayer, U. (1999). Evolution of the Northeast German Basin — inferences from a 3D structural model and subsidence analysis. *Tectonophysics, 313* (1–2), 145-169.

Scheck-Wenderoth, M., & Lamarche, J. (2005). Crustal memory and basin evolution in the Central European Basin System—new insights from a 3D structural model. *Tectonophysics, 397* (1), 143-165.

Schoenball, M., Baujard, C., Kohl, T., & Dorbath, L. (2012). The role of triggering by static stress transfer during geothermal reservoir stimulation. *Journal of Geophysical Research: Solid Earth, 117* (B9).

Schubert, A., Höferle, R., & Böhm, F. (2007). Geothermal Doublets Munich Riem and Pullach i . Isartal in Comparison : Geological and Drilling Concepts for Minimizing the Geological Risk in the Deep Malm Aquifer. *Proceedings of European Geothermal Congress, Unterhaching, Germany, 30 May–1 June,* , 5.

Schultz, R., Stern, V., Novakovic, M., Atkinson, G., & Gu, Y. J. (2015). Hydraulic fracturing and the Crooked Lake Sequences: Insights gleaned from regional seismic networks. *Geophysical Research Letters, 42* (8), 2750-2758.

Schumacher, M. E. (2002). Upper Rhine Graben: Role of preexisting structures during rift evolution. *Tectonics, 21* (1), 6-1; 6-17.

Segall, P., & Fitzgerald, S. D. (1998). A note on induced stress changes in hydrocarbon and geothermal reservoirs. *Tectonophysics, 289* , 117.

Segall, P. (1989). Earthquakes triggered by fluid extraction. *Geology, 17* (10), 942-946.

Segall, P., Grasso, J. R., & Mossop, A. (1994). Poroelastic stressing and induced seismicity near the Lacq gas field, southwestern France. *Journal of Geophysical Research, 99* (B8), 15.

Segall, P., & Lu, S. (2015). Injection-induced seismicity: Poroelastic and earthquake nucleation effects. *Journal of Geophysical Research: Solid Earth, 120* (7), 5082-5103.

Segall, P. (1985). Stress and subsidence resulting from subsurface fluid withdrawal in the epicentral region of the 1983 Coalinga Earthquake. *Journal of Geophysical Research: Solid Earth, 90* (B8), 6801-6816.

Seibt, P., Kabus, F., & Hoth, P. (2005). The Neustadt-Glewe geothermal power plant–practical experience in the reinjection of cooled thermal waters into sandstone aquifers. *Proceedings World Geothermal Congress 2005, Antalya, Turkey, 24-29 April 2005*.

Seibt, P., & Wolfgramm, M. (2008). Practical experience in the reinjection of thermal waters into sandstone. *Proceedings of the Workshop for decision makers on direct heating use of geothermal resources in Asia. Tianjin, China*

Sewell, S., Cumming, W., Bardsley, C., Winick, J., Quinao, J., Wallis, I., Sherburn, S., & Bourguignon, S. (2015). Interpretation of microseismicity at the Rotokawa Geothermal Field, 2008 to 2012. *Interpretation, 19* , 25.

Shapiro, S. A., & Dinske, C. (2009). Fluid-induced seismicity: Pressure diffusion and hydraulic fracturing. *Geophysical Prospecting,* , 301.

Shen, B., King, A., & Guo, H. (2008). Displacement, stress and seismicity in roadway roofs during mining-induced failure. *International Journal of Rock Mechanics and Mining Sciences, 45* (5), 672-688.

Sherburn, S., Sewell, S., Bourguignon, S., Cumming, W., Bannister, S., Bardsley, C., Winick, J., Quinao, J., & Wallis, I. (2015). Microseismicity at rotokawa geothermal field, New Zealand, 2008–2012. *Geothermics, 54* , 23-34.

Simpson, D. W., Leith, W. S., & Scholz, C. H. (1988). Two types of reservoir-induced seismicity. *Bulletin of the Seismological Society of America, 78* (6), 2025-2040.

Siskind, D. E., Stagg, M. S., Kopp, J. W., & Dowding, D. H. (1980). Structure response anddamage produced by ground vibrations from surface blasting. *Report No. Report of Investigations 8507, Washington, DC: US Bureau of Mines.*

SODM. (2016). Methodiek voor risicoanalyse omtrent geïnduceerde bevingen voor gaswining - Tijdelijke leidraad voor adressering MBB. *Report No. VERSIE 1.2, Den Haag: State Supervision of Mines.*

Spetzler, J., & Dost, B. (2017). Hypocentre estimation of induced earthquakes in Groningen. *Geophysical Journal International, 209* (1), 453-465.

Suckale, J. (2009). Induced seismicity in hydrocarbon fields. *Advances in Geophysics, 51.*

Sumy, D. F., Cochran, E. S., Keranen, K. M., Wei, M., & Abers, G. A. (2014). Observations of static Coulomb stress triggering of the November 2011 M5.7 Oklahoma earthquake sequence. *Journal of Geophysical Research: Solid Earth, 119* (3), - 2013JB010612.

Talwani, P., & Acree, S. (1984). Pore pressure diffusion and the mechanism of reservoir-induced seismicity. *Pure and Applied Geophysics, 122* (6), 947-965.

Tenzer, H., Park, C., Kolditz, O., & McDermott, C. I. (2010). Application of the geomechanical facies approach and comparison of exploration and evaluation methods used at Soultz-sous-Forêts (France) and Spa Urach (Germany) geothermal sites. *Environmental Earth Sciences, 61* (4), 853-880.

ter Heege, J., Osinga, S., Wassing, B., Candela, T., Orlic, B., Buijze, L., & Chitu, A. (2018). Mitigating induced seismicity around depleted gas fields based on geomechanical modeling. *The Leading Edge, 37* (5), 334-342.

TerHeege, J., Osinga, S., & Carpentier, S. (2018). The Geomechanical Response of Naturally Fractured Carbonate Reservoirs to Operation of a Geothermal Doublet. *52nd US Rock Mechanics/Geomechanics Symposium*

Tischner, T., Krug, S., Pechan, E., Hesshaus, A., Jatho, R., Bischoff, M., & Wonik, T. (2013). Massive hydraulic fracturing in low permeable sedimentary rock in the GeneSys project. *Proceedings, Thirty-Eighth Workshop on Geothermal Reservoir Engineering, Stanford University, Stanford, California, February 11-13,* 2013, SGP-TR-198.

TNO, & EBN. (2018). Play-based portfoliobenadering, eerste inzicht in zes voordelen voor veilig en verantwoord, kosteneffectief versnellen van geothermie. Utrecht.

Trautwein, U., & Huenges, E. (2005). Poroelastic behaviour of physical properties in Rotliegend sandstones under uniaxial strain. *International Journal of Rock Mechanics and Mining Sciences, 42* , 924.

Trugman, D. T., Shearer, P. M., Borsa, A. A., & Fialko, Y. (2016). A comparison of long-term changes in seismicity at The Geysers, Salton Sea, and Coso geothermal fields. *Journal of Geophysical Research: Solid Earth, 121* (1), 225-247.

Ungemach, P., Antics, M., & Papachristou, M. (2005). Sustainable geothermal reservoir management. *Proceedings World Geothermal Congress 2005, Antalya, Turkey, 24-29 April 2005.*

Urbancic, T., & Zinno, R. (1998). Cotton Valley Hydraulic Fracture Imaging Project: Feasibility of determining fracture behavior using microseismic event locations and source parameters. *1998 SEG Annual Meeting.*

USACE. (1972). Systematic drilling and blasting for surface excavations. *Report No. EngineeringManual EM 1110-2-3800., Washington: US Army Corps of Engineers.*

Van Adrichem Boogaert, H. A., & Kouwe, W. F. P. (1993-1997). *Stratigraphic Nomenclature of the Netherlands. TNO.*

Van de Graaf, T., Haesebrouck, T., & Debaere, P. (2018). Fractured politics? The comparative regulation of shale gas in Europe. *Journal of European Public Policy, 25* (9), 1276-1293.

van Thienen-Visser, K., & Breunese, J. (2015). Induced seismicity of the Groningen gas field: History and recent developments. *The Leading Edge, 34* (6), 664-671.

Van Wees, J. D., Buijze, L., Van Thienen-Visser, K., Nepveu, M., Wassing, B. B. T., Orlic, B., & Fokker, P. A. (2014). Geomechanics response and induced seismicity during gas field depletion in the Netherlands. *Geothermics, 52* (0), 206-219.

Veldkamp, J.,G, Mijnlieff, H., Bloemsma, M., Donselaar, R., Henares, S., Redjosentono, A., & Weltje, G. J. (2015). Permian Rotliegend Reservoir Architecture of the Dutch Koekoekspolder Geothermal Doublet. *World Geothermal Congress 2015 Melbourne.*

Vidal, J., & Genter, A. (2018). Overview of naturally permeable fractured reservoirs in the central and southern Upper Rhine Graben: Insights from geothermal wells. *Geothermics, 74* , 57-73.

Vidal-Gilbert, S., Nauroy, J. -., & Brosse, E. (2009). 3D geomechanical modelling for CO2 geologic storage in the Dogger carbonates of the Paris Basin. *International Journal of Greenhouse Gas Control, 3* , 288.

Walsh, F. R., & Zoback, M. D. (2015). Oklahoma's recent earthquakes and saltwater disposal. *Science Advances, 1* (5).

Wassing, B. B. T., Buijze, L., & Orlic, B. (2017). Fault reactivation and fault rupture in producing gas fields with elastic and visco-elastic caprocks. *51st Rock Mechanics Symposium San Francisco, ARMA 17-355.*

Wiemer, S., Kraft, T., Trutnevyte, E., & Roth, P. (2017). "Good Practice" Guide for Managing Induced Seismicity in Deep Geothermal Energy Projects in Switzerland. *Report , Zürich: Swiss Seismological Service.* doi: https://doi.org/10.3929/ethz-b-000254161

Willems, C. J. L. (2017). *Doublet deployment strategies for geothermal Hot Sedimentary Aquifer exploitation. Application to the Lower Cretaceous Nieuwerkerk Formation in the West Netherlands Basin.* (PhD, Technical University Delft).

Wiprut, D., & Zoback, M. D. (2000). Fault reactivation and fluid flow along a previously dormant normal fault in the northern North Sea. *Geology, 28* (7), 595-598.

Wolfgramm, M., Bartels, J., Hoffmann, F., Kittl, G., Lenz, G., Seibt, P., Unger, H. J. (2007). Unterhaching geothermal well doublet: structural and hydrodynamic reservoir characteristic; Bavaria (Germany). *Proceedings European Geothermal Congress, Unterhaching, Germany, 30 May-1 June 2007.*

Wong, I. (1985). Mining-induced earthquakes in the Book Cliffs and eastern Wasatch Plateau, Utah, USA. *International Journal of Rock Mechanics, Mining Science and Geomechanics Abstracts, 22* , 263-270.

Wong, I. G., Humphrey, J. R., Adams, J. A., & Silva, W. J. (1989). Observations of mine seismicity in the eastern wasatch plateau, utah, USA: A possible case of implosional failure. *Seismicity in Mines* (pp. 369-405 Springer.

Yerkes, R. F., & Castle, R. O. (1976). Seismicity and faulting attributable to fluid extraction. *Engineering Geology, 10* (2–4), 151-167.

Yuliang, H., Zuyuan, L., Oingyuan, Y., Xiancheng, C., Ping, H., Wentao, M., & Jun, L. (1996). Induced seismicity at Wujiangdu Reservoir, China: A case induced in the karst area. *Pure and Applied Geophysics, 147* (2), 409-418.

Zang, A., Oye, V., Jousset, P., Deichmann, N., Gritto, R., McGarr, A., Majer, E., & Bruhn, D. (2014). Analysis of induced seismicity in geothermal reservoirs – An overview. *Geothermics, 52* (0), 6-21.

Zemach, E., Drakos, P., Spielman, P., & Akerley, J. (2017). Desert Peak east Enhanced Geothermal Systems (EGS) project. *Draft Final Report , Ormar Nevada, Inc.*

Zhao, P., Kühn, D., Oye, V., & Cesca, S. (2014). Evidence for tensile faulting deduced from full waveform moment tensor inversion during the stimulation of the Basel enhanced geothermal system. *Geothermics, 52* , 74-83.

Ziegler, P. A. (1990). Geological atlas of western and central Europe.

Zimmermann, G., Moeck, I., & Blöcher, G. (2010). Cyclic waterfrac stimulation to develop an enhanced geothermal system (EGS): Conceptual design and experimental results. *Geothermics, 39* (1), 59.

Zimmermann, G., Tischner, T., Legarth, B., & Huenges, E. (2009). Pressure-dependent Production Efficiency of an Enhanced Geothermal System (EGS): Stimulation Results and Implications for Hydraulic Fracture Treatments. *Pure and Applied Geophysics, 166* , 1089 - 1106.

Appendix A

In this Appendix a selection of geothermal sites is described in detail. The geothermal sites that were included were limited to deep geothermal sites used for the generation of electricity or district/space heating.

These case studies include geothermal systems where induced seismicity was recorded, but also those where no induced events were observed. The case studies are grouped per geothermal area or basin, and are located in different countries to ensure diversity. The geothermal systems have different purposes, e.g. the generation of electricity or district heating, and therefore target different rock types, with different temperatures, at different depths.

Case studies were selected based on data availability and diversity in terms of rock type, location, depth, and temperature. Many of the best-documented geothermal sites where notable seismicity has occurred have been studied.

A.1 Upper Rhine Graben, Germany/France

The Upper Rhine Graben is a 300 km long NNE trending rift system running from the Jura Mountains in the south to Frankfurt in the north (Figure A-1). It is on average 30 – 40 km wide and is flanked by shoulders which rise 400 m (north) to 1200 m (south) above the graben floor (Grimmer et al., 2017). The graben is bounded by large normal faults on the east and west side, and contains many smaller internal faults along the same orientation. The main tectonic structures are inherited from the Variscan orogeny (Late Paleozoic: Permo-Carboniferous). During this time NNE-SSW striking sinistral shear zones formed, which disrupted ENE trending Permo-Carboniferous troughs and highs (Grimmer et al., 2017; Schumacher, 2002). These troughs were filled with Late Carboniferous – Early Triassic sediments, which increased in thickness towards the north. Later sedimentation up to the Upper Jurassic was more homogeneous over the graben. The tectonic structures were reactivated during the Eocene (Cenozoic) as a result of Alpine orogeny. Multiple phases of deformation caused uplift and subsidence along NNE trending faults. Cenozoic sediments were deposited over the Mesozoic sediments, increasing in thickness towards the east of the graben up to 3.5 km (Grimmer et al., 2017). The current-day stress field is marked by a normal faulting to strike-slip regime (transtensional) with the maximum horizontal stress trending NW-SE. The region is seismically active with frequent small events and some destructive events in recent history (M_L 6.5 – 6.9 in 1356). The graben is the site of a large temperature anomaly, with temperatures of 75 – 150 °C at 2 km depth (Baillieux et al., 2013).
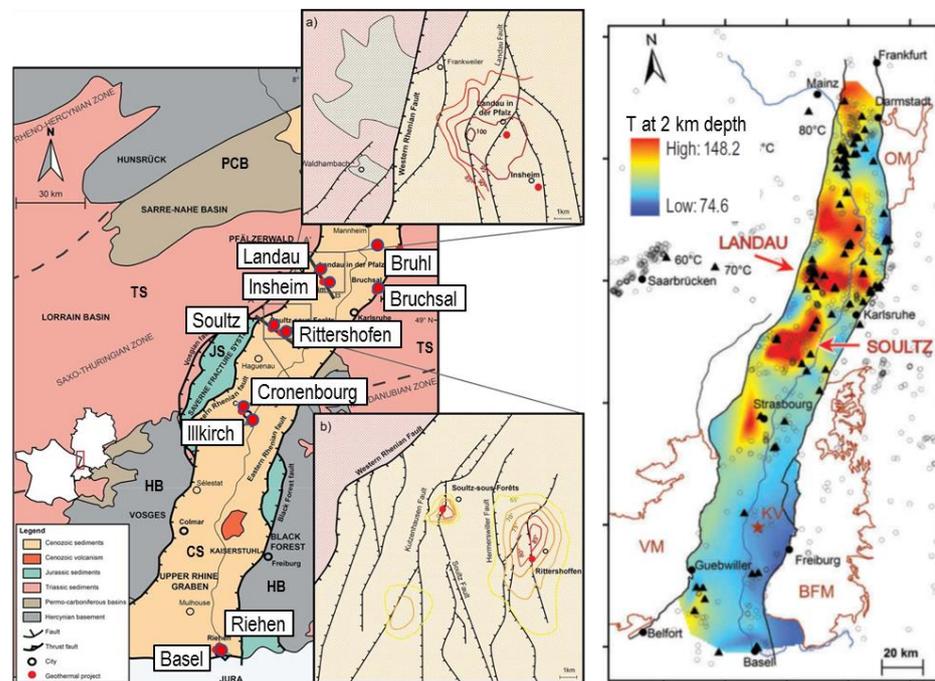

Figure A-1   Structures, temperature and location of geothermal sites in the Upper Rhine Graben. a) Geological map of the Upper Rhine Graben showing the locations of geothermal systems. HB: Hercynian Basement, PCB: Permo-Carboniferous Basement, JS: Jurassic Sediments, TS: Tertiary Sediments, CS: Cenoizoic Sediments. Close-ups show the local fault orientations(Modiefied from Vidal & Genter, 2018, Copyright Elsevier, published under a Creative Commons License). b) Temperature at 2 km depth (From: Baillieux et al., 2013, Copyright Taylor & Francis, reproduced with permission).

A.1.1   Basel, Switzerland (M 3.4)

Country & place:	Switzerland, Basel	
Activity:	Geothermal EGS	
Start date – End date:	02 – 12 - 2006	08 – 12 – 2006
Fluid + Fluid balance:	Water	Injection
Activity depth:	5 km	
Activity rocktype:	Granite	
In-situ T	190 °C	
Cumulative ΔV:	11,570 m^3	
Maximum Top Hole Pressure:	29.6 MPa	
Maximum flowrate:	55 l/s	
Monitoring system:	Yes	
Maximum magnitude + Date:	3.4	08 – 12 - 2006
Distance M_{max} – activity:	0.1 km	
Intensity [EMS]:	IV-V	
Damage:	Slight non-structural damage	
Interpretation	Induced by pore pressure increase	

Tectonic setting and geology: The Basel EGS is located in northwestern Switzerland at the southern end of the Upper Rhine Graben. The Basel EGS targeted fractured granitic basement, the top of which was encountered from 2557 m depth (Häring et al., 2008). At 5 km depth the reservoir temperature was estimated at 190 °C. Clay-filled fracture zones were identified in the wellbore.

Activity design: A single vertical wellbore (Basel 1) was drilled into the basement to a depth of 5 km. The bottom part of the well was an open hole section from 4.63 – 5 km.

Operations and monitoring: A low-rate injection test was conducted on 23 November 2006, injecting ~600 m^3 at a flowrate of 0.16 l/s and a maximum wellhead pressure of 7.4 MPa was reached. The main stimulation started on 2 December 2006. Over the course of 6 days a total of 11,570 m^3 water was injected, at a maximum flowrate of 55 l/s and a maximum wellhead pressure of 29.6 MPa (Figure A-2) (Deichmann et al., 2014; Häring et al., 2008). On 8 December 2006 injection rate was reduced because of the high seismicity rate. Five hours later the well was shut in, and then bled-off because seismicity did not decrease. Since then 3400 m^3 of flowback was recorded. A microseismic monitoring array was in place, operative since February 2006 throughout the stimulation and subsequent months. The monitoring system consisted of 6 borehole stations at depths between 320 and 2745 m. In addition seismicity was recorded by the national network.
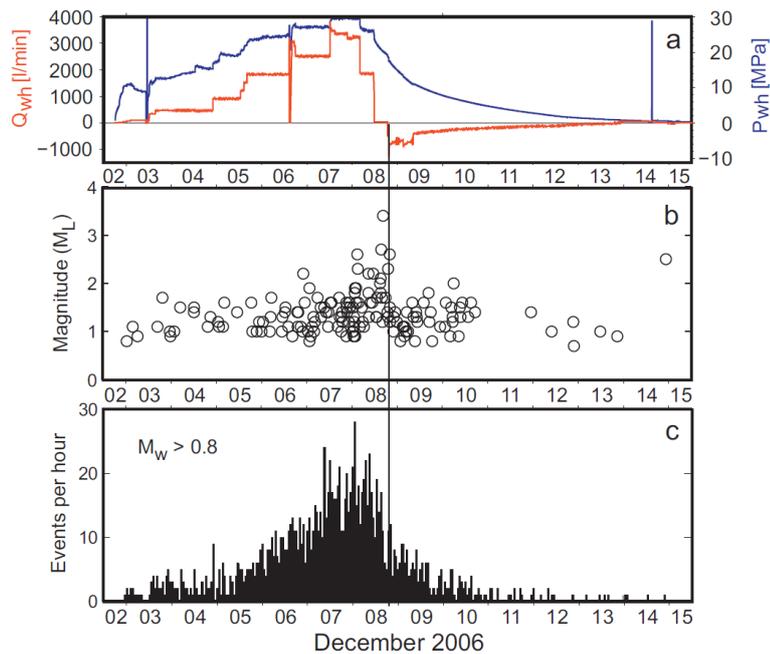
Figure A-2   Operational data and recorded seismicity during the main stimulation of the Basel 1 well. The wellhead flowrate Q_{wh} is shown in l/min, and the wellhead pressure P_{wh} in MPa (From Deichmann et al., 2014, Copyright Elsevier, reproduced with permission).

Occurrence of seismicity: The first seismic events were detected a few hours after stimulation started. During the whole stimulation 11,200 events were detected with $-1 < M_L < 3.4$. The largest event with a M_L 3.4 occurred just after bleed-off of the well. Seismic activity declined but continued for months after bleeding off the well, with several $M_L > 3$ occurring in January and February 2007 and smaller events occurring up to 2013 (Deichmann et al., 2014). Events occurred at a distance up to 1 km from the well, highlighting a steep plane, striking in the direction of the maximum horizontal stress (Figure A-3).
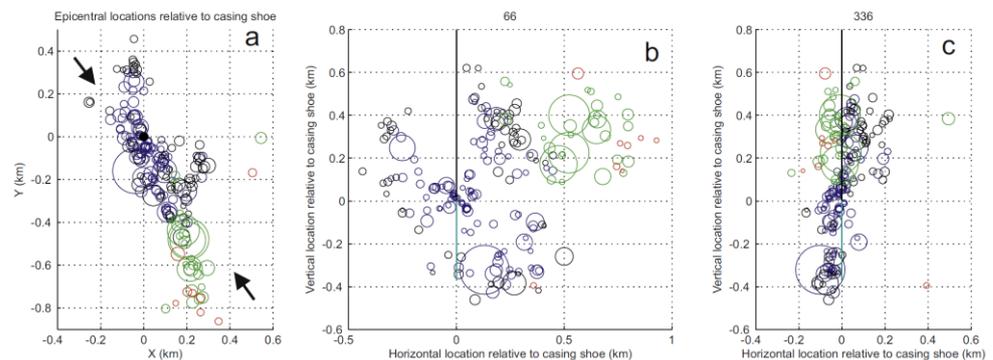

Figure A-3   Location of seismic events at the Basel 1 EGS. Darkblue: events recorded during stimulation from 2 to 8 December 2006, black: 9 to 31 December 2006, green: 1 January to 30 November 2007, red: eight events in 2010, 2012, 2013. The size of the circles gives the relative magnitude. The borehole is indicated with the black line, and the open hole section with a light blue line. Arrows indicate the maximum horizontal stress (From Deichmann et al., 2014, Copyright Elsevier, reproduced with permission).

Interpretation: The elevated pore pressures from the main stimulation caused reactivation of pre-existing faults and fractures. Diffusion of pore pressure caused post-injection seismicity and expansion of the seismic cloud after shut-in. Focal planes and detailed analysis of the seismic cloud showed that the internal structure of the stimulated fault zone was complex with numerous small faults and fractures oriented at different orientation compared to the main trend in Figure A-3a (Deichmann et al., 2014).

A.1.2   Bruchsal, Germany

Country & place:	Germany, Bruchsal	
Activity:	Geothermal	
Start date – End date:	2002	To date
Fluid + Fluid balance:	Water	Circulation
Activity depth:	2.5 km	
Activity rocktype:	Sandstones	
In-situ T	134 °C	
Cumulative ΔV:	Balanced	
Maximum Top Hole Pressure:	0.5 MPa	
Maximum flowrate:	28 l/s	
Monitoring system:	Yes (Since June 2010)	
Maximum magnitude + Date:	N/A	N/A
Distance M_{max} – activity:	N/A	
Intensity [EMS]:	N/A	
Damage:	N/A	
Interpretation	N/A	

Tectonic setting and geology: The Bruchsal geothermal system is located in the central part of the Upper Rhine Graben, close to the Eastern boundary fault (Figure A-1) The area around Bruchsal is characterized by 3 dominant fault structures; NNE-SSW striking normal faults dipping 60-80° to the W-NW, parallel and synthetic to the Eastern boundary fault; the second set of faults are NE-SW to N-S antithetic normal faults and the third set are NW-SE striking transfer faults (Figure A-4) accommodating a 500 m vertical offset between the two wells of the geothermal system (Meixner et al., 2016). The present day stress field at the Bruchsal geothermal site is characterized by a transitional normal faulting to strike-slip regime with a maximum horizontal stress orientation of N142°E ± 20° (Meixner et al., 2016). The Bruchsal site has a low seismic hazard level (Evans, K. F. et al., 2012). The geothermal reservoir is located between 1.8-2.5 km depth and consists of highly fractured Lower Triassic sandstones (Bundsandstein) and Upper Permian sandstones and breccia conglomerates (Rotliegend and Zechststein). The temperatures in the reservoir range between 100-135 °C and the reservoir shows slight underpressure conditions (Meixner et al., 2014). The permeability in the reservoir is controlled by water bearing fractures (Meixner et al., 2016).
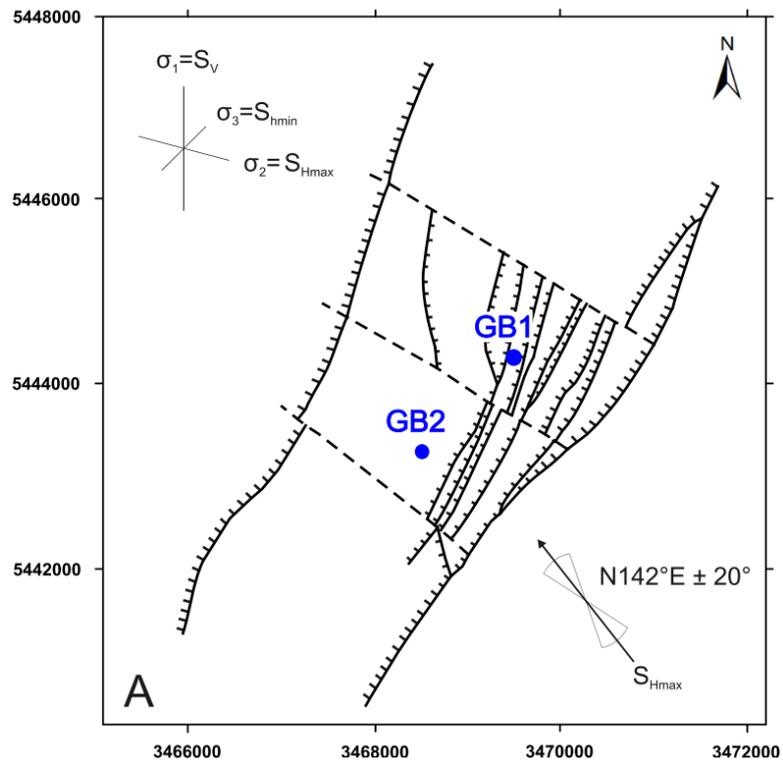
Figure A-4   Fault pattern around the Bruchsal geothermal doublet at a depth of 1000m below sea-level (From Meixner et al., 2016, Copyright Elsevier, reproduced with permission).

Activity design: The first well (GB1) was drilled vertically in 1983 to a depth of 1932 m, followed by the second well (GB2) in 1987 to a depth of 2542 m. The two wells are 1.5 km apart (Herzberger et al., 2010). In the initial configuration the GB1 well served as the production well, this configuration was later changed. The doublet is aligned parallel to the Eastern boundary fault and separated by a NW-SE striking fault with a vertical offset of 500 m. Due to this separating fault, the GB1 well intersects the top of the Bundsandstein at 1685 m, whereas the GB2 well intersects the top of the Bundsandstein at 2220 m (Meixner et al., 2016). The GB1 well is drilled through NNE-SSW striking normal faults (Evans et al., 2012).

Operations and monitoring:
The well was first put into operation in 1987, when it circulated at up to 15 l/s, producing at GB1 and injecting at GB1. The system produced water with temperatures of 100 °C. For economic reasons the system was abandoned in 1990. It was reactivated in 2002 using the deeper GB2 well as the production well. After the change in configuration, circulation tests showed flow rates of 28.5 l/s and wellhead temperatures of 120 °C (Herzberger et al., 2010). Since 2009 a power (Kalina) plant has been in operation. The system has been producing at a flow rate of 24 l/s. A seismic monitoring system composed of 4 stations has been in place since June 2010. Each station consists of 3 orthogonal geophones, which are installed at 100 m depth. The stations are positioned within a radius of 2.5 km from the doublet (Gaucher, 2016).
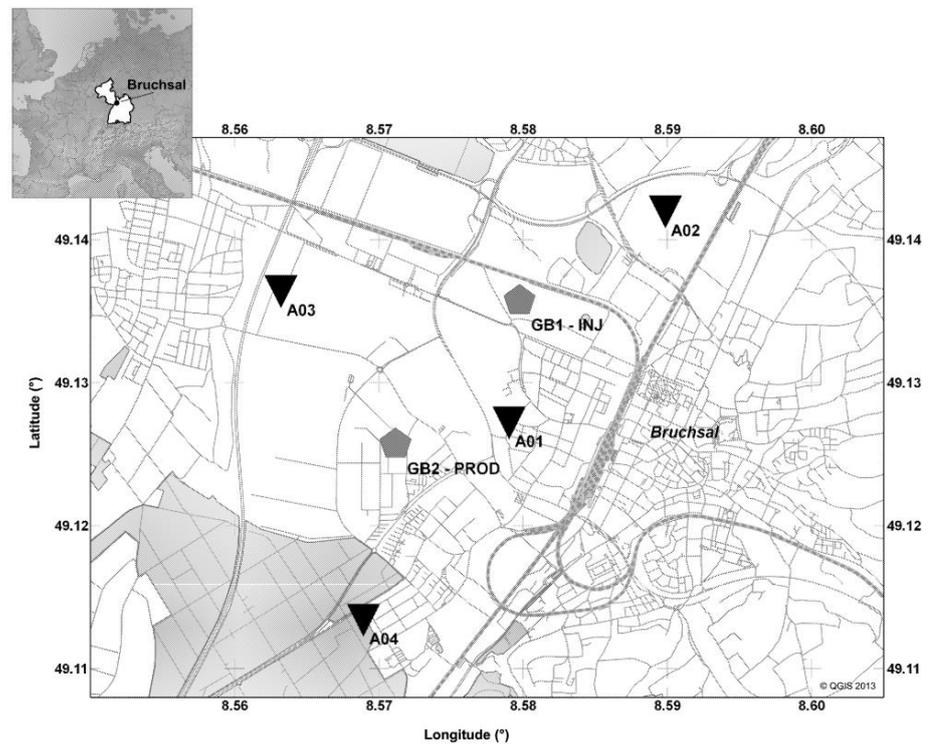
Figure A-5 Locations of Bruchsal doublet and seismic monitoring stations (From Gaucher, 2016, Copyright Wiley, reproduced with permission).

Occurrence of seismicity: There are no reports of felt micro seismicity in the area that can be linked to the operation of the geothermal system (Evans, K. F. et al., 2012). Taking the detection capability of the monitoring system into account, it can be stated with 95% certainty that no earthquake with a local magnitude (M_L) larger than 0.7 has occurred in the area, since the start of monitoring in 2010 (Gaucher, 2016).

Interpretation: The graben parallel faults (NE-SW to NNE-SSW) are characterized by low reactivation potential for both shear and tensile failure in the present day stress field. The transfer faults (NW-SE) have a high reactivation potential for tensile failure, but are also characterized by a low potential for shear reactivation (Meixner et al., 2016).The orientation of the faults relative to the present day stress field may explain the absence of induced seismicity.

A.1.3   Insheim, Germany (M_L 2.4)

Activity:	Geothermal EGS (electricity generation)	
Start date – End date:	7 – 4 – 2010	14 – 4 – 2010
Fluid + Fluid balance:	Water	Injection, circulation
Activity depth:	3.6	
Activity rocktype:	Bundsandstein and Rotliegend sandstones, granitic basement	
In-situ T	165°C	
Cumulative ΔV:	9000 (stimulation), balanced (circulation)	
Maximum Top Hole Pressure:	9 MPa (stimulation), 1.2 MPa (circulation)	
Maximum flowrate:	180 l/s (stimulation), 62 l/s	
Monitoring system:	Yes	
Maximum magnitude + Date:	2.4	09-04-2010
	2.1	08-2013
Distance M_{max} – activity:	< 1 km	
Intensity [EMS]:		
Damage:	felt at the surface	
Interpretation	The pressure gradient between the wells induced faulting on pre-existing fault planes	

Tectonic setting and geology: The Insheim geothermal site is located in the Upper Rhine Graben, 6 km southwest of Landau and 30 km northeast of Soultz-sous-Forêts (Figure A-1, Figure A-6a). The target formations at Insheim are the Triassic (Muschelkalk, ~200 - 300 m thick, Bundsandstein 200 – 300 m thick) and Permian (Rotliegend ~400 m thick) sediments, and the top 100 m of the granitic basement which lies at a depth of 2824 – 3537 m (Figure A-6b).

Activity design: The GTI 1 well was drilled in 2008, reaching a maximum depth of 3.4 km. The 1000 m open-hole section covered Bundsandstein and Rotliegend sandstones, and the upper 100 m of the granitic basement, where temperatures were 165°C (Kuperkoch). A second well GTI 2 was drilled in 2009 from the same location (3.6 km deep). The wells were deviated from 1500 m downwards, and were 1000 m apart at 3.6 km. Both wells were drilled through two of the west-dipping faults in Figure A-6b. A sidetrack from GTI 1 was drilled in 2010 (GTI 1b) from 2.6 to 3.6 km as the injectivity was low in GTI 1.
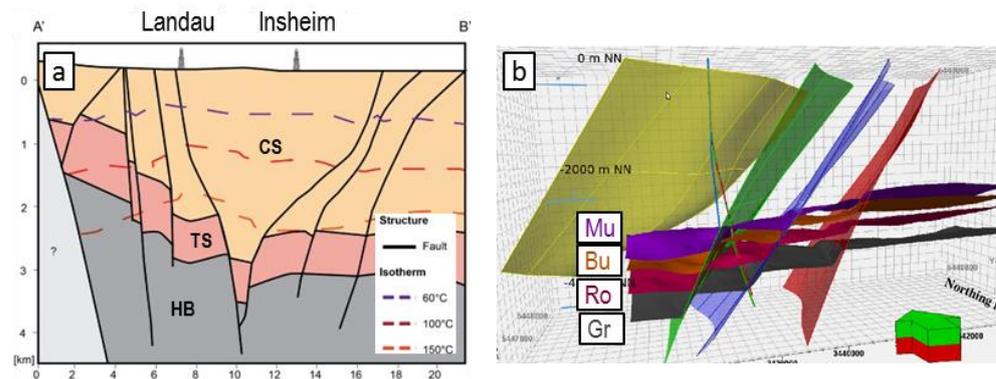
Figure A-6   Faults and formations at Insheim. a) Vertical cross-section showing the subsurface below Landau and Insheim, including faults (black lines) and main formations. HB: Hercynian Basement, TS: Triassic Sediments, and CS: Cenozoic Sediments. Isotherms are shown (dashed lines).(Modified from Vidal & Genter, 2018, Copyright Elsevier, published under a Creative Commons license). b) 3D geological model below Insheim. The top of the Triassic Muschelkalk (Mu) and Bundsandstein (Bu), the Permian Rotliegend (Ro), and the granitic basement (Gr) are shown. Four major west-dipping faults are indicated with the yellow, green, purple, and red planes. Well paths for GTI 1 (red), GTI 1b (green), and GTI 2 (blue) are shown (From Küperkoch et al., 2018, Copyright Seismological Society of America, reproduced with permission).

Operations and monitoring: Several well tests were performed in injection well GTI 1 in March 2010, followed by hydraulic stimulations in April 2010 (Baumgärtner et al., 2013). These stimulations were conducted in four phases, injecting a total volume of 9000 m^3 with a maximum wellhead pressure of 9 MPa and maximum flowrates of 120 l/s. Production of heat through circulation of water started in October 2012 (Küperkoch et al., 2018). Microseismic monitoring was in place during stimulation and circulation with three permanent borehole stations, as well as permanent and temporary surface stations.

Occurrence of seismicity: During stimulation in April 2010 tens of events were recorded, with a reported maximum M_L 2.4 (Baumgärtner et al., 2013). From the start of circulation to the end of 2015 ~600 events were recorded with a 0.4 < M_L 2.1 (Küperkoch et al., 2018). The events occurred predominantly in the granitic basement from 3 – 5 km, near and between both wells (Figure A-7). In particular some of the large events occurred near the production well. Focal mechanisms indicated oblique normal faulting on N-S striking planes consistent with the larger fault structures. Early during the injection also a NW-SE trending fault was reactivated (Figure A-7a).
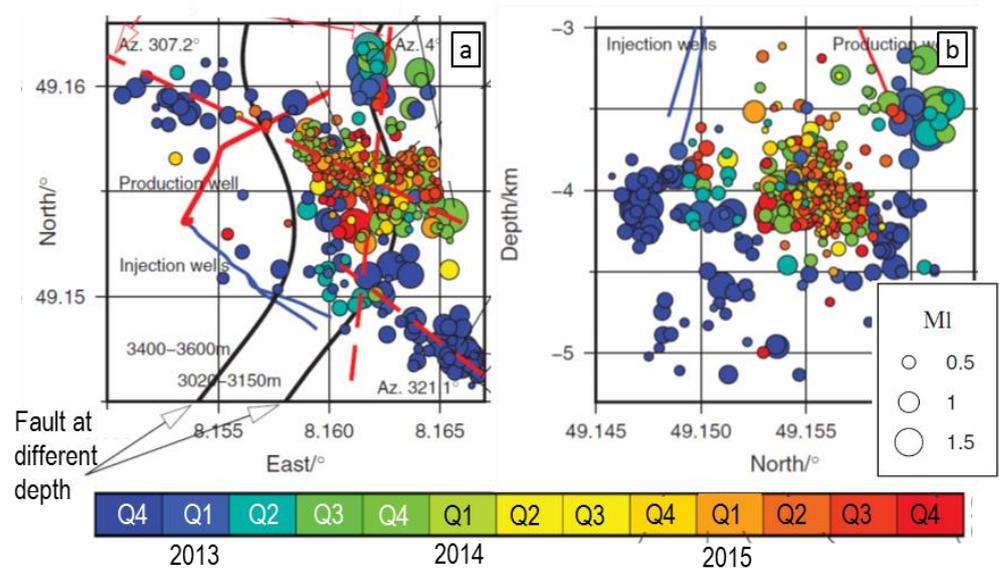
Figure A-7　　Seismicity observed at Insheim from late 2012 to end 2015 (From Küperkoch et al., 2018, Copyright Seismological Society of America, reproduced with permission). The color scale indicates the timing of the events. The injection (blue lines) and production wells (red line) are drawn, as well as one of faults (black line). a) Top view of seismicity. Dashed lines indicate the orientation of the reactivated faults. b) Cross-section view of seismicity.

Interpretation: The pressure gradient between the wells induced faulting on pre-existing fault planes. Most of the seismicity occurred in the granitic basement.

A.1.4   Rittershoffen, France (ML 1.6)

Activity:	Geothermal stimulation, thermal, chemical and hydraulic	
Start date – End date:	2012	2014
Fluid + Fluid balance:	Water, acid	Injection, circulation
Activity depth:	2.5 – 2.7 km	
Activity rocktype:	Sandstones and hydrothermally altered granite	
In-situ T	160 °C – 180 °C	
Cumulative ΔV:	Stimulation: 4230 m^3 (T)+300 m^3 (C)+4100 m^3 (H) Circulation: 2.590.000 m3	
Maximum Top Hole Pressure:	3 MPa	
Maximum flowrate:	80 l/s	
Monitoring system:	Yes	
Maximum magnitude:	M_L 1.6 (stimulation) M_L 1.3 (circulation)	
Distance M_{max} – activity:	< 1km	
Intensity [EMS]:	No felt events	
Damage:	-	
Interpretation	Pore pressure increase and static stress transfer	

Tectonic setting and geology: The Rittershoffen ECOGI geothermal site is located in the western part of the Upper Rhine Graben, 6 km east of the Soultz-sous-Forêts geothermal site (Figure A-1). The target formations at Rittershoffen are the Lower Triassic Bundsandstein (sandstones) and the top of the hydrothermally altered granitic basement. The top of the crystalline basement is located at a depth of 2200 m. The wells target the normal fault in the crystalline basement (Rittershoffen Fault), which bounds the local graben structure in which the wells are located (Figure A-8). The Rittershoffen Fault has a N355°E strike and dips 45° in a western direction, with a vertical offset of more than 250 m. The temperature logs in the wells suggest an advection-dominated temperature regime in the Buntsandstein and crystalline basement rocks, with important natural flow in the targeted fault zone (Baujard, C. et al., 2017; Vidal & Genter, 2018).
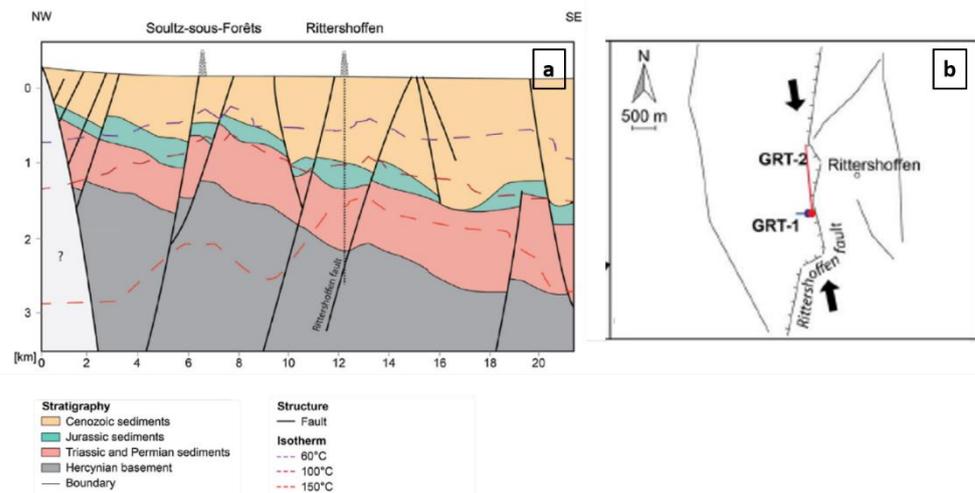
Figure A-8   a) Simplified geological cross-section of Rittershoffen, presenting main fault structures and temperature anomalies in the region. The vertical dotted line represents the location of the GRT-1 well, intersecting the Rittershoffen fault. b) Location of wells GRT-1 and GRT-2 (From Baujard, C. et al., 2017 and Vidal & Genter, 2018, both Copyright Elsevier, published under a Creative Commons License).

Activity design: The Rittershoffen ECOGI doublet consists of two wells, GRT-1 and GRT-2. The sub-vertical GRT-1 well was drilled from September to December 2012, reaching a maximum depth of 2580 m. From mid-March to end July 2014 a second well, GRT-2, was drilled, which is deviated 37° to the north and reaches a depth of 2708 m (TVD). Both wells have open-hole sections, the top of which is encountered at a depth of 1800 m (GRT-1) and 1872 m depth (GRT-2). The open-hole sections cross the Buntsandstein and Permian sandstones and the crystalline basement of hydrothermally altered fractured granites as well as intact granites (Baujard, C. et al., 2017; Vidal & Genter, 2018).

Bottom hole temperatures in the wells are 160 °C (GRT-1) to 180 °C (GRT-2). The wells are approximately 3 km apart at depth. A hydraulic connection between GRT-1 and GRT-2 has been identified.

Operations and monitoring: From December 30th 2012 to January 10th 2013 well clean-up operations and several production tests were performed in GRT-1. A total volume of 6400 m3 of fluids were produced during these operations. To enhance the initially low productivity index, well GRT-1 was stimulated in three stages. Between April 23rd and April 25th 2013, a thermal stimulation was performed with low-rate cold fluid injection. The total volume of fluids injected during this first phase of stimulation was 4230 m^3. Fluids were injected at a constant temperature of 12°C, at six different injection rates ranging between 10 l/s and 25 l/s . The maximum wellhead pressure reached during thermal stimulation was 28 bar. Between June 22nd and June 27th 2013, a chemical stimulation was applied. A total volume of 216 m3 of environmentally friendly acids was injected at three isolated depth intervals in the Buntsandstein and granitic basement. Finally, immediately following the chemical stimulation, on June 27th and June 28th, the well was hydraulically stimulated with several step rate injections with maximum flowrates up to 80 l/s (Baujard, C. et al., 2017). Wellhead pressures during stimulation reached 30 bar overpressure. A total volume of 4100 m3 of fluids was injected into the reservoir. Decisions whether or not

to proceed with a next injection step were based on observed seismicity rates, recorded by an advanced seismological monitoring network composed of 18 surface stations, allowing for real-time localization of the seismic events (Maurer et al., 2015).

Well development in GRT-2 was not necessary, due to the high initial productivity index (Baujard et al., 2017).

The geothermal plant at Rittershoffen has been in commercial operation since September 2016 (Baujard et al., 2017). Since the start of commercial operations, 630.000 m3 (2016) and 1.960.000 m3 (2017) of brine have been circulated for heat production (Baujard et al., 2018). Seismic monitoring continued since the start of commercial operations at the site.

Occurrence of seismicity: The thermal stimulation generated 113 seismic events, with a maximum reported magnitude of M_L 1.2 (Baujard, C. et al., 2017). No seismic events were detected during the chemical stimulation of the well. During and following the hydraulic stimulation, in total 1395 events were detected (Lengline et al., 2017). First seismic activity during stimulation was recorded at injection rates above 40 l/s, linked to overpressures of 25 bar (exceeding the maximum flowrate of the thermal stimulation) (Baujard et al., 2017; Lengline et al., 2017). Seismicity stopped after injection, but a second swarm of seismic events was recorded 4 days after shut-in of the well, with a maximum reported magnitude of M_L 1.6. The maximum allowable threshold of M_L 1.7 was not reached and seismic events could not be felt by the local population (Baujard et al., 2017; Maurer et al., 2015). Almost all seismic events occurred within a distance of 1 km from the GRT-1 injection well, at a depth between 2200 m and 2400 m (Lengline et al., 2017). The well development strategy applied to GRT-1 was considered successful, as a significant increase of the injectivity index by a factor 5 was achieved with very limited induced seismicity.

Seismic monitoring in 2017 revealed a total of 734 seismic events, mostly located within a distance of 600 m of GRT-1. The maximum reported local magnitude is M_L 1.3 (PGV 0.24 mm/s), well below the pgv threshold of 1.5 mm/s (Baujard et al., 2018).

Interpretation: The seismicity during injection is related to the overpressures and associated pore pressure diffusion, which induced seismicity on a pre-existing critically-stressed fault structure in the granite basement. The second swarm of seismic events, which occurred after a 4 days seismically quiet period after shut-in has been explained by the occurrence of aseismic slip on the fault and associated static slip transfer (Lengline et al., 2017).

A.1.5   Soultz-sous-Forêts, France (M_L 2.9)

Activity:	Geothermal EGS	
Start date – End date:	1989	
Fluid + Fluid balance:	Water	Injection
Activity depth:	4.7 - 5 km	
Activity rocktype:	Granite	
In-situ T	200 °C	
Cumulative ΔV:	22,680 m^3 in GPK2	30-6-2000 to 6-7-2000
	37,300 m^3 in GPK3	27-5-2003 to 7-6-2003
	9,300 m^3 in GPK4	13-9-2004 to 16-9-2004
	12,340 m^3 in GPK4	
Maximum Top Hole Pressure:	13 - 19 MPa	
Maximum flowrate:	45 - 90 l/s	
Monitoring system:	Yes	
Maximum magnitude + Date:	2.9	10 – 06 - 2003
Distance M_{max} – activity:	0.35 km	
Intensity [EMS]:	IV	
Damage:	slight non-structural damage	
Interpretation	Induced by pore pressure increase	

Tectonic setting and geology: The Soultz-sous-Forêts site is situated in the Upper Rhine Graben, ~5 km from its main western bounding fault (Figure A-1). The Rhine Graben is tectonically active, with extension in the east-west direction as a result of the Alpine orogeny (Dorbath et al., 2009; Tenzer et al., 2010). The maximum horizontal stress is oriented 170°, and the stress regime determined from focal mechanisms is transitional from normal faulting to strike-slip (Horálek et al., 2010). The Soultz-sous-Forêts system targets the fractured granitic basement, which starts at a depth of 1.4 km, and reaches a temperature of 200 °C at 5 km depth (Dorbath et al., 2009; Tenzer et al., 2010).

Activity design: The Soultz-sous-Forêts system consists of multiple wells, which were drilled at various times between 1989 and 2004 (e.g. Tenzer et al., 2010). GPK1 reached 3.6 km in 1992, and GPK2 was drilled to 3.9 km depth in 1995. GPPK2 was deepened to 5 km in 1999, and two other wells (GPK3, GPK4) were drilled from the same location and were deviated from 2.5 km downwards, so they are spaced 500 – 600 m apart at the maximum depth of 5 km (Figure A-9).

Operations and monitoring: Many injection and circulation experiments were conducted from 1991 to date, including a number of large volume stimulations. The GPK1 and GPK2 well were stimulated at 3.6 and 3.9 km depth in 1993 and 1995, with total volumes of 44,500 m^3 and 28,000 m^3. Later stimulations were conducted at 5 km depth in GPK2 (2000), GPK3 (2003), and GPK4 (2004,2005) where volumes of 9,300 – 37,300 m^3 water were injected (see table above) (Dorbath et al., 2009). Maximum wellhead pressures were between 14 and 17 MPa, and flow rates were up

to 50 l/s (GPK2), 100 l/s (GPK3), and 45 l/s (GPK4, 2004 & 2005). Microseismic monitoring was performed in different boreholes; for the stimulations in the 90's sensors were placed in the ESP1 well and abandoned oil wells (Cornet 1997), and for the later stimulations the network included also GPK1 (Dorbath et al., 2009). Also a surface network was in place.
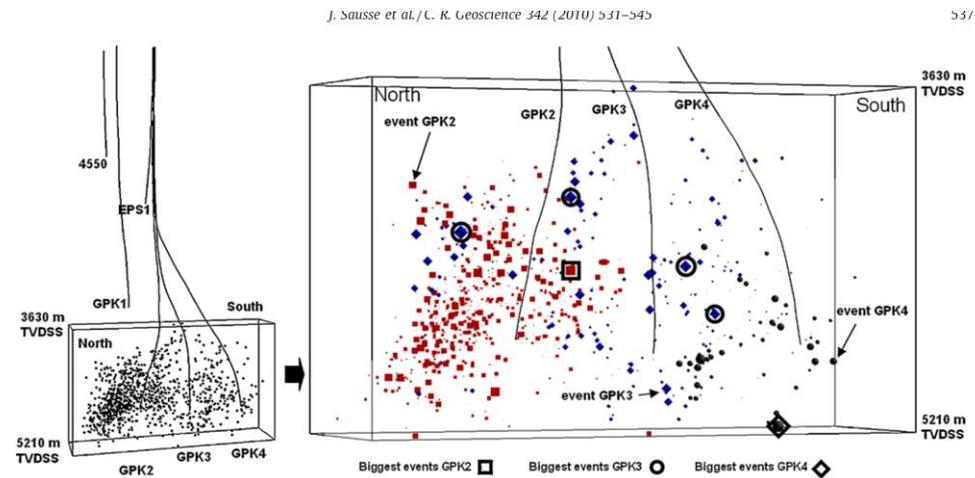

Figure A-9   Distribution of microseismicity for the GPK2, GPK3, and GPK4 stimulations (From Sausse et al., 2010, Copyright Elsevier, reproduced with permission).

Occurrence of seismicity: Micro-seismicity occurred during all main stimulations, with thousands of events being located. Maximum reported seismic magnitudes were 1.9 (GPK1, 1993), 0.3 (GPK2, 1995), 2.5 (GPK2, 2000), 2.9 (GPK3, 2003), 2.3 (GPK4, 2004), and 2.7 (GPK4, 2005) (Charléty et al., 2007; Dorbath et al., 2009). The seismic clouds clustered around the injection wells (height ±500 m) and spanned ~1.5 km along the north-south direction (Figure A-9). Seismic events showed normal faulting and strike-slip faulting, and focal planes coincided with the regional structures. The largest events sometimes occurred after bleeding off the well, i.e. for GPK3 and GPK4 (2004).

Interpretation: Seismicity was induced on pre-existing fractures and faults by elevated fluid pressure and diffusion of pressure away from the well.

### A.2 Molasse Basin, Germany/Switzerland/Austria
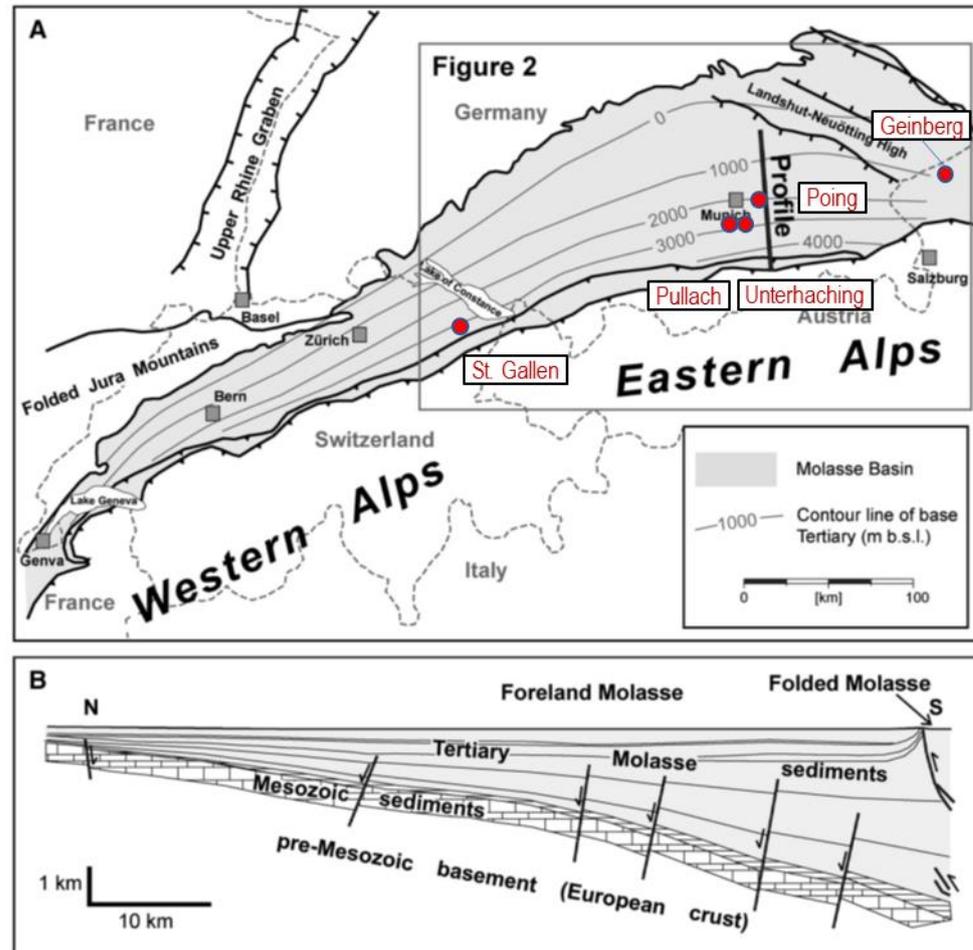
Figure A-10   Overview of the Molasse Basin. a) Extent of the Molasse Basin in Switzerland and Germany and thickness of the Tertiary sediments (contour lines). The location of sites described in this section are indicated with red dots. b) Cross-section through the Molasse Basin along profile line in a. (From Reinecker et al., 2010, Copyright Elsevier, reproduced with permission)

The Molasse Basin (North Alpine Foreland Basin) is a typical foreland basin found directly north of the Alps, ranging from Geneva in the west to Bavaria in the east (Figure A-10). Flexure of the lithosphere due to the Alpine mountain building caused the formation of a deep foreland basin in the Eocene, which was filled by Tertiary Molasse sediments (e.g. Bachmann, G. H. et al., 1987; Reinecker et al., 2010). The deepest, oldest formation below the basin is the Variscan Basement, which consists of gneisses and granites. During the Variscan orogeny in the Carboniferous NW-SE troughs developed locally (similar as in the Rhine Graben), which were filled with Permo-Carboniferous sediments (Bachmann, G. H. et al., 1987). The basement outside of the troughs was subject to erosion. During the Triassic lithospheric cooling and subsidence caused the formation of a basin (part of the Thetys Ocean) which extended eastwards (e.g. Mazurek et al., 2006). Triassic sediments were deposited unconformably on top of the basement, or locally the Permo-Carboniferous troughs. The Triassic sediments are thickest in the west and were deposited increasingly to the east with time; the Early Triassic Bundsandstein is found only up to the

westernmost tip of the current-day Molasse Basin, the Middle Triassic was deposited up to halfway between Zurich and Munich, and the Upper Triassic Keuper and Lower Jurassic sediments were deposited almost up to Munich (Bachmann, G. H. et al., 1987). The Middle Jurassic pelitic and oolitic limestones of the Dogger are present below almost the entire Molasse Basin, ranging in thickness from 0 m in the SE to 200 m the NE. The Upper Jurassic Malm limestones are also ubiquitous below the basin, and vary in thickness from 600 m in the south to 400 m in the north. Subsequent uplift caused karstification of the Jurassic sediments, and eroded parts of the Jurassic sediments and the Cretaceous sediments, before the Alpine orogeny caused the formation of the Molasse Basin and infill with Tertiary and Cenozoic sediments.

During subsidence of the Molasse Basin E-W striking normal faults developed (Figure A-10b), but these are currently inactive. Stress measurements and focal mechanisms indicate the present day stress regime to be transpressional (strike-slip to thrust faulting). The maximum horizontal stress is oriented N-S in the eastern parts of the basin, and gradually rotates to NNW-SSE in the west (Reinecker et al., 2010).

The main geothermal target in the Molasse Basin is the karstified Malm limestone formation which has a high permeability. It is located between 1.5 and 5.5 km with temperatures up to 160 °C.

A.2.1   Geinberg, Austria

Country & place:	Austria, Geinberg	
Activity:	Geothermal	
Start date – End date:	1980 (production) 1998 (circulation)	1998 (production) Still circulating
Fluid + Fluid balance:	Water, Acid	Production, stimulation/circulation
Activity depth:	2.2 km	
Activity rocktype:	Carbonates	
In-situ T	105 °C	
Cumulative ΔV:	Production: ~ 93.600.000 m^3 Stimulation: 60 m^3 hydrochloric acid Circulation: ~ 85% is re-injected	
Maximum Top Hole Pressure:	< 0.2 MPa	
Maximum flowrate:	Production: 22 l/s Circulation: 25 l/s (production), 21 l/s (injection)	
Monitoring system:	No	
Maximum magnitude + Date:	N/A	N/A
Distance M_{max} – activity:	N/A	
Intensity [EMS]:	N/A	
Damage:	N/A	
Interpretation	N/A	

Tectonic setting and geology: Geinberg is located in Austria, at the east side of the Molasse Basin (Figure A-10). The area is characterized by Pre-Tertiary, NNW-SSE striking faults, showing vertical throws of about 1000 m and Tertiary (Oligocene) faults, striking E-W and displaying vertical throws of about 300 m (Goldbrunner, 1999). The only stress field orientation data in the area comes from the Simbach-Braunau geothermal site (~20 km to the west) and shows a N-S trend for the maximum horizontal stress (Evans, K. F. et al., 2012). The target reservoir rocks are the Late Jurassic Malm carbonates with a maximum thickness of 750 m, directly overlying the crystalline basement, (Goldbrunner, 1999; Nachtmann & Wagner, 1987). The permeability in the reservoir is controlled by fault zones and karstification.

Activity design: The present day Geinberg geothermal system consists of two wells. A vertical injection well (Geinberg 1) reaching a depth of 2120 m and a deviated production well (Geinberg Thermal 2), the well bottom of which is situated 1600 m away from Geinberg 1 at a depth of 2225 m (Figure A-11). The Geinberg 1 well intersects the top of the Malm at 2126 m, whereas the Geinberg Thermal 2 well intersects the Malm at 2117 m. Both wells cross the same synthetic fault, Geinberg 1 at a depth of 2083 m and the Geinberg Thermal 2 well much shallower in the Campanian Marls. The Geinberg Thermal 2 well also intersects an antithetic fault around 1900 m (Goldbrunner, 1999; Karytsas et al., 2009). The bottom of the Geinberg Thermal 2 well represents an 276 m open hole section which is mostly situated in the Malm (Evans, K. F. et al., 2012).
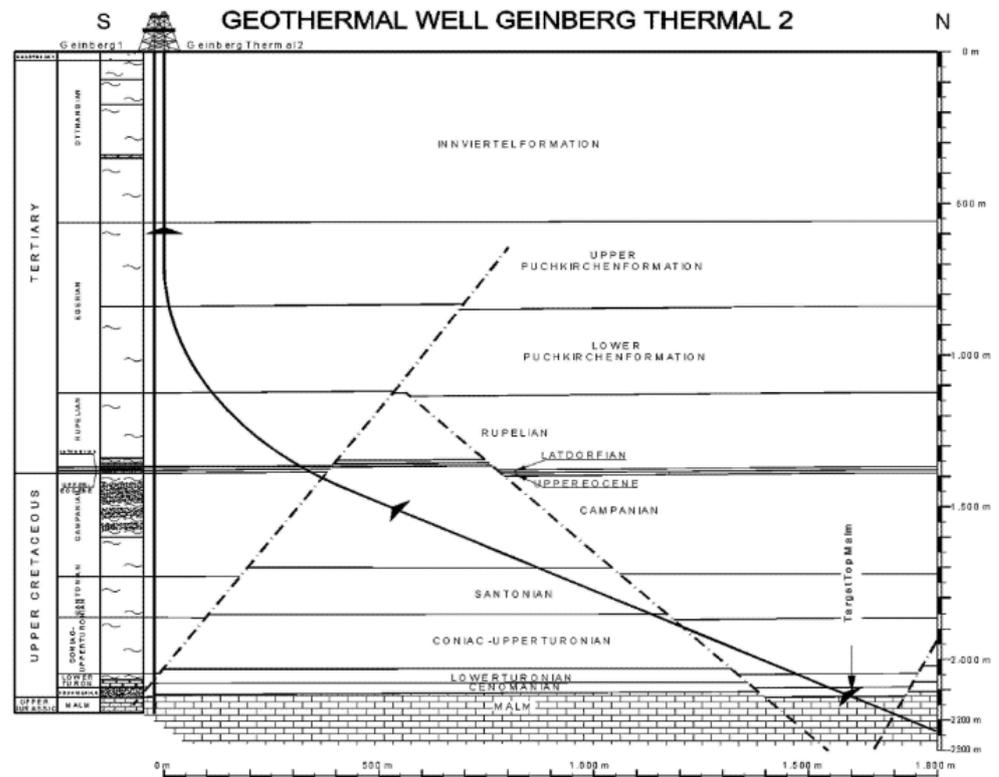
Figure A-11 Well trajectory of the Geinberg geothermal doublet (From Goldbrunner, 1999; Karytsas et al., 2009, Copyright Taylor & Francis, reproduced with permission).

Operations and monitoring: Geinberg 1 was originally drilled as a hydrocarbon exploration well in 1974, but no oil or gas was found. In 1978 it was re-completed as a geothermal production well and it started producing in 1980 as a single well. The well operated with artesian overflow and initial flowrates of 22 l/s, producing water of about 100 °C. Due to reservoir pressure decreases the flowrate dropped to 4-10 l/s (artesian overflow) in the 1990's. To counter further declining reservoir pressures a second well (Geinberg Thermal 2) was drilled in 1998 so that water could be reinjected. A chemical stimulation was applied in this Geinberg Thermal 2 well, using 60 m^3 of hydrochloric acid. The stimulation increased the maximum production rate from 18 l/s to 50 l/s. The doublet started producing water of 100-105 °C by artesian overflow and flowrates of 25 l/s from the Geinberg Thermal 2 well in late 1998. Re-injection of 30 °C water occurred at a flow rate of 21 l/s in the Geinberg 1 well without additional pumping (Goldbrunner, 1999; Karytsas et al., 2009). About 4 l/s is not re-injected, but is used for thermal spa.

Occurrence of seismicity: There have been no events reported by local population or regional/local network (Evans et al., 2012).

A.2.2   Poing, Germany (M$_L$ 2.1)

Activity:	Geothermal (district heating)	
Start date – End date:	December 2012	still producing
Fluid + Fluid balance:	Water	Circulation
Activity depth:	3.05 km	
Activity rocktype:	Carbonates	
In-situ T	85 °C	
Cumulative ΔV:	Balanced	
Maximum Top Hole Pressure:	< 1 MPa	
Maximum flowrate:	100 l/s	
Monitoring system:	Several stations present < 10 km	
Maximum magnitude + Date:	2.1	09-09-2017
Distance M$_{max}$ – activity:		
Intensity [EMS]:	III-IV	
Damage:	Felt, light damage to old buildings	
Interpretation	Reactivation of critically stressed faults?	

Tectonic setting and geology: The Poing geothermal system is situated in the Molasse Basin, 15 km west of Munich (Figure A-10). No natural seismicity was recorded near Poing. The target formation is the Malm, which at Poing has a thickness of 660 m, and is encountered at 2.3 – 2.5 km depth (TVD) (www.geotis.de). The underlying Lower Jurassic Dogger has a thickness of ~60 m (Bachmann, G. H. et al., 1987). The temperature within the Malm reservoir is 85°C.

Activity design: The Poing doublet consists of two wells which were drilled in 2008, the injection well TH1 and the production well TH2 (Figure A-12). The wells were drilled to depths of 3050 and 3014 m TVD, and were oriented along a N-S line which is perpendicular to the dominant fault trend in the region.
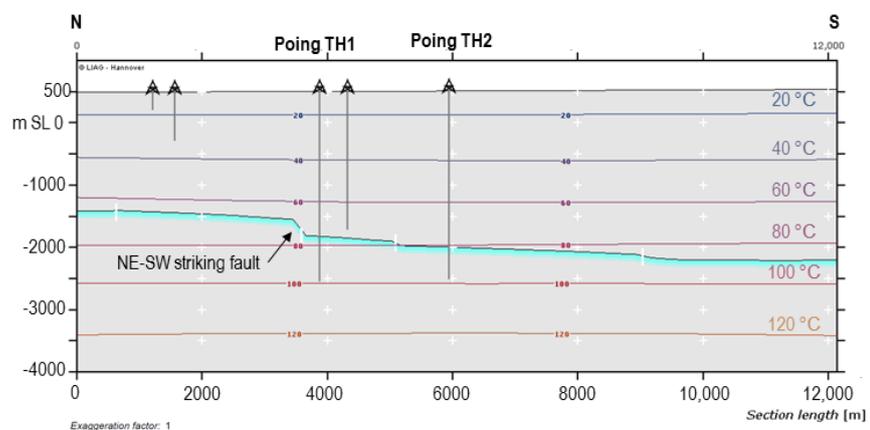

Figure A-12   Vertical cross-section along the Poing doublet (Source: www.geotis.de).

Operations and Monitoring: Circulation started in December 2012, with average flow rates of 85 l/s and maximum flow rates of 100 l/s (www.geotis.de). After the occurrence of seismicity in 2016 and 2017 circulation was stopped and temporarily halted in September 2017, but circulation recommenced in October 2017 at a lower flowrate of 65 l/s. No specific microseismic monitoring was in place, but there were 5 stations located in the vicinity of the project (1 – 10 km). An additional station was placed near Poing in 2017 (LIAG, 2018).

Seismicity: In November and December 2016 four earthquakes were recorded with local magnitudes 1.0 to 2.1 (LIAG, 2018). The last two with M_L 2.1 and 1.8 were felt by the local population. On 9 September 2017 another event of M_L 2.1 occurred, at a depth of 3.1 km (± 1 km). Peak Ground Velocities of 1.6 mms^{-1} were recorded in Poing, which translated into an Intensity of IV. Light damage was reported to old buildings.

Interpretation: The injection well was located close to a regional fault, and also a fault was present between the wells (Figure A-12). However, the exact cause of the induced events is unclear, as pore pressure and thermally-induced stress changes were likely very small. Reactivation of critically stressed faults may have occurred (LIAG, 2018).

A.2.3　　Pullach, Germany

Country & place:	Pullach, Germany	
Activity:	Geothermal	
Start date – End date:	November 2005	To date
Fluid + Fluid balance:	Water	Circulation
Activity depth:	3.4 km	
Activity rocktype:	Carbonates	
In-situ T	107 °C (Th1a)	
Cumulative ΔV:	Balanced	
Maximum Top Hole Pressure:	1.5 MPa	
Maximum flowrate:	95 l/s (Operating at 88 l/s)	
Monitoring system:	No	
Maximum magnitude + Date:	N/A	N/A
Distance M_{max} – activity:	N/A	
Intensity [EMS]:	N/A	
Damage:	N/A	
Interpretation	N/A	

Tectonic setting and geology: The Pullach geothermal site is located in the Molasse Basin, about 10 km west of the Unterhaching geothermal site (Figure A-10). The target reservoir are the carbonates from the Malm formation which lies at a depth of ca. 2984-3440 m, directly overlying the granitic basement (Böhm et al., 2010).

Activity design: The present day geothermal system consists of 3 wells, two production wells (Th1/1a and Th2) and one injection well (Th3). Th1a is a sidetrack of Th1. Th1/1a and Th2 were not drilled into fault zones and the bottoms of these wells are 3.1 km apart (Figure A-13). The wells intersect the top of the Malm at 2810 m (Th1a), 2819 m (Th1) and 2958 m (Th2) TVD (Böhm et al., 2010). The intersection depth of Th3 with the top of the Malm is unknown. The wells have a total depth (TVD) of 3389 m (Th1), 3370 m (Th1a), 3443 m (Th2) and 3505 m (Th3).
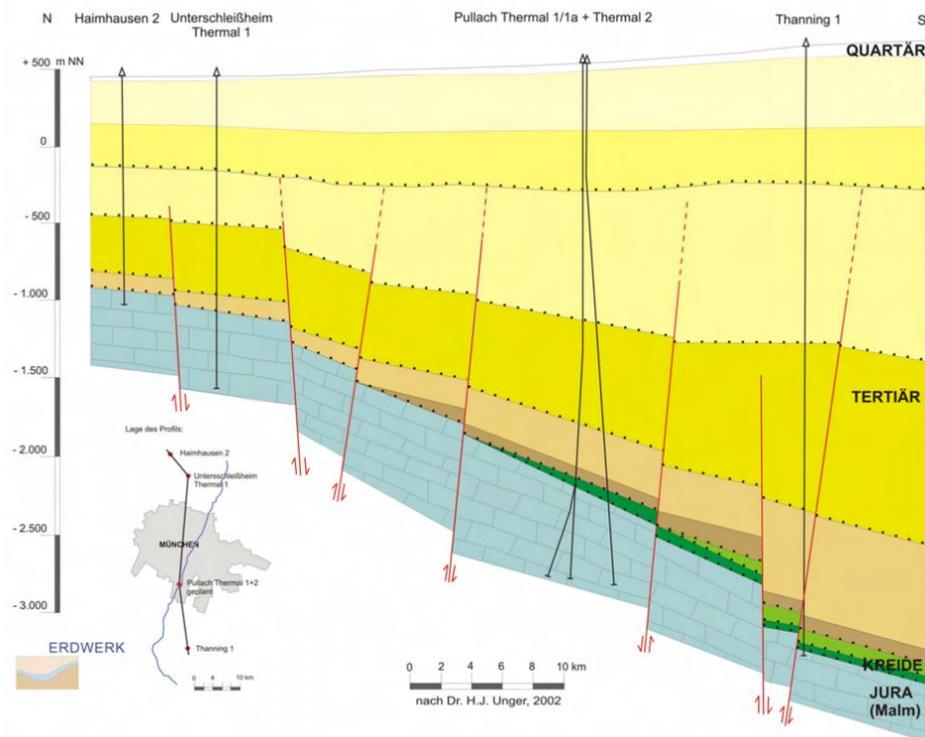
Figure A-13   N-S cross-section through Munich including a schematic well trajectory of the Pullach Th1, Th1a and Th2 wells (From Schubert et al., 2007, Copyright Erdwerk, reproduced with permission).

Operations and monitoring: The drilling of Pullach Th 1 started in December 2004 and was finished at a final depth of 3300 m (MD) in February 2005. In the same month they started drilling well Th2, which was completed   in May 2005 with a final measured depth of 4120 m. Injection tests in Pullach Th1 revealed insufficient injectivity of the well, after which the Th1 well was deepened. This did still not result in the desired injectivity, so a sidetrack (Th1a) was drilled deviating from Th1 at a depth of 2814 m (MD) and reaching a final measured depth of 3930 m. Due to a lack of fault inventory, the Th1a sidetrack was drilled directionally, to cover the greatest possible drilling distance in the Malm (Schubert et al., 2007). The doublet system started operating in November 2005.

In January 2011 a third well (Th3) was drilled. The injection in well Th2 stopped on the 17th November 2011, after which the water from the Th1a well was injected in the Th3 well. The Th3 well was chosen as new injection well due to its high productivity, which is caused by the larger diameter of the injection interval of the well. A pump was installed in Th2 after which in December 2011 the first tests started using Th2 as an additional production well (Baumann et al., 2017), turning the system into a triplet. The actual production of the triplet started in October 2012. Since then Th1a has been producing at a rate of 53 l/s and the production rate of the Th2 well has increased from 20 l/s to about 35 l/s (Agemar, T. et al., 2014; Agemar, Thorsten et al., 2014; Baumann et al., 2017). The wellhead temperature of Th2 has been increasing since the conversion from injection to production well (Figure A-14).
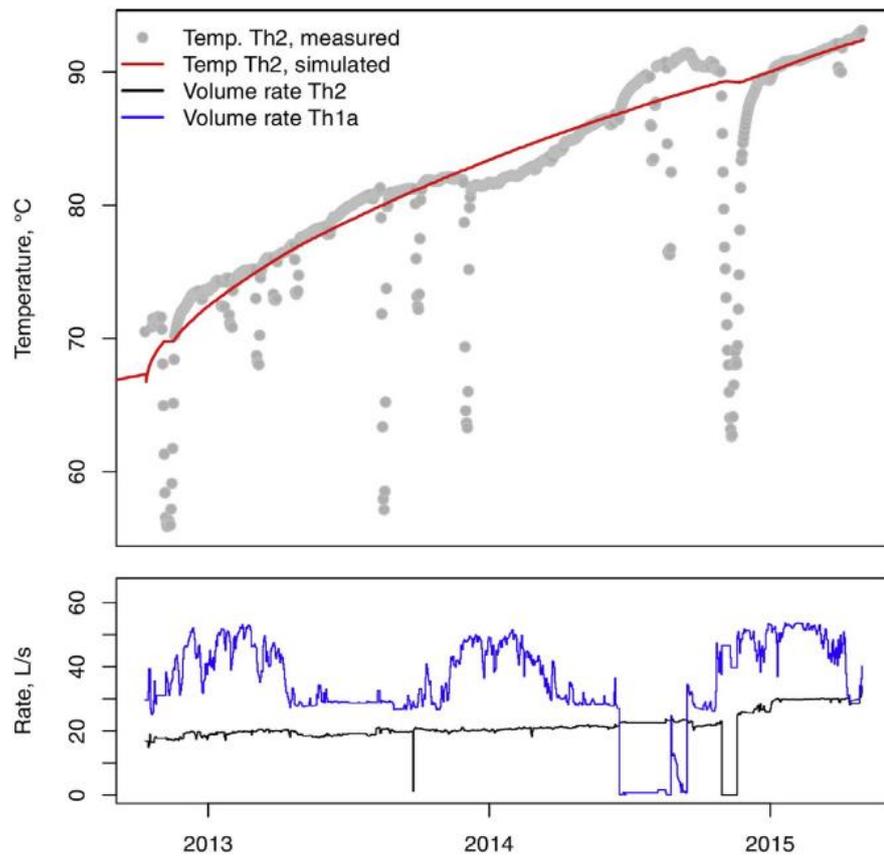
Figure A-14 Top: Increasing wellhead temperatures at Th2 after conversion from injection to production well. Bottom: Production flow rates of Th1a and Th2 (From Baumann et al., 2017, Copyright Elsevier, reproduced with permission).

Occurrence of seismicity: There have been no events reported by local population or regional/local network (Evans et al., 2012).

A.2.4   Sankt Gallen, Switzerland (M 3.5)

Activity:	Drilling of geothermal well	
Start date:	14 – 7 – 2013 16 – 07 – 2013 19 – 07 - 2013	cold-water test acid stimulation mud pumping
Fluid + Fluid balance:	Drilling mud	injection
Activity depth:	4.25 km	
Activity rocktype:	Carbonate (Malm)	
In-situ T	145°C	
Cumulative ΔV:	150 m^3 (test), 145 x 2 m^3 (acid), 700 m^3 (mud)	
Maximum Top Hole Pressure:	7.5 MPa (test), 8 MPa (acid), 9 MPa (mud)	
Maximum flowrate:	52 l/s (test), 42 l/s (acid)	
Monitoring system:	Yes (M$_c$ 0.1)	
Maximum magnitude + Date:	3.5	20 – 07 – 2013
Distance M$_{max}$ – activity:	400 m	
Intensity [EMS]:	IV	
Damage:	Widely felt, minor damage	
Interpretation	Reactivation of critically stress fault	

Tectonic setting and geology: Sankt Gallen is situated in the southwestern part of the Molasse basin, 50 km east of Zürich (Figure A-10). Several medium sized earthquakes occurred within 50 km since 1984 (Diehl et al., 2017). The geothermal well targeted the fractured and faulted carbonates of the Upper Jurassic Malm formation and the Triassic Muschelkalk at 3.8 – 4.5 km depth (Figure A-15). The 700 meter thick Mesozoic sediments were cross-cut by a pronounced NNE-SSW striking fault zone of 30 km in length and 100 m in width (Obermann et al., 2015). The normal faults dip steeply to the SE, bounding a Permo-Carboniferous trough locally underlying the Mesozoic formation (Moeck et al., 2015). The stress regime is strike-slip with the maximum horizontal stress striking NNW-SSE, and the faults were oriented optimally for reactivation. The temperature of the Malm is 145 °C.

Activity design: In 2013 a single injection well GT-1 was drilled, reaching the top of the Malm at 3.8 km in March (Moeck et al., 2015). The well reached a total depth of 4.25 km on 6th of July 2013, with an open-hole section of 400 m.
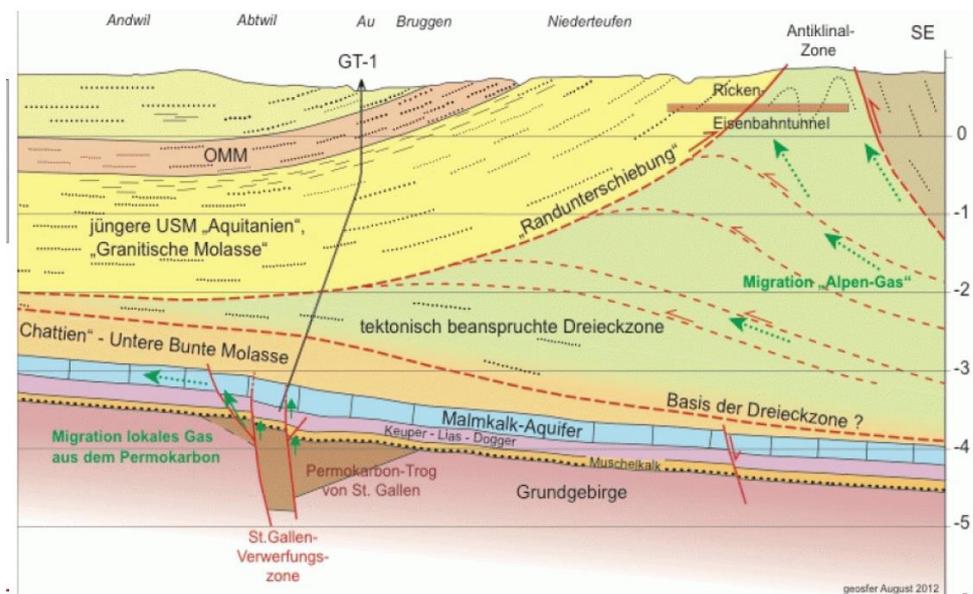
Figure A-15 Local geology and well trajectory at Sankt Gallen (From Moeck et al., 2015, Proceedings World Geothermal Congress, Melbourne).

Operations and monitoring: After reaching the target depth, a cold water injection test was done on 14 July. A total of 175 m^3 was injected over 2 hours, reaching a maximum wellhead pressure of 7.5 MPa and a maximum flow rate of 52 l/s (Obermann et al., 2015). On 16 July two acid stimulations were done with each 145 m^3 of HCl at maximum wellhead pressures of 8 MPa and flow rates of 42 l/s. On 19 July gas suddenly entered the borehole, increasing the wellhead pressure to 9 MPa. A total volume of 700 m^3 of drilling mud was pumped into the well to suppress the inflow of gas. On 25 July well control operations ended. In October a small production test was conducted. A local monitoring network was in place during the drilling and testing, with a magnitude of completeness of M_L 0.0 (Diehl et al., 2017).

Occurrence of seismicity: During and after the cold water injection test 12 events were detected with M_L < 0.1. During two days following the acid stimulations 40 events were detected with M_L up to 0.2. During pumping of mud to push back the gas seismic activity increased, culminating in a M_L 3.5 on 20 July 2013. After well control finished on the 25th of July the seismicity stopped, but seismicity rates increased in September, likely related to well cleaning operations. In total 350 locatable earthquakes occurred from 14 July to November, with M_L from -1.2 to 3.5 (Diehl et al., 2017). The earthquakes occurred ~200 – 400 m below the open hole section, predominantly in the Permo-Carboniferous sediments (Figure A-16). The focal mechanism was strike-slip. Seismicity migrated along the fault plane to the SW and NE, and locations delineated a NW dipping fault which was not seen on seismics.

Interpretation: A hydraulic connection (likely the F2 fault) is proposed between the borehole and the deeper parts of the reactivated fault (Figure A-16b). Pressure perturbations could be transferred to depth and could reactivate critically stressed faults.
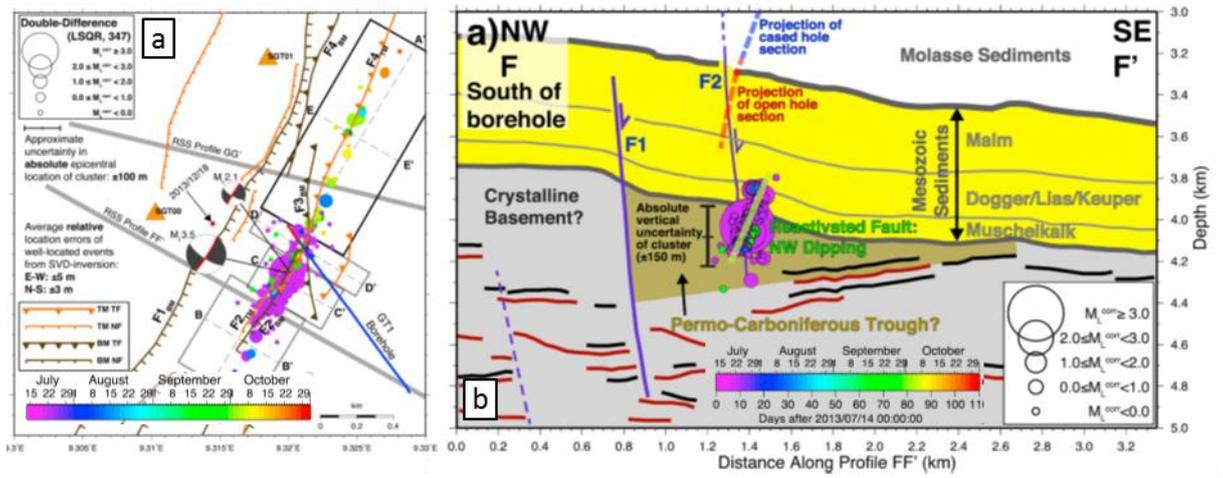
Figure A-16 Seismicity at the St. Gallen geothermal well. a) Top view of located events and faults.
b) Cross-section view along FF' in a of located events and faults. (From Diehl et al.,
2017, Copyright John Wiley & Sons, reproduced with permission).

A.2.5   Unterhaching, Germany (M 2.4)

Country & place:	Germany, Unterhaching	
Activity:	Geothermal, district heating	
Start date – End date:	October 2007	To date
Fluid + Fluid balance:	Water	Circulation
Activity depth:	3.4 km	
Activity rocktype:	Carbonates	
In-situ T	122 °C	
Cumulative ΔV:	Balanced	
Maximum Top Hole Pressure:	< 1 MPa	
Maximum flowrate:	120 l/s (Increased to 140 l/s after 2014)	
Monitoring system:	Yes (since January 2010)	
Maximum magnitude + Date:	2.4	03-07-2008
Distance M_{max} – activity:	~ 0.5 km (injection well)	
Intensity [EMS]:	II - III	
Damage:	None	
Interpretation	Induced by pore pressure perturbation, due to cold water re-injection	

Tectonic setting and geology: The Unterhaching geothermal system is situated in the Molasse Basin in Southern Germany (Figure A-10). The target reservoir rocks are the Malm carbonates which are found at 3 km depth and have a thickness of 600 m. The area is characterized by NE-SW striking antithetic faults (Figure A-17) which extend at least 100-200 m into the crystalline basement underlaying the Malm carbonates (LIAG, 2012; Megies & Wassermann, 2014; Wolfgramm et al., 2007).
No natural seismicity has been recorded within 40 km of the well location, prior to the start of the operation (Evans et al., 2012; Leydecker, 2011).

Activity design: Two wells were drilled, the production well (GT1a) and injection well (GT2), to vertical depths of 3.35 and 3.59 km respectively. The wells intersect the top of the Malm reservoir at 3002 (GT1a) and 2977 m (GT2) TVD. GT2 was drilled into one of the main NE-SW trending faults (Figure A-17), showing a normal offset of 160-240 m. GT1a was drilled into a NNW to NW striking fault, 3.6 km from GT2 at the reservoir depth (Megies & Wassermann, 2014).
The fault systems are assumed to be connected (Wolfgramm et al., 2007). The bottom section of the GT1a well is secured by a slotted liner of 446 m, whereas the GT2 well represents an open-hole of 695 m (Wolfgramm et al., 2007).
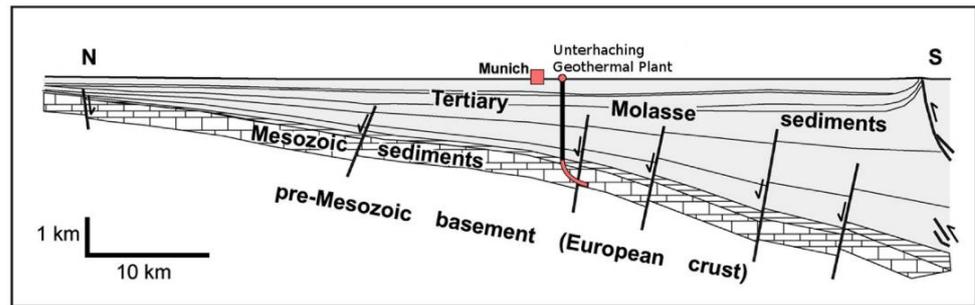
Figure A-17   North-South profile through the Molasse basin close to Munich. Faults and well geometry are displayed schematically. Injection interval of the well is indicated in red (From Megies & Wassermann, 2014, Copyright Elsevier, reproduced with permission).

Operations and monitoring: The Unterhaching system started operating in October 2007 for district heating and in February 2009 electricity production was added. The system circulates at a rate of 120 l/s with a wellhead pressure below 1 MPa and the production temperature is 122 °C (Megies & Wassermann, 2014). The system operates without hydraulic stimulation. According to the geotIS database the circulation rate has been increased up to 140 l/s, after 2014 (Agemar, T. et al., 2014; Agemar, Thorsten et al., 2014). After the detection of several M 1.9 – 2.3 earthquakes in February and July 2008 by the regional network, single temporary seismometers were positioned closer to the epicentral region (July 2008 to December 2009). To improve the location accuracy and in order to detect smaller earthquakes, a local network of five stations was deployed around the re-injection (GT2) well in January 2010 (Evans, K. F. et al., 2012).

Occurrence of seismicity: In February 2008 an earthquake of magnitude M_L 2.3 was detected by the Bavarian Earthquake Service, followed by three additional earthquakes in July 2008 of magnitudes M_L 2.4, 2.1 and 1.9. Until January 2012 a total 136 seismic events were detected in the region with local magnitudes ranging from -0.8 to 2.4. Approximately 90% of the events have magnitudes smaller than 1.0, 11 events had a magnitude in between 1.0 and 2.0 and 5 event magnitudes exceeded 2.0 (Megies & Wassermann, 2014). The locations of the larger seismic events were estimated to be about 1700 m below the injection well bottom (Figure A-18) on the foot wall site of the main fault in the crystalline basement (Megies & Wassermann, 2014).
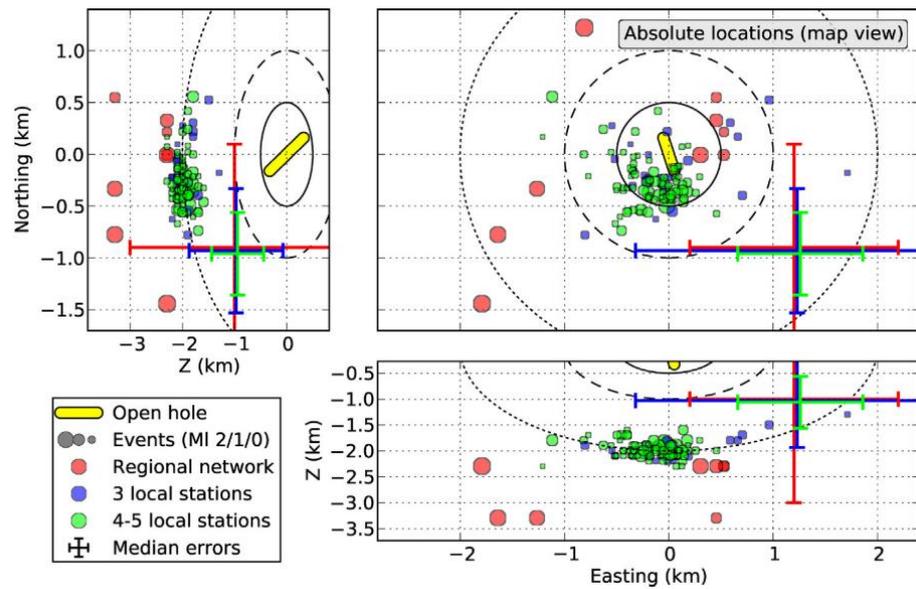
Figure A-18 Absolute locations of all recorded seismic events. The open hole section of the re-injection well is indicated in yellow (From Megies & Wassermann, 2014, Copyright Elsevier, reproduced with permission).

Interpretation: The larger events, and possibly also the smaller events are assumed to be triggered by local stress changes and pore pressure perturbations as a result of the re-injection of cold water. The spatial pattern of the events suggests a repeated rupture of part of the main fault (NE-SW) intersecting the injection well. The orientation of this fault is favorable for reactivation in the present day stress field (Megies & Wassermann, 2014).

A.3 North German Basin, Germany

The North German Basin is part of the Central European Basin, and covers the north of Germany and the south of Denmark (Figure A-19a). The basin formed in the late Carboniferous to Early Permian in the foreland of Variscan orogeny, where rifting and wrench faulting occurred (Scheck & Bayer, 1999). The basin was oriented NW-SE, defined by the Teisseyre-Tornquist Zone (TTZ) which forms the northeastern boundary, and the Elbe Fault zone which forms the southwestern boundary. Both fault zones have been active from the Carboniferous. Extensive volcanism and magmatism occurred around 300 Ma, depositing widespread volcanic sequences with thicknesses up to 2500 m in the northeast of Germany. Thermal subsidence during the Permian and Triassic led to the deposition of thick Lower Permian Rotliegend sequences (>2000 m,Figure A-19b), Upper Permian Zechstein salt formations, and Triassic Bundsandstein up to 1500 m in thickness (Scheck & Bayer, 1999; Scheck-Wenderoth & Lamarche, 2005; Ziegler, 1990). N-S graben formation started in the Triassic due to E-W extension, and subsidence along these grabens continued up to the Late Cretaceous. The Bundsandstein is overlain by the Middle Triassic Muschelkalk (<500 m) and the Upper Triassic Keuper (<1000 m). Jurassic sediments were only preserved in the south and east of the basin. The total thickness of the Zechstein up to the Lower Cretaceous reaches up to >7000 m (Figure A-19c). In the Upper Cretaceous the basin was inverted along NW-SE trending faults, resulting in local highs and troughs. In the Cenozoic subsidence continued, depositing up to 2000 m of sediments in northern Germany.
NW-SE striking faults are most dominant in the basin, sub-parallel to the old, large bounding faults. NNW-SSE striking faults are also present, related to the Triassic E-W extension. The stress regime is complex and varies from transpressive in the western part of the basin to transtensional in the eastern parts. The Zechstein salt may decouple pre-Permian stress and faults from the overburden (Scheck-Wenderoth & Lamarche, 2005). The maximum horizontal stress is oriented N-S in the west part of the basin, and rotates to NW-SE near the Elbe Fault zone (Scheck-Wenderoth & Lamarche, 2005). Natural seismicity is rare.

The main geothermal targets in the North German Basin are Mesozoic sediments, including the Middle Bundsandstein sandstones, the Lower, Middle, and Upper Keuper sandstones and shales (Rhaetian reservoir), Lower and Middle Jurassic deltaic deposits, and the Lower Cretaceous sands, shales, and marls. More uncertain targets are the tighter, deeper, Rotliegend sediments (2.5 – 5.5 km).
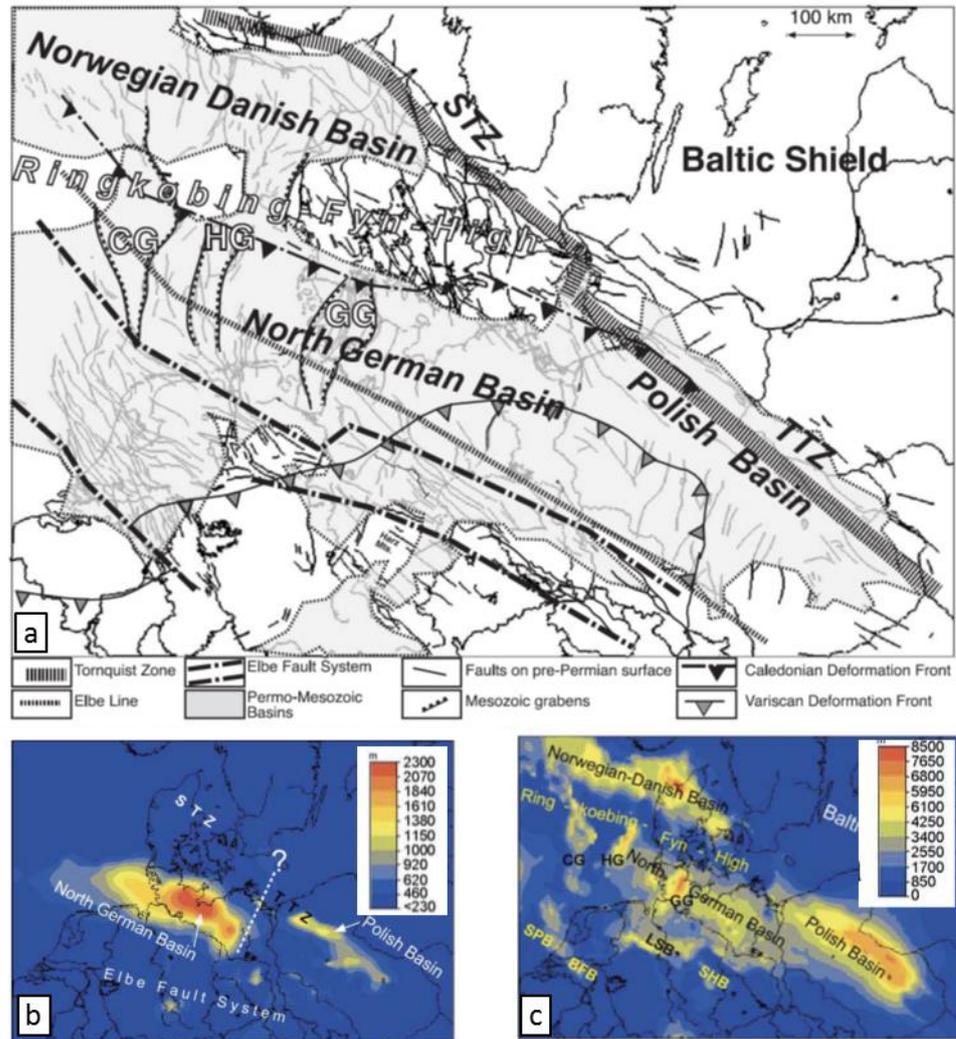
Figure A-19   Overview of the North German Basin. a) Main structural elements of the North German Basin. b) Thickness of Rotliegend deposits. c) Thickness of Upper Permian Zechstein to Lower Cretaceous sediments. (From Scheck-Wenderoth & Lamarche, 2005, Copyright Elsevier, reproduced with permission).

A.3.1   Gross Schönebeck, Germany

| Country & place (lat, lon):	Germany, Gross Schönebeck	
Activity:	Geothermal stimulation	
Start date – End date:	10 – 08- 2007	15 – 08 – 2007
Fluid + Fluid balance:	Water	Injection
Activity depth:	4.2 km	
Activity rocktype:	Sandstones and volcanics	
In-situ T	150 °C	
ΔT in-situ – fluid:	80 °C	
Cumulative ΔV:	13,000 m^3	
Maximum Top Hole Pressure:	58 MPa	
Maximum flowrate:	150 l/s	
Monitoring system:	Yes	
Maximum magnitude:	-1	
Distance M_{max} – activity:	0.5 km	
Intensity [EMS]:	I	
Damage:	N/A	
Interpretation	Induced by pore pressure increase	
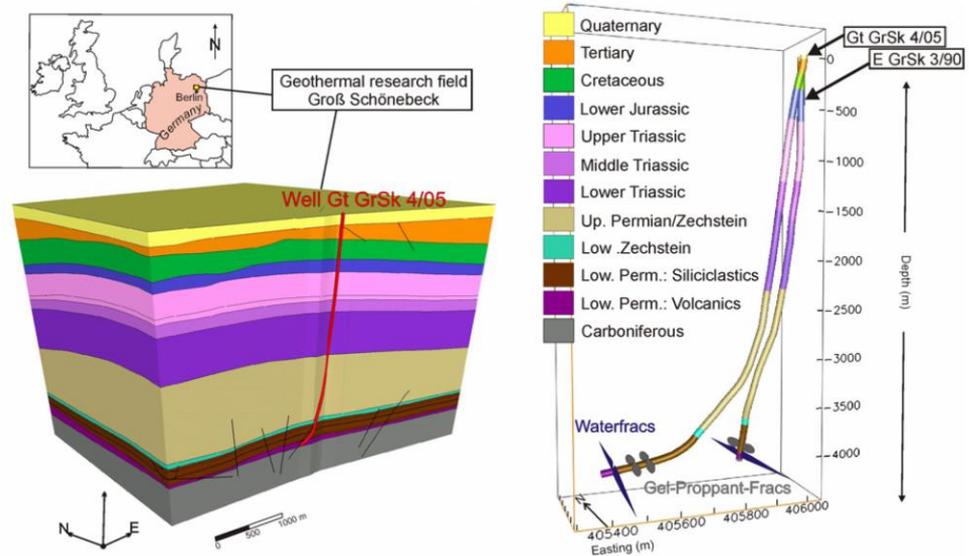
Figure A-20 Overview of the Gross Schönebeck geothermal research site (From Zimmermann et
al., 2010, Copyright Elsevier, reproduced with permission).

Tectonic setting and geology: The Gross Schönebeck research site is located
northeast of Berlin in the Northeast German Basin (Figure A-19). The current day
stress field at the Gross Schönebeck site is transitional from normal faulting to strike-
slip faulting, with the maximum horizontal stress S_{Hmax} oriented 18.5° (Moeck, I. et al.,

2009). Major faults in the Rotliegend are trending NW-SE and minor faults striking NE-SW to NNE-SSW. The minor faults have the most critical orientation in the present day stress field (Moeck, I. et al., 2009). The target formation is the Rotliegend Group which is composed of 400 m of siltstones, sandstones, conglomerates and andesites at depths of 3874–4294 m with temperatures around 150°C (Zimmermann et al., 2009). The prime geothermal formations were the Dethlingen formation (including Lower Elbe subgroup) which consisted of fluvial sandstones with a porosity of 8 – 10% and permeability of 10 – 100 mD (Trautwein & Huenges, 2005) with an average thickness of 80 m, and 60 m thick fractured volcanic rocks (andesites) of the Lower Rotliegend Group (Figure A-20). The Rotliegend is overlain by 1300 m of Zechstein rocksalt.

Activity design: The Gross Schönebeck system consists of two deep wells forming a doublet. A former gas well was drilled nearly vertical in 1990 (EGrSk 3/90) and was deepened to 4294 m in 2000 and deepened further to 4309 m in 2003, reaching the top of the Carboniferous (Figure A-20). In 2006 the second well (Gt GrSk4/05) was drilled to 4198 m with an increasing deviation, so that the distance between the two wells was 500 m and they were aligned with the minimum horizontal stress (Zimmermann et al., 2010).
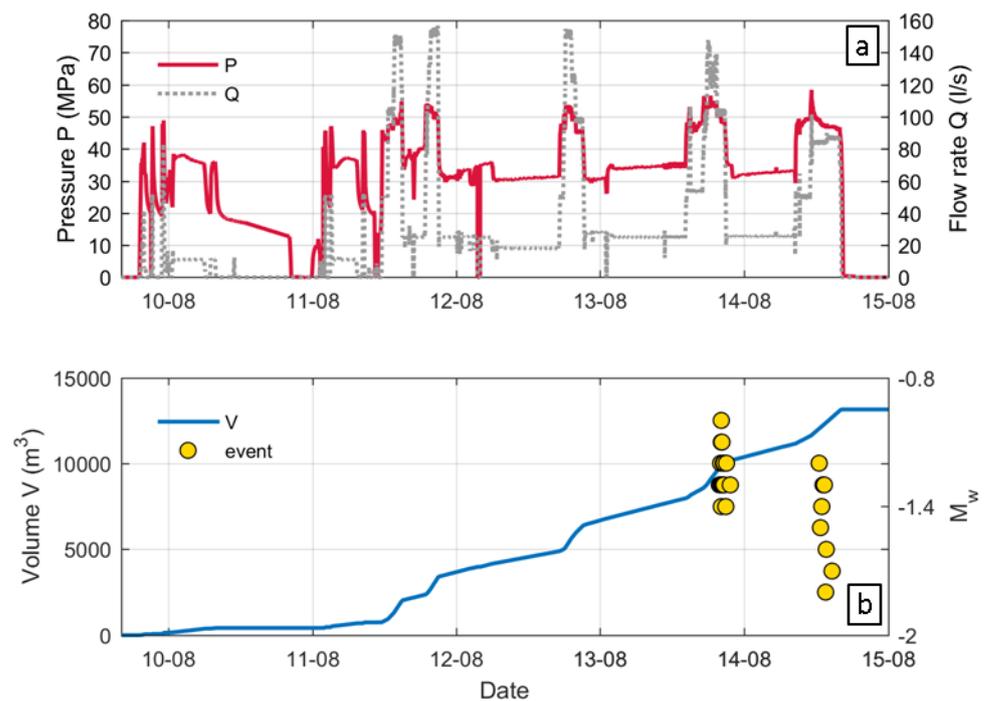

Figure A-21   Operational data and microseismic events during the waterfrac in the volcanics. a) Pressures and flowrates, b) Cumulative injected volume and seismic events (From Kwiatek et al., 2008; Zimmermann et al., 2010, Copyright Elsevier, reproduced with permission).

Operations and monitoring: Several stimulations were conducted from 2001 – 2004 to test enhancing productivity of the reservoir, including two hydraulic fracturing experiments using gel-proppants in the sandstone intervals (~300 m^3), and a waterfrac stimulation (4284 m^3) in the andesites (Zimmermann et al., 2009). Microseismic monitoring was performed using 6 shallow borehole seismometers, but

no events were picked up during the treatments. The Gt GrSk4/05 well was stimulated in 2007, with a massive waterfrac targeting the volcanic formation using 13170 m^3 water and 24 ton quartz (Zimmermann et al., 2010). The stimulation lasted 6 days and a maximum top hole pressure of 58 MPa and maximum flow rate of 150 l/s were attained (Figure A-21). Additionally two smaller gel-proppant fracturing experiments targeting the sandstone formations were performed. The total injected volumes were 280 m^3 and 310 m^3, with pressures of 41.6 MPa, and flow rates of up to 67 l/s and 58 l/s. During the stimulations in Gt GrSk4/05 a 3-component borehole sensor in EGrSk 3/90 was added to the network to detect smaller events.

Occurrence (or lack of) of seismicity: Only minor and low magnitude seismicity was observed during the stimulations in 2007. A total of 80 events were detected by the borehole sensor during the waterfrac, and only 2 very weak events during fracturing of the sandstones (Kwiatek et al., 2010). Magnitudes and locations were determined for 29 events indicating a M_w -1.8 to -1.0 and alignment on a planar structure with a strike of 17° and dip 52°, similar to the orientation of the minor fault in the vicinity of the well and the orientation of S_{Hmax}.

Mechanisms: The inferred mechanism of seismicity was the increase in pore pressure which led to shearing, likely on a pre-existing fault in the vicinity of the well. (Moeck et al., 2009). The fault orientations were not critical under the in-situ stress conditions, but the increased fluid pressure induced fault reactivation (Blöcher et al., 2018). Modeling indicated no changes in temperature during the waterfrac and thermal stresses did not play a role in generating the seismicity.

A.3.2   Hannover GeneSys project, Germany

Activity:	Geothermal, research	
Start date:	30 – 03 – 2011 23 – 05 – 2011	30 – 03 – 2011 (steptest) 27 – 05 – 2011 (waterfrac)
Fluid + Fluid balance:	Water	injection
Activity depth:	3.091 km	
Activity rock type:	sandstone (tight)	
In-situ T	169°C	
Cumulative ΔV:	120 m^3, 20,000 m^3	
Maximum Top Hole Pressure:	42 MPa, 47 MPa	
Maximum flowrate:	12 l/s, 90 l/s	
Monitoring system:	Yes, detection limit M_w -0.5	
Maximum magnitude + Date:	N/A	
Distance M_{max} – activity:	N/A	
Intensity [EMS]:	N/A	
Damage:	N/A	
Interpretation	N/A	

Tectonic setting and geology: The GeneSys demonstration project near Hannover is a follow-up of the Horstberg project. It is situated in the northeast of Hannover in the west of the North German Basin (Figure A-19), in a horst-like structure between two salt diapirs (Figure A-22b). The project targets low permeable sandstones of the Lower Triassic Middle Bundsandstein formation from 3440 to 3670 m depth (Figure A-22a) (Tischner et al., 2013). These include the Solling, Volpriehausen (20 m thick) and Detfurth sandstone (10 m thick) sequences, which have very low permeabilities between 10^{-18} - 10^{-16} m^2. The maximum horizontal stress is striking NW-SE, and the stress regime is normal faulting. Stress measurements in the well indicate a minimum horizontal stress which is 90% of the vertical stress, so that the stress state is near isotropic. The stress field was likely influenced by the salt diapirs (Rioseco et al., 2013). Natural seismicity rates are low.

Activity design: The project consists of a single well (Groß Buchholz Gt1) which was drilled to 3834 m depth in 2009 (Figure A-22). The casing was perforated in the Volpriehausen sandstone interval (3656 – 3662 m).
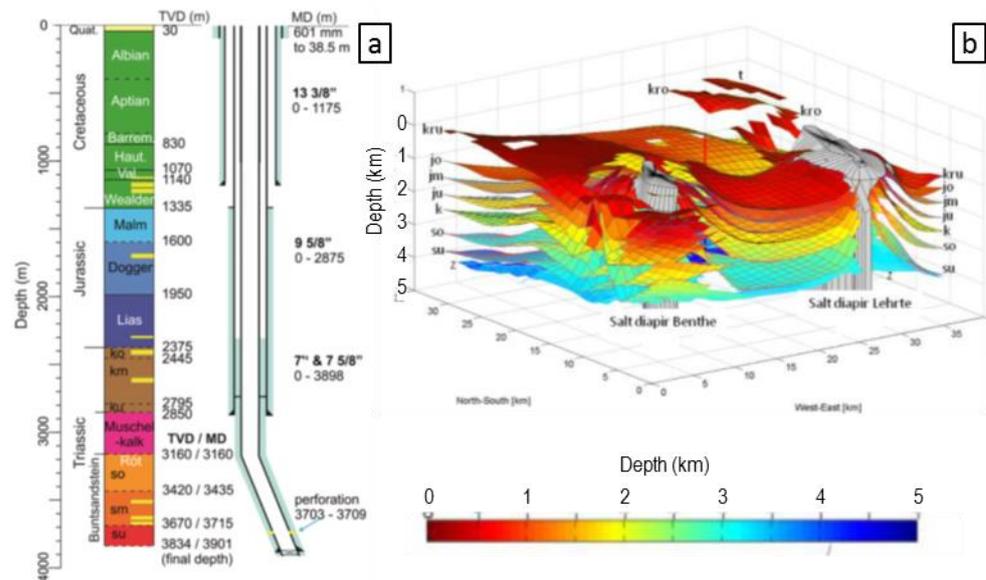
Figure A-22 Lithology and local geology of the GeneSys project near Hannover. a) Stratigraphy encountered in the borehole (From: Tischner et al., 2013). b) Local geology (From Rioseco et al., 2013, Copyright BGR, reproduced with permission).

Operations and monitoring: After conducting a minifrac test in 2010 (2.5 m^3), a step rate injection test was conducted on 30 March 2011 (Tischner et al., 2013). Over 5 hours 120 m^3 water was injected at flowrates up to 12 l/s with wellhead pressures up to 42 MPa. A massive waterfrac was conducted from 23 May to 27 May 2011. A total 20,000 m^3 was injected in 5 phases, with flowrates up to 90 l/s and wellhead pressures up to 47 MPa. Two short injection tests were performed in July and October, each injecting 90 m^3. Microseismic monitoring was operative throughout the tests, with 4 shallow borehole stations from < 1km from the well, and 4 borehole stations and 4 surface stations < 4 km from the well (detection limit M_w -0.5).

Occurrence of seismicity: No seismicity was recorded.

Interpretation: Successful creation of a conductive fracture (but problems with salt plugging). The stable state of stress and the local geology (absence of fractures, sandstone) may have prevented seismicity.

A.3.3   Horstberg GeneSys project, Germany

Activity:	Geothermal, research	
Start date:	27 – 10 – 2003	1 – 11 – 2003 (waterfrac)
Fluid + Fluid balance:	Water	injection
Activity depth:	3.083 km	
Activity rocktype:	sandstone (tight)	
In-situ T	158°C	
Cumulative ΔV:	20,000 m^3	
Maximum Top Hole Pressure:	34 MPa	
Maximum flowrate:	50 l/s	
Monitoring system:	Yes, detection limit M_L 0.0	
Maximum magnitude + Date:	N/A	
Distance M_{max} – activity:	N/A	
Intensity [EMS]:	N/A	
Damage:	N/A	
Interpretation	N/A	

Tectonic setting and geology: This GeneSys research project employed an abandoned gas well located 80 km NE of Hannover, in the North German Basin (Figure A-19). The target formations were low permeability sandstones of the Lower Triassic Middle Bundsandstein formation from 3636 to 3926 m depth, see Figure A-23 (Orzol et al., 2005). These include the Solling, Volpriehausen, and Detfurth sandstone sequences which are each 6 – 20 m thick. The temperature at the well bottom was 158 °C. The minimum horizontal stress was relatively high, 70% - 80% of the vertical stress.

Activity design: The project consists of a single well (Horstberg Z1) which was drilled in 1987 to a depth of 3834 m (Orzol et al., 2005). The casing was perforated in the Solling sandstone (3664 – 3668 m), Detfurth sandstone (3787 – 3791 m), and Volpriehausen sandstone interval (3920 – 3926 m).
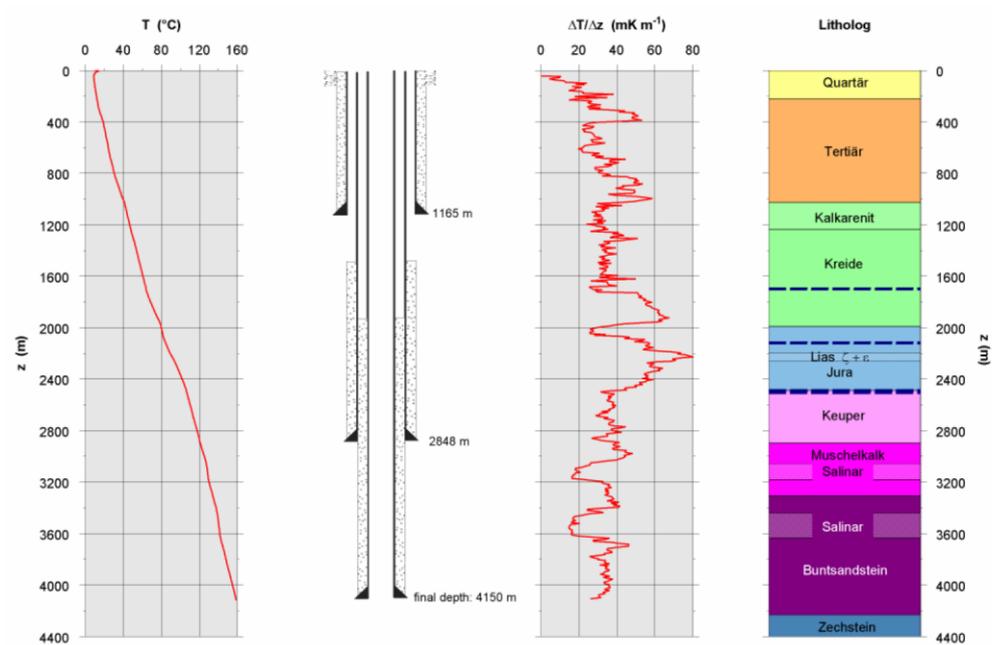
Figure A-23 Well data from Horstberg Z1 well, with temperature profile, well design, temperature gradient, and the stratigraphy (From Orzol et al., 2005, Proceedings World Geothermal Congress, Melbourne).

Operations and monitoring: The first waterfrac was performed in the Volpriehausen sandstone, where 1000 m^3 was injected at an injection pressure of 46 MPa, with flowrates up to 25 l/s (Orzol et al., 2005). In October - November 2003 a massive waterfrac was conducted in the Detfurth sandstone, with 20,000 m^3 water injected at wellhead pressures up to 34 MPa and flowrates up to 50 l/s, Orzol). After the waterfrac a venting test was conducted where in two weeks 7000 m^3 was produced from the fracked sandstone. In January and February 2004 cyclic tests were performed, one weekly test where 2,500 m^3 was injected at 20 l/s and 30 MPa wellhead pressure, and then produced over five intervals in the following week. Also daily tests were performed with an injection of 400 m^3, a shut-in phase, and a production phase. Microseismic monitoring was performed with 8 stations at 0.8 – 1.6 km from the well. The detection limit was -0.5 < M_L < 0.0.

Occurrence of seismicity: Only 11 events were detected. The events were too weak to be located.

Interpretation: Successful creation of a conductive fracture. The stable state of stress and the local geology (sandstone) may have inhibited seismicity.

A.3.4   Neuruppin, Germany

Activity:	Geothermal, district heating & balneology	
Start date:	2007 (commissioned	To date
Fluid + Fluid balance:	Water	Circulation
Activity depth:	1.6 km	
Activity rocktype:	Sandstone (Dogger)	
In-situ T	64°C	
Cumulative ΔV:	Balanced	
Maximum Top Hole Pressure:	?	
Maximum flowrate:	17 l/s	
Monitoring system:	No	
Maximum magnitude + Date:	N/A	
Distance M_{max} – activity:	N/A	
Intensity [EMS]:	N/A	
Damage:	N/A	
Interpretation	N/A	

Tectonic setting and geology: The Neuruppin geothermal doublet is situated 50 km NW of Berlin, in the North German Basin. The system targets the Middle Jurassic Dogger sandstones (Aalenian formation), which lies at a depth of 1620 m with a temperature of 64 °C (Seibt & Wolfgramm, 2008). Well logs from nearby wells show that the Dogger is underlain by Lower Jurassic sediments (marl, siltstone, claystone), Triassic sediments, and Permian evaporites (Beer, Wolfgramm). It is overlain by ~200 m siltstones and claystones, and the Malm carbonates.

Activity design: The production well Neuruppin/Seetorviertel 1 was drilled in 2006 to a depth of 1702 m. The injection well Neuruppin/Seetorviertel 2 was drilled from the same well path and deviated, so that at reservoir level the wells are 875 m apart.

Operations and monitoring: Operations started in 2007. Flowrates are up to 17 l/s, and the water is reinjected into the same formation.

Seismicity: No seismicity was reported for this geothermal plant.

**Interpretation:** Successful geothermal plant without seismicity.
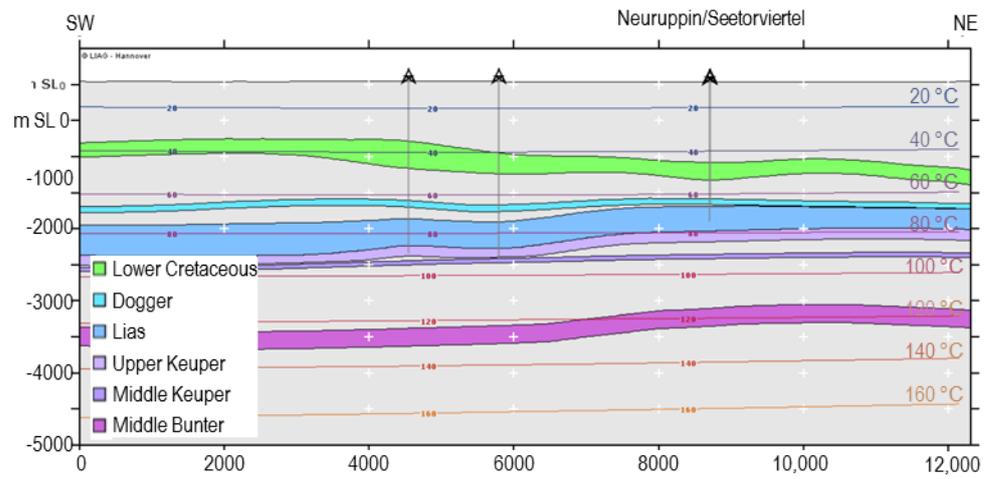
Figure A-24 Local stratigraphy near Neurupping. The well Neuruppin/Seetorviertel is shown. (Source: www.geotis.de).

A.3.5   Neustadt-Glewe, Germany

Activity:	Geothermal, powerplant, district heating	
Start date – End date:	1 – 1 – 1995	to date
Fluid + Fluid balance:	Water	circulation
Activity depth:	2.2 km	
Activity rocktype:	Sandstones	
In-situ T	99°C	
Cumulative ΔV:	Balanced (circulation)	
Maximum Top Hole Pressure:	0.5 MPa	
Maximum flowrate:	35 l/s	
Monitoring system:	No	
Maximum magnitude + Date:	N/A	
Distance M_{max} – activity:	N/A	
Intensity [EMS]:	N/A	
Damage:	N/A	
Interpretation		

Tectonic setting and geology: Neustadt-Glewe is situated in the North German Basin (Figure A-19), circa 100 km SSE of Hamburg. The area is a seismically quiet region. The target formations for geothermal exploration are Upper Triassic Contorta sandstones (Rhaetian reservoir, or Rhätkeuper) of the Middle Keuper Formation (Seibt et al., 2005). These sandstones are located between 2200 and 2300 m depth, with a total thickness of 60 m. The average porosity is 22% and the average permeability is good with 0.5×10^{-12} m^2. The reservoir temperature is 99 °C.

Activity design: Neustadt-Glewe is a classical doublet with two wells (Gt NG1/88: production, Gt NG2/89: injection) that were drilled in 1989-1990, to depths of 2455 and 2335 m (Figure A-25). The distance between the wells is 2 km, along a WSW-ENE profile. The productive horizons of the Middle Keuper Contorta sandstones were encountered between 2241 and 2320 m (Seibt et al., 2005).
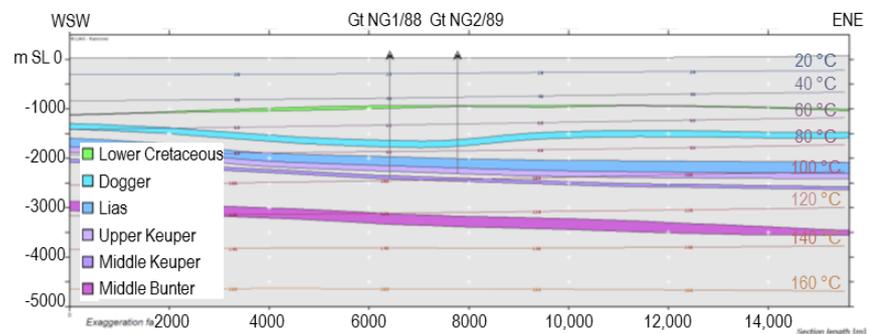

Figure A-25 Overview of the Neustadt-Glewe geothermal system and local geology (Source: www.geotis.de).

Operations and monitoring: Operations started in 1995 and have been continuing since, producing hot water of 99 °C and reinjecting it into Gt NG1/88 at a temperature of 50 - 60 °C. Flowrates ranged from 11 – 35 l/s, at a small injection pressure of 0.3 – 0.5 MPa. Acidization was used to remove carbonate precipitation in 1998 and 2007, with temporary higher flowrates of 90 – 100 l /s with an injection pressure of 0.6 – 0.8 MPa (Seibt & Wolfgramm, 2008). No microseismic monitoring was in place.

Seismicity: No seismicity has been recorded over the lifetime of the geothermal system.

Interpretation: Successful geothermal project and the first geothermal electricity plant in Germany.

A.3.6   Sønderborg, Denmark

Activity:	Geothermal, district heating	
Start date:	2013	To date
Fluid + Fluid balance:	Water	circulation
Activity depth:	1.2 km	
Activity rocktype:	Sandstone (Keuper)	
In-situ T	40°C	
Cumulative ΔV:	Balanced	
Maximum Top Hole Pressure:	?	
Maximum flowrate:	97 l/s	
Monitoring system:	No	
Maximum magnitude + Date:	N/A	
Distance M_{max} – activity:	N/A	
Intensity [EMS]:	N/A	
Damage:	N/A	
Interpretation	N/A	

Tectonic setting and geology: The Sønderborg geothermal plant is located in the south of Denmark close to the German border. It is situated in the north of the North German Basin (Figure A-19) 25 km southwest of the Ringkøbing High, which forms the southern boundary of the Norwegian Danish Basin. The target formation is the Upper Triassic Gassum (equivalent to Rhaetian) sandstone reservoir, which has a temperature of 48 °C at 1.1 km depth (Røgen et al., 2015). The effective thickness of the Gassum is 40 m, with an average porosity of 28%.

Activity design: The production and injection wells Sønderborg-1 and Sønderborg-2 were drilled in 2010 to a depth of 2592 m and 1405 m (Røgen et al., 2015) The initial target Bundsandstein was not found in the first well, and the Upper Triassic Gassum sandstone was targeted instead at a depth of 1.2 km. At the reservoir level the two wells are 0.8 km apart.

Operations and monitoring: Operations started in 2013 with the production of 48°C saline water, and reinjection at 12 °C. The maximum flowrate was 96 l/s, but injectivity decreased over time (Røgen et al., 2015).

Seismicity: No seismicity was reported for this geothermal plant.

Interpretation: Successful geothermal plant without seismicity.

A.3.7   Waren, Germany

Activity:	Geothermal, district heating	
Start date:	1984	To date
Fluid + Fluid balance:	Water	circulation
Activity depth:	1.5 km	
Activity rocktype:	Sandstone (Keuper)	
In-situ T	61°C	
Cumulative ΔV:	Balanced	
Maximum Top Hole Pressure:	5 MPa, 1 MPa (> 1986)	
Maximum flowrate:	14 l/s, 17 l/s (> 1986)	
Monitoring system:	No	
Maximum magnitude + Date:	N/A	
Distance M_{max} – activity:	N/A	
Intensity [EMS]:	N/A	
Damage:	N/A	
Interpretation	N/A	

Tectonic setting and geology: The Waren geothermal plant is the oldest operational geothermal heating plant in Germany. It is situated 120 km NNW of Berlin in Mecklenburg Vorpommern in the north of the North German Basin (Fig). The geothermal plant targets the Upper Triassic sandstones (Rhätkeuper) of the Contorta formation encountered at a depth of 1560 m, as well as the overlying Lower Jurassic Hettangian sandstone at 1506 m depth (Kabus & Jäntsch, 1995). Also the Middle Jurassic Aalen formation (1159 m depth) was used temporarily for reinjection. The effective thickness of the Contorta is 24 m, with a porosity of 29%. The Hettangian sandstones have an effective thickness of 30 m, and a porosity of 27%, and the Aalen sandstones also have an effective thickness of 30 m and a porosity of 28%. The reservoir temperature is 61 °C in the Contorta sandstone, 58 °C in the Hettangian sandstones, and 46 °C in the Aalen sandstone.
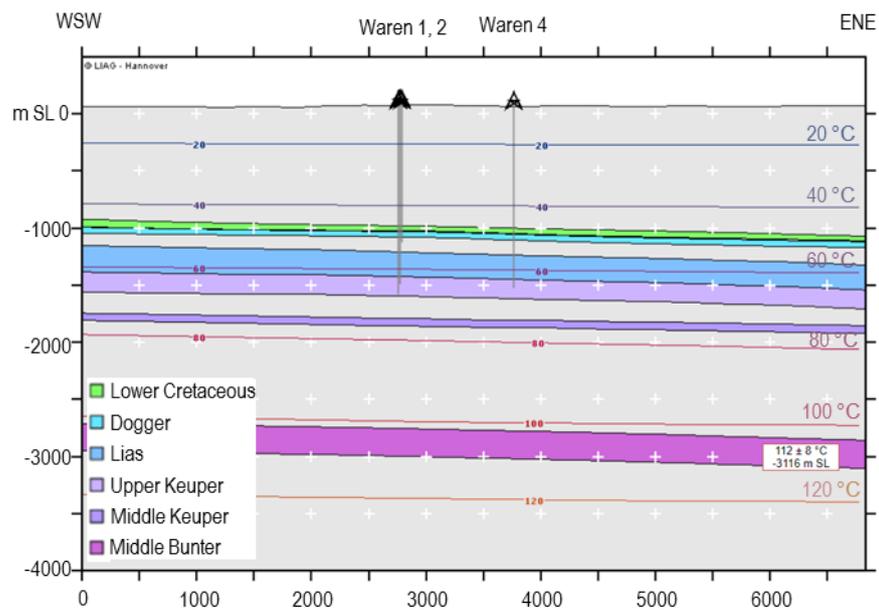
Figure A-26   Local geology at the Waren geothermal plant (Source: www.geotis.de).

Activity design: In 1981 the production well Waren 1 was drilled into the Contorta formation to a depth of 1656 m, and a shallower injection well Waren 2 was drilled into Aalen formation to a depth of 1200 m (Kabus & Jäntsch, 1995). The horizontal distance between the two wells was 50 m (Figure A-26). In 1986 a second injection well Waren 4 was drilled 1.3 km from the production well to a depth of 1565 m, targeting the Hettangian sandstone.

Operations and monitoring: Operations started in 1984, with the production from the Contorta sandstone. Reinjection into the shallow injection well occurred at maximum pressures of 5 MPa reaching flowrates up to 14 l/s (Evans, K. F. et al., 2012). The injection well did not meet the expectations, and reinjection into the Hettangian sandstones started in 1986 at injection pressures of 1.1 MPa and flowrates 17 l/s. The reinjection temperature was 45 °C.

Seismicity: No seismicity was reported for this geothermal plant.

Interpretation: Successful geothermal plant without seismicity.

A.4 Paris Basin, France

The Paris Basin is a nearly circular sedimentary basin which covers the northern part of France. It lies in between four crystalline basement bodies (Vosges, Ardennes, Massif Central and Massif Armoricain), see Figure A-27. The basin formed during a period of rifting in Permo-Triassic times. From Triassic to late-Jurassic, the Paris Basin was characterized by an extensional regime, related to the opening of the Tethys and the Atlantic Ocean (Guillocheau et al., 2000). During this time the depositional sedimentary environment fluctuated between alluvial plain, coastal plain and open marine.
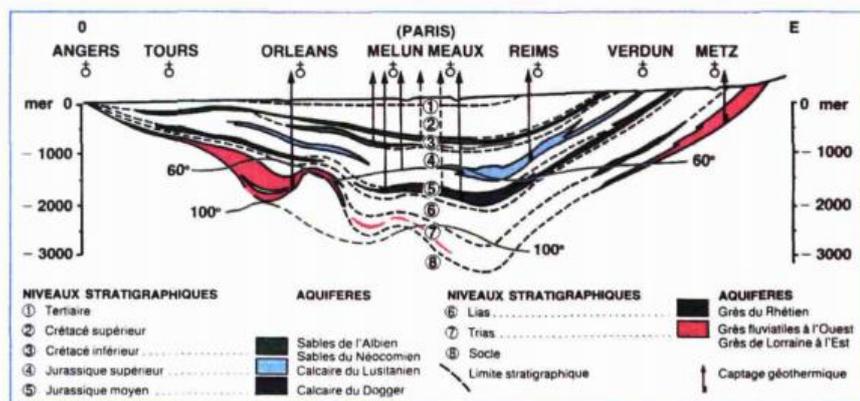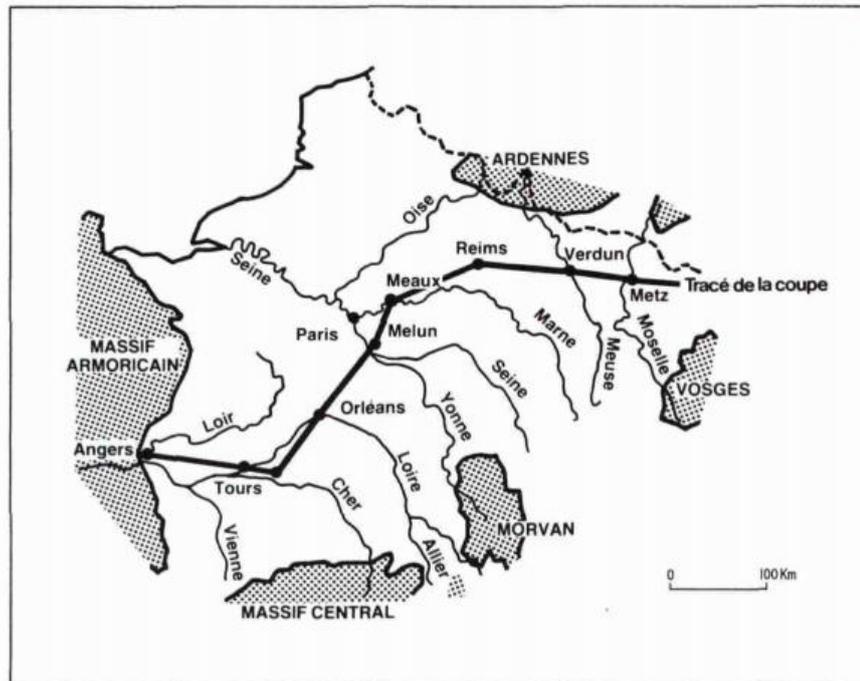

Figure A-27   Schematic cross section through the Paris Basin, number 5 indicates the Dogger geothermal reservoir (From Rojas et al., 1989, Copyright BRGM/RR-30169-FR, reproduced with permission).

The geothermal target in the Paris Basin are the mid-Jurassic (Dogger) carbonate rocks, which consists of several units. The most productive layers in the Dogger strata are the Bathonian aged carbonate platforms, which have a thickness of 100-150 m and lay at a depth of 1500-2000 m (Lopez et al., 2010). The reservoir temperature is between 55 °C and 80 °C and the average porosity is about 15% (Rojas et al., 1989). The porosity is generally matrix controlled, although in some units fracturing and dissolution has increased the porosity which may therefore locally be fracture-controlled.

The fault pattern characterizing the Paris basin is visualized in Figure A-28. The present day stress regime is at the limit between normal faulting and strike slip faulting and the orientation of the maximum horizontal stress is N 145° (Cornet & Burlet, 1992; Vidal-Gilbert et al., 2009). The Paris Basin is a seismically inactive region.
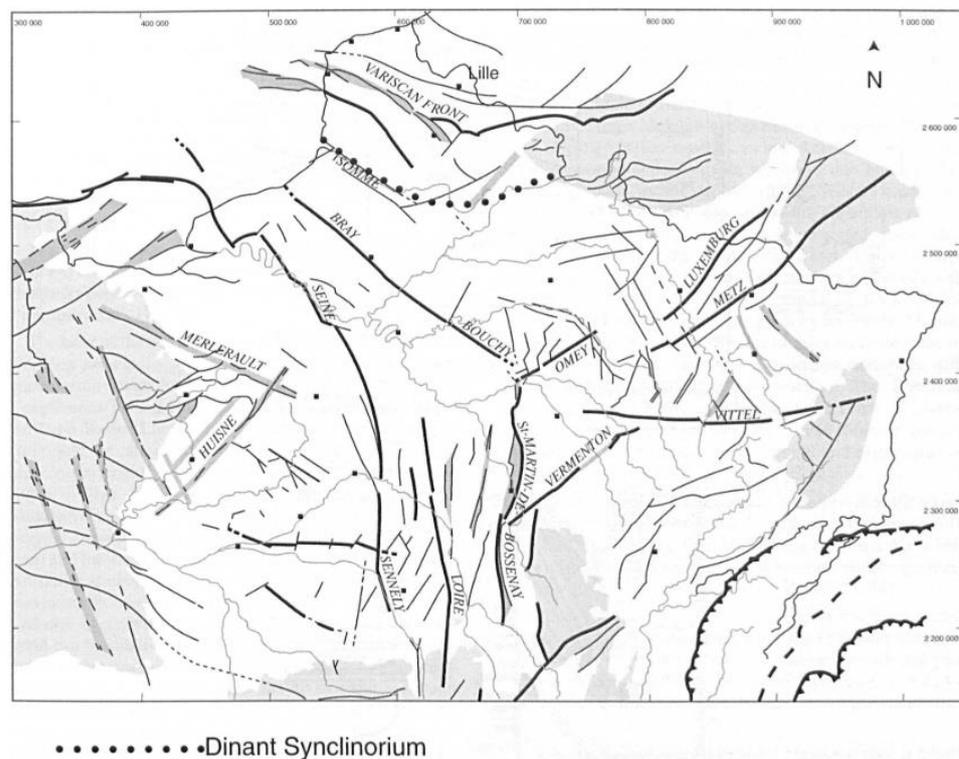

Figure A-28   Major faults in the Paris Basin (From Guillocheau et al., 2000, Copyright Taylor & Francis, reproduced with permission).

Since 1970 fifty-five doublets have been implemented in the Dogger formation of the Paris Basin, thirty-four of which are still in operation (Table A-1). The well depths range between 1600 and 2300 m and the well head temperatures range between 55-85 °C. The systems are all closed (circulating) doublets or triplets with flow rates ranging between 14 l/s to 167 l/s (average: 68 l/s). Nearly all the wells are completed with an 8-inch open hole section through the Bathonian deposits of the Dogger formation. Twenty-one doublets were abandoned for technical (corrosion and scaling problems) and economic (low fossil-fuel prices) reasons. There have been no indications for induced seismicity as a result of the geothermal exploration in the area.

Geothermal plant[a]	Year of commissioning	Year of shutdown	Wellhead temperature (°C)	Average flow rate (m³/h)	Brine salinity (g/l)	Additional energy source	Geothermal contribution to heat supply (%)
Melun (L'Almont)	1969		71	220	12.7	cg gz	63
Villeneuve-la-Garenne	1976	1994	57	50			
Le Mee-sur-Seine	1978		72	200	13	gz df	34
Montgeron	1982		72.5	220	12.2	gz	77
La Courneuve (Sud)	1982		56	180	21.9	cg gz	32
Cergy-Pontoise – Ville Nouvelle	1982	1991	57	200	14		
Coulommiers	1981		85	240	30.5	cg gz	95
Meaux (Collinet)	1982		79	250	32.6	cg gz df	35
Evry – Ville Nouvelle	1983	1999	72	175	10.4		
Aulnay-sous-Bois 1	1982	1994	71	220	25.7		
Clichy-sous-Bois	1985		71	200	19.3	cg gz	33
Orly 1	1984		76	240	12.2	hf df gz	65
Paris 16eme (Porte de Saint Cloud)	1984	1989	62	200	14.4		
Fontainebleau (Ecole des Mines)	1983	1991	74	130	6		
Meaux (Beauval)	1983		78	600	38.8	cg gz df	35
Meaux (Hopital)	1983		75	250	31.5	cg gz	44
Acheres	1983	1989	55	200	12.6		
La Celle Saint-Cloud	1983	1989	62	170	11.4		
Ris-Orangis	1983		72	225	11.5	cg gz df	42
Blanc-Mesnil (Nord)	1983		67.5	250	27	gz df	62
La Courneuve (Nord)	1983		58	200	23.8	gz	64
Sevran	1983	1990	69	275	25		
Vaux-le-Penil	1983	1998	72	140	12.5		
Chatenay-Malabry	1984	1997	67	175	10		
Chatenay-Malabry	1984	1997	67	175	10		
Ivry-sur-Seine	1983	1994	63.8	120	16		
Garges-les-Gonesse	1984	1994	67.7	250	29.1		
Epinay-sous-Senart	1984		75.2	250	14	gz	72
Aulnay-sous-Bois 2	1984	1994	70.5	275	24.9		
Bondy	1984	1989	64	250	16.4		
Tremblay-en-France	1984		74	275	26.1	gz	90
Cachan 1 & 2	1984		70	340	16.2	cg gz hf	78
Sucy-en-Brie	1984		78	140	24.9		100
Vigneux sur Seine	1985		71.9	300	12.5	gz df	66
Champigny-sur-Marne	1985		78.2	280	27.7	cg gz	71
Chevilly-Larue/L'Hay-les-Roses	1985		75	600	14.7	cg gz	55
Creteil	1985		78.9	300	23.3	cg df	37
Maisons-Alfort 1	1985		73	300	21.4	cg gz df	67
Villiers-le-Bel	1985		67	290	26.1	cg hf	39
Chelles	1986		69	280	21.2	cg gz hf	42
Alfortville	1986		74	260	19.5	gz	74
Bonneuil-sur-Marne	1986		79.3	300	22	gz	66
Fresnes	1986		71.7	200		cg gz df	50
Maisons-Alfort 2	1986		74	260	20.3	cg gz df	35
Orly 2	1986		76.8	250	14.8	hf df gz	65
Thiais	1986		76	250	17.8	gz	87
Villeneuve Saint Georges	1987		76	350	19.9	cg gz df	61
Paris 19eme (La Villette)	1990	1990					

Abbreviations: cg, gz, df and hf denote cogeneration, gas, diesel fuel and heavy fuel oil, respectively. Data are from Vathaire et al. (2006) and Huchon (2008).

[a] Today, all operating geothermal plants in the Paris basin are located in the Ile-de-France region. Plants outside the Ile de France region have been shut down.

Table A-1   Overview of geothermal projects in the Paris Basin. (From Lopez et al., 2010, Copyright Elsevier, reproduced with permission).

A.5 Norwegian Danish Basin

The Norwegian Danish Basin was part of the Permian basin, and formed around the same time as e.g. the North German Basin. Rifting in the Upper Carboniferous and Lower Permian caused the basin to develop along a NW-SE orientation (Figure A-29). It is bounded in the south by the Ringkøbing High, and in the north it is separated from the Fennoscandian shield by the Sorgenfrei-Tornquist Zone. The oldest sediments overlying the basement are Lower Rotliegend sandstones and volcanics at a depth of up to 6 km. Subsidence continued in the Triassic and Jurassic as a result of thermal cooling, and thick sequences of Zechstein halite were deposited, overlain by Triassic sandstones, mudstones, carbonates, and evaporites. These include the Lower Triassic Bunter sandstone formation which has a thickness of 300 – 600 m, and the Upper Triassic sandstone Gassum Formation (time equivalent to the Rhaetian in the North German Basin) which is 30 – 300 m thick (Kristensen et al., 2016). The Jurassic sediments are predominantly mudstones and sandstones, and the Cretaceous sediments consist of carbonates and chalk. Inversion occurred in the Cenozoic along the basin boundaries. Major fault structures run NW-SE, and smaller faults SW-NE (Figure A-29). The maximum horizontal stress is oriented NW-SE and the regional stress regime is tensional. Seismic activity on the onshore parts of the basin is low (Gregersen & Voss, 2014).
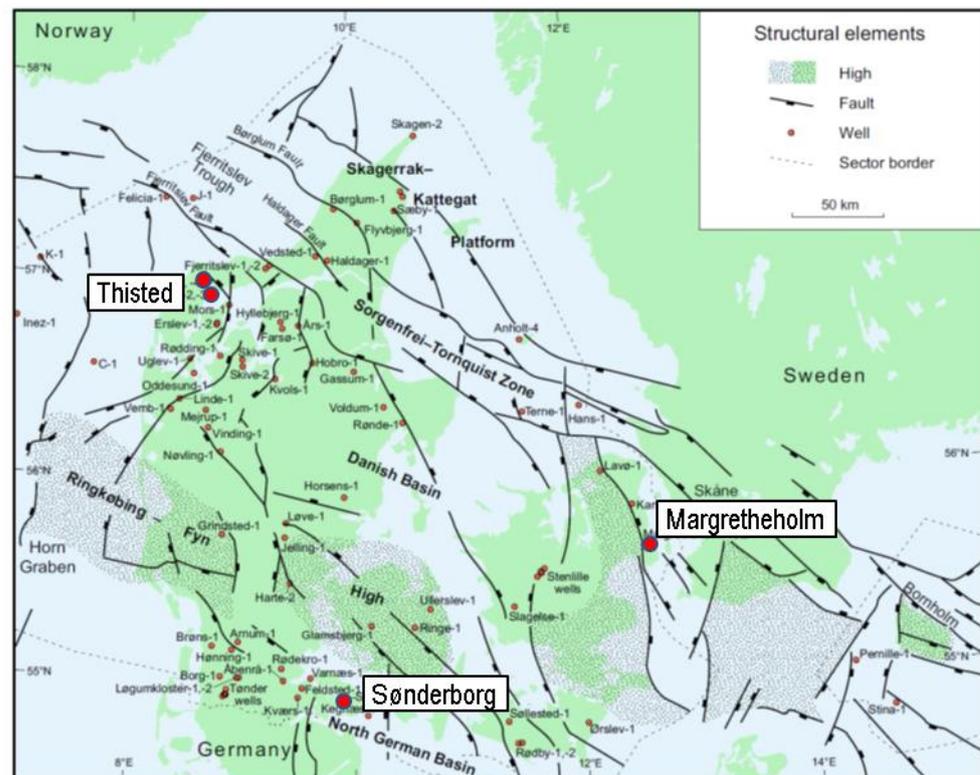

Figure A-29 Structural elements of the Norwegian Danish Basin (From Frederiksen et al., 2001, Copyright Elsevier, reproduced with permission).

The main geothermal targets are the Bunter sandstone and the Gassum sandstone formations, which have temperatures up to 80°C.

A.5.1 Thisted, Denmark

Activity:	Geothermal, district heating	
Start date:	1 – 1 – 1984	start drilling
Fluid + Fluid balance:	Water	circulation
Activity depth:	1.25 km	
Activity rocktype:	Sandstone	
In-situ T	45°C	
Cumulative ΔV:	?	
Maximum Top Hole Pressure:	1.7 MPa	
Maximum flowrate:	56 l/s	
Monitoring system:	No	
Maximum magnitude + Date:	N/A	
Distance M_{max} – activity:	N/A	
Intensity [EMS]:	N/A	
Damage:	N/A	
Interpretation	N/A	
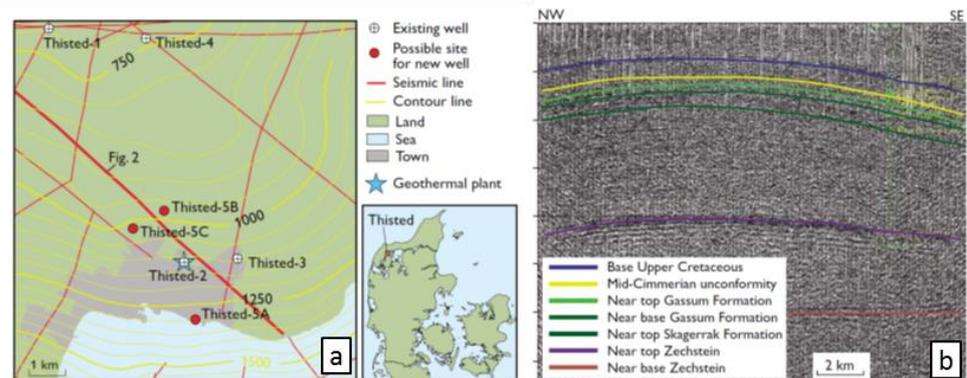
Figure A-30   Location and local geology of the Thisted geothermal system. (From Hjuler et al., 2014, Copyright GEUS, published under a Creative Commons license).

Tectonic setting and geology: The Thisted geothermal plant is located in the northern part of the Norwegian Danish Basin (Figure A-29, Figure A-30). The target formation is the permeable sandstone Upper Triassic to Lower Jurassic Gassum Formation (time-equivalent to Rhaetian Formation in Germany), which is encountered at a depth of 1.2 km and has a thickness of 135 m (Hjuler et al., 2014). The Gassum has an average porosity of 28% and a permeability of $1 – 5 \times 10^{-12}$ m^2, and a reservoir temperature of 45° C. The area is characterized by diapirism; Thisted is situated just southwest of a Zechstein salt pillow. The Zechstein is overlain by the Triassic Skagerrak Formation (or Bunter Sandstone), which consists of sandstones, conglomerates, siltstones and shales. The Gassum Formation is overlain by Jurassic formations (silts, mudstones) and a thick layer of Cretaceous chalk and limestone, all dipping to the SE. A few medium size earthquakes have occurred within 20 km of the geothermal site (Gregersen & Voss, 2014).

Activity design: The production well Thisted-2 was drilled in 1983 to a total depth of 3.3 km (Mahler, 1995). It was packed at 1300 m and filled with gravel, producing from 1250 m depth. The cooled water of 12°C is reinjected into Thisted-3, which is drilled to 1242 m, at a distance of 1.5 km east of Thisted-2.

Operations and monitoring: Operation of the geothermal plant started with a pilot in 1984, when water was circulated at 10 l/s. In 1988 the plant was expanded, reaching flowrates of 42 l/s at an injection pressure of 0.9 MPa (Mahler, 1995). In 2001 the capacity was increased further to 56 l/s, with injection pressures of 1.7 MPa (Mahler & Magtengaard, 2005).

Seismicity: No seismicity was reported for this geothermal plant.

Interpretation: Successful geothermal plant without seismicity.

A.5.2   Margretheholm, Denmark

Activity:	Geothermal, district heating	
Start date:	1 – 1 – 2005	To date
Fluid + Fluid balance:	Water	circulation
Activity depth:	2.6 km	
Activity rocktype:	Sandstone (Bundsandstein)	
In-situ T	73°C	
Cumulative ΔV:	Balanced	
Maximum Top Hole Pressure:	0.7 MPa	
Maximum flowrate:	65 l/s	
Monitoring system:	No	
Maximum magnitude + Date:	N/A	
Distance M_{max} – activity:	N/A	
Intensity [EMS]:	N/A	
Damage:	N/A	
Interpretation	N/A	
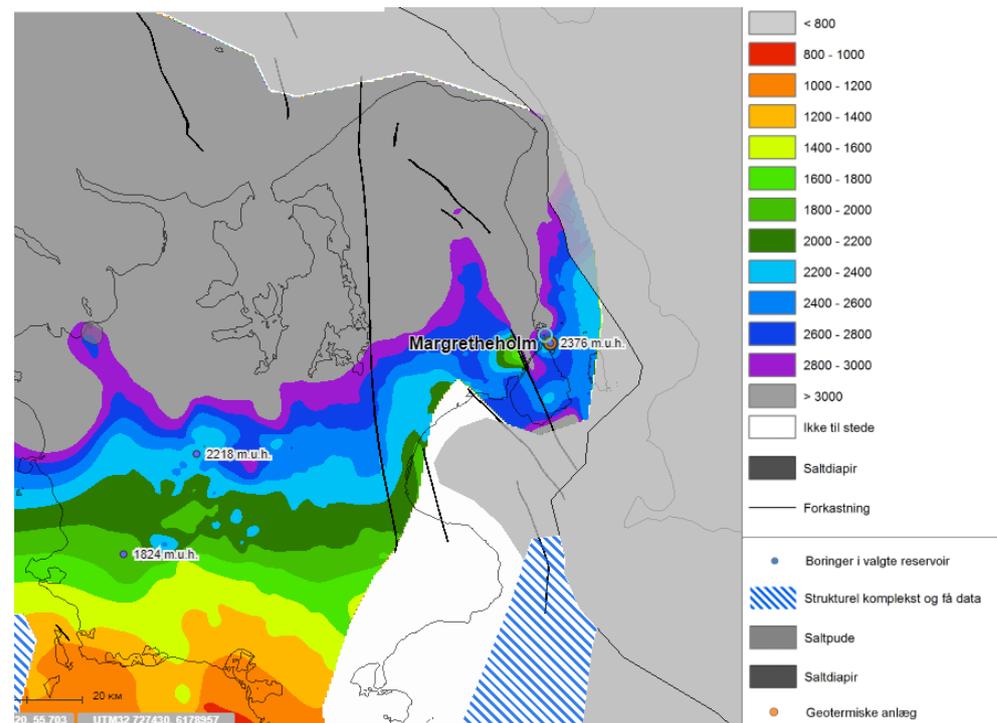
Figure A-31 Depth of the Bundsandstein formation in northeast Denmark (Source: http://data.geus.dk/).

Tectonic setting and geology: The Margretheholm pilot geothermal system is situated in the northeast of Denmark at the east side of Copenhagen (Figure A-31). The site is located in the Øresund Basin (Erlström et al., 2018), which is a

substructure of the Norwegian-Danish Basin (NDB). It is bounded in the northeast by the Sorgefrei-Tornquist fault zone (STF), which separates the basin from the Fennoscandian shield (Figure A-29). The west and southwest are bounded by large normal faults (Amager and Øresund faults) striking NW-SE, parallel to the STF. The geothermal system targets the Lower Triassic Bundsandstein (mainly Hammar and Flommen formations) which is found between depths of 2470 – 2660 m with a temperature of 73 °C (Erlström et al., 2018). It consists of sandstone layers interbedded with sandy claystone layers (Figure A-32), with an average permeability of 4 x 10^{-13} m^2. It is underlain by a few m of Permian conglomerates, which lie directly over the Precambrian granitic basement (top depth 2700 m). The reservoir is capped by Lower Jurassic sandy claystones and siltstones.
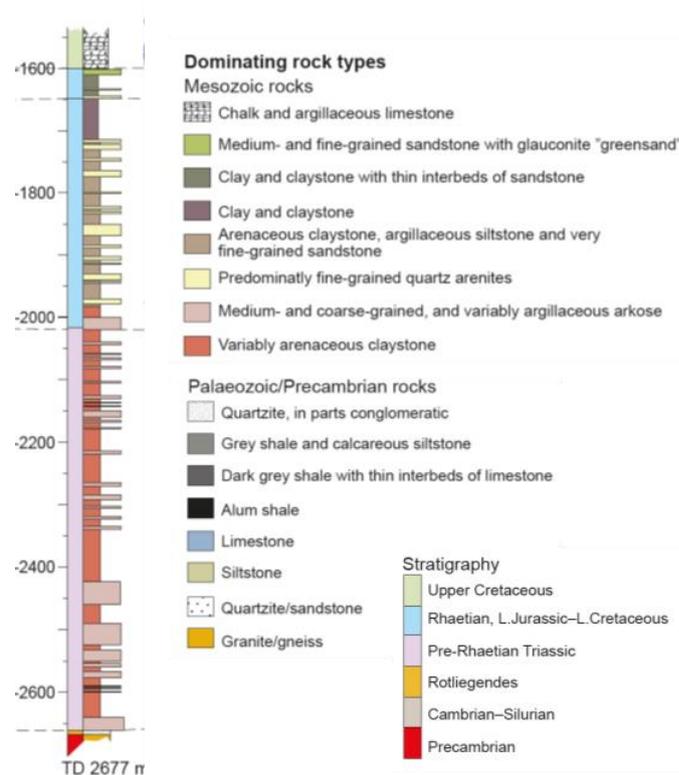
Figure A-32   Stratigraphy in the Margretheholm-1 well. (From Erlström et al., 2018, Copyright Dansk Geologisk Forening, reproduced with permission).

Activity design: The Margretheholm-1 well was drilled in 2002 to a depth of 2700 m, reaching the granitic basement. In 2003 a second deviated well Margretheholm-2 was drilled to the same depth, at 1.3 km from the first well.

Operations and monitoring: Circulation of brine started in 2005, with flowrates of 65 l/s. The hot water of 71 °C was produced at a pressure of 1.5 MPa, and 15 °C water was reinjected into the injection well at a reinjection pressure of 0.7 MPa. Over the years the injection pressure needed to be increased to ~7 MPa (Røgen et al., 2015). Acidization was used repeatedly to lower injection pressure. No local seismic monitoring systems are in place.

Seismicity: No seismicity was reported for this geothermal plant.

Interpretation: Successful geothermal plant without seismicity.

A.6 Rosemanowes, United Kingdom (M2.0)

Activity:	Geothermal EGS, research	
Start date – End date:	1982	Nov 1988
Fluid + Fluid balance:	Water	Stimulation(1982,1985) Circulation(1983,1985)
Activity depth:	2.0, 2.6 km	
Activity rocktype:	Granite	
In-situ T	80, 95 °C	
Net ΔV:	18,500 m^3 water (2A stimulation) 225,000 m^3 water (2A circulation) 5,700 m^3 viscous gel (2B viscous stimulation) 490,000 m^3 water (2B/C circulation) 530 m^3 viscous gel (3 stimulation) 4,000 m^3 viscous gel (3 stimulation)	
Maximum Top Hole Pressure:	14.2 MPa (2A stim), 15 MPa (2B stim.), 11.8 MPa (2B cir.), 24 MPa (3 stim.)	
Maximum flowrate:	100 l/s (2A stim.), 200 l/s (2B stim.), 35 l/s (2B cir.), 85 l/s (3 stim.)	
Monitoring system:	Shallow borehole, downhole system	
Maximum magnitude + Date:	0.6 (2A), 2.0 (2B cir.)	
Distance M$_{max}$ – activity:	0.6 km	
Intensity [EMS]:		
Damage:	Mildly felt	
Interpretation	Pressure increase in faults	

Tectonic setting and geology: The Rosemanowes experimental geothermal site is located in the Rosemanowes granite quarry in Cornwall, in the southwest of the United Kingdom. This is one of the outcrops of the Carnmenellis pluton which intruded in the Late Carboniferous and Early Permian. The rocks surrounding the batholith are mudstones, shales, and conglomerates of primarily Devonian age, which may be locally metamorphosed. The stress regime is strike-slip with the maximum horizontal stress striking NW-SE. The granite is naturally fractured with fracture orientations NNW-SSE, and WSW-ENE (Batchelor, 1982). No major faults were observed in the outcropping granite at the Rosemanowes site (Parker, 1999).

Activity design: Two boreholes (RH11 and RH12) were drilled in 1980 to 2 km depth with a 400 m open-hole section at the bottom (Richards et al., 1994). At the reservoir level the boreholes were ~200 m apart, oriented (mistakenly) NW-SE, perpendicular to the minimum horizontal stress (see Figure A-33). In 1983, after stimulation of RH12 both boreholes were deepened by 150 m. A third deep borehole RH15 was drilled in 1984 to 2.6 km with a 500 m open-hole section. The horizontal spacing between RH15 and RH12 was ~200 m, and the vertical spacing 450 m. RH15 and RH12 were aligned SW-NE, parallel to the minimum horizontal stress.
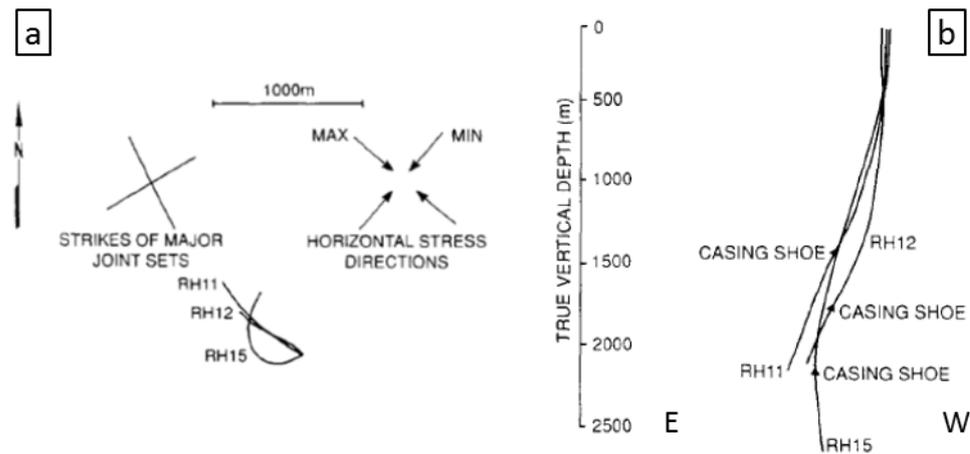
Figure A-33 Well paths at Rosemanowes. a) Top view of deep wells RH11, RH12, and RH15, orientation of the major joint sets, and the minimum and maximum horizontal stress, b) Vertical section of the three deep wells. (From Richards et al., 1994, Copyright Elsevier, reproduced with permission).

Operations and monitoring: In 1982 (following an explosive stimulation) Phase 2A started with the hydraulic stimulation of injection well RH12 with a total volume of 18,500 m³ at maximum pressure of 14.2 and flowrates of 100 l/s (Batchelor et al., 1983). Afterwards circulation was established between RH12 and RH11. During circulation large water losses of up to 70% were observed, which amounted to a net ΔV 225,000 m³ (Richards et al., 1994). During Phase 2B in July 1985 a viscous stimulation of RH15 was performed, with 5500 m³ of gel and 200 m³ of water at an injection pressure of 15 MPa and flowrates of 200 l/s (Parker, 1999). After this stimulation and a flow test, a long term circulation experiment was conducted between RH12 (injection) and RH15 (production) until 1988. Injection pressure during circulation reached 11.8 MPa with flow rates up to 35 l/s (Richards et al., 1994). The fraction of water loss was smaller, but over the 4 years the net water losses accumulated to 490,000 m³. Two additional stimulations were performed in 1989 and 1990 (Phase 3) to improve the thermal performance of the system and reduce the short circuit between the wells (Parker, 1999). In early 1989 530 m³ of viscous gel and 55 tonnes of sand were injected in RH15 at a maximum pressure of 24 MPa and flowrates up to 85 l/s. In 1990 another 4,000 m³ of viscous gel and proppant were injected. Microseismicity was monitored with 8 surface stations at 1 – 6 km from the wells, as well as a downhole array in RH11 (Batchelor, 1982; Batchelor et al., 1983).

Seismicity: Thousands events were recorded during Phase 2. During the Phase 2A stimulation seismicity was located between the wells, and migrated predominantly downwards with injection time (Batchelor et al., 1983). The maximum reported magnitude was 0.6. During the Phase 2B stimulation much less seismicity was generated, and locations showed it migrated vertically from injection well RH12 to RH15 (Figure A-34b). During both circulations a large rock volume showed microseismicity, extending far beyond the region between the wells (Figure A-34c, d). The largest magnitude of M_L 2.0 occurred at 3.1 km depth during circulation in 1987 (Evans, K. F. et al., 2012). The event was mildly felt by local inhabitants. Another M_L 1.7 event occurred in January 1988 but it was not felt at the surface.

Interpretation: Shearing on critically stressed joints and fractures. The downwards migration in Phase 2A may be due to poor conductivity between the wells as they were oriented along the maximum horizontal stress direction. Seismicity rates during circulation may have been relatively high due to the large water losses (net injection).
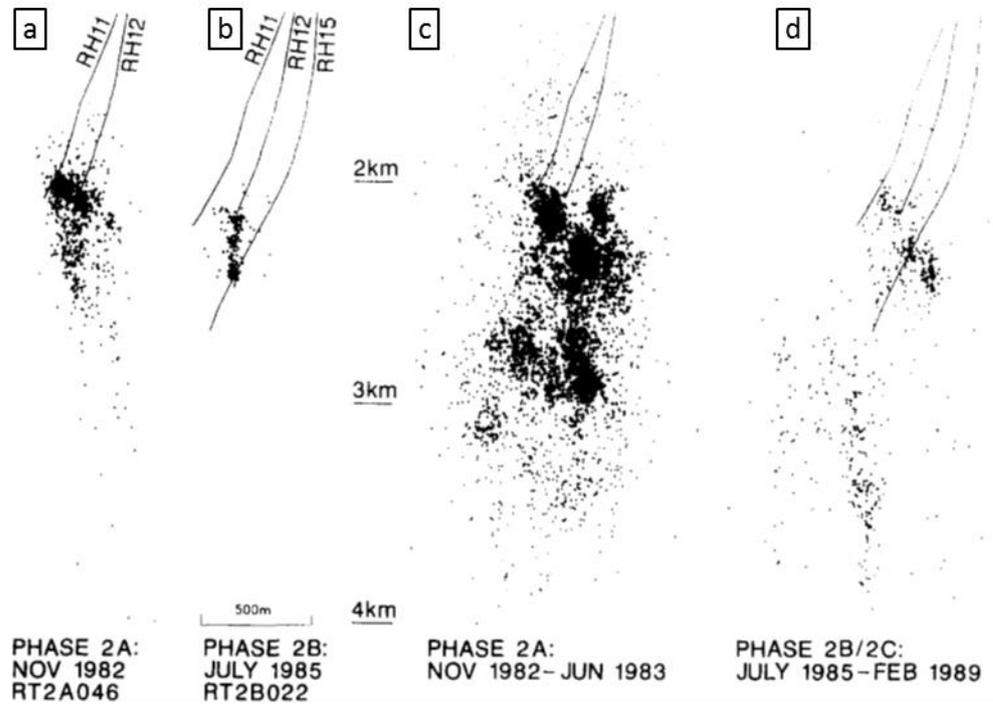

Figure A-34 Microseismicity recorded at Rosemanowes during different stages in Phase 2 (From Richards et al., 1994, Copyright Elsevier, reproduced with permission).

A.7 Pohang, South Korea (M 5.4)

Country & place:	South-Korea, Pohang	
Activity:	Geothermal EGS	
Start date – End date:	January 2016	September 2017
Fluid + Fluid balance:	Water	Injection
Activity depth:	~ 4.0 – 4.3 km	
Activity rocktype:	Granodiorite with gabbroic dykes, granitic gneiss	
In-situ T	140 °C	
Cumulative ΔV:	Gros 12,800 m^3, net 6000 m^3	
Maximum Top Hole Pressure:	27.7 MPa (PX-1) and 89.2 MPa (PX-2)	
Maximum flowrate:	18 l/s (PX-1, 1st stimulation) and 47 l/s (PX-2, first stimulation)	
Monitoring system:	Yes	
Maximum magnitude + Date:	5.4	15 – 11 - 2017
Distance M_{max} – activity:	< 1 km	
Intensity [EMS]:	VI	
Damage:	Heavy structural damage, casualties	
Interpretation	Pore pressure increase induced earthquakes on a previously unmapped fault, which triggered the mainshock of M 5.4	

Tectonic setting and geology: The Pohang EGS is located in the southeastern part of the Korean peninsula, in the sedimentary Pohang Basin, which formed in the Early to Middle Tertiary during the opening of the Japan Sea. As a result of the opening of the Japan Sea in a back arc setting, in this region predominantly NNE striking strike slip and NNE to NE striking normal faults developed (Figure A-35). Some of these faults have been reactivated as either strike slip or reverse faults in the current-day compressional stress field (Kim, Kwang-Hee et al., 2018). This stress field is marked by a strike-slip regime, with the maximum horizontal stress trending between N65° E and N136° E (Kim, Hanna et al., 2017; Park et al., 2017), with a most likely orientation of N114° E (Min, 2018). The Korean peninsula is characterized by low to moderate intraplate seismic activity. The catalogue of historical earthquakes for this region shows a long term history of natural earthquakes (of which three with M>7), which indicates some of the major fault structures are still active. September 2016, a M_w 5.5 event was recorded on the Yangsan Fault, the epicenter located some 30 km to the south of the EGS site (Grigoli et al., 2018; Kim, Kwang-Hee et al., 2018; Kim, Kwang-Il et al., 2018).
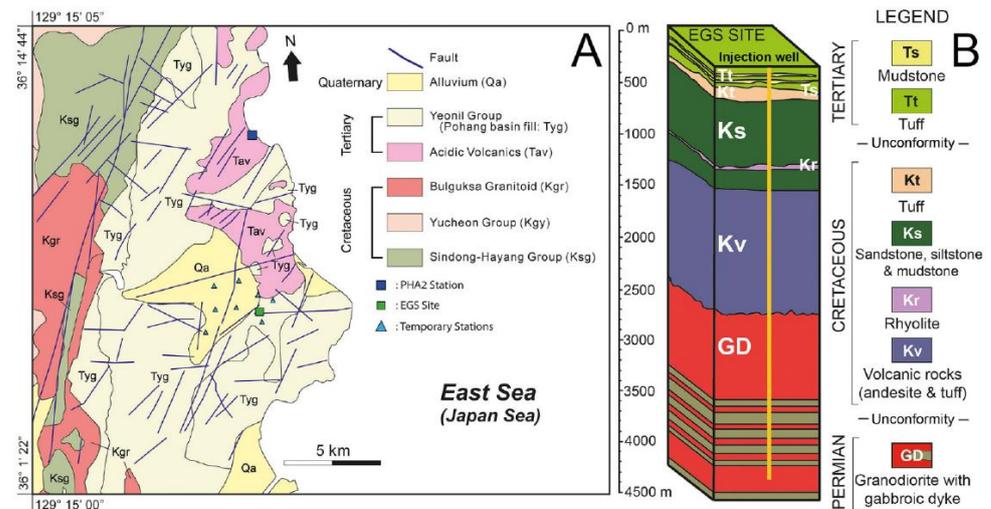
Figure A-35　Geology of the Pohang EGs site. Left: Map of regional surface geology, showing predominant fault orientations. Right: Lithological sequence at the Pohang EGS site. (From Kim, Kwang-Hee et al., 2018, Copyright AAAS, reproduced with permission).

The Pohang EGS targets fractured granodiorites in the basement, the top of which is encountered at 2400 m depth (Figure A-35). At 4.2 km depth bottom hole temperatures of 140 °C, measured three days after drilling, were reported (Kim, Kwang-Hee et al., 2018; Min, 2018).

Activity design: Drilling activities at the Pohang site started in September 2012 and were completed in November 2015. A deviated production well (PX-1) and a vertical injection well (PX-2) were drilled into the basement rocks up to a depth of 4217 to 4348 m. PX-1 and PX-2 have open-hole sections at the bottom of the well of 313 m, respectively 140 m. The distance between the wells is 600 m at the bottom of the wells. Both wells have been hydraulically stimulated during multiple phases to enhance flow in the rocks. The Pohang EGS site has not been in operation, all activities on site having been suspended since the occurrence of the November 2017 Mw 5.4 event (Kim, Kwang-Hee et al., 2018).

Operations and monitoring: The hydraulic stimulation of the Pohang EGS site comprised 5 phases, during which well PX-1 (stage 2,3,4) and PX-2 (stage 1,3,5) have been stimulated alternatingly (Figure A-36). The stimulation activities at the Pohang site started January 29th 2016 with stimulation of well PX-2 (Figure A-37). In the period from January 29th to February 20th 2016, a total volume of 1970 m3 of water has been injected into the open hole section of the well. Injection rates varied between 1 and 47 l/s and a maximum wellhead pressure of 89.2 MPa was reached. Various injection strategies were tested (step rate, cyclic injection, long term injection, long term shut-in and bleed-off). During the injection activities, a seismic monitoring network was in place, composed of nine borehole seismometers, four surface seismometers and one three-component borehole geophone installed at 1360m depth in the PX-1 well (Park et al., 2017). Between January 29th and February 24th, 271 seismic events have been recorded by the network. The largest earthquake recorded during this first injection phase had a magnitude of M_w 1.4 (M_L 1.7). Largest seismicity rates and magnitudes of seismic events were observed during shut-in (Min, 2018; Park et al., 2017).

Following stimulation of PX-2, well PX-1 has been stimulated from December 15th to 28th, 2016 (Figure A-38). A total volume of 3907 m3 of fluids was injected, with a net volume of 2689 m3 remaining in the system after bleed-off. Maximum well head pressures of 27.7 MPa were reached, with maximum injection rates of 18 l/s. Similar to the first stimulation of PX-2, various injection schedules were used, comprising cyclic injection, long term injection, shut-in and bleed-off. A total of 837 seismic events were recorded during this phase, two largest events of M$_L$ 2.2 being recorded during shut-in of the well. No details are given on monitoring networks in place during stimulation of well PX-1. During both first stimulations of PX-1 and PX-2 a traffic light system was used to manage the risks of induced seismicity (Kim, Kwang-Il et al., 2018; Min, 2018).
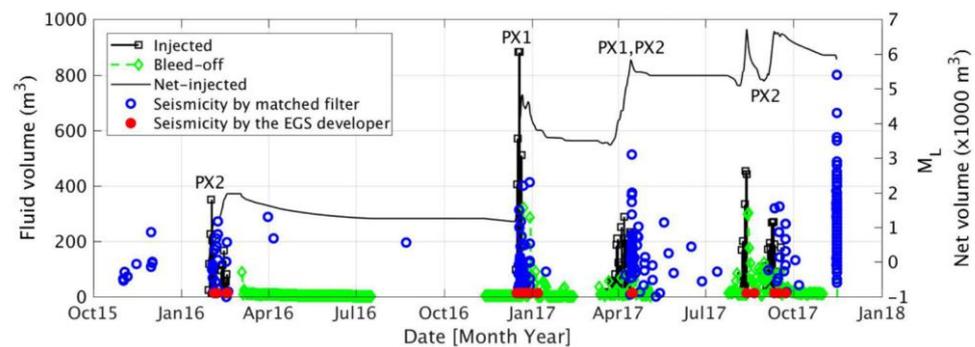
Figure A-36 Different hydraulic stimulation stages and associated seismicity at the Pohang EGS site (From Kim, Kwang-Hee et al., 2018, Copyright AAAS, reproduced with permission).
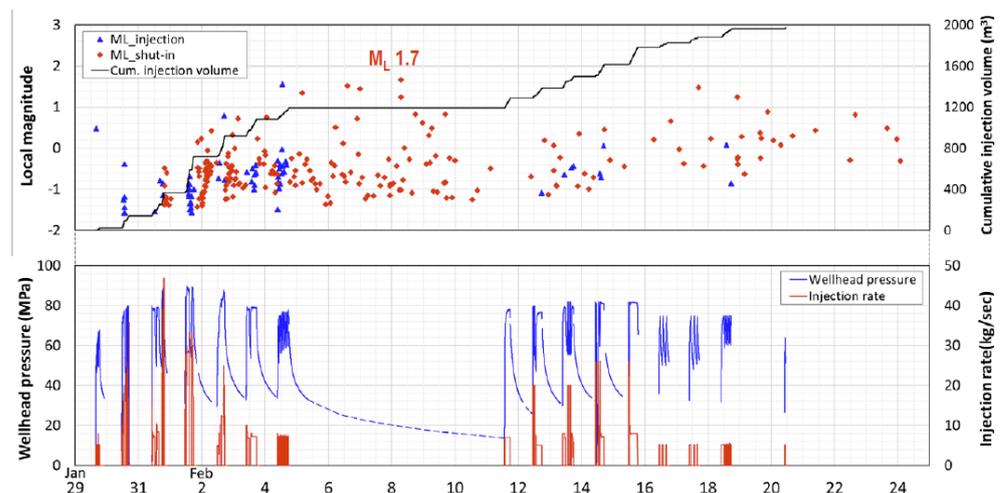

Figure A-37 Hydraulic stimulation data of well PX-2. First hydraulic stimulation from January 29th to February 20th, 2016. Upper graph shows magnitudes of seismic events during stimulation, distinguishing between seismic events during injection and shut-in, and cumulative Injection volume. Lower graph presents wellhead pressures and injection rates (From Min, 2018, Powerpoint presentation downloaded on 15 April 2019 from http://www.destress-h2020.eu/stay-informed/news-and-events/bsds-blog/Home-DESTRESS-met-for-a-fruitful-exchange-in-Glasgow/).
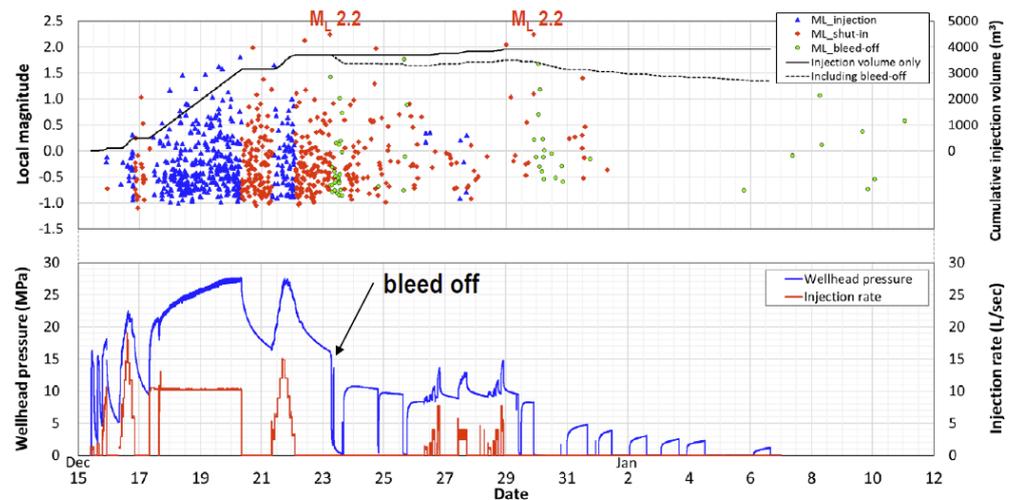
Figure A-38 Hydraulic stimulation of well PX-1(Min, 2018). Hydraulic stimulation from December 15th to 28th, 2016. Upper graph shows events during stimulation, distinguishing between events which occurred during injection, shut-in and bleed-off. Lower graph shows wellhead pressures and injection rates (From Min, 2018, Powerpoint presentation downloaded on 15 April 2019 from http://www.destress-h2020.eu/stay-informed/news-and-events/bsds-blog/Home-DESTRESS-met-for-a-fruitful-exchange-in-Glasgow/).

These stimulations were followed by 3 additional hydraulic stimulations in April 2017, August 2017 and September 2017 (Figure A-36). On 15th of April 2017, during the third stimulation phase, a M_L 3.1 seismic event was recorded near the injection site (Kim, Kwang-Hee et al., 2018). To date, little data on injection schemes, pressures, monitoring networks and observed seismicity during the April 2017 and September 2017 stimulations can be found in literature. August 2017, a cyclic soft stimulation of well PX-1 was performed. The cyclic stimulation consisted of 3 phases of stimulation, with maximum flowrates up to 10 l/s and maximum wellhead pressures up to 22 MPa. A monitoring network was installed and a traffic light system was used to mitigate induced seismicity during the soft cyclic stimulation. After the occurrence of a M_w 1.9 seismic event, injection was stopped, and the total injected fluid volume was recovered by means of flowback (Hofmann et al., 2018). During the 5 stimulations a cumulative volume of 12,800 m3 of fluids was injected, with a net volume of approximately 6000 m3 remaining in the rocks after bleed-off of the wells (Kim, Kwang-Hee et al., 2018).

November 15th 2017, approximately two months after the last stimulation, a magnitude M_w 5.4 event occurred at a distance of less than 1 km of the injection site (Grigoli et al., 2018; Kim, Kwang-Hee et al., 2018). Both Grigoli et al. (2018) and Kim et al. (2018) suggest the M_w 5.4 earthquake was induced by the fluid from the EGS site, being injected into, or very close to a near-critically stressed large-scale fault structure. The potential relation between the hydraulic stimulations at the Pohang EGS site and the occurrence of the M_w 5.4 event has been investigated by different research teams (Grigoli et al., 2018; Kim, Kwang-Hee et al., 2018). Recent research has indicated that EGS activities at the Pohang site induced earthquakes on a previously unmapped fault, which triggered the mainshock. Once triggered the earthquake grew to a magnitude M5.4 event through the release of tectonic strain (ORAC, 2019).

A.8 Hellisheiði, Iceland (M 4.0)

Country & place:	Húsmúli re-injection wells, Hellisheiði, Iceland	
Activity:	Waste water injection from a geothermal Field	
Start date – End date:	September 2011	2015
Fluid + Fluid balance:	Water from Hellisheiði	Re-Injection
Activity depth:	~ 1.9 – 3.0 km	
Activity rocktype:	Basalt, hyaloclastites	
In-situ T	220 - 250 °C	
Cumulative ΔV:	Re-injected ~ 13,000,000 m3	
Maximum Top Hole Pressure:	2.8 MPa	
Maximum flowrate:	550 l/s	
Monitoring system:	Yes	
Maximum magnitude + Date:	4.0	15 – 10 – 2011
Distance M_{max} – activity:	0 - 3 km	
Intensity [EMS]:	Felt @12 km	
Damage:	No considerable structural damage	
Interpretation	Pore pressure diffusion and increase; additional Coulomb stressing by production in Hellisheidi	

Tectonic setting and geology: The Hellisheiði high temperature geothermal field is located in the southwest of Iceland, within the Hengill Volcanic System. The Hengill-Hellisheiði area is seismically active, with recent earthquakes of magnitude M_w 5.4 and M_w 5.1. The Hengill area is structurally dominated by a large NE-SW striking fault and fracture system, intersected by E-W striking structures. Wells in Húsmúli target faults and volcanic fissures in the basaltic lava layers, hyaloclastites and dykes (Agustsson et al., 2015; Gunnarsson et al., 2015). The formation temperature in the Húsmúli area is 220-250 °C (Gunnarsson, 2013). The Hengill volcanic system itself is positioned in a tectonically active region, at the junction of two active rift zones and a seismically active transform zone, the South Iceland Seismic Zone (SISZ). In May 2008 two Mw 6.0 earthquakes were recorded in the SISW, some 15 km to the east of the Húsmúli injection site. The in-situ stress field in this region is characterized by a NW-direction of the minimum horizontal stress and a strike slip to normal stress regime (Agustsson et al., 2015).

Activity design: There are 47 production and 17 reinjection wells in the Hellisheiði geothermal field (Figure A-39). Borehole depths are between 1.9 and 3.0 km and injection temperatures are around 60- 80°C.
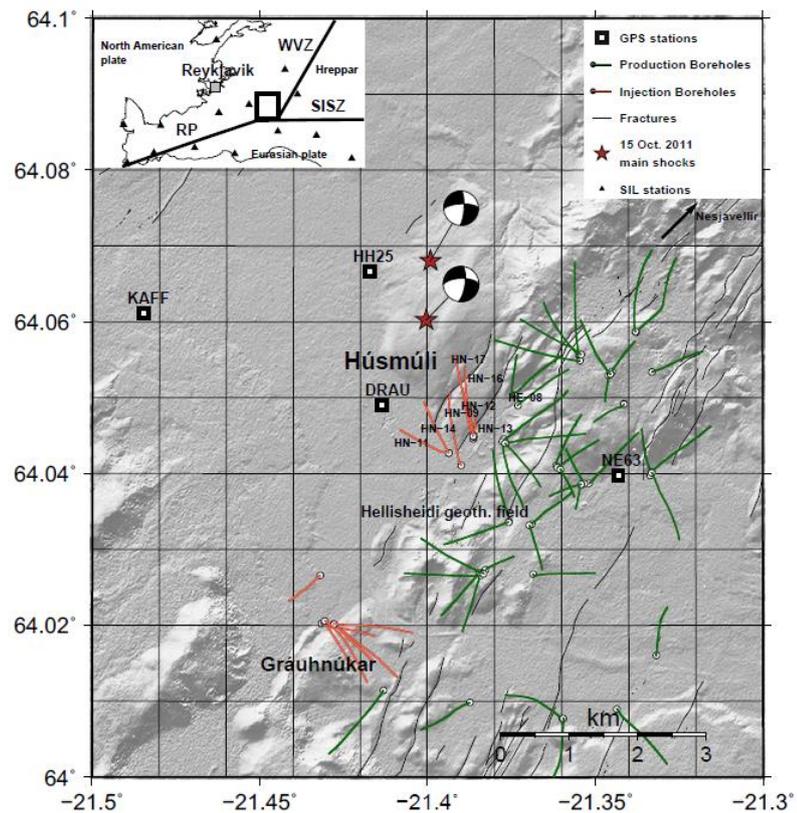
Figure A-39   Hellisheiði geothermal field and associated Húsmúli reinjection zone. Black lines present mapped surface fractures, green lines show trajectories of production boreholes, red lines show trajectories of injection boreholes and red stars show the location of the two M 4.0 mainshocks. Stations of the national seismic monitoring network are shown as black triangles in the inset at the top (From Juncu et al., 2018, Copyright Elsevier, published under a Creative Commons license).

Operations and monitoring: The production of geothermal energy at the Hellisheiði Field started in 2006. Production rates at the Hellisheiði field increased from 7 Mton/year in 2006 to 30 Mton/year in 2011. In order to maintain pressures in the reservoir and counteract surface subsidence, reinjection of waste water was started at the Grauhnúkar site in 2007, followed by injection at the Húsmúli site in September 2011 (Juncu et al., 2018). Injection started at the Húsmúli injection site on September 1st 2011, and injection rates of 550 l/s were reached within several days. Injection initially took place in four boreholes (HN-09, HN-12, HN-14 and HN-17) and injection into a fifth borehole (HN-16) started on September 23rd 2011. Injection overpressures mounted to a maximum of 2.8 MPa. The total volume injected between September 2011 and May 2012 is estimated at 13 x 10^6 m^3. Injection continued after May 2012, and injection rates were kept approximately constant over the period 2012 – 2015, with rates between 300 and 450 l/s (Juncu et al., 2018).

Seismic activity in Iceland is continuously monitored by a national seismic network, in operation since 1991. Twelve seismic stations were located within a distance of 50 km, of which 5 stations are positioned within a distance of 5 km of the injection sites

Occurrence of seismicity: A number of seismic swarms have been observed at the Húsmúli injection site, both during the testing and drilling of the boreholes (with magnitudes up to M 2), and during the injection activities. After the start of injection

an increase of micro-seismic activity was observed from September 10th 2011 (Figure A-40) around the wells HN-12, HN-14 and HN-17 (Figure A-39; Figure A-40), and migrating northward. It highlighted a 2 km large NNE-SSW striking fault structure. From September 17th 2011, a second N-S oriented fault structure was highlighted. Two mainshocks were recorded on October 15th 2011, with maximum reported magnitudes M_L 4.0, which were felt in a nearby village ~ 12 km from the injection site (Agustsson et al., 2015; Gunnarsson, 2013; Juncu et al., 2018). For three months seismicity continued and focused within this area, whereas mid-January 2012, seismic activity shifted to a third structure located 1 km westward, which remained seismically active until May 2012. After May 2012 period recurrent intervals of increased seismic activity were reported in Húsmúli. Focal mechanisms of seismic events mainly indicate strike-slip faulting, with a minor dip-slip component on N-S oriented, steeply eastward dipping faults. The depth of seismicity is located mostly between 1.5 and 4.5 km (Juncu et al., 2018).

The injection at Grauhnúkar with an average injection rate of 170 kg/s caused only very little micro-seismicity (Juncu et al., 2018).
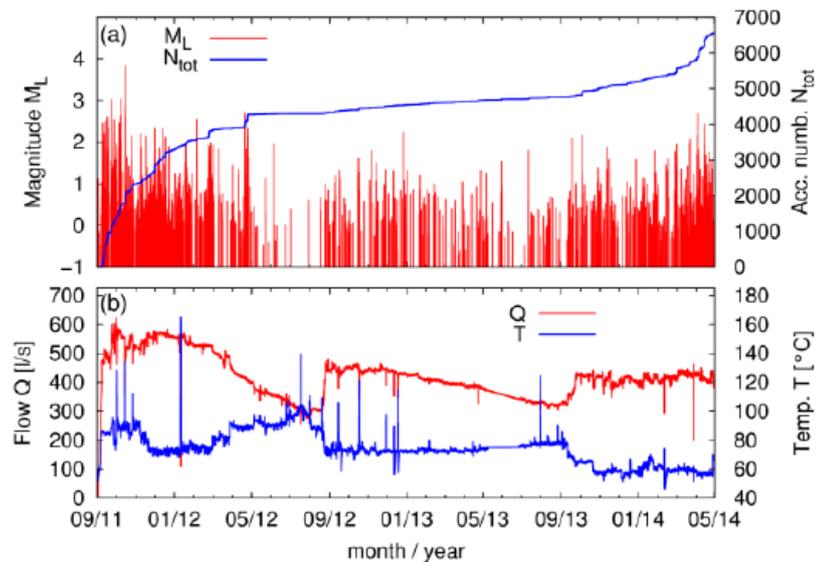

Figure A-40   Relation between injection activities and induced seismicity at the Húsmúli injection site. a) Magnitudes of earthquakes (red) and cumulative number of seismic events (blue) versus time. b) Total flow into the injection wells in the Húsmúli area (red); temperature of the injection water (blue) (From Gunnarsson et al., 2015, Proceedings World Geothermal Congress, Melbourne).

Interpretation: The authors state that re-injection and the associated pressure increase triggered earthquakes and released stresses that were already built up in the area. As the Húsmúli site is on the edge of the Hellisheiði geothermal field, production and associated subsidence may have caused additional stress changes on the faults in the Húsmúli area (Gunnarsson, 2015).

A.9　Habanero, Cooper Basin, Australia (M 3.7)

Activity:	Geothermal EGS	
Start date – End date:	07 – 11 – 2003 10 – 09 – 2005 14 – 11 - 2012	23 – 12 – 2003 H-1 20 – 09 – 2005 H-1 30 – 11 – 2012 H-4
Fluid + Fluid balance:	Water	Injection
Activity depth:	4.4 km	
Activity rocktype:	Granite	
In-situ T	200 °C	
Cumulative ΔV:	20,000 m^3 , 22,500 m^3 , 34,000 m^3	
Maximum Top Hole Pressure:	70 MPa, 62 MPa, 50 MPa	
Maximum flowrate:	40 l/s, 31 l/s, 60 l/s	
Monitoring system:	Yes	
Maximum magnitude + Date:	3.7	5 - 12 - 2003
	3.0	12 – 9 – 2005
	3.0	
Distance M_{max} – activity:	?	
Intensity [EMS]:	?	
Damage:	N/A	
Interpretation	Induced by pore pressure increase	

Tectonic setting and geology: The Habanero geothermal field (EGS) is located in the Cooper Basin, in the northeast of South Australia (Baisch, S. et al., 2006). The regional stress regime is compressive, with the maximum horizontal stress of ~150 MPa oriented east-west, i.e. a high gradient ($\Delta S_{Hmax}/\Delta Z$) of the maximum principal stress (ΔS_{Hmax}) with depth (Z) of ~34 MPa/km (Holl & Barton, 2015). Natural seismic activity in the region is low. The pilot project targeted the granitic basement, which is encountered below 3.6 km of sediments. Overpressured fractures were observed in the wells, with overpressures up to 35 MPa at 4.4 km depth.

Activity design: The Habanero -1 injection well was drilled in 2002 to a depth of 4.4 km, with an open hole section from 4.1 to 4.4 km (Baisch, S. et al., 2006; Baisch, S. et al., 2009). The in-situ temperature at 4.4 km depth was 250°C. A second production well Habanero-2 was drilled in 2004 at 500 m from Habanero-1. Later the system was expanded with Habanero-3 and Habanero-4 (2012), at a distance of 560 and 705 m from Habanero-1 (Figure A-41).
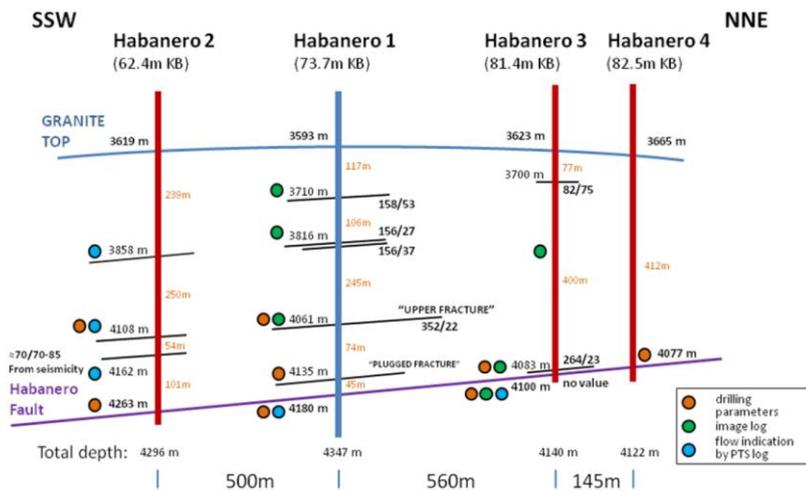
Figure A-41 The Habanero field structure (From Holl & Barton, 2015, Proceedings World Geothermal Congress, Melbourne).

Operations and monitoring: Habanero-1 was stimulated twice, in 2003 and 2005, with 20,000 m^3 and 22,500 m^3 water injected (Baisch, S. et al., 2006; Baisch, S. et al., 2009). Wellhead pressures were 70 MPa and 62 MPa, and maximum flowrates were 40 l/s and 60 l/s, respectively. Habanero-4 was stimulated in 2012, with the injection of 34,000 m^3, with a maximum wellhead pressure of 50 MPa and maximum flowrates of 60 l/s (Baisch, Stefan et al., 2015). Microseismic monitoring was performed with shallow (<370 m) and one deep borehole sensor (1800 m).

Occurrence of seismicity: During the Habanero-1 stimulation over 1,500 events occurred daily with a maximum reported magnitude of M$_L$ 3.7 (Baisch, S. et al., 2006). During the re-stimulation in 2005 16,000 events were detected with a maximum of M$_L$ 3.0 (Baisch, S. et al., 2009). The maximum reported magnitude during the Habanero-4 stimulation was 3.0 (Baisch, Stefan et al., 2015). The events highlighted a sub-horizontal plane, extending >1500 m from the well. Most focal mechanisms were consistent with this structure and indicated thrust faulting on a shallow plane.
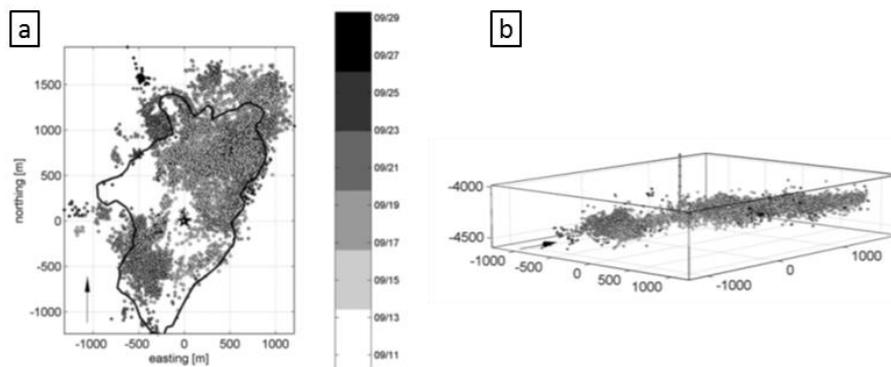

Figure A-42 Microseismicity recorded during the stimulation of Habanero-1 in 2005. Colors indicate the event date (From Baisch et al., 2009, Copyright Seismological Society of America, reproduced with permission).

<u>Interpretation</u>: The high pressures induced slip along a large, pervasively fractured, pre-existing fault zone. This fault was recognized in all four Habanero wells (Figure A-41).

A.10 Tuscan-Latium geothermal area: Larderello, Italy (M 3.2)

Activity:	Geothermal field, powerplant	
Start date – End date:	1 – 1 – 1926	to date
Fluid + Fluid balance:	Water	production (<1974) circulation (>1974)
Activity depth:	<3.5 km	
Activity rocktype:	Carbonates, metamorphic rock	
In-situ T	150 – 350 °C	
Cumulative ΔV:	10^9 m^3 (production), balanced (circulation)	
Maximum Top Hole Pressure:		
Maximum flowrate:	830 l/s (field-wide)	
Monitoring system:	Since 1976	
Maximum magnitude + Date:	3.2	1978
Distance M_{max} – activity:	?	
Intensity [EMS]:	?	
Damage:	none reported	
Interpretation	Interaction of natural seismicity and induced seismicity in and around the geothermal field	

Tectonic setting and geology: The Larderello geothermal field is located south of Florence in the inner Appenines, near the Travale and Lago geothermal fields. Post-collisional extension started in the Early Miocene causing crustal thinning and magmatism, resulting in a high heat flow (Brogi et al., 2003). Steam is mostly produced from the shallower Triassic evaporites and Jurassic carbonates (TN1, TN2 in Figure A-43), and also from deeper, fractured metamorphic rocks between 2 and 4 km deep (MRU 2, 1) (Batini, Fausto et al., 2003). The geothermal reservoir is covered by an impermeable cover, and pressures are subhydrostatic, with only 2 MPa at 1 km depth. Temperatures in the shallow formations range from 150 – 260 °C, and up to 350 °C in the deeper metamorphic rocks. The region is characterized by an extensional stress and NW-SE trending normal faults dipping to the NE (Figure A-43). Recent seismic activity is moderate (M 4.1 in 1970), but in 1724 a large event occurred in the region with intensity up to VII-VIII (Batini, F. et al., 1985).
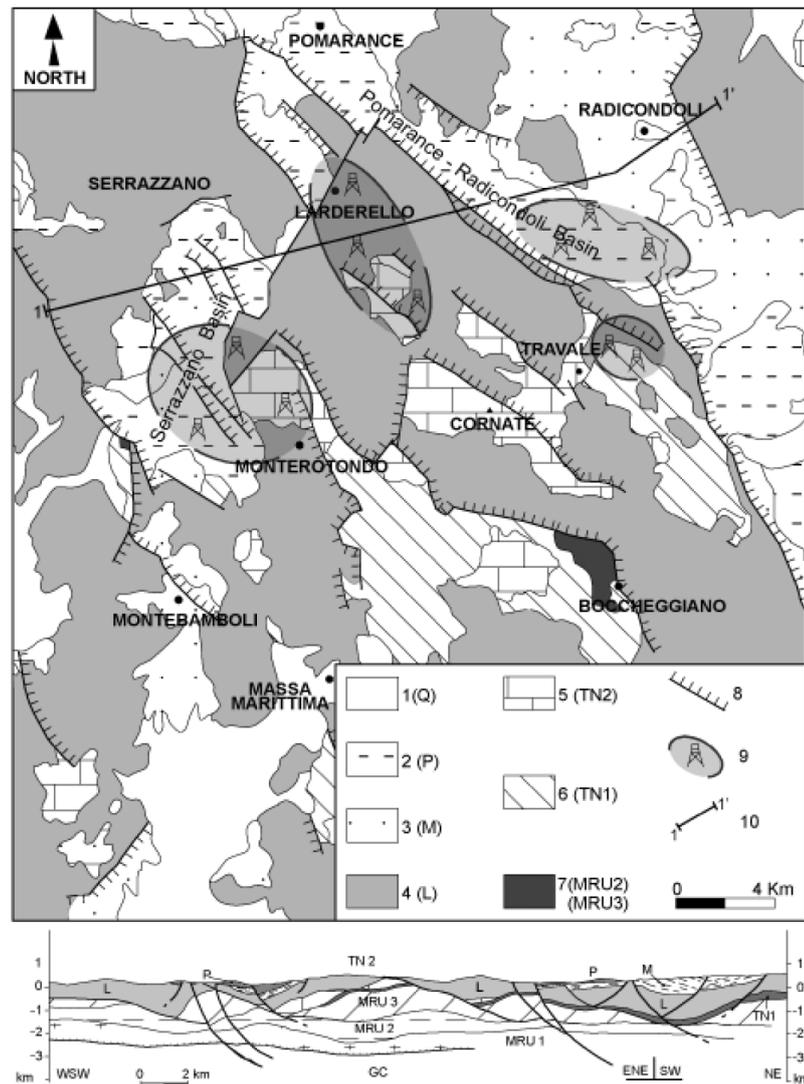
Figure A-43 Geological map of the Larderello-Travale geothermal area. 1) Quaternary sediments, 2) Pliocene marine sediments, 3) Miocene continental and marine sediments, 4) Jurassic – Eocene Ligurian sediments of oceanic crust and sediments, 5) Tuscan Nappe Late Triassic – Miocene carbonates, 6) Tuscan Nappe Triassic evaporites, 7) Paleozoic and Triassic metamorphic rocks, GC) Geniss complex. (From Batini et al., 2003, reproduced with permission from the author).

Activity design: Larderello is the oldest steam-producing geothermal field, with the first commercial powerplant in 1926. The first well was drilled in 1926 and 426 production wells were drilled up to the 1970, to depth of 0.2 to 1 km targeting the shallow carbonate reservoir. Eight reinjection wells were drilled from 1979 to 1983. From the 1980s also wells were drilled to the deeper metamorphic rocks at depths up to 3.5 km.

Operations and monitoring: The operational history of the field is long and complex. The production rate of the entire field increased to a maximum of 830 kg/s in the 1960s (Cappetti & Stefani, 1994). As production declined and pressure dropped more wells were drilled, and reinjection started in the 1974. Reinjection occurred at the top of the reservoir in the Valle Secolo area at 80 l/s. Field-wide production stabilized at

700 – 800 kg/s (individual wells up to 6 kg/s). A microseismic monitoring network was built in 1976 – 1978 consisting of over 15 stations (Batini, F. et al., 1985).

Seismicity: After placing the seismic network, over 1000 events were recorded near Larderello and neighboring Travale field from 1978 – 1982, with magnitudes 0.0 to 3.2 (Batini, F. et al., 1985). Seismicity continued to occur but did not exceed M 3.2. Events occurred up to 8 km deep and showed normal faulting to strike-slip mechanisms. Seismicity clustered around certain active injection and production wells.

Interpretation: The area has natural seismicity, and induced seismicity in and around the geothermal field. Seismicity rates may have increased with injection but magnitudes did not (Batini, F. et al., 1985).

A.11 The Netherlands

The aquifers that are targeted for geothermal energy production are largely the same as those that have been explored for oil and gas exploration for many decades (Figure A-46). Their occurrence and thickness have been mapped for the entire Netherlands (on- and offshore) by TNO, resulting in the DGM-Deep model (Digital Geological Model) (Kombrink et al., 2012). This model stores for the main stratigraphic units the distribution, depth and thickness. The model can be viewed and downloaded as GIS-layers from the www.nlog.nl and www.dinoloket.nl websites. Detailed lithostratigraphic descriptions are available from the online stratigraphic nomenclature https://www.dinoloket.nl/nomenclature-deep. Descriptions of the main tectonic units can also be found in the www.dinoloket.nl site (Van Adrichem Boogaert & Kouwe, 1997). Figure A-47 shows an instructive SW-NE cross section. The West Netherlands Basin in the Southwest has until now been the most important target for geothermal exploration. Here, rocks of Jurassic and Cretaceous age offer the best geothermal potential. In the northeastern part, rocks of Permian (Rotliegend) age are targeted.

The main stratigraphic units were divided into aquifers for the development of the online geothermal potential assessment tool ThermoGIS (www.thermogis.nl) (Kramers et al., 2012). Also, the main properties porosity and permeability have been mapped for the onshore part of the Netherlands for ThermoGIS (Pluymaekers et al., 2012). An update of ThermoGIS was published in 2018. For this version, both the structural framework of DGM-Deep and the property maps were updated.

Brief descriptions of the aquifers that are most important for geothermal exploration are given below. The descriptions are mostly derived from (Van Adrichem Boogaert & Kouwe, 1997).
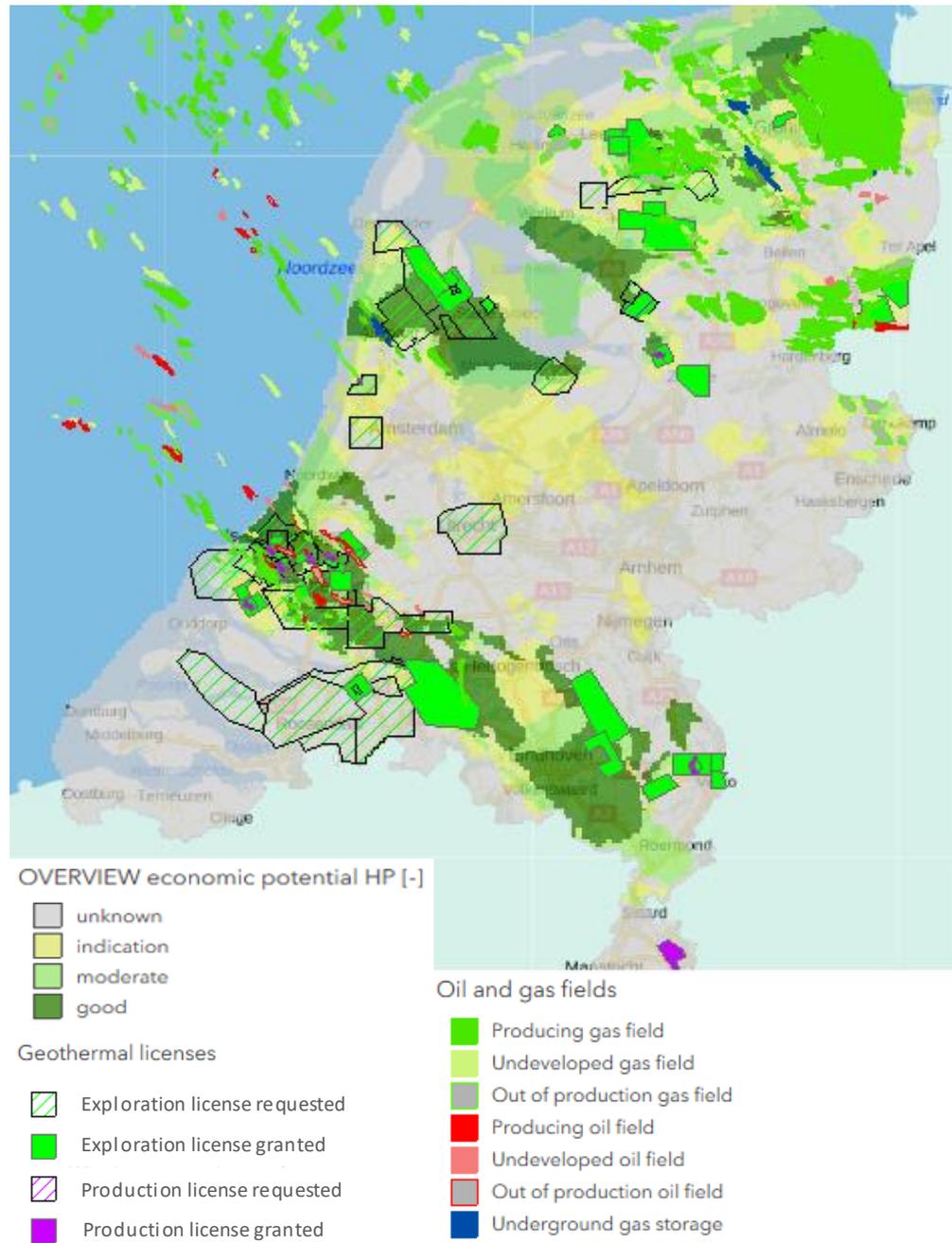
Figure A-44 Overview of geothermal potential, licenses and oil & gas fields in the Netherlands (Souirce: www.thermogis.nl; figure produced by TNO).
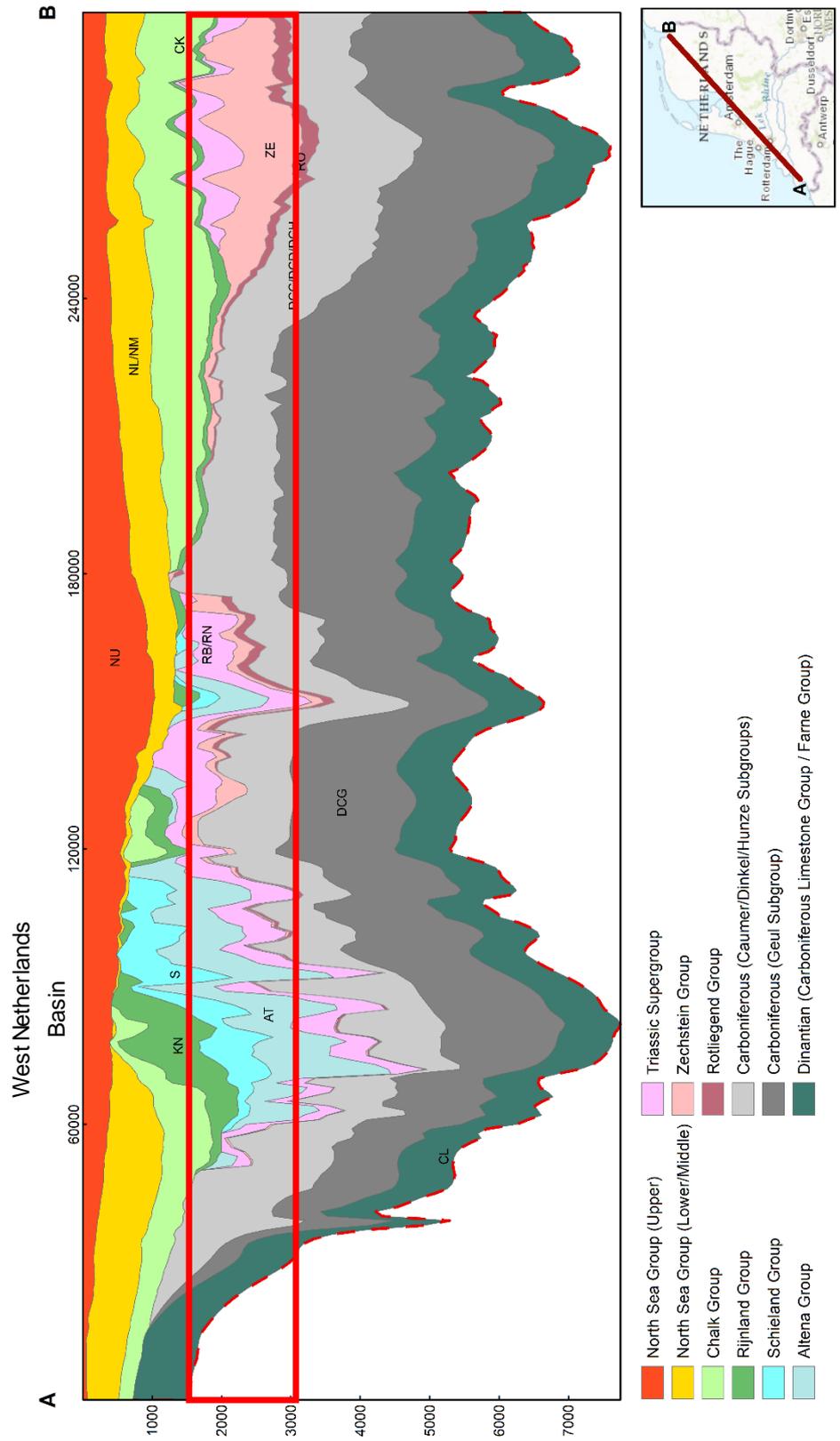
Figure A-45 General cross section through the Netherlands showing the main lithostratigraphical units. The red box indicates the depth interval of the current geothermal operations. From: DGM-Deep v4 (Source: www.nlog.nl; figure produced by TNO).

Carboniferous

Zeeland Formation

The lower part of the Carboniferous of the Netherlands consists of limestones that were deposited in shallow marine environment as carbonate platforms (northern part of the Netherlands), or as carbonate ramps (southern part) (Kombrink, 2008), (Reijmer et al., 2017). They are grouped in the Zeeland Formation. The rocks are well known in the south of the country, where they are found at relatively shallow depth (Figure A-48). In the northern part, their depth is around ~4 kilometres. Here, the rocks were drilled twice for oil and gas exploration purposes, but both wells were dry, and the rocks tight. In most parts of the country, however, the rocks are buried very deeply (>4 km), and were therefore not drilled and poorly visible on seismic. Hence, their nature is largely unknown. Possibly, the rocks are platform carbonates, similar to the northern occurrences, or ramp carbonates, similar to the south, but another possibility is that during the Early Carboniferous shallow to deep intra-platform basins existed where clay-rich deposits accumulated. The thickness of the rocks ranges between ~0 and about ~900 meters. The primary porosity is very low (a few percent), but locally the rocks were karstified during one or more subaerial exposure events leading to secondary porosity and permeability. Also, fracture permeability may occur. Because the permeability is still poorly understood and few wells drilled this formation, no porosity or permeability maps have yet been produced.
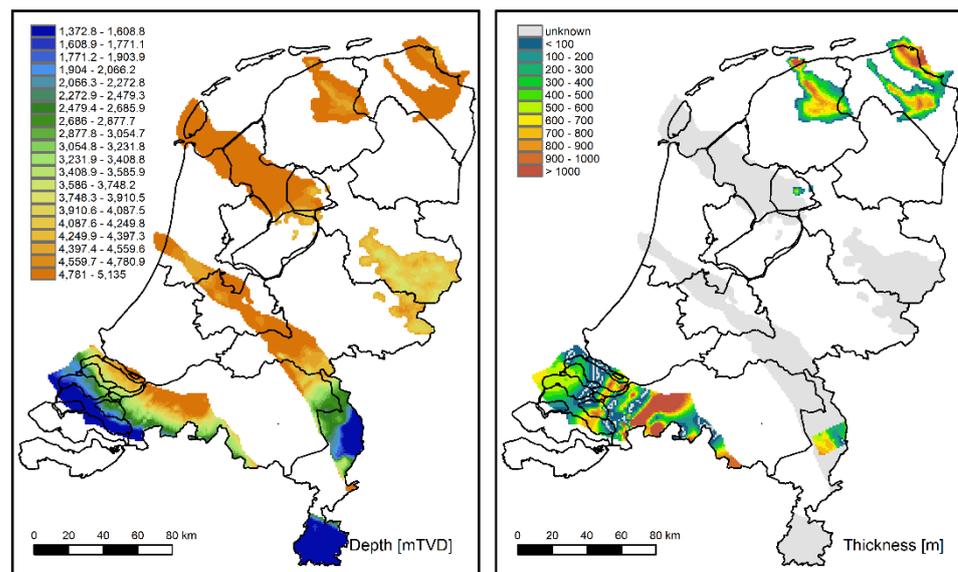

Figure A-46 Lower Carboniferous aquifer (Zeeland Formation). Only depth and thickness (partly) were mapped on a national scale (Source: www.thermogis.nl; figure produced by TNO).

The underlying rocks of Devonian age are poorly known. In the two doublets that were drilled in the southern part of the Netherlands, they are mostly quartzites that have very low primary porosity and permeability. The overlying rocks vary throughout the country, but most often the seal is constituted by Namurian shales.

Hunze and Dinkel Groups

The Upper Carboniferous of the Netherlands is for the largest part characterized by shales, but in the eastern part of the country and in the West Netherlands Basin also

sandstones occur. The sandstones were formed as sheet flood and fluvial channel sandstones. The expected permeabilities are low, with the exception of the eastern part of the Netherlands, coinciding with a shallow depth and therefore relatively low temperature (Figure A-49). In the largest part of the West Netherlands Basin, the rocks are buried too deep for conventional geothermal application (i.e., based on natural permeability without the necessity of stimulation). The sand bodies are difficult to map on seismic. The aquifers contained in these Groups are currently not considered as favourable geothermal targets, and no active exploration is ongoing. The aquifer is underlain by Namurian shales, and overlain by sandstones of the Rotliegendes.
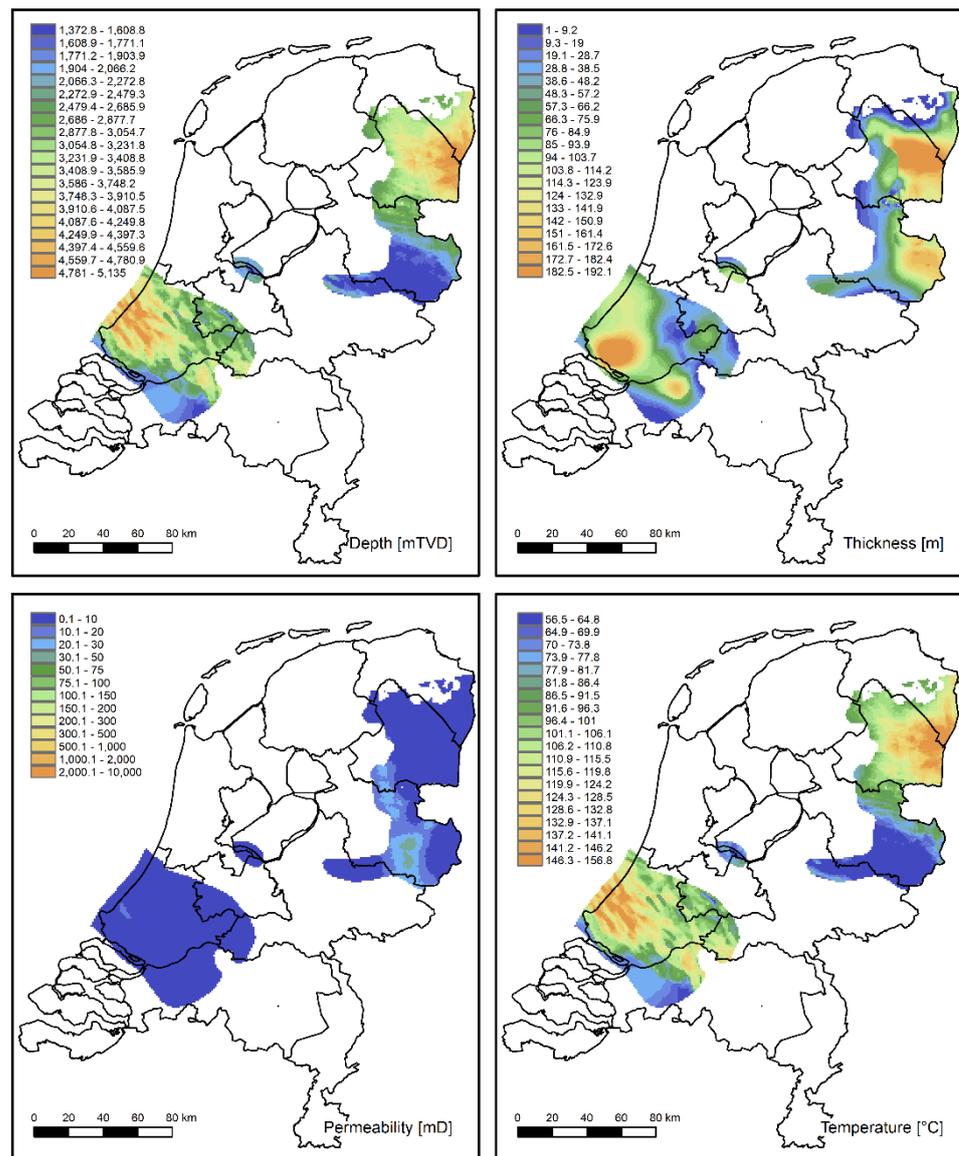

Figure A-47   Upper Carboniferous aquifers (Hunze and Dinkel Groups) (Source: www.thermogis.nl; figure produced by TNO).

Permian

The sandstones that were deposited in the Southern Permian Basin during the Early Permian in the Netherlands are grouped in the Slochteren Formation. The rocks occur in the largest part of the country, with the exception of the southernmost part and various locations that were elevated areas during the Permian, such as the Texel-IJsselmeer High (Figure A-50). The majority of Dutch gas fields, including the Groningen field, produce from rocks of the Slochteren Formation. The sandstones were deposited in an arid, desert-/playa-lake complex environment. The dominant facies are aeolian and fluvial. During deposition, the Silverpit lake, which existed north of the Netherlands, occasionally expanded southward, causing the deposition of interfingering shales. In the northern provinces (Groningen and Drenthe) the shales can be several tens of meters thick, causing the definition of the Lower and Upper Slochteren Members, separated by the Ameland Member.
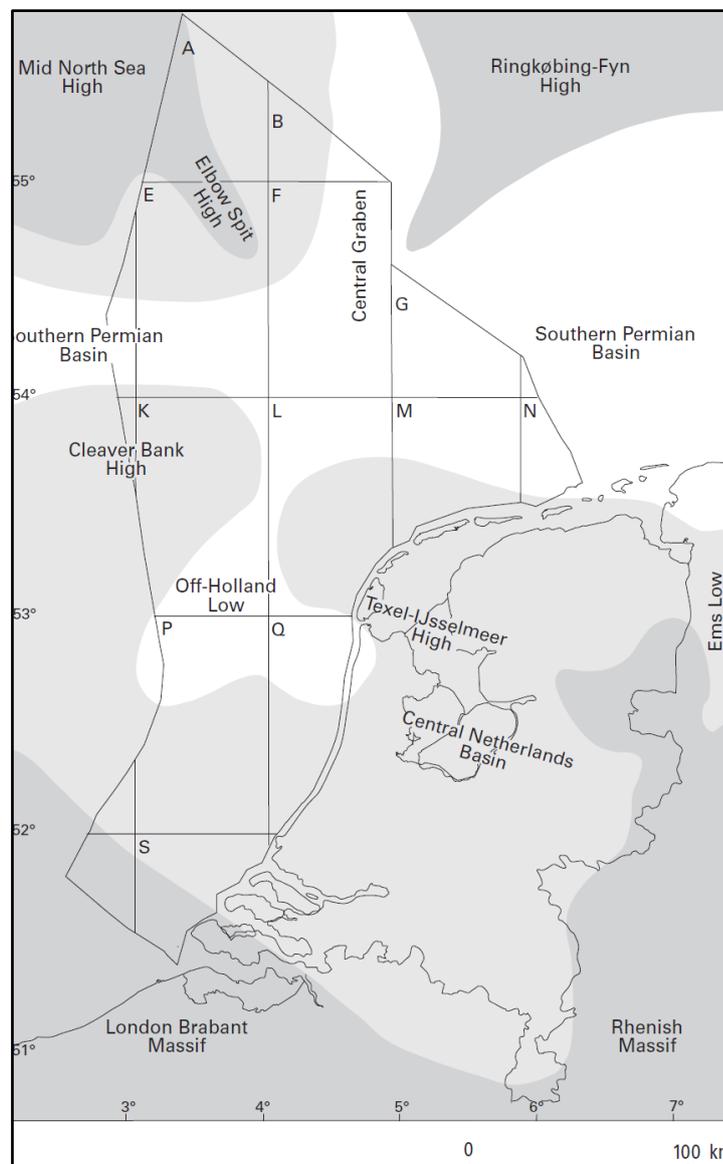

Figure A-48 Early Permian structural elements (Source Van Adrichem Boogaert & Kouwe, 1993-1997, Stratigraphic Nomenclature of the Netherlands, TNO).

The thickness of the sandstones ranges from several meters of absent in the South, to 300 meters locally in the North (Figure A-51).
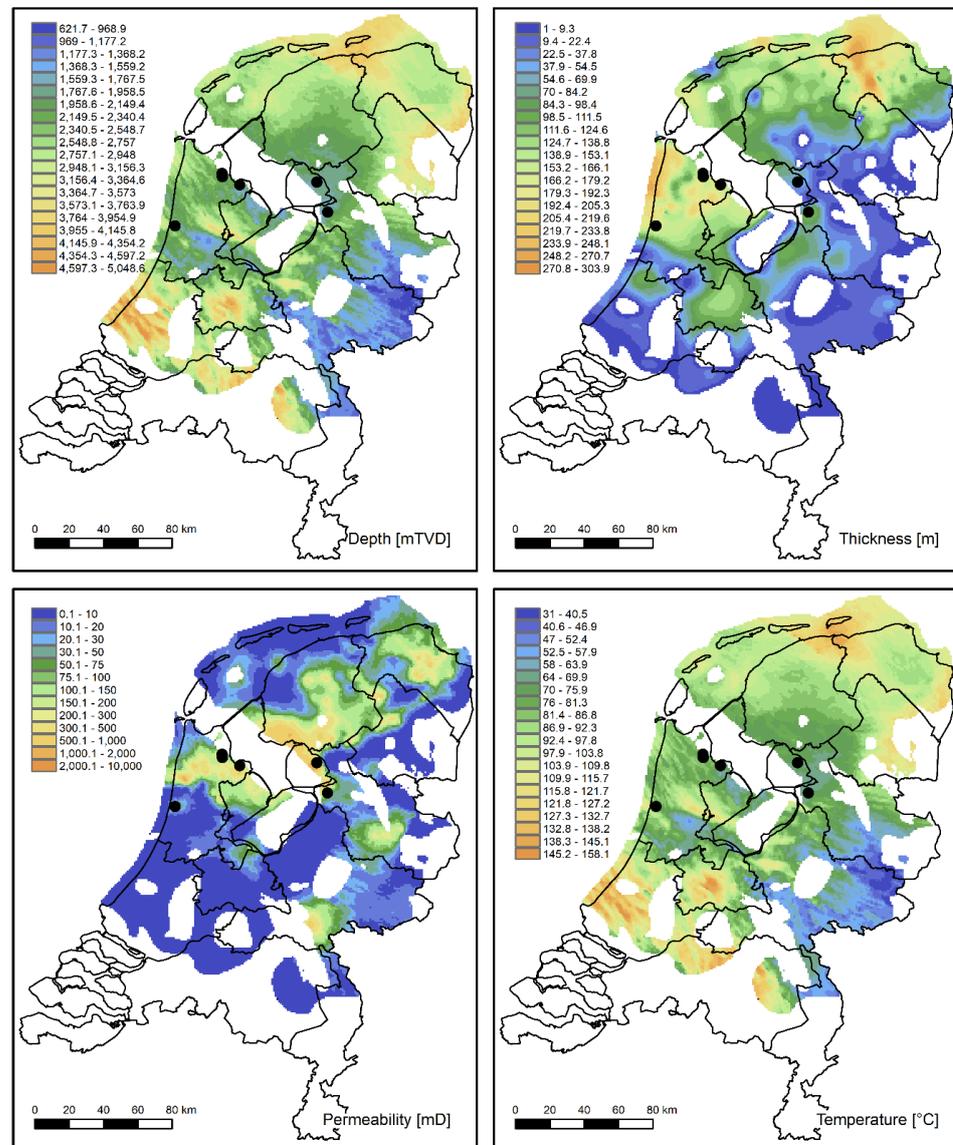

Figure A-49   Permian geothermal aquifers (Slochteren Formation). Black dots indicate geothermal wells (Source: www.thermogis.nl; figure produced by TNO).

The aquifer characteristics are usually favourable for geothermal applications, between several tens of mD to more than a Darcy. In the southern part, however, the permeability is low due to deep burial and inversion.

The Slochteren Formation unconformably overlies rocks of Carboniferous age that may be either shales or sandstones (Base Permian Unconformity). The rocks are overlain by Permian Zechstein evaporites, claystones and carbonates that thin towards the south – south of approximately the city of Amsterdam the thickness of the Zechstein is very small or zero, and the Rotliegend may be covered by the Triassic Main Claystone.

Triassic

Most of the sandstones that were deposited during the Triassic belong to the Main Buntsandstein Group (part of the Lower Germanic Trias). The relevant units are (from old to young) the Nederweert Sandstone, Volpriehausen, Detfurth and Hardegsen Formations. The overlying Röt Fringe and Solling Sandstones belong to the Upper Germanic Trias. The sandstones were deposited in aeolian and fluvial depositional environments, when rifting started to occur in the Southern Permian Basin. The different units represent different tectonic phases. All units are well known throughout the Netherlands and Germany, with the exception of the Nederweert Sandstone which occurs only in the southeastern part of the Netherlands.
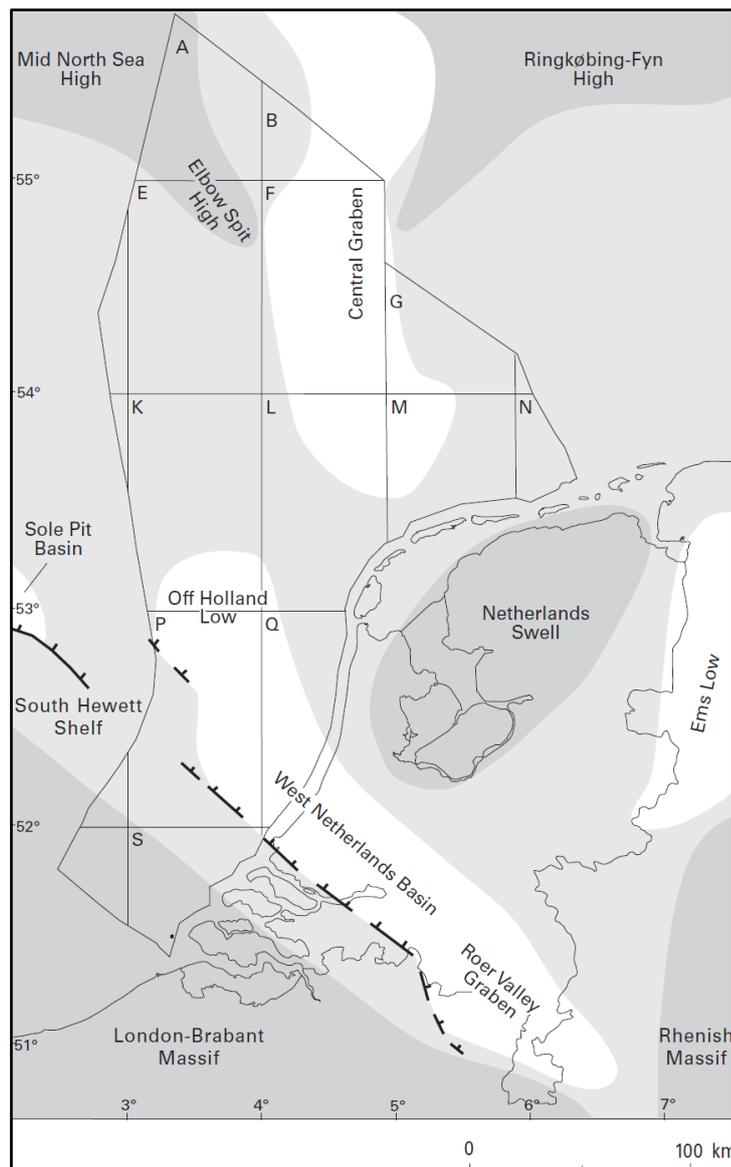

Figure A-50 Triassic to Liassic structural elements, source Source Van Adrichem Boogaert & Kouwe, 1993-1997, Stratigraphic Nomenclature of the Netherlands, TNO).

The clastic input that is the origin of the sandstones has its origin in the south and southeast. This is also where the thickest deposits are found (Roer Valley Graben (RVG), West Netherlands Basin and the German Lower Saxony Basin, Figure A-53),

from several hundreds of meters in the WNB to over 500 meters in the Roer Valley Graben. The thickness in the North, where the Netherlands Swell existed during deposition, is between 0 and ~100 meters.
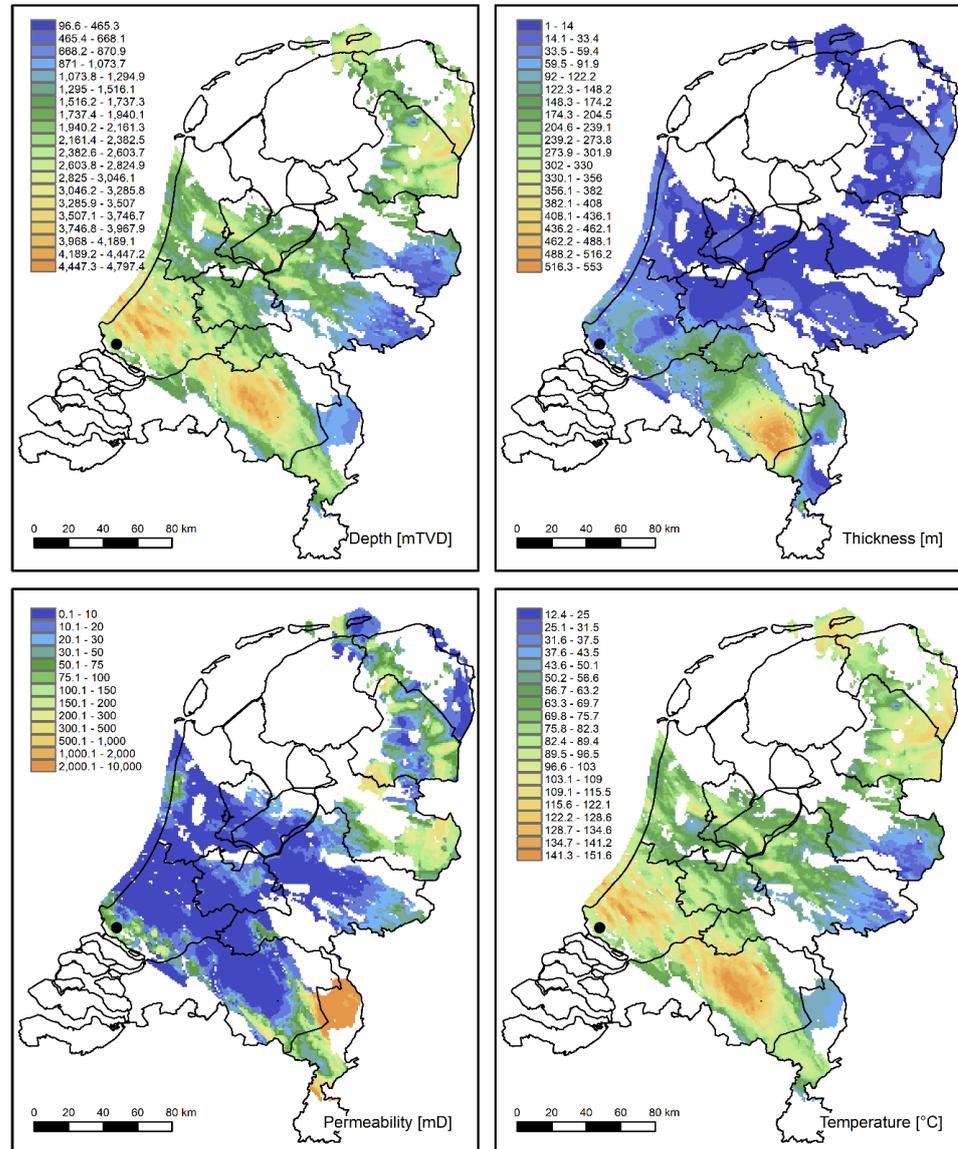

Figure A-51 Triassic geothermal aquifers. Black dot indicates geothermal well (Source: www.thermogis.nl; figure produced by TNO).

The aquifer properties vary widely: where the thickest deposits occur, deep burial followed by inversion has decreased the permeability in the central parts of the WNB and RVG, but along their southern border, where burial and inversion were less severe, the aquifer properties may still be favourable for geothermal exploration. Few data exist on the aquifer properties of the thick Nederweert Sandstone in the Southeast. Given the shallow burial, this may be an interesting target for geothermal exploration. Favourable aquifer properties also exist in the North and Northeast, but here the current depth is relatively shallow and therefore the temperature is low.

The sandstones conformably overlay the lower Triassic Main Claystone. They are overlain by evaporites, claystones and carbonates of the Upper Germanic Trias Group.

Jurassic / Cretaceous

The most important target for geothermal exploration from Jurassic and Cretaceous age are the Nieuwerkerk Formation (Upper Jurassic / Lower Cretaceous) and the Rijnland Group (Cretaceous) (Figure A-54).
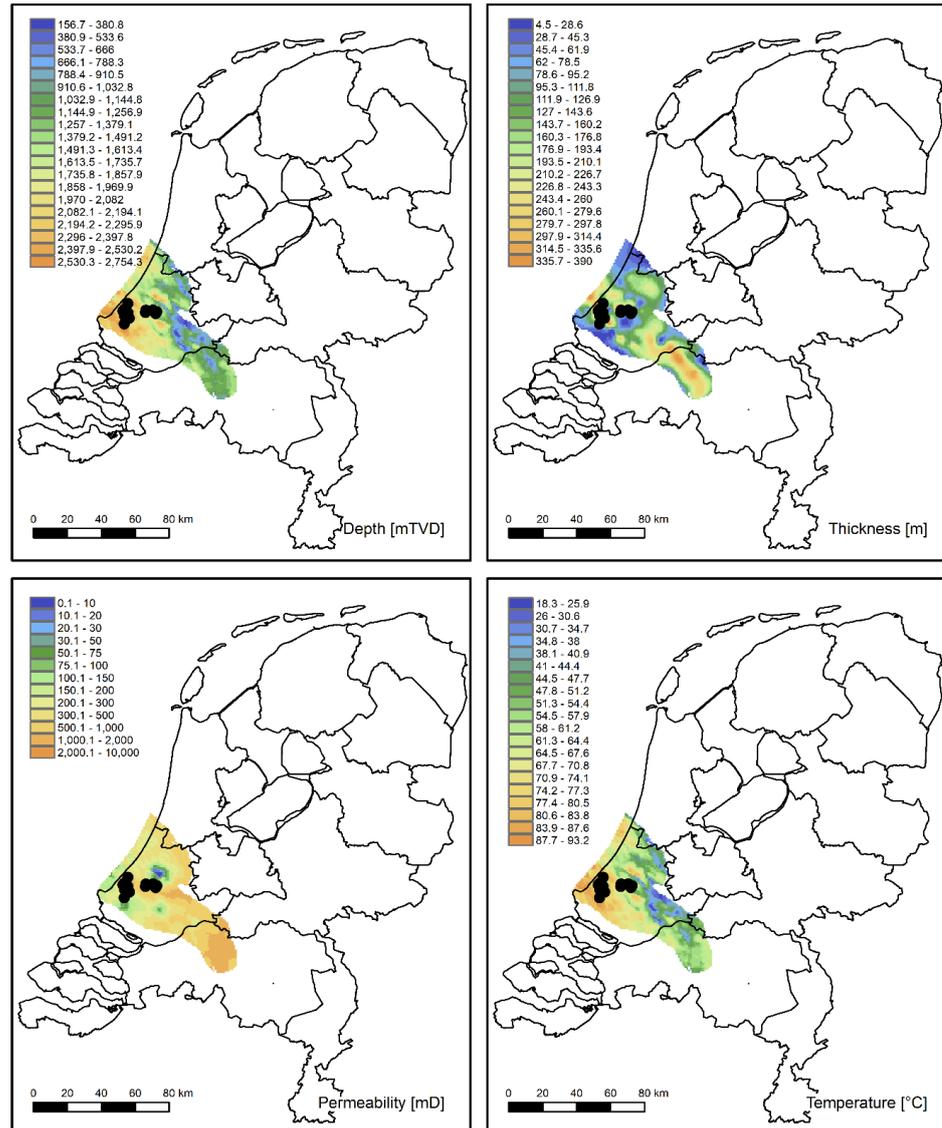

Figure A-52 Upper Jurassic / Lower Cretaceous geothermal aquifers (Nieuwerkerk Formation). Black dots indicate geothermal wells (Source: www.thermogis.nl; figure produced by TNO).

Highs

Platforms

Cretaceous or Paleogene on top on top of Zechstein
Cretaceous or Paleogene on top of Triassic

Basins

Strongly inverted
Mildly or not inverted

Boundary of structural element

Abbreviations

DH	Dalfsen High
ESH	Elbow Spit High
LBM	London-Brabant Massif
LH	Limburg High
TIJH	Texel-IJsselmeer High
WH	Winterton High
ZH	Zeeland High

ADB	Anglo-Dutch Basin
AP	Ameland Platform
COP	Central Offshore Platform
CP	Cleaverbank Platform
ESP	Elbow Spit Platform
FP	Friesland Platform
GP	Groningen Platform
IP	Indefatigable Platform
LT	Lauwerszee Through
MNSH	Mid North Sea High
NHP	Noord Holland Platform
OP	Oosterhout Platform
PMC	Peel-Maasbommel Complex
RFH	Ringkøbing Fyn High
SGP	Schill Grund Platform
IJP	IJmuiden Platform

|	
BFB	Broad Fourteens Basin
DCG	Dutch Central Graben
CNB	Central Netherlands Basin
LSB	Lower Saxony Basin
ORB	Outer Rough Basin
RVG	Roer Valley Graben
SG	Step Graben
TEG	Tail End Graben
TB	Terschelling Basin
VB	Vlieland Basin
WNB	West Netherlands Basin

Figure A-53 Late Jurassic to Early Cretaceous structural elements (Source: Van Adrichem Boogaert & Kouwe, 1993-1997, Stratigraphic Nomenclature of the Netherlands, TNO).

Nieuwerkerk Formation

Rocks belonging to the Nieuwerkerk Formation have until now been the most popular geothermal exploration target. This is due to the combination of abundant demand in the Westland area, defined by the greenhouses present, and the favourable aquifer properties of the rocks of the Nieuwerkerk Formation.

The presence of the Nieuwerkerk Formation is limited to the West Netherlands Basin. The Formation consists of (from old to young) the Alblasserdam Member, the Delft Sandstone Member and the Rodenrijs Claystone Member. The latter serves as seal. The Delft Sandstone Member is the most prominent target, together with the Alblasserdam Member, which has a lower N/G than the Delft Sandstone Member. The boundary between Delft and Alblasserdam cannot be mapped seismically. In wells, the uppermost part of the Alblasserdam is usually completed together with the Delft if it is sandy. The first (major) claystone is then considered to be the lower boundary of the aquifer. The rocks formed as braided river and meandering channel fill deposits in a subsiding basin that consisted of separate tectonic blocks that had varying subsidence and uplift rates.

The thickness varies between 0 on the margins of the WNB to over 300 meters in the central parts of the Basin. The permeability ranges from about ~50 to ~2000 mD. The rocks are often found to be loosely consolidated only, therefore sand production can be a problem if sand screens are not installed.

The Nieuwerkerk Formation unconformably overlies the marine claystones and sandy carbonates of the Altena Group. The Formation is overlain by the Rijnland Group, some interfingering occurs. The underlying unit may also be of Triassic age along the southern margin of the West Netherlands Basin.

Rijnland Group
Deposition of the sediments of the Rijnland Group mainly took place in the West Netherlands Basin, where subsidence, that started with the deposition of the Nieuwerkerk Formation, continued. Also in the Northern part of the Netherlands deposition took place. The depositional environment varies between coastal and shallow to deep (open) marine, and was in part controlled by differential subsidence and uplift of the various tectonic block in the WNB. The Rijnland Group is divided in a (lower) Vlieland Sandstone and an (upper) Vlieland Claystone Formation, followed by the Holland Formation. The largest geothermal potential is found in the Vlieland Sandstone Formation, that in itself consists of various sandstone and claystone rich members.

The thickness of the sandstones of the Rijnland Group is largest in the West Netherlands Basin, where it may be as thick as 300 meters. In the North, the thickness is usually limited to a few tens of meters only, with the exception of the (offshore) Vlieland Basin where the thickness is up to ~100 meters (Figure A-56).

The depth of the rocks of this unit is usually between ~1500 and ~2500 meters, which ensures high permeability, around 50-2000 mD. This makes it an attractive target for geothermal exploration. The rocks may be unconsolidated.

The rocks of the Rijnland Group are overlying those belonging to the Schieland Group (WNB) or Niedersachsen Group (Northern part). The Vlieland Sandstone is overlain by the Vlieland Claystone Formation. The Holland Formation is overlain by the marly limestones of the Chalk Group.
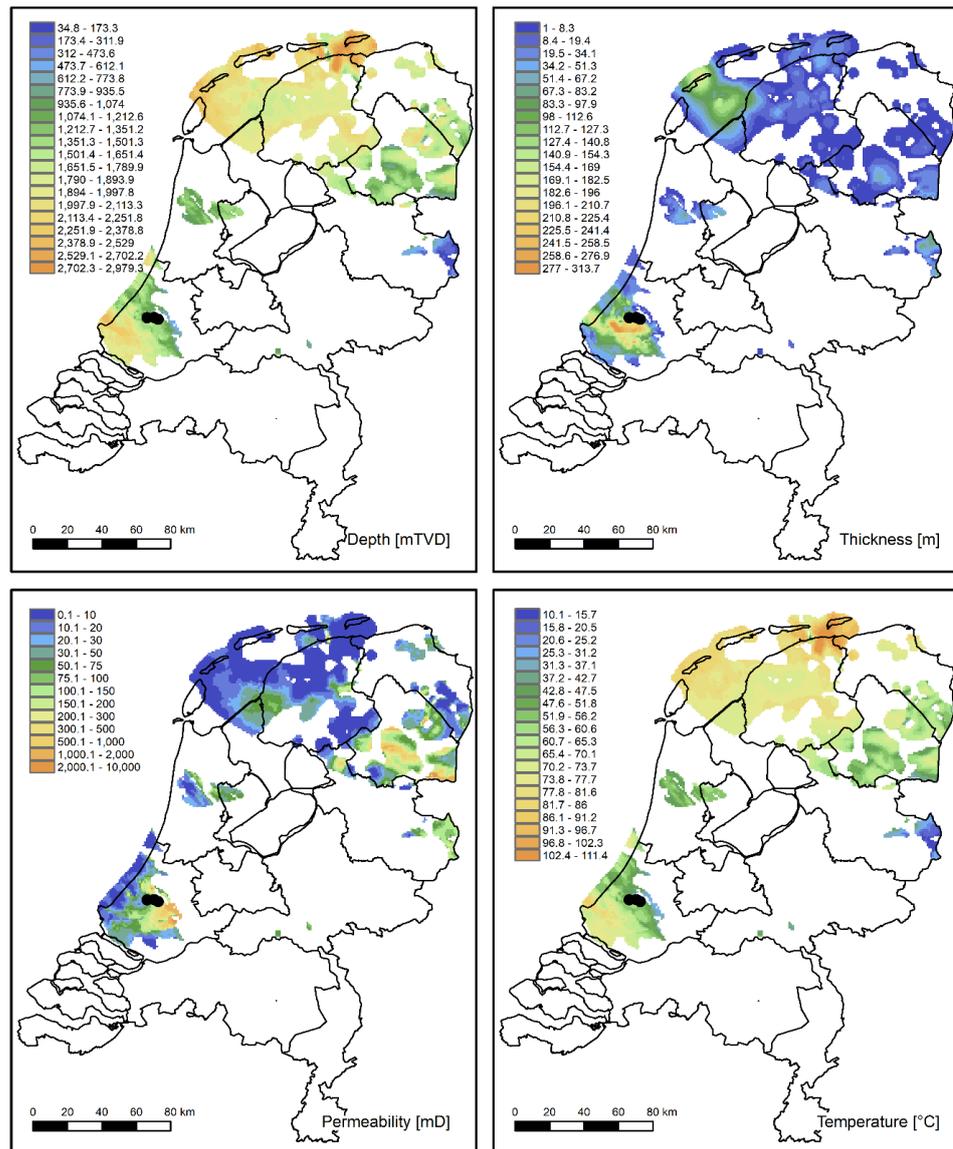
Figure A-54 Cretaceous geothermal aquifers (Rijnland Group). Black dots indicate geothermal wells (Source: www.thermogis.nl; figure produced by TNO).

Cenozoic

Rocks of Cenozoic age (Paleogene, Neogene[10] and Quaternary occur nearly everywhere in the Netherlands at depths ranging from zero to about 1300 meters, with larger depths up to 1800 meters locally in the Roer Valley Graben (Figure A-57). The thickness is mostly up to about 100 meters, locally in the Roer Valley Graben and West Netherlands Basin up to 200-300 meters. The rocks constitute loosely consolidated sandstone, siltstone and claystone of predominantly marine origin. The boundary with the underlying limestones of the Chalk Group (and locally older rocks) is an unconformity. The rocks are usually unconformably overlain by the sandstones, siltstones and claystones of the Breda Formation.

---

[10]The well know Tertiairy was replaced officially in 2004 by the Paleogene and Neogene

Due to the relatively shallow depth, the temperature of the reservoirs is also relatively low. Therefore the reservoirs have not attracted much attention for geothermal exploration.
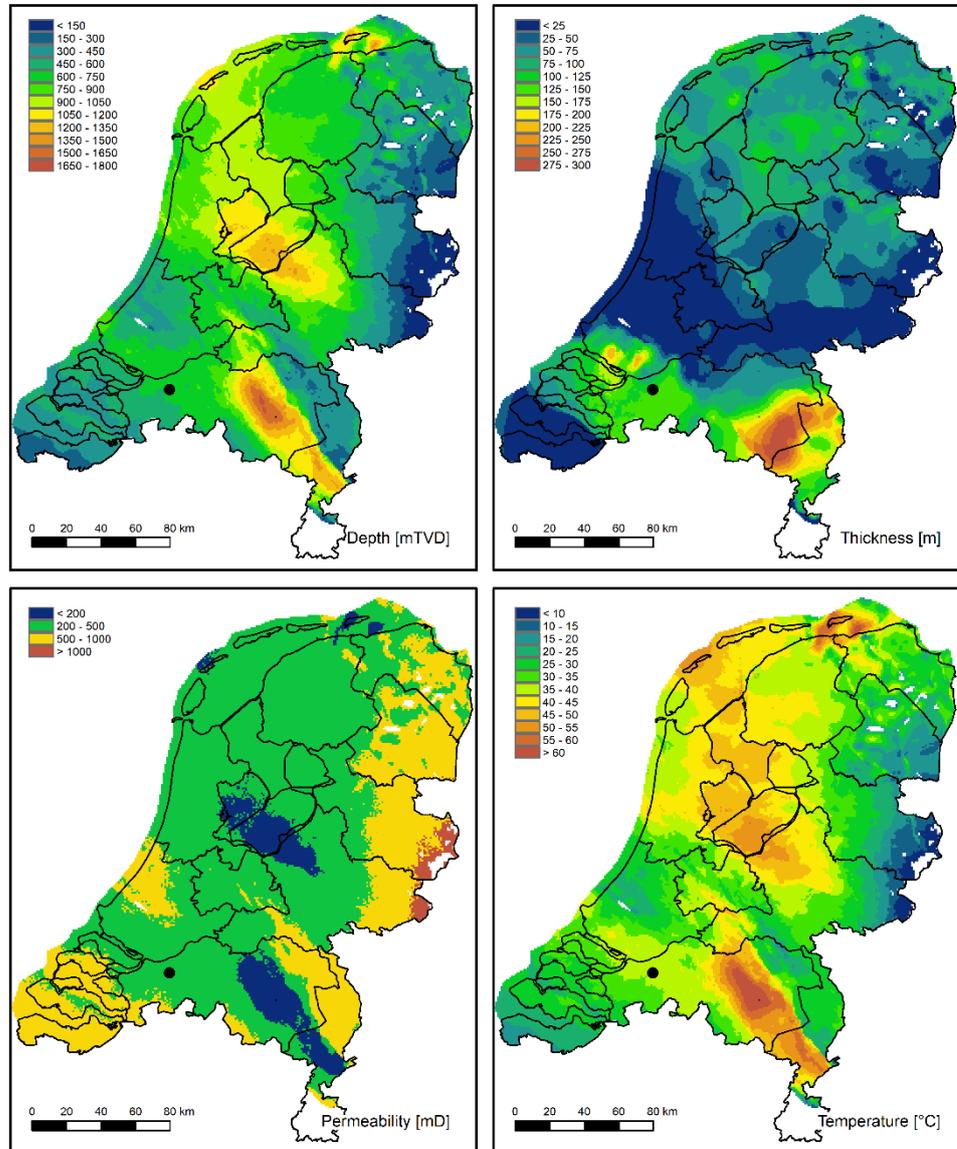

Figure A-55 Cenozoic geothermal aquifers (Middel and Lower Northsea Group). Black dot indicates geothermal well (Source: www.thermogis.nl; figure produced by TNO).

A.11.1   Koekoekspolder, The Netherlands

Country & place (lat, lon):	The Netherlands, Koekoekspolder (52.58095582, 5.9504193)	
Activity:	Geothermal production	
Start date – End date:	10 – 09- 2011	In operation
Fluid + Fluid balance:	Water	Circulation
Activity depth:	1.9 km	
Activity rocktype:	Sandstone	
In-situ T	76 °C	
ΔT in-situ – fluid:	45 °C	
Cumulative ΔV:	5.1 Mm^3	
Maximum Top Hole Pressure:	unknown	
Maximum flowrate:	43 l/s	
Monitoring system:	no	
Maximum magnitude:	n/a	
Distance M_{max} – activity:	n/a	
Intensity [EMS]:	n/a	
Damage:	n/a	
Interpretation		

Tectonic setting and geology: The Koekoekspolder geothermal doublet is located in the central part of the Netherlands. It produces from sandstones belonging to the Slochteren Formation that were deposited during the Late Permian in the Southern Permian Basin (Figure A-58) (Henares et al., 2014). This large scale basin was bounded by the London-Brabant Massif and the Rhenisch Massif in the south and southeast, and the Ringkobing-Finn High in the North (Geluk, 2005). The rocks are unconformably overlying Late Carboniferous rocks comprising mainly shales and coal that were drilled in the nearby Kampen-01 well (Figure A-58). They are overlain by rocks of the Permian Zechstein comprising mainly anhydrite and dolomite. The location is adjacent to the Texel IJsselmeer High, a fault bound, northwest-southeast local structural high that already existed during the Permian ((Gaupp & Okkerman, 2011), (Geluk, 2005)), which had a gently NNE dipping flank (Mijnlieff & Geluk, 2011). Therefore immediately west of the operation the thickness of the reservoir decreases to about zero. The reservoir itself, which is partly covered by 3D and partly by 2D seismic, is about horizontal and does not contain faults that are visible on seismic (Veldkamp et al., 2015).

At the Koekoekspolder site, the sandstones, that were deposited in an aeolian facies ((Henares et al., 2014), Mid-Netherlands Sand Sea' (Gaupp & Okkerman, 2011)), contain abundant detrital anhydrite which significantly lowered the reservoir porosity and permeability.

The area is tectonically inactive, no earthquakes have been recorded.
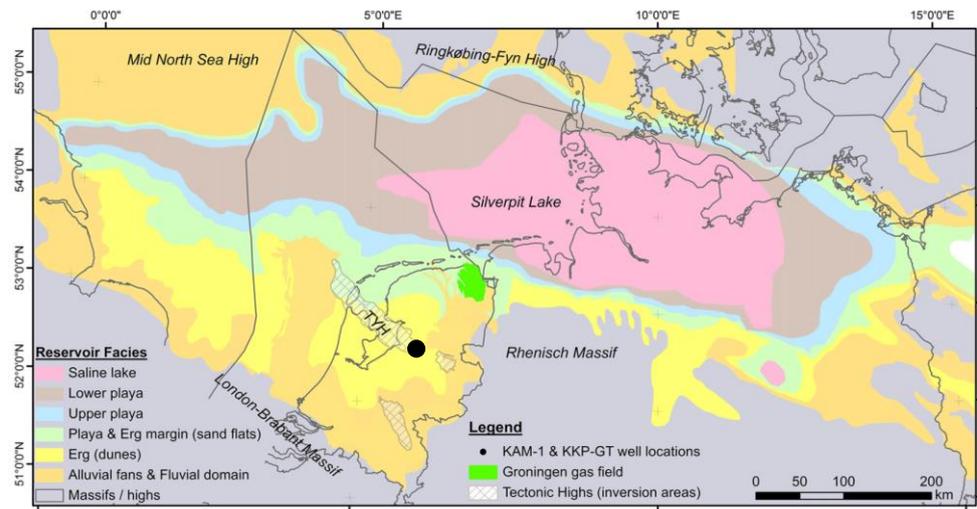
Figure A-56　Paleogeography of the Southern Permian Basin during the Upper Rotliegend. Black dot indicates the Koekoekspolder location. TYH: Texel IJsselmeer High (From Henares et al., 2014, Copyright Elsevier, reproduced with permission).
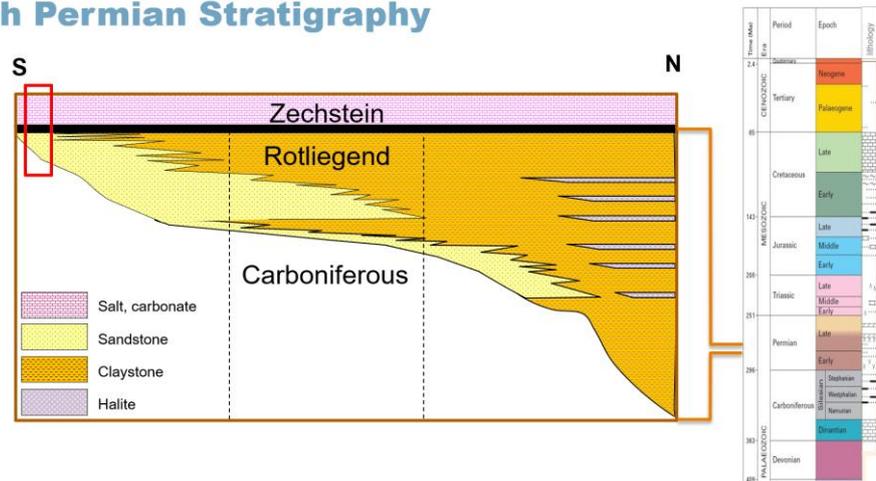

Figure A-57　Schematic stratigraphy of the Koekoekspolder area. The doublet is located in the red rectangle (figure produced by TNO.

A.11.2   Vierpolders, The Netherlands

Country & place (lat, lon):	The Netherlands, Vierpolders (51.87253053, 4.16042624)	
Activity:	Geothermal production	
Start date – End date:	01 – 01 – 2016	In operation
Fluid + Fluid balance:	Water	Circulation
Activity depth:	2.1 km	
Activity rocktype:	Sandstone	
In-situ T	85 °C	
ΔT in-situ – fluid:	61 °C	
Cumulative ΔV:	3.2 Mm^3	
Maximum Top Hole Pressure:	unknown	
Maximum flowrate:	83 l/s	
Monitoring system:	no	
Maximum magnitude:	n/a	
Distance M_{max} – activity:	n/a	
Intensity [EMS]:	n/a	
Damage:	n/a	
Interpretation		

Tectonic setting and geology: The Vierpolders geothermal doublet is located in the southwestern part of the Netherlands. It produces from sandstones belonging to the Volpriehausen, Detfurth and Hardegsen Formations (Main Buntsandstein Group) and Basal Solling Sandstone that were deposited during the Triassic. Tectonically, the location is situated on the southwestern border of the West Netherlands Basin (Figure A-58). The tectonic history of the basin is complex, and was controlled by the progressive fragmentation of the Southern Permian Basin (Geluk, 2005). The deposition of the sediments of the Main Buntsandstein Group comprises four tectonic pulses. Deposition of the sediments of the Group was controlled by extensional tectonics, hence the Volpriehausen, Detfurth and Hardegsen Formations are tectono-stratigraphic units. In the Late Cretaceous and Tertiary, the West Netherlands Basin was inverted. Therefore locally deeply buried Triassic rocks were uplifted to shallow depth, maintaining their compaction-related low porosity. However, the determination of whether local tectonic blocks are presently at their maximum burial depth or were uplifted, is difficult.

The sandstones of the Main Buntsandstein Group were deposited in a fluvio-lacustrine facies (Geluk, 2005), and all three Formations consist of a first-order fining upward cycle of sandstone at the base, followed by siltstones and claystones. Due to erosional phases in between the deposition, parts of the successions may be absent. For instance, the maximum remaining thickness of the Hardegsen Formation in the West Netherlands basin is only 70 meters. In the southern part of the Netherlands, though, the entire succession is sandstone of fluvial origin (northwards they are dominantly aeolian) (Geluk, 2005). The Basal Solling Sandstone (separated from the underlying Hardegsen Formation by the Hardegsen Unconformity) consists of aeolian

sands (Geluk, 2005). At the project location, the net thickness is 188 meter at the production well (gross: 204 meter, N/G 0.9) (Mijnlieff, 2017). The area is tectonically inactive, no earthquakes have been recorded.
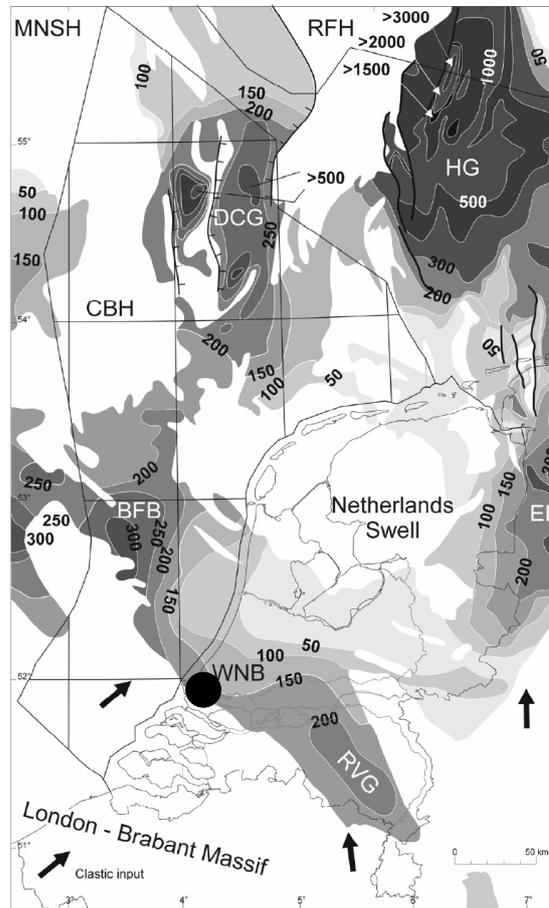

Figure A-58   Isopach map of the Main Buntsandstein Subgroup (in m) (From: Geluk, 2005, Stratigraphy and tectonics of Permo-Triassic basins in the Netherlands and surrounding areas, PhD Thesis, Utrecht University). Black dot indicates the Vierpolders doublet location.

A.11.3   Honselersdijk, The Netherlands

Country & place (lat, lon):	The Netherlands, Honselersdijk (52.01614293, 4.22663824)	
Activity:	Geothermal production	
Start date – End date:	13 – 03 - 2012	In operation
Fluid + Fluid balance:	Water	Circulation
Activity depth:	2.4 km	
Activity rocktype:	Sandstone	
In-situ T	88 °C	
ΔT in-situ – fluid:	56 °C	
Cumulative ΔV:	4.0 Mm^3	
Maximum Top Hole Pressure:	unknown	
Maximum flowrate:	32 l/s	
Monitoring system:	no	
Maximum magnitude:	n/a	
Distance M$_{max}$ – activity:	n/a	
Intensity [EMS]:	n/a	
Damage:	n/a	
Interpretation		

Tectonic setting and geology: The Honselersdijk geothermal doublet is located in the southwestern part of the Netherlands (Figure A-59). It produces from sandstone belonging to the Delft Sandstone Member of the Nieuwerkerk Formation, in the West Netherlands Basin (see the description of the Vierpolders doublet).
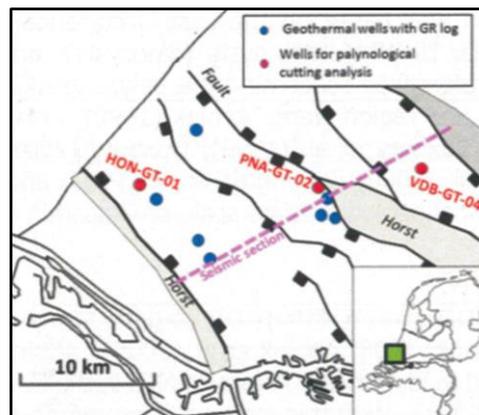

Figure A-59 Setting of the Honselersdijk doublet (HON-GT) (From Willems, 2017, Doublet deployment strategies for geothermal hot sedimentary aquifer exploitation. application to the Lower Cretaceous Nieuwerkerk formation in the West Netherlands Basin. PhD Thesis, TU Delft).
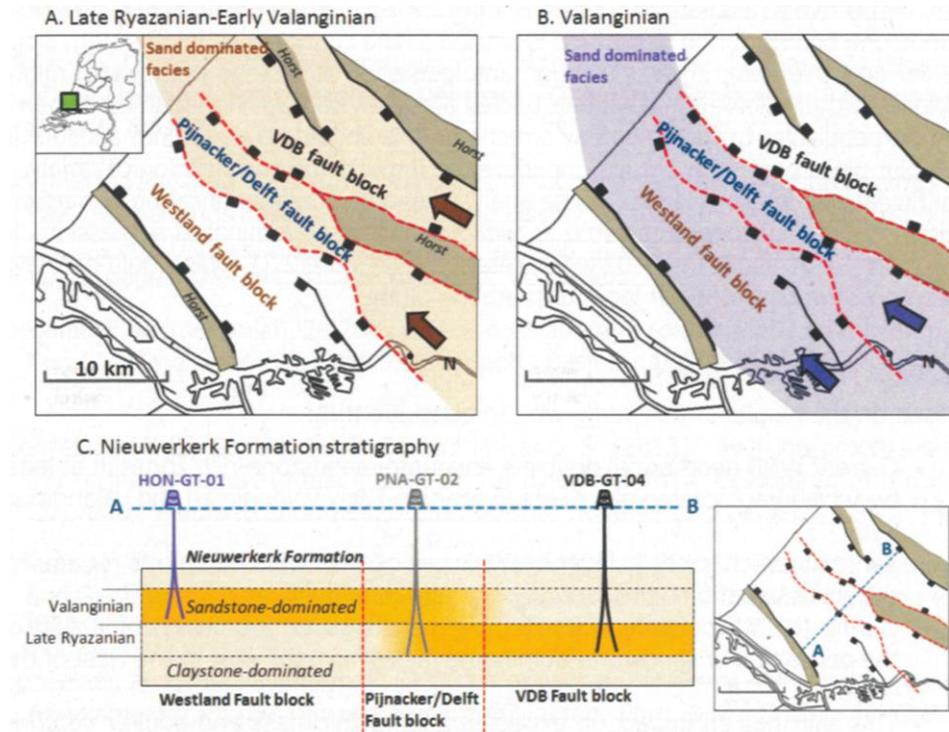
Figure A-60   Locations of sand-dominated sedimentation during the Early Cretaceous (From: Willems, 2017, (From Willems, 2017, Doublet deployment strategies for geothermal hot sedimentary aquifer exploitation. application to the Lower Cretaceous Nieuwerkerk Formation in the West Netherlands Basin. PhD Thesis, TU Delft).

During the Triassic, the West Netherlands Basin strongly deepened towards the North (Figure A-58, see the description of the Vierpolders installation). After the Triassic, the developed further in various tectonic blocks with different subsidence and uplift rates. Uplifted blocks were eroded, while sedimentation took place on subsiding blocks (Figure A-60). For the sediments belonging to Nieuwerkerk Formation this resulted in early (Ryazanian) sedimentation in the northern blocks (Pijnacker / Delft and Van den Bosch), and later (Valanginian) sedimentation on the Honselersdijk site (Westland block). The basin was inverted along older faults during the Late Cretaceous and Tertiary. Older normal faults were reactivated as strike-slip and oblique-slip faults.

The sandstones of the Delft Sandstone Member were deposited as braided-river valley fills and meandering single-channel fills and as crevasse-splays in a flood-plain to lower-coastal-plain setting (Ministry of Economic Affairs and Climate Policy, 2018). Sands occur in sheets, isolated or stacked channels. They are overlying the claystones and sandstones of the Alblasserdam Member of the Nieuwerkerk Formation (of which the sandstones are known to be productive too). They are overlain by the claystones of the Rodenrijs Claystone Member of the Nieuwerkerk Formation.

The area is tectonically inactive, no earthquakes have been recorded.

A.11.4   Californië, The Netherlands

Country & place (lat, lon):	The Netherlands, Californië Californië Wijnen Geothermie (CWG) (51.42218805, 6.09139302) Californië Lipzig Gielen (CLG) (51.43318034, 6.08359037)	
Activity:	Geothermal production	
Start date – End date:	20 – 01- 2013 (CWG) 01 – 07- 2017 (CLG)	Closed-in Temp. suspended
Fluid + Fluid balance:	Water	Circulation
Activity depth:	2.1 km (CWG) ~2.7 km (CLG)*	
Activity rocktype:	Limestone, quartzite	
In-situ T	82 °C (CWG) ~80°C (CLG)	
ΔT in-situ – fluid:	47 °C (CWG)	
Cumulative ΔV:	9.1 Mm^3	
Maximum Top Hole Pressure:		
Maximum flowrate:	107 l/s (CWG) 104 l/s (CLG)*	
Monitoring system:	Yes	
Maximum magnitude:	n/a**	
Distance M_{max} – activity:	n/a**	
Intensity [EMS]:	n/a**	
Damage:	n/a**	
Interpretation	Natural or induced seismicity, under investigation	

*Data from Platform Geothermie (www.geothermie.nl), official CLG data is not public yet (publication expected April 2021, www.nlog.nl). **During the course of this study, seismicity occurred in the vicinity of the Californië projects. The seismicity is not indicated in the table because potential relations between geothermal operations and the seismicity are under investigation (www.sodm.nl).

Tectonic setting and geology: The Californië Wijnen Geothermie (CWG) geothermal triplet and Californië Lipzig Gielen (CLG) doublet are located in the southeastern part of the Netherlands. They target fractured limestones of the Zeeland Formation which is of Early Carboniferous (Dinantian) age, and possibly hydraulically connected to underlying quartzites of Devonian age. The limestones of the Zeeland Formation were deposited in varying environments: marginal marine to shallow marine carbonates and mudflats, open marine shelf carbonate shoals with restricted lagoonal platform carbonates, and open marine carbonate slopes (Reijmer et al., 2017). The rocks have a very low primary porosity. In contrast to all other current Dutch doublets that target sandstone with large primary porosity, the geothermal systems rely on secondary porosity to obtain high flow rates. For the Zeeland Formation in this area, two sources of secondary porosity are known: karst- and fault-related porosity. Due to (repeated) subarial exposure events, karstification has sometimes led to high secondary porosity, like for example in case of the limestones

targeted for gas storage in Loenhout (Belgium). The area is located in the tectonically most active area of the country, directly adjacent to the Roer Valley Graben between the Tegelen and Viersen Fault zones (Figure A-61) (Houtgast & Van Balen, 2000). The Tegelen Fault separates the Peel Horst and Venlo Fault blocks, and had its main period of activity in the Early Quaternay (Bisschops et al., 1985).
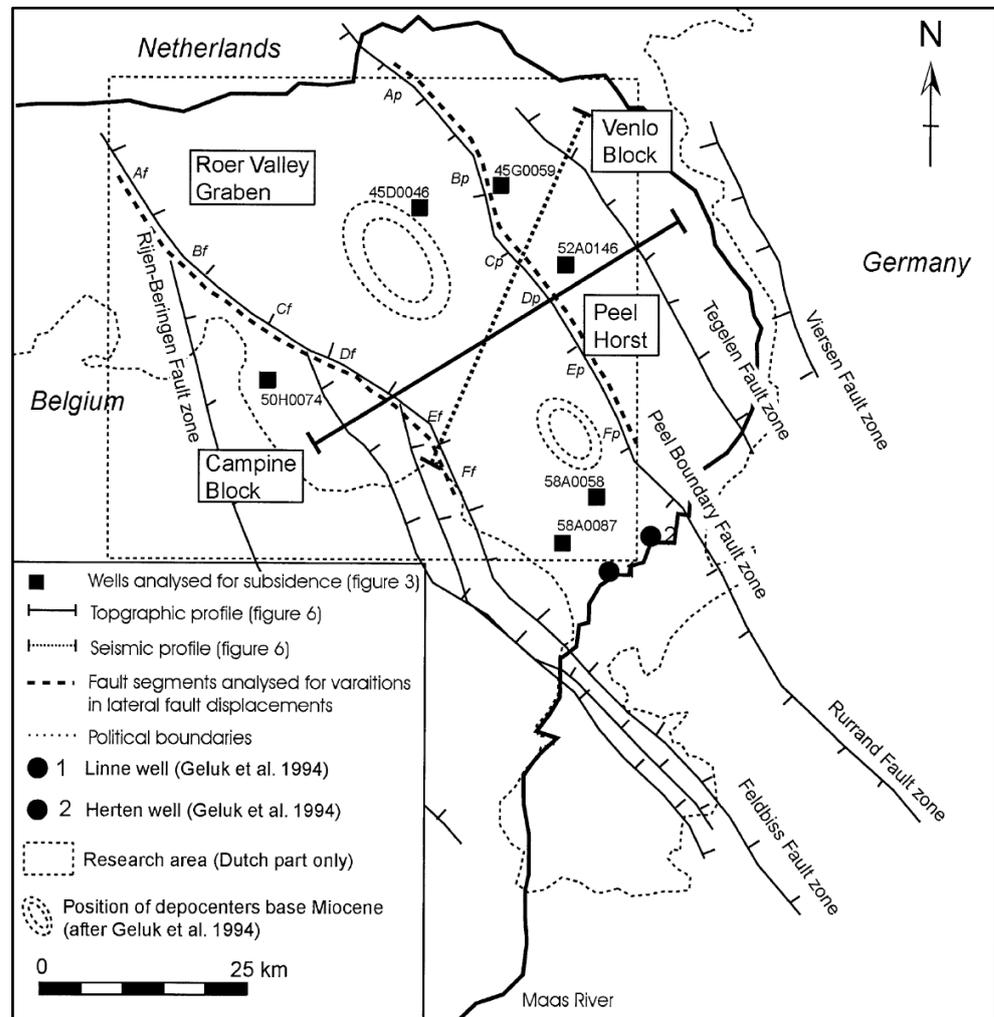

Figure A-61 The Roer Valley Rift System tectonic units (From Houtgast & Van Balen, 2000, Copyright Elsevier, reproduced with permission).

Activity design: The CWG triplet (CAL-GT-01 to CAL-GT-03) was originally designed to have two production wells, 1 and 3 drilling into the Tegelen Fault Zone, and a single injector 2, drilled away to the northeast from the Tegelen Fault Zone, and intended to inject into karst zones (Figure A-62, Figure A-63). However, the injector well became clogged quickly after start of injection operations. It was decided to inject instead in well 3, which had collapsed in the fault zone reservoir section. Injection therefore takes place in the younger strata of the Zeeland Formation. Pending a workover of well 2, the doublet has produced until May 2018 when the project was stopped and wells closed in after consultancy with the State Supervision of the Mines (SodM). The CLG doublet (CAL-GT-04 & CAL-GT-05) is situated ~1.5 km from the CWG triplet and also targets the Dinantian limestones of the Zeeland Formation.
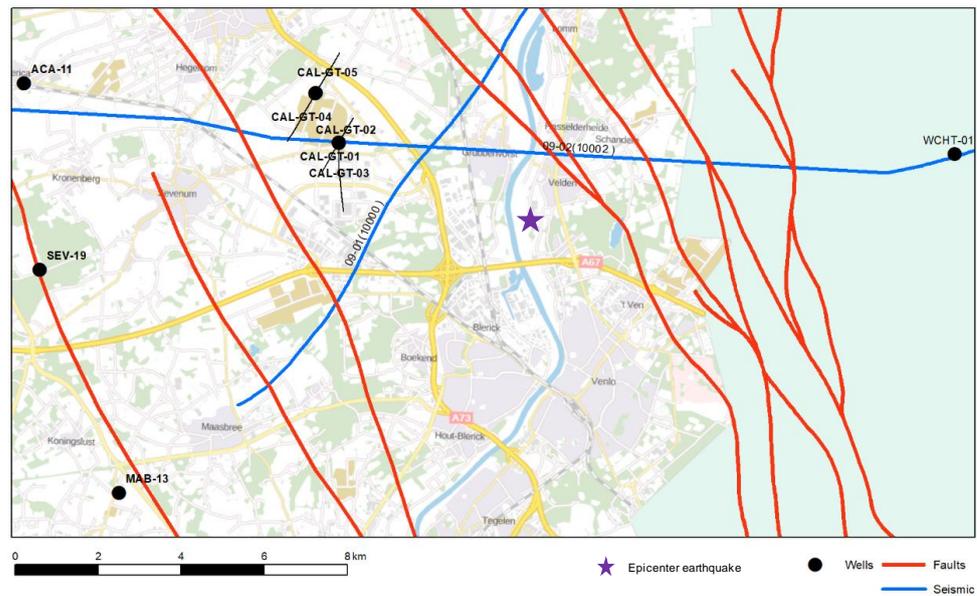
Figure A-62   Location of the Californië geothermal wells (CAL-GT-01 to CAL-GT-05) and approximate epicenter location of the M 2.0 seismic event that occurred on September 3rd 2018 (from KNMI). The Tegelen fault is located immediately southwest of the Californië geothermal wells (figure produced by TNO).
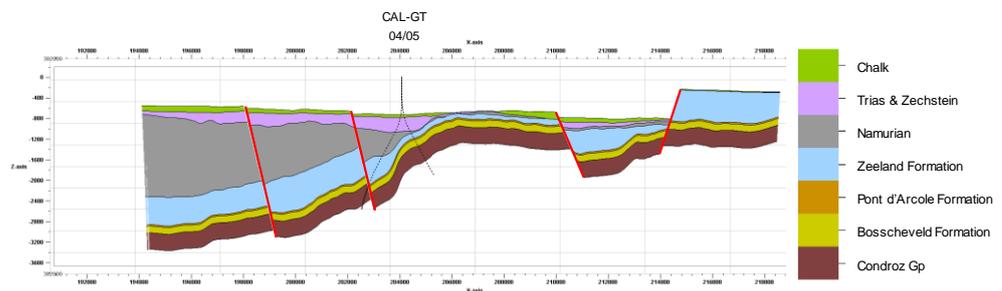

Figure A-63   West-East cross section along the (entire) seismic line 09-02 shown in Figure A-64 (figure produced by TNO).

Operations and monitoring: Operation of the CWG geothermal system started 20-01-2013, and was stopped in May 2018. A maximum flow rate of 107 l/s was reported. A maximum flow rate of 107 l/s and temperature of ~80°C was reported for the CLG geothermal system based on a production test on February 3rd, 2016 (www.geothermie.nl). A traffic light system for seismicity is operational. Operations are currently suspended following detection of seismicity in the area.

Occurrence (or lack of) of seismicity: Minor seismicity was detected near Grubbenvorst (Velden) at ~5 km distance from the Californië projects. A small event with peak ground velocity (PGV) of 0.03 mm/s occurred on August 25th 2018, followed by a M 2.0 event (PGV 1.7 mm/s) on September 3rd 2018. The area is known for the occurrence of natural seismicity (Figure 1-2, Figure A-64). Also of interest for the Dinantian fractured or karstified carbonate geothermal play in general is the seismicity that occurred in the vicinity of the Balmatt geothermal project near Mol in

Belgium (Figure A-65). Between December 28th 2018 and February 28th 2019 around 47 seismic event with M between 0 and 2.3 were recorded (local network of seismometers, maximum reported magnitude M_L 1.5 on January 18th 2019 as detected by the regional seismic network of the KSB). It is suggested that the seismicity is related to the injection of cold water (see www.vito.be for more details).

Mechanisms: Potential relations between geothermal operations and the seismicity are under investigation (see www.sodm.nl for latest information). It is currently not clear if relations with the geothermal projects exist or if the seismicity is natural. The analysis is hampered by poor vertical resolution of hypocenter depth due to limited accuracy of the regional velocity model.
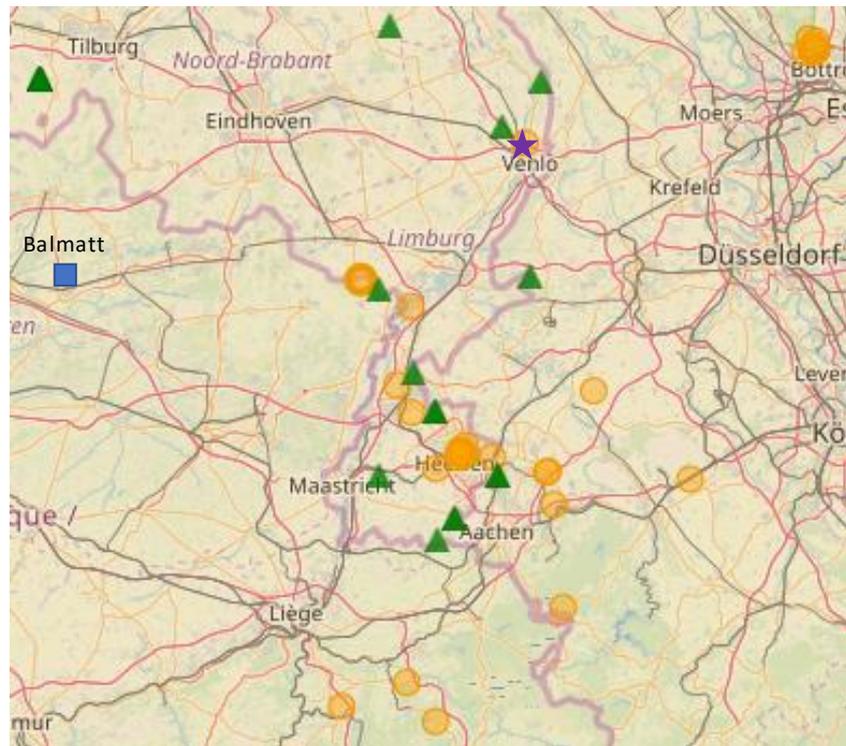

Figure A-64   Occurrence of seismicity in the southeast of the Netherlands over a yearly period (between 28 – 02 – 2018 and 28 – 02 – 2019) as recorded by the KNMI regional seismic network. Note that the seismic events with reported depth $\geq$ 5 km are natural events associated with tectonic processes in the Roer Valley Graben. Differences in depth be used as one of the indicators in the assessment of the (absence of) spatial relations between seismicity and anthropogenic operations (note that uncertainties in depth are not indicated, but may be km's). The M2.0 seismic event detected in the vicinity of the Californië geothermal projects is located close to the village of Velden (see Table below). The location of the Balmatt geothermal site near Mol in Belgium is indicated for reference. The seismicity near the Balmatt site is not reported in this dataset, but is reported by the local seismic network operated by VITO (Figure A-65). Source of map and seismic data: KNMI (http://rdsa.knmi.nl/dataportal/).

Figure A-64, continued.

| Origin Time	Mag.	Type	Latitude	Longitude	Depth	Location
2019-01-26T23:47:48	1.1	MLs	51.1410	5.8640	18.0	Stevensweert
2019-01-11T03:20:14	2.2	MLs	51.0050	6.3300	12.0	Linnich (Duitsland)
2019-01-07T19:11:34	1.2	MLs	50.5320	5.8550	12.0	Theux (België)
2019-01-06T20:08:47	1.2	MLs	50.9060	5.9910	9.0	Heerlen
2019-01-06T13:39:45	1.4	MLs	50.9100	5.9920	9.0	Heerlen
2018-12-31T01:51:18	1.3	MLs	50.8210	6.2290	9.0	Eschweiler (Duitsland)
2018-12-22T06:27:22	1.4	MLs	50.8750	6.2140	15.0	Alsdorf (Duitsland)
2018-12-17T04:34:46	1.0	MLs	50.9700	5.8670	15.0	Munstergeleen
2018-11-29T19:36:09	1.7	MLs	50.8980	6.0720	9.0	Eygelshoven
2018-11-17T05:25:02	2.6	MLs	50.6540	6.2520	5.0	Roetgen (Duitsland)
2018-09-13T22:31:18	2.4	MLs	50.4930	5.6890	5.0	Sprimont (België)
2018-09-03T18:20:34	2.0	MLs	51.4030	6.1560	1.0	Velden
2018-08-09T19:31:23	2.0	MLs	51.5480	6.8670	1.0	Oberhausen (Duitsland)
2018-08-08T22:45:44	0.5	MLs	50.9170	6.0030	9.0	Heerlen
2018-08-08T21:37:40	0.6	MLs	50.9010	5.9970	9.0	Landgraaf
2018-08-08T20:09:10	0.5	MLs	50.8990	5.9980	9.0	Landgraaf
2018-08-08T19:59:10	1.9	MLs	50.9040	5.9950	9.0	Landgraaf
2018-08-05T05:39:15	3.0	MLs	51.5530	6.8900	1.0	Bottrop (Duitsland)
2018-08-01T02:05:17	2.4	MLs	51.5700	6.8780	1.0	Bottrop (Duitsland)
2018-07-30T01:15:09	0.6	MLs	50.9030	5.9980	9.0	Landgraaf
2018-07-30T01:13:51	1.7	MLs	50.9040	5.9910	9.0	Heerlen
2018-07-30T01:13:49	0.7	MLs	50.9050	6.0020	9.0	Landgraaf
2018-07-27T15:17:57	2.6	MLs	50.3830	7.4030	10.0	Saffig (Duitsland)
2018-07-23T22:14:16	1.9	MLs	50.8970	5.9860	7.0	Heerlen
2018-07-23T22:14:02	1.3	MLs	50.9050	5.9880	9.0	Heerlen
2018-07-23T08:39:03	1.5	MLs	50.9040	5.9940	7.0	Landgraaf
2018-07-23T08:38:04	2.4	MLs	50.9040	5.9860	5.0	Heerlen
2018-07-18T03:40:50	2.6	MLs	50.3580	7.3950	10.0	Ochtendung (Duitsland)
2018-07-07T13:10:51	0.7	MLs	50.8730	6.2100	12.0	Alsdorf (Duitsland)
2018-05-25T22:43:27	3.2	MLs	51.1840	5.7380	15.0	Kinrooi (België)
2018-05-03T18:23:26	0.9	MLs	50.4680	5.9280	18.0	Spa (België)
2018-04-28T22:16:43	1.1	MLs	51.0140	5.8290	12.0	Guttecoven
2018-04-21T11:47:47	3.0	MLs	50.8620	6.5750	7.0	Kerpen (Duitsland)
2018-04-16T13:16:40	2.9	MLs	51.5660	6.8950	7.0	BOT (Duitsland)
2018-03-16T18:56:35	1.5	MLs	50.8790	5.9290	5.0	Voerendaal
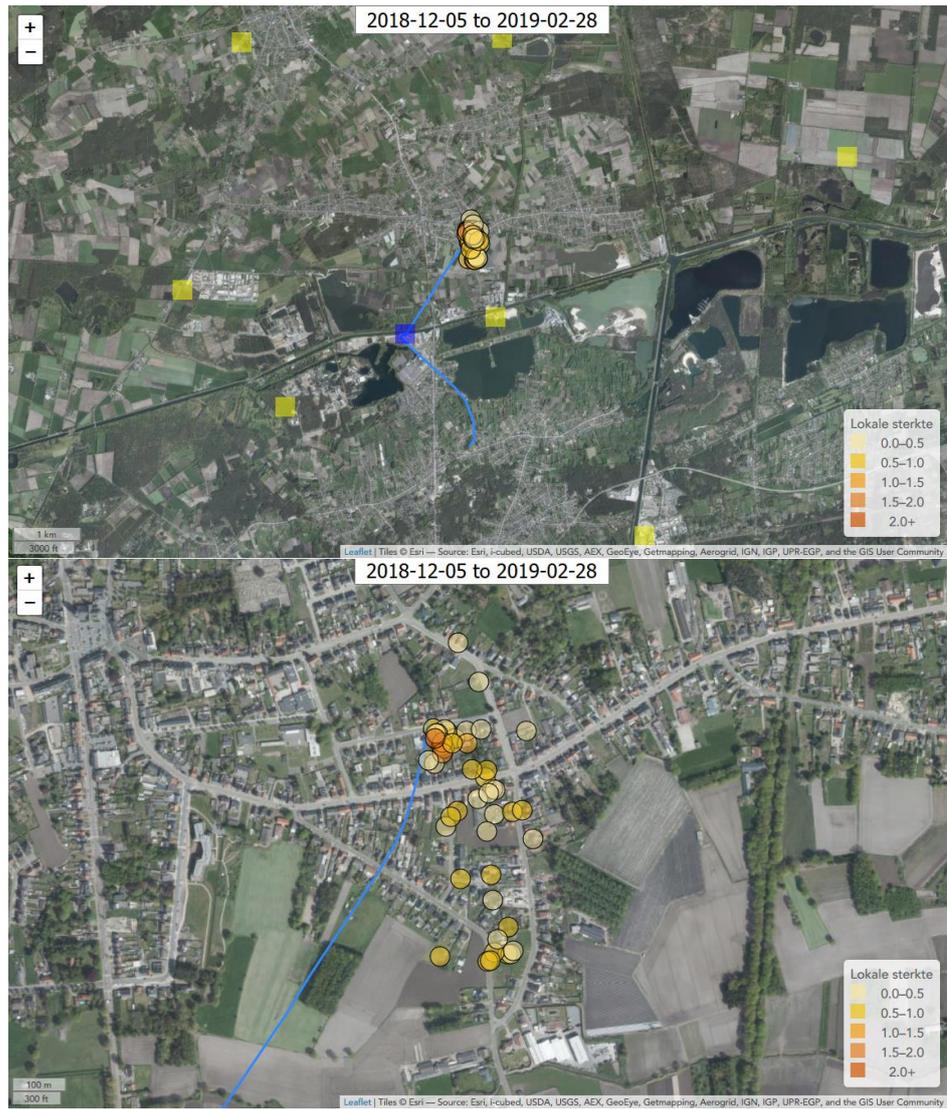
Figure A-65   Location of local seismometers (yellow squares), geothermal plant (blue square), subsurface well trajectories (blue lines) and seismic events (circles color coded according to calculated local magnitude, see legend). Upper figures shows location of seismic cloud relative to the geothermal plant, wells and seismometers, lower figures is a blow-up of the seismic cloud(Source: www.vito.be).

A.12 The Geysers, California, USA (M$_w$ 5.0)

Activity:	Geothermal field, powerplants	
Start date – End date:	1969	to date
Fluid + Fluid balance:	Steam Steam + water	production (<1969) production + reinjection (>1969)
Activity depth:	1 – 2.8 km	
Activity rocktype:	metamorphic rock (greywacke)	
In-situ T	240 °C, 400 °C (High temperature zone)	
Cumulative ΔV:	2 x 10^9 m^3 (production – injection) water	
Maximum Top Hole Pressure:	-0.1 MPa	
Maximum flowrate:	70 l/s (EGS)	
Monitoring system:	yes	
Maximum magnitude + Date:	M$_w$ 5.0 M$_w$ 3.9 (EGS project)	14 – 12 – 2016
Distance M$_{max}$ – activity:	within	
Intensity [EMS]:	V – VI (M$_w$ 5.0)	
Damage:	none reported	
Interpretation		

Tectonic setting and geology: The Geysers field is the largest producing geothermal field in the world. It is located in Northern California, about 80 km east of the San Andreas fault (Garcia et al., 2016). The field is situated in a region between two large active NNW-SSE striking strike-slip faults. The decrease in deformation rates on these faults with distance from the San Andreas Fault causes a transtensional environment (normal faulting to strike-slip). The Geysers field itself is bounded by two NNW-SSE striking faults that have been inactive for at least 15,000 years. Inside the field also inactive SE-NW faults are present. The maximum horizontal stress strike NNW-SSE parallel to the dominant fault motion in the region. The reservoir is situated in greywacke (competent, poorly sorted sandstone), that has been intensely deformed, faulted, and metamorphosed. Matrix porosities are < 2%. The reservoir can be divided in a normal temperature reservoir (NTR) between ~1 – 2.6 km with temperatures up to 240 °C, and a high temperature reservoir (HTR) which underlies the NTR in the northwest Geysers area and where temperatures can be over 400 °C (Figure A-66). At 4 km depth a recent granitic pluton is found. The reservoir is capped by low permeability unfractured greywacke. The field is vapor dominated, and initial pressure were 3 – 4 MPa between 0.5 and 3 km depth (Allis, 1982).
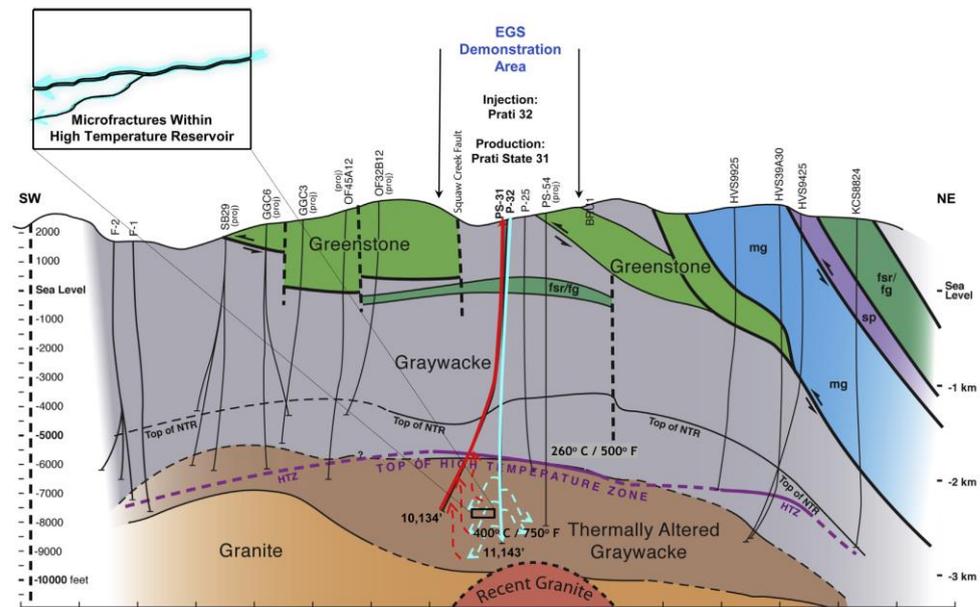
Figure A-66 Cross-section of the northwest of the Geysers geothermal field and the EGS demonstration project (From Rutqvist et al., 2015, Copyright Springer Nature, published under a Creative Commons license).

Activity design: In 2012 – 2013 there were 58 active injection wells and 320 production wells across the field. The EGS demonstration project is situated in the north, making use of two abandoned exploration wells Prati 32 (injection) and Prati State 31 (production) that were reopened and deepened to 2.9 and 3.3 km, within the HTR which was found below 2.6 km depth.

Operations and monitoring: Geothermal production started in 1960, when the first powerplant was installed (Majer et al., 2017). The production rate increased to ~4 x 10^9 kg/year of steam in 1969. From 1969 the number of powerplants grew, production increased and condensed steam was reinjected, about ~25% of the production mass (Figure A-67a). As field pressures decreased in the early 1980's, also rain water was reinjected. After peak production of 80 x 10^9 kg/year in 1987, the productivity of the field declined because of overdevelopment. To enhance productivity additional river water was injected from 1997, and waste water from 2004, so that in total about 60% was reinjected, which increased to 80% in 2015. The cumulative net depletion (steam produced – water injected) in 2010 was 1.4 x 10^{12} kg . In 2011 the Northwest Geysers EGS demonstration project was started to stimulate the deep HTR. Water was injected at initial rates of 70-76 l/s under gravity drive (no extra wellhead pressure) in the P 32 well (Figure A-67b). The water can enter the reservoir because the steam cools and collapses, creating a vacuum (vacuum pressure 0.09 MPa at the wellhead). In the nearby wells the injection caused the pressure to increase by ~0.7 MPa (Garcia et al., 2016). Later injection rates varied between 25 and 63 l/s, continuing for multiple years. The total volume injected at the EGS site was 0.5 – 1 million m^3 per year .
From 1975 eight permanent USGS stations are present over the field with a magnitude of completeness of 2. Since 2003 a permanent local monitoring network (LBNL network) is operative throughout the Geysers, currently consisting of 32 seismic stations (Garcia et al., 2016). Two temporary networks were installed around the EGS project, with a total of 21 stations.
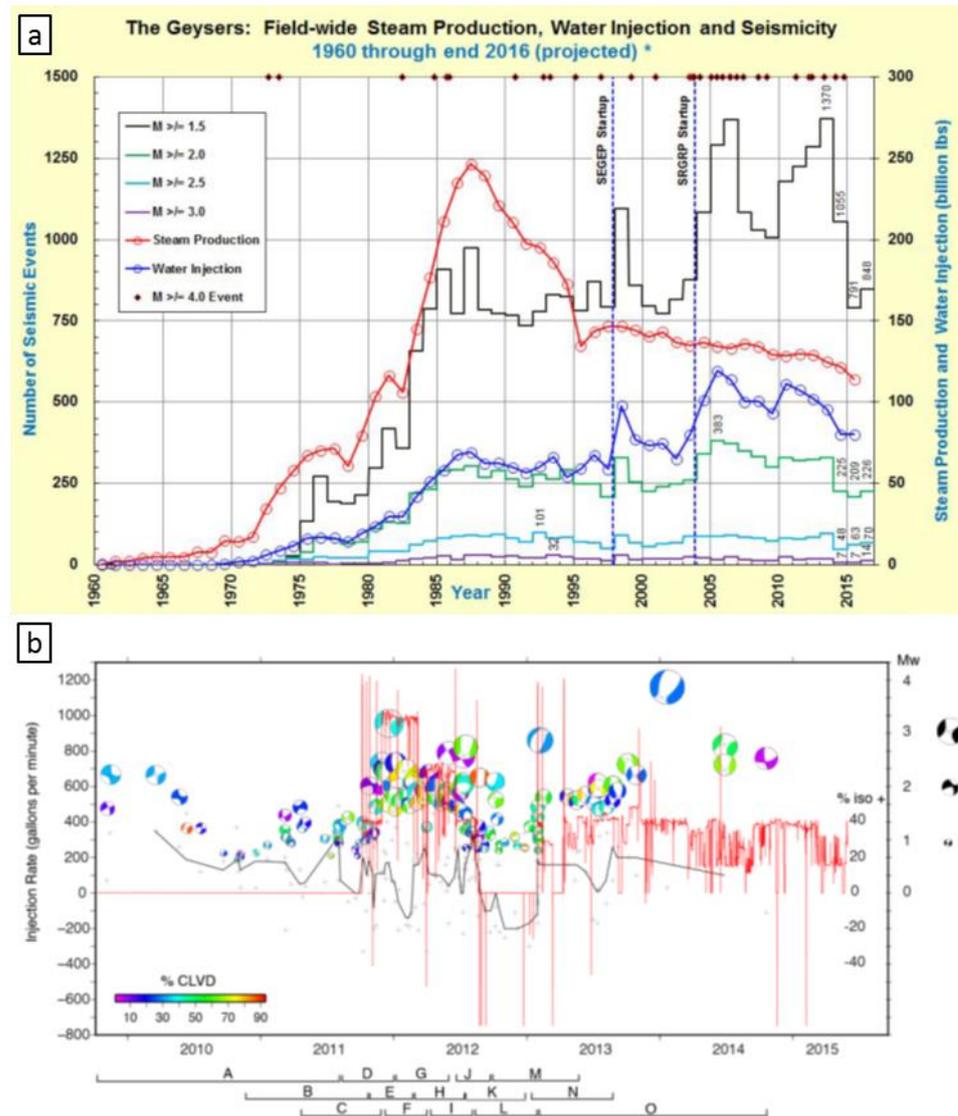
Figure A-67   Operational parameters of the Geysers field as a whole and of the EGS demonstration project versus induced seismicity. a) depletion of the Geysers field (total production – injected water) and injected water with time. 1 billion lbs = 4.5 x 10^8 kg. The number of events with M > 1.5, 2.0, 2.5, and 3.0 are also shown, as well as M > 4 events (top axes). SEGEP and SRGRP indicate the start of injection of river water and waste water. (From Majer et al., 2017 (From Dreger et al., 2018, Report No. DOE/EE-0662, U.S. Department of Energy) b) Injection rate (red line) and seismicity at the EGS demonstration project (100 gallons per minute = 6.3 l/s) (From Dreger et al., 2018, Proceedings 43rd Workshop on Geothermal Reservoir Engineering, Stanford University).

Occurrence of seismicity: Since the early 1980's more than 750 events were recorded annually in the Geysers geothermal field (Figure A-67a). The number of seismic events correlates with the injection rates. Since 2003 20 M > 4.0 events were recorded, with the maximum M_w 5.0 occurring on the 14th of December 2016 (Majer et al., 2017). Hypocenters are mostly located between 1 and 5 km depth (Figure A-68a), with a significant part of the events below the reservoir > 2.8 km depth (Jeanne et al., 2015; Martínez‑Garzón et al., 2014). Seismicity is more frequent and deeper in the northwestern part of the field. During the initial two years of the EGS

stimulation most events were observed near the injection well (Figure A-68b). Larger events lined up SW-NE consistent with surface traces of faults (Garcia et al., 2016). The largest event recorded during the EGS stimulation was a M_w 3.9 in 2013 (Figure A-67b). The events have mainly normal faulting to strike-slip mechanisms.

Interpretation: The mechanisms of seismicity at the Geysers are complex, involving poroelastic stressing, cooling and thermoelastic stressing, and pore pressure changes. Volumetric strain and reservoir compaction were associated with seismicity, but in general seismicity correlates well with injection (Trugman et al., 2016). Microseismic and modeling studies suggest that thermoelasticity plays a large role, in particular close to the wellbore, whereas small changes in steam pressure can induce events up to a kilometer from the wells (Martinez – Garzon 2016, Rutqvist 2016, Jeanne 2016).
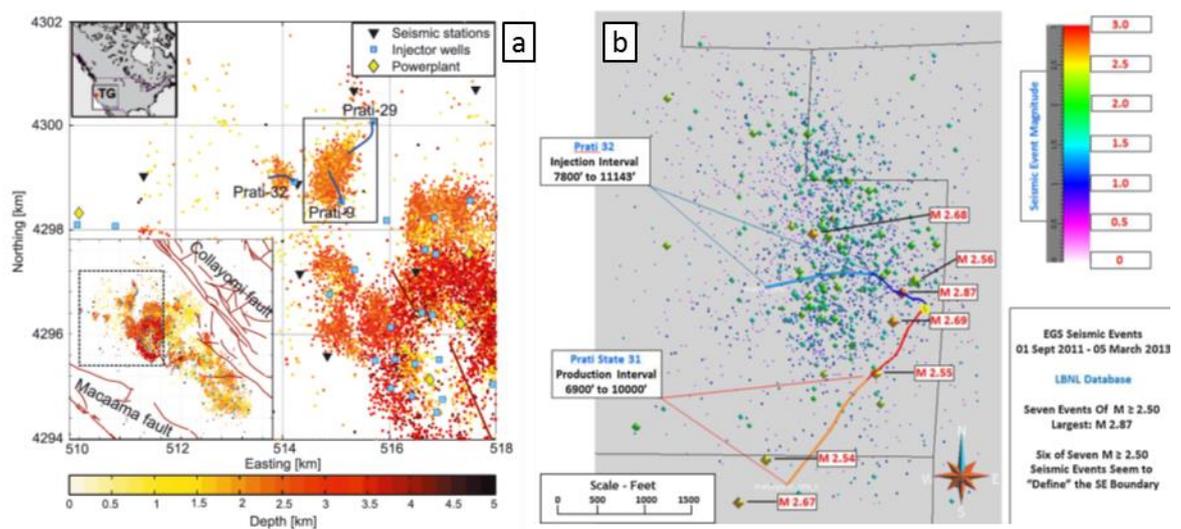

Figure A-68   Seismicity in the Geysers field. a) Seismicity recorded between 2007 and 2012. The position of injection wells and seismic stations is indicated by the blue squares and black triangles (From Martínez ‑ Garzón et al., 2014, Copyright American Geophysical Union, reproduced with permission), b) Map view of seismicity recorded during the first 1.5 years (September 2011 to March 2013) of EGS stimulation in the northwestern Geysers. The well paths of Prati 32 (injection well) and Prati State 31 (production well) are shown in blue and red (From Garcia et al., 2016, Copyright Elsevier, reproduced with permission).

A.13 Salton Sea, California, USA (M$_w$ 5.1)

Activity:	geothermal field, electricity production	
Start date:	1986	to date
Fluid + Fluid balance:	Water, steam	production, injection net extraction
Activity depth:	1 – 2.5 km	
Activity rocktype:	sandstone, siltstone	
In-situ T	< 390 °C	
Cumulative ΔV:	~450,000,000 m^3	
Maximum Top Hole Pressure:		
Maximum flowrate:	3733 l/s (field cumulative)	
Monitoring system:		
Maximum magnitude + Date:	M$_w$ 5.1	01 – 09 – 2005
Distance M$_{max}$ – activity:	< 2.5 km	
Intensity [EMS]:	N/A	
Damage:	N/A	
Interpretation	causal relation with largest event unclear	

Tectonic setting and geology: The Salton Sea geothermal field is located in southern California, at the transition from the diverging East Pacific Rise to the strike-slip San Andreas Fault system (McGuire et al., 2015). The field is situated in a tensional region between NW-SE striking strike-slip faults. It is a water dominated geothermal field located in sandstone, siltstones, and shales, which are only slightly altered at shallow levels (1 – 2 km and < 280°C) and more altered and cemented at deeper levels where temperatures exceeded 300 °C (Figure A-69). Porosity in the shallow formations is 10 – 30% but decreases strongly with depth and alteration. Deeper rocks are however extensively fractured providing permeability. The reservoir is capped by a 400 m thick caprock consisting of silt, clay, sand, and anhydrites. Locally five rhyolite intrusions are present, as well as some intruded dikes and sills. Natural seismicity in the region is high. The main structure in the reservoir is the Main Central Fault, a SW-NE striking strike-slip fault.
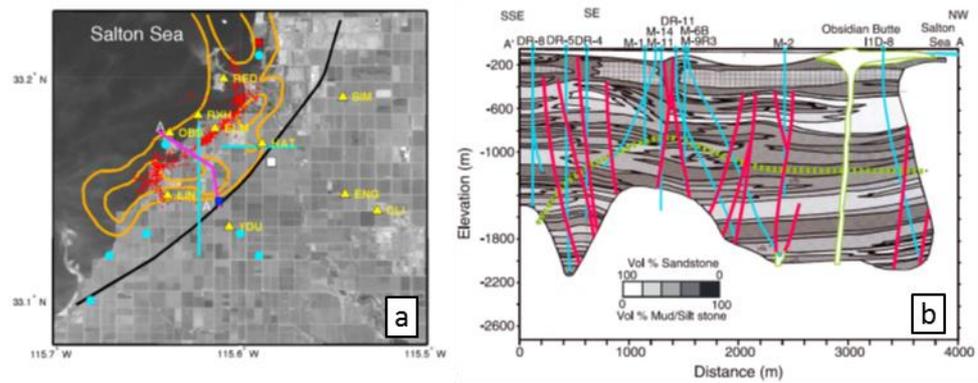
Figure A-69 Salton Sea geothermal field a) orange lines show the outline of the geothermal anomaly of the Salton Sea field. The red dots show hypocenters of the 2005 earthquake swarm which occurred at 3.5 – 5 km depth. The black line is the surface trace of the Main Central Fault b) Cross-section of the Salton Sea geothermal field along the pink line in a. Red lines are interpreted fault, with the Main Central fault strands at ~1200 m distance. Shaded colors indicate the sand content vs clay content, with white indicating 100 % sandstone. Geothermal wells are shown with the blue lines (From McGuire et al., 2015, Copyright American Geophysical Union, reproduced with permission).

Activity design: From 1980 onwards 28 production and 41 injection wells have been drilled into the geothermal field, mainly targeting depths of 1 – 2.5 km. A total of 10 power plants are present in the area.

Operations and monitoring: Production of steam started in 1986, and was increased towards the end of the 1980's (Figure A-70). From 1990 onwards production and injection rates were 5 – 10 million m^3 per month. The net production was 1 – 2 million m^3 per month.
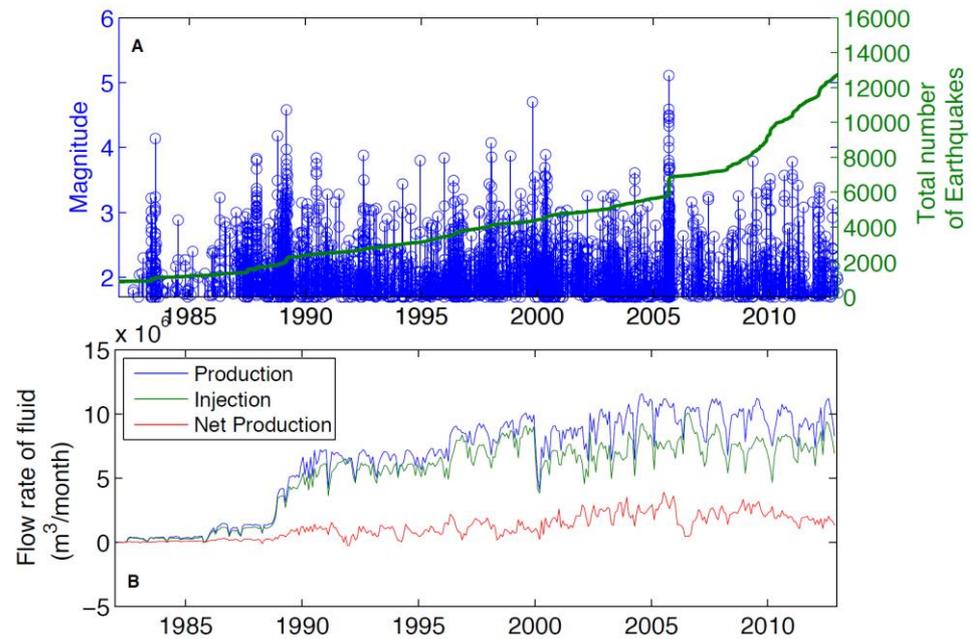
Figure A-70 Seismicity and injection and production in the Salton Sea geothermal field. a) number of events recorded from 1981 to 2012. All events with a depth shallower than 15 km were taken into account. b) monthly production and injection rates, and net production (production – injection) (From Brodsky & Lajoie, 2013, Copyright AAAS, reproduced with permission).

Occurrence of seismicity: The area has high natural seismic activity which is observed from the start. With increasing operation the activity rates increased. From 1985 - 2011 over 12000 earthquakes with M > 1.75 were recorded (Figure A-71; Brodsky & Lajoie, 2013). Events were mostly directly below the geothermal reservoir, 3 – 7 km. The largest observed event was a M 5.1. which was part of a large earthquake swarm with also a number of M > 4 events. Most of this swarm occurred on the Main Central Fault at depths between 3.5 and 5 km (McGuire et al., 2015). Later swarms were more diffuse.
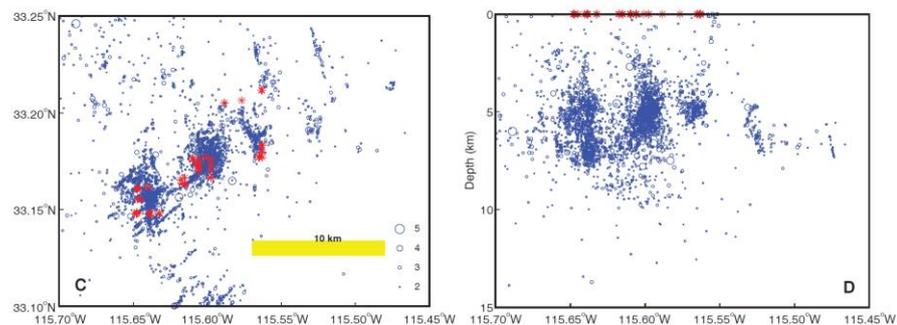

Figure A-71 Seismicity recorded between 1981 and 2012 (From Brodsky & Lajoie, 2013, Copyright AAAS, reproduced with permission).

Interpretation: Contrary to the Geysers field seismicity did not correlate well with operational parameters. Seismicity rates increased after the field started producing, but the correlation with operations was unclear and variable with time (Brodsky & Lajoie, 2013; Trugman et al., 2016). The best correlation was obtained for a combination of net production and injection (Brodsky & Lajoie, 2013). Aseismic slip is also inferred in the shallow porous sediments, and may have triggered the earthquake swam in 2005 including the M 5.1 event. Stress transfer due to the aseismic slip could have elevated the stresses so that more earthquakes were induced and the correlation with operations increased after 2005 (McGuire et al., 2015; Trugman et al., 2016). These studies highlight the difficulty in differentiating induced seismicity from natural seismicity in this tectonically active area.

A.14 Desert Peak, Nevada, USA (M$_w$ 1.7)

Activity:	Geothermal field, EGS, powerplants	
Start date – End date:	1969	to date
Fluid + Fluid balance:	circulation injection (EGS)	1985 – to date 2011 - 2013
Activity depth:	1 – 1.7 km	
Activity rocktype:	volcanics	
In-situ T	207 °C	
Cumulative ΔV:	~150,000 m^3 (shallow EGS) ~40,000 m^3 (deeper EGS)	
Maximum Top Hole Pressure:	8 MPa	
Maximum flowrate:	100 l/s (EGS)	
Monitoring system:	yes 14 stations	
Maximum magnitude + Date:	M$_w$ 1.7	2013
Distance M$_{max}$ – activity:	< 500 m	
Intensity [EMS]:	not felt	
Damage:	none	
Interpretation	increased pressure	

Tectonic setting and geology: The Desert Peak is located in west Nevada, USA, within the Humboldt structural zone in the Northern Hot Spring Mountains (Faulds et al., 2010). This zone is characterized by strike-slip and normal faulting along northeast striking faults and northwest – southeast extension. The Northern Hot Spring Mountains contains seven geothermal fields, including the Desert Peak geothermal field. The field is located above a horst structure, in a step in the Rhyolite Ridge Fault zone which is defined by a number of NNE striking fault blocks (Figure A-72; A-73). The maximum horizontal stress is parallel to these faults. The geothermal reservoir with temperatures up to 207 °C is situated in Tertiary volcanic and sedimentary rocks with porosities 4 - 11%, overlying Mesozoic metamorphic and granitic basement (Benato et al., 2016; Lutz et al., 2010). The main reservoir rocks are metamorphosed diorites and metavolcanics rocks of the Jurassic (Lutz et al., 2010).
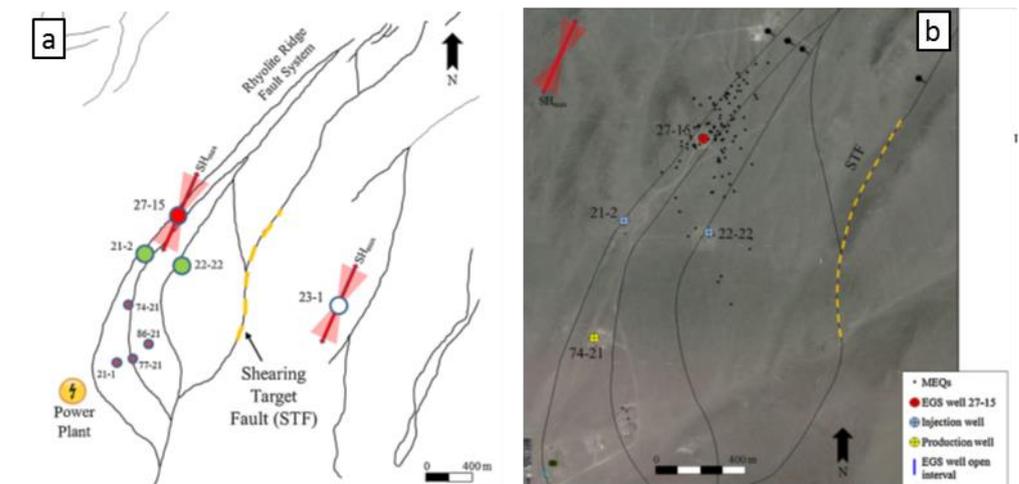
Figure A-72   Surface traces of faults, wells and seismicity. a) Surface traces of faults of the Rhyolite Ridge Fault System. Production wells (purple), injection wells (green), and the EGS well 27-15 (red) are shown. The horizontal stress is indicated at two wells. b) Seismic events during the deep stimulation in January 2013 (From Benato et al., 2016, Copyright Elsevier, reproduced with permission).

Activity design: After drilling several test wells well 21 – 1 and 21 – 2 were drilled in 1976 to depths of 1260 m and 1050 m (Zemach et al., 2017). Between 1982 and 1984 production wells 86-21 and 67-21 was drilled to 1000 and 1250 m, and injection well 22-22 to 2051 m. In 2003 and 2004 two more successful production wells were drilled (74-21 and 77-21). Currently there are 7 active producers, and 2 injectors 21-2 and 22-2. Well 27-15 was drilled in 2004 and found unsuccessful; this well was later used for the EGS project.
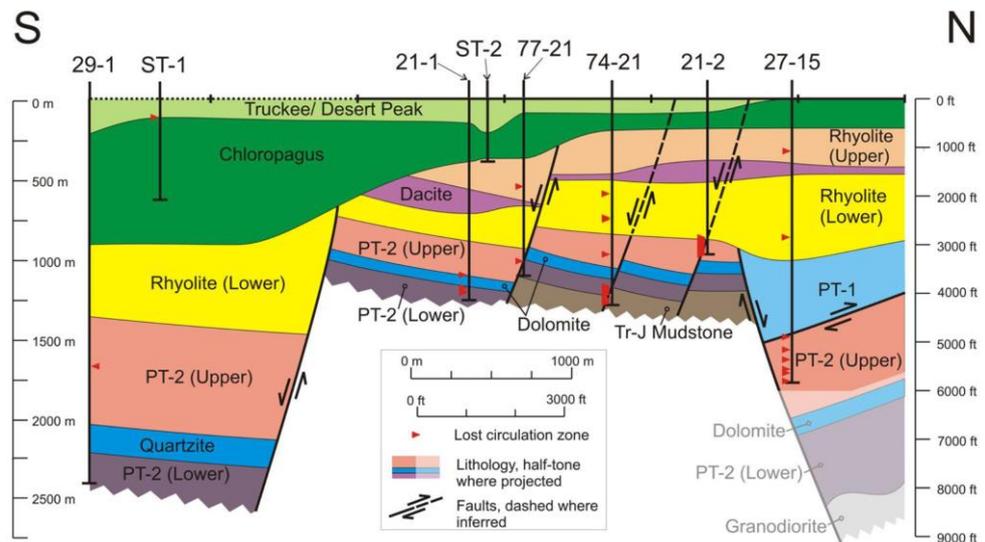

Figure A-73   North-south cross-section through the Desert Peak geothermal field. PT-1 is Pre-Tertiary Unit 1 which are metasedimentary rocks of Jurassic age (mudstones, dolostones, shale), and PT-2 are metamorphosed rocks of Triassic – Jurassic age. (From Lutz et al., 2010, Rock mechanical testing and petrologic analysis in support of well stimulation activities at the Desert Peak Geothermal Field, Nevada, Proceedings Thirty-Fifth Workshop on Geothermal Reservoir Engineering, Stanford University).

Operations and monitoring: Generation of electricity started in December 1985, with 67-21 and 86-21 used for production and 21-2 for injection (Zemach et al., 2017). Well 21-1 was first producing and converted to an injection well from 2003 to 2006. In 2006 a new powerplant was installed. Four of the wells were self-flowing. From September 2010 to March 2013 several stimulation treatments were performed in a shallow section of well 27-15 (914 – 1067 m in the lower rhyolites). Flow rates ranged from 5 to 100 l/s, with wellhead pressures of 3.8 to 8 MPa. The largest volumes was injected during the 13 day stimulation in April 2012 with 133,000 m^3 at a maximum pressure of 7.2 MPa. At the start of 2013 the deeper part of the well (1.5 m depth) was stimulated with maximum injection pressure of 10.3 MPa and maximum flowrates of 60 l/s (Zemach et al., 2017). This stimulation was followed by a long term injection test.

Seismicity was monitored with 15 local stations and the network was upgraded at the end of December 2011 (Benato et al., 2016).
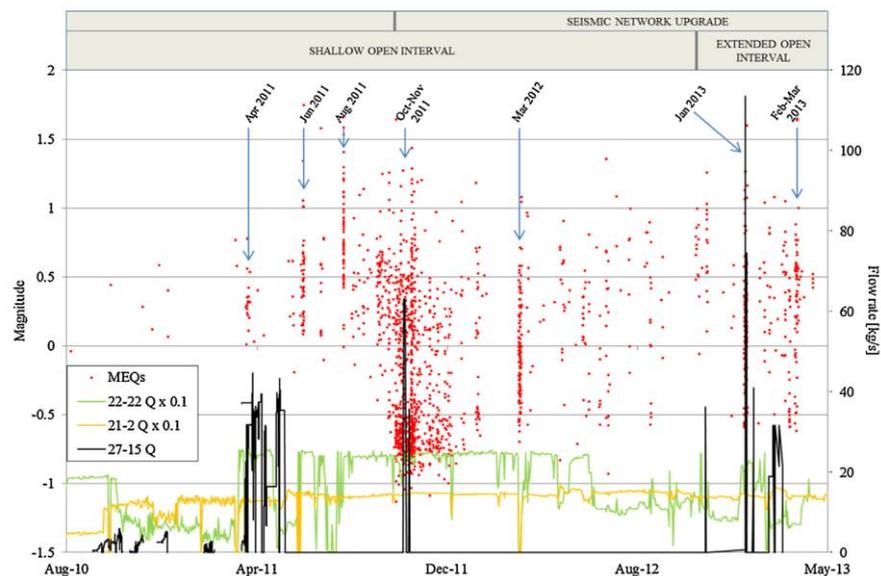

Figure A-74 Stimulations in 27-15 EGS well. The flow rate in well 27-15 is shown in black, the flow rates in the nearby injection wells 21-2 and 22-22 in yellow and green (10 times amplified). Red dots show the recorded microseismicity. In January and August 2011, and May 2012, no stimulations were conducted in 27-15 but seismicity is recorded in response to changes in injection in 21-2 and 22-22 (From Benato et al., 2016, Copyright Elsevier, reproduced with permission).

Occurrence of seismicity: Microseismicity was recorded during the different stimulations. During the April 2011 stimulation 15 locatable events occurred with magnitudes not exceeding M_w 0.8 (Benato et al., 2016). During later stimulations, and changes in injection rate in the other injection wells, several 100's of events were recorded with M_w up to 1.7. During stimulation of the deeper parts of the well ~200 events were recorded with a maximum of 1.7 (Figure A-74). During the long term injection test in 2013 events lined up between the EGS well and the other injection wells (Zemach).

Interpretation: Shearing due to increases in pressure and cooling-induced thermoelastic stress changes (Benato et al., 2016; Dempsey et al., 2014).

A.15 Rotokawa, New Zealand (M 3.3)

Activity:	Geothermal field, powerplants	
Start date – End date:	1997	to date
Fluid + Fluid balance:	circulation net production	1997 - 2010 2010 – to date
Activity depth:	1 – 1.7 km	
Activity rocktype:	volcanics (andesite)	
In-situ T	340 °C	
Cumulative ΔV:	1.5×10^8 m^3 production (1997 – 2015) 1.1×10^8 m^3 injection (1997 – 2015) 3.6×10^7 m^3 net production	
Maximum Top Hole Pressure:	1 MPa reinjection pressure 3.5 MPa reservoir depletion	
Maximum flowrate:	462 l/s (whole field)	
Monitoring system:	yes 10 stations	
Maximum magnitude + Date:	M_w 3.3	2013
Distance M_{max} – activity:	< 700 m	
Intensity [EMS]:	not felt	
Damage:	none	
Interpretation	cooling and thermoelastic stressing, pressure increases	

Tectonic setting and geology: The Rotokawa geothermal field is located in the Taupo Volcanic Zone (TVZ), which runs NE-SW in the center of the North Island, New Zealand (Figure A-75). It is a water-dominated geothermal reservoir about 6 km in diameter, situated in fractured andesites at 1 – 2.5 depth (Sherburn et al., 2015). The reservoir is underlain by greywacke basement rocks. A number of major faults run though the field NE-SW parallel to the TVZ which offset the greywacke basement. Temperatures at 2 km depth are ~300 °C.

Activity design: The first exploration wells were drilled in the 1960's, and the first powerplant was operational 1997. Since then 31 wells have been drilled, with a second powerplant becoming operational in 2010. In 2015 18 wells were active, 13 of which were producing and 5 injecting. Some older wells are abandoned due to casing failure. The geothermal reservoir is ~3 x 4 km in dimension.
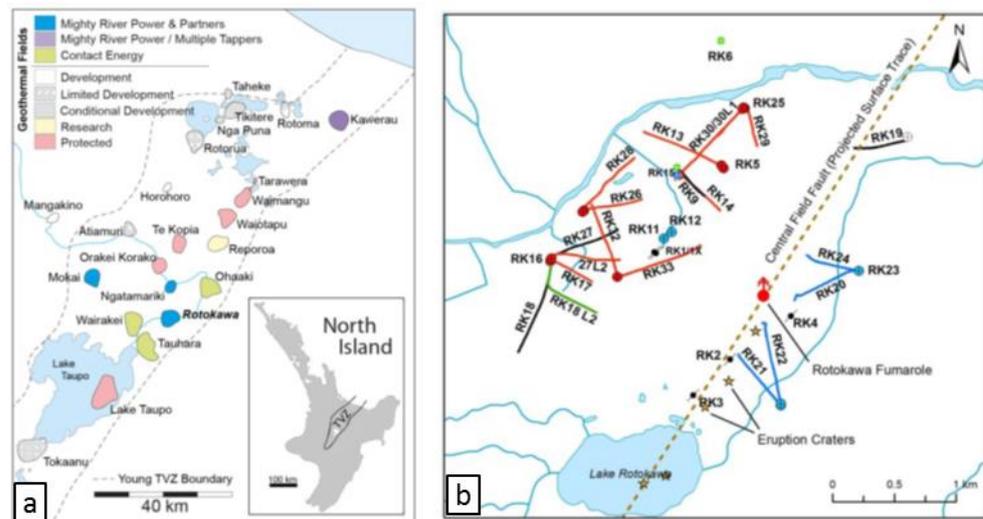
Figure A-75 Rotokawa geothermal field location and wells. a) The Taupo Volcanic Zone and geothermal fields including Rotokawa. b) Map view showing the wells drilled in the field, with in red the production wells, in blue the injection wells, and in black abandoned wells. The projected trace of the of the Central Field Fault is shown by the dashed line (From Sewell et al., 2015, Interpretation of microseismicity at the Rotokawa Geothermal Field, 2008 to 2012, Proceedings World Geothermal Congress 2015, Melbourne).

Operations and monitoring: Electricity generation started in 1997, with production from wells RK5 and RK9 between 1 and 2 km depth (Figure A-75). Reinjection occurred in RK1, RK11, and RK12 in the center of the field, at shallower depths of 0.5 – 1 km (Sherburn et al., 2015). After pressures increased by ~1 MPa at these shallow depths, injection was shifted to RK16 and RK18 wells in the southwest in 2005. These wells injected at a total rate of 500 tonnes/hour at a depth of 1 – 3 km (Figure A-76) . In October 2008 injection was shifted to the southeast in well RK20. Production in this period occurred in RK5, RK13, and RK14 in the north. Up to this time almost 100% of produced fluid was reinjected. Early 2010 a new powerplant came online (NAP) and additional injection in RK21 and RK22 increased the total to 2000 tonnes/day which was equal to 80% of the production. At the end of 2010 injection from RK21 and RK22 was shifted to RK24. After the increased production rates in 2010 the reservoir pressure decreased between 0.5 and 3.5 MPa. Pressure measurements showed that the field was compartmentalized, likely by sealing faults. Microseismicity is monitored by the regional network. A single station was added above the field in 2005, a 10 station network operated for several months in 2006, and a 10-station network operated continuously from October 2008. The magnitude of completeness decreased from ~2.5 to 2 (Figure A-76).
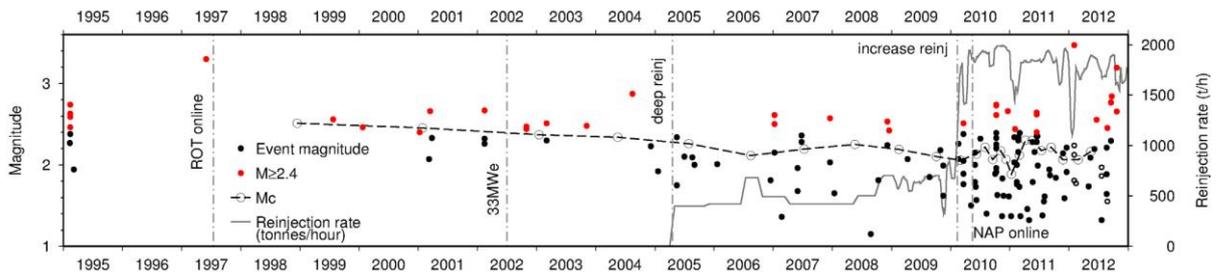
Figure A-76 Injection and seismicity measured by the regional network at Rotokawa (From Sherburn et al., 2015, Copyright Elsevier, reproduced with permission).

Occurrence of seismicity: Microseismicity showed a close correlation to injection wells, and shifted as the injection was shifted to different wells (Sewell et al., 2015; Sherburn et al., 2015). In 2005 seismicity ~350 events were recorded <2.5 km from the active injection wells RK16 and RK18 in the southwest, with a maximum magnitude of 2.3. In 2006 the local network recorded 200 events near these wells with a maximum of M 1.7. In 2008 seismicity occurred mainly in the north near the production zone (Figure A-77). From 2008 onwards seismicity clustered predominantly near the active injectors RK20 and RK24 at a depth between 1.5 and 3 km (Figure A-77). The maximum reported magnitude was an M_w 3.3 in July 2011. The Central Field Fault was interpreted as a (semi-permeable) barrier to migrating fluids, as microseismicity did not migrate across it, and temporary reservoir pressure differences were observed across the fault. Little seismicity was observed in the south where RK21 was still injecting.
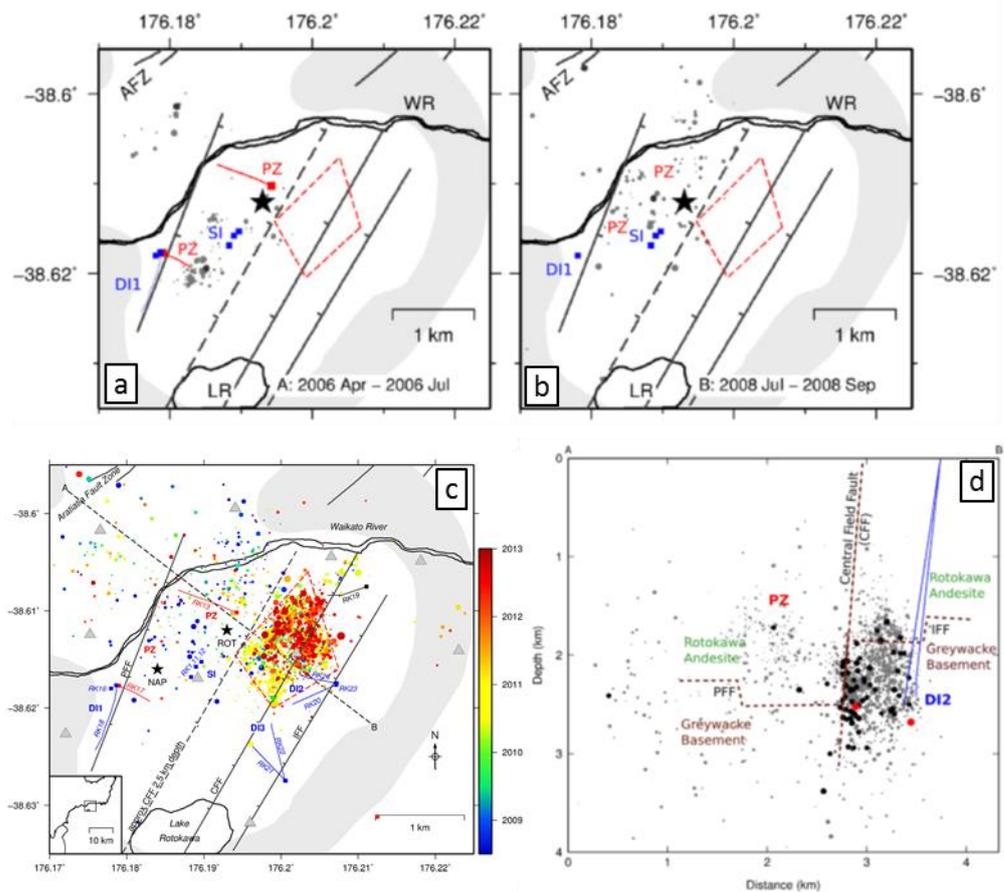
Figure A-77 Seismicity in the Rotokawa geothermal field. a) Seismicity from April 2006 to July 2006 (a temporary local network was in place), b) Seismicity from July 2008 to September 2008. c) Seismicity from 2008 to 2012 (10-station network in place), d) depth of seismicity and interpretation of the geology (From Sherburn et al., 2015, Copyright Elsevier, reproduced with permission).

Interpretation: Cooling and contraction (thermoelastic stressing) has been suggested as the main mechanism for the seismicity (Sherburn et al., 2015). The temperature difference between the reservoir (340 °C) and reinjected fluids (80 – 130 °C) are large, and pressure changes in the east are small (0.1 MPa). The local geology and presence of fractures is key, as indicated by the lack of seismicity at some wells, and the presence of seismicity at other wells.

Appendix B

In this Appendix an overview of other activities related to induced seismicity is given. These include hydraulic fracturing for hydrocarbon production, waste water injection, hydrocarbon depletion, secondary and tertiary recovery, drilling-induced seismicity, reservoir impoundment, and mining.

B.1 Hydraulic fracturing

The purpose of hydraulic fracturing is to enhance the permeability of initially impermeable formations by creating new fractures and reactivate pre-existing fractures. It is generally applied to stimulate flow in formations with low permeability such as tight sandstones or shales, thereby enabling production of hydrocarbons or obtaining flow rates required to successfully develop geothermal energy. During hydraulic fracturing fluids (and solids) are injected at high pressures exceeding the minimum horizontal stress. This process leads to the creation of tensile fractures or the reactivation of pre-existing fractures (see section 2.4.2). The injected solids (proppants) help to keep the newly created fractures open as pressure drops after injection is stopped.

Hydraulic fracturing for oil and gas production has a long history and is widely employed worldwide (King, 2010). The accelerated development of shale gas and oil in the United States has dramatically increased the scale of fracturing operations in the United States. U.S. EPA (2016)estimates that 275,000 wells have been drilled and likely hydraulically fractured between 2000 and 2013 in the United States, with 25,000-30,000 new oil and gas wells that have been hydraulically fractured each year between 2011 and 2014. Prime shale targets include are the Barnett Shale in Texas, the Marcellus Shale, the Bakken Shale, and the Haynesville Shale with recently increasing focus on oil production from the Bakken Shale in North Dakota and the Permian Region in Texas (www.eia.gov). Also in Canada (predominantly Alberta and British Columbia) hydraulic fracturing is ubiquitous with over 180,000 fractured wells in 2016 in Alberta alone (www.nrcan.gc.ca). Hydraulic fracturing for oil and gas production is also widely employed in Europe, but much more for production from tight sandstone or carbonate reservoirs. Hydraulic fracturing of shale plays in Europe is limited, with more than 70 wells targeting shales drilled in Poland (74 in 2015 with 25 hydraulically fractured wells and 12 horizontal hydraulically fractured wells, Pieńowski, 2015), and start of fracturing operations in a horizontal well in Lancashire, England in October 2018 after initial fracturing of a vertical well near Blackpool in 2011. In many other European countries shale gas exploration is not pursued due to difficult economics as well as public concerns and resistance regarding the environmental impact of hydraulic fracturing (Van de Graaf et al., 2018). In the Netherlands, a recent screening of ~252 wells with conventional hydraulic fracturing operations for tight sandstone and carbonate reservoirs indicated no negative consequences for human health and natural environment (TNO & EBN, 2018).

Compared to the number of wells, the number of felt events related to hydraulic fracturing is very small. Up to 2010, no seismicity with M > 2 was reported. However, since 2011 a number of large events with M_L up to 4.8 have been reported in relation to hydraulic fracturing (Foulger et al., 2018). Nearly all of the large events occurred in Canada (e.g. Atkinson et al., 2016), but events up to M_w 4.7 also occurred in the Sichuan Basin, China (Lei et al., 2017). In section B.1.1 the seismicity observed near Crooked Lake, Canada, is described in more detail.

Comparison to geothermal: Pioneering work on field tests of hydraulic fracturing for enhanced heat extraction for geothermal energy production has been performed at the Fenton Hill site in New Mexico by researcher of the Los Alamos National Laboratory (Dash and Murphy, 1981). Subsequently, hydraulic fracturing has been used in many enhanced geothermal sites worldwide (see appendix A;

The scale of the injection wells (several km) and the injected volumes (1,000 - 100,000 m^3) are similar or larger in hydraulically fractured oil & gas wells than for example in EGS systems, but the injection pressure is usually much larger. Pressure diffusion plays a dominant role both in hydraulic fracturing for hydrocarbon productions and in geothermal systems. Temperature effects are not very relevant for hydraulic fracturing, although injection of large volumes of cold fluid may result in thermal fracturing.

B.1.1   Crooked Lake, Canada (M$_w$ 3.9)

Activity:	Hydraulic fracturing	
Start date:	17 - 12 - 2014	8 – 1 – 2015
Fluid + Fluid balance:	Water	injection
Activity depth:	3.4 km	
Activity rocktype:	shale	
In-situ T		
Cumulative ΔV:	61148 m^3 (2 wells, 2 x 25 frac stages)	
Maximum Top Hole Pressure:	70 MPa	
Maximum flowrate:	17 l/s	
Monitoring system:	no	
Maximum magnitude + Date:	3.9	23 – 01 – 2015
Distance M$_{max}$ – activity:	0.8 km	
Intensity [EMS]:	N/A	
Damage:	N/A	
Interpretation	pressure diffusion and fault reactivation extending into the basement	

Tectonic setting and geology: Crooked Lake is a region 20 km west of Fox Creek, Alberta Canada, ~250 ENE of Edmonton. It is located in the Western Canada Sedimentary Basin (WCSB), a large sedimentary basin east of the Rocky Mountains, covering most of Alberta and parts of British Columbia and Saskatchewan (Figure B-1). Shale gas exploration increased exponentially since 2005, with over 12,000 hydraulically fractured wells in 2015 (Atkinson et al., 2016). The main shale plays in the WCSB are the Lower Triassic Montney, the Devonian Horn River Shale, and the Upper Devonian Duvernay, which is the main play targeted near Crooked Lake. The Duvernay Shale consists of organic-rich shales and carbonates, and is located at a depth of 3.4 km with a thickness of 40 m at the location of this case study (Schultz et al., 2015). It is underlain by limestones and shales of the Majeau formation, limestones of the Cooking formation, and carbonates of the Swan Hills formation (https://ags.aer.ca), and the distance to the basement is 500 m (Figure B-1b). Natural seismic activity in the basin is low. The maximum horizontal stress strikes SW-NE and the regional faulting regime is strike-slip.

Activity design: This case study focuses on a specific well pad with two horizontal wells (UWI 02/15-07-063-22W5/0 and 00/15-07-063-22W5/2). The horizontal wells with a length of 2 km were drilled into the Duvernay shale at a depth of 3.4 km (Bao & Eaton, 2016).

Operations and monitoring: Hydraulic fracturing started on 17 December 2014 and finished on 8 January 2015 (Bao & Eaton, 2016). Maximum wellhead pressures reached 70 MPa, with maximum flowrates of 17 l/s. A total of 61148 m^3 was injected in 2 x 25 fracturing stages. Four local stations were present at distances of 2.5 – 7 km from the well pad, in addition to regional broadband stations.
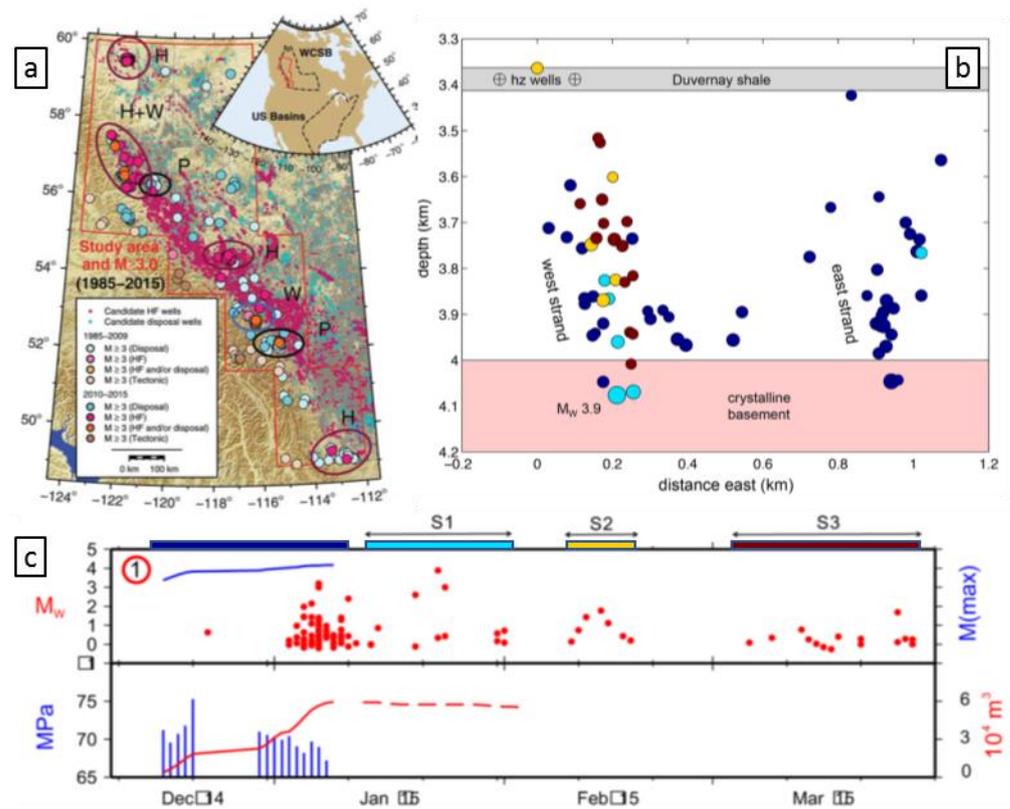
Figure B-1   Seismicity and injection data near Crooked Lake. a) hydraulic fracturing (HF) wells in the Western Canada Sedimentary Basin (WCSB) and occurrence of seismicity with M > 3 (From Atkinson et al., 2016, Copyright Seismological Society of America, reproduced with permission). b) east-west cross-section of wellpad 1 (UWI 02/15-07-063-22W5/0 and 00/15-07-063-22W5/2) near Crooked Lake (lat: 54.4, lon: 117.3, center oval with H in a), and located seismic events. Colors indicate the timing of seismicity, with dark blue: during stimulation, cyan: S1 (see c), yellow: S2, red: S3. c) Injection data and seismicity of wellpad 1. (From Bao & Eaton, 2016, Copyright AAAS, eproduced with permission).

Occurrence of seismicity: Seismicity started in January 2015 during the second stage of hydraulic fracturing (Figure B-1). The number of seismic events increased, with magnitudes up to M_w 3.2 (07 – 01 – 2015). After fracturing finished seismicity continued to occur for three months, with a maximum reported magnitude M_w 3.9 on 23 January 2015. Nearly all of the seismicity occurred below the Duvernay shale, extending into the crystalline basement to 4.1 km depth (Bao & Eaton, 2016).

Interpretation: Increased pressure and pressure diffusion caused reactivation on pre-existing faults extending into the basement. A study investigating seismicity in the entire WCSB suggests that the proximity to the basement is one of the dominant controlling factors on the occurrence of hydraulic fracturing induced seismicity, along with overpressure in the Duvernay, and the proximity to the Swan Hills reef formation (Pawley et al., 2018).

B.2 Waste water injection

One of the first examples of induced seismicity associated with waste water injection occurred at the Rocky Mountain Arsenal waste water injection site in Denver (Evans, D., M., 1966; Healy et al., 1968). From March 1962 to September 1965 a total of ~550,000 m³ of waste water was injected into fractured Precambrian basement at a depth of 3.7 km. Shortly after the start of injection earthquakes were recorded which were closely correlated to the injection activities in space (<5 km from injection well) and time, with magnitudes M_L <4.5. The largest earthquake (m_b 4.9) occurred in 1967, after termination of injection. Since then, a large number of cases have been reported where fluid injection has led to induced seismicity.

The most famous example is the significant increase in seismicity rates in the Central USA, due to the large-scale waste water injection projects. Since 2009, a dramatic increase in seismicity rates has been observed in the central and eastern United States, in the states of Arkansas, Colorado, New Mexico, Virginia, Texas, Ohio and Oklahoma (Ellsworth, 2013; Keranen, K. M. et al., 2014; Walsh & Zoback, 2015). Multiple large magnitude and damaging earthquakes have been recorded, amongst others the M 5.7 earthquake near Prague in Oklahoma (Keranen, Katie M. et al., 2013), the M 4.7 event near Guy-Greenbrier, Arkansas (Horton, 2012) and the M 4.0 earthquake in Youngstown, Ohio (Kim, Won-Young, 2013). The increase in seismicity has generally been related to the injection of large volumes of salty wastewater (co-produced from hydrocarbon production, or a by-product from hydrofracking) into the subsurface (Ellsworth, 2013; Goebel et al., 2017; Keranen et al., 2014; Kim, 2013). The waste water is either re-injected into the hydrocarbon producing formations, or disposed of in saline sedimentary aquifers with high porosity and permeability. In Oklahoma, extremely large volumes of waste water, mainly co-produced formation water from hydrocarbon production and some waste water from fracturing operations, were injected into the highly permeable Arbuckle Group. Injection wells are continuously operating with injection rates of 10,000m³/month to 100,000 m³/month. Similarly, in North-Central-Arkansas, large amounts of waste-water as a by-product of hydrofracking operations, are injected into the Springfield and Ozark aquifer (Horton, 2012). The region of North-Texas experienced a significant increase in seismicity since 2008, which can be attributed to the injection of waste water in the Ellenburger Formation (Hornbach et al., 2016). In Guy and Greenbriar (Arkansas, USA) for example, large volumes of wastewater (~200,000 m³) were injected at 2 – 3.5 km depth from July 2010 to February 2011 (Horton, 2012). The injection occurred in the Arbuckle formation (part of the Ozark aquifer), a fractured, karstified dolostone. Following the injection a swarm of earthquakes was recorded with magnitudes up to M 4.7. The hypocenters illuminated a pre-existing fault plane which extended up to 10 km from the well (Figure B-2a). Seismicity occurred below the Ozark aquifer at depths of 3 – 7 km within the granitic Precambrian basement (Figure B-2b).

Most seismicity related to wastewater injection does not occur in the sedimentary formation targeted for injection, but in the underlying crystalline basement rocks, at depths up to 10 km below the injection intervals. Seismicity associated to waste water injection has been reported up to distances of 10 to 40 km from the nearest injection well (Goebel et al., 2017; Horton, 2012; Keranen, K. M. et al., 2014; Kim, Won-Young, 2013).
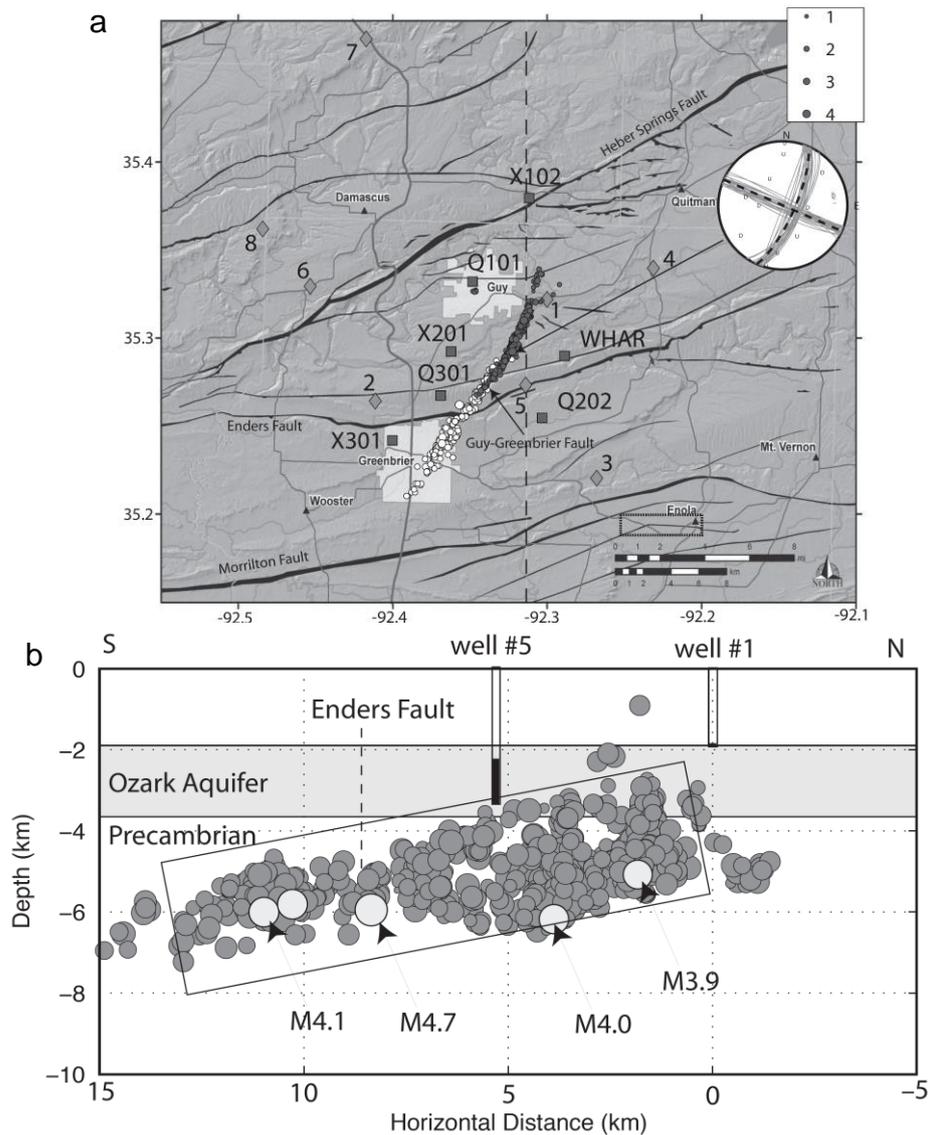
Figure B-2   Location of induced seismicity at Guy-Greenbrier (From Horton, 2012, Copyright Seismological Society of America, reproduced with permission). a) Map view of seismicity, with black dots indicating seismicity from 1 October 2010 to 15 March 2011, and white dots indicating seismicity from 16 February to 8 March. b) Depth distribution of seismic events.

Comparison to geothermal: The scale of the waste water injection operations is generally much larger than for geothermal operations. Waste water is injected via multiple injection wells, at injection rates of several 10,000 m3 to 100,000 m3 per months, over prolonged periods of several months to years, which means extended areas can be affected by the pore pressure change. Injection pressures are generally low and comparable to conventional geothermal operations. Waste water is either injected into depleted hydrocarbon reservoirs, with reservoir pressures well below virgin reservoir pressures, or into sedimentary aquifers at virgin reservoir pressures. Both pressure diffusion and poroelastic stressing can play a role in the reactivation of faults and the generation of seismicity (Goebel et al., 2017). The role of temperature has not been explicitly mentioned in the literature, but as large volumes of cold fluids are injected into the deep subsurface, thermal stresses may also play a role in the generation of seismicity.

B.2.1   Prague, Oklahoma (M 5.7)

Country & place (lat, lon):		
Activity:	Waste water injection into the Wilzetta Oil Field	
Start date – End date:	1993	To date
Fluid + Fluid balance:	Water	Injection
Activity depth:	1.3 to 2.1 km	
Activity rocktype:	(dolomitic) limestones	
In-situ T	n.a.	
ΔT in-situ – fluid:	n.a.	
Cumulative ΔV:	~ 170.000 m3 ((cumulative volume in 2011)	
Maximum Top Hole Pressure:	3.6 MPa	
Maximum flowrate:	~ 1500 m^3/month	
Monitoring system:	Yes	
Maximum magnitude:	5.7	
Distance M_{max} – activity:	~ 5 km	
Intensity [EMS]:	VIII	
Damage:	Yes	
Interpretation	Induced by pore pressure increase or triggering from stress transfer by earlier events	

Tectonic setting and geology: The Wilzetta Oil Field is located within the Wilzetta fault system in Oklahoma, USA. Oil production in the Wilzetta Oil Field predominantly occurred in the 1950's and 1960's, with only limited production ongoing today. Oil is produced from the porous limestones of the Hunton Formation, trapped in isolated reservoir compartments offset along steeply dipping faults. Since 1993 waste water has been injected into the Wilzetta Oil Field. The injection wells target the Hunton limestones and the dolomitic limestones of the Arbuckle group below at depths between 1.3 and 2.1 km. The maximum horizontal stress in the area is oriented ENE-WSW (Keranen, Katie M. et al., 2013).
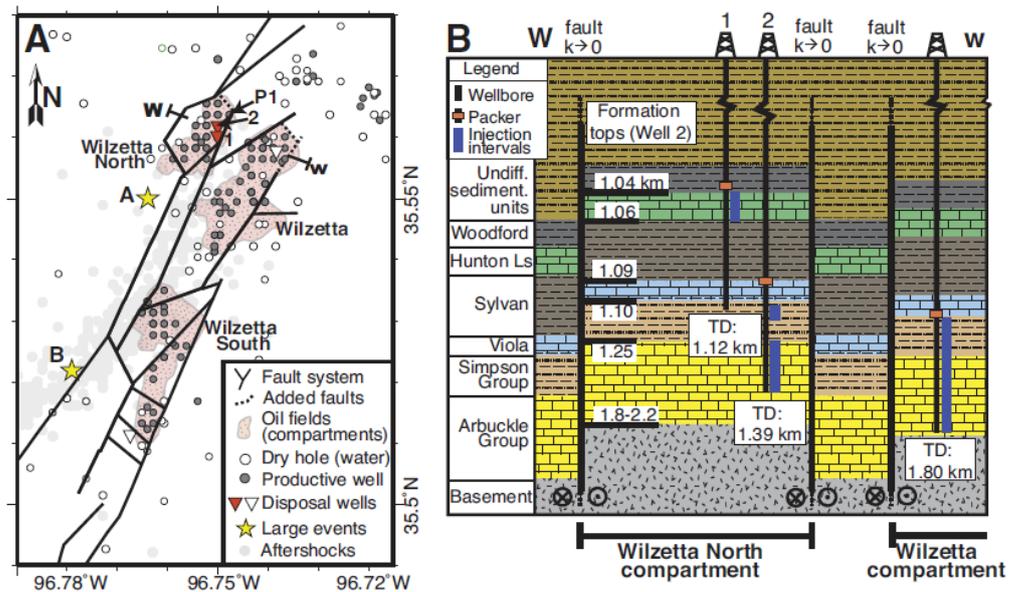
Figure B-3   Geology of the Wilzetta oilfields in Oklahoma, USA. A: Wilzetta fault system, injection and production wells and earthquakes and location of 3 large magnitude events, i.e. A Mw 5.0, B Mw 5.7 and C Mw 5.0 seismic event. B: Cross section of the lithology of the Wilzetta oilfield showing high-permeability limestone reservoirs are interbedded with shales. Faults are low-permeability barriers (From Keranen et al., 2013, Copyright The Geological Society of America, reproduced with permission).

Activity design: Injection activities started in 1993. Initially waste water was injected in well 1 (Figure B-3) into the underpressured Hunton limestone reservoir at zero wellhead pressure. Wellhead pressure reached a maximum of 3.6 MPa in 2006, at which time a second injection well was added (Keranen, Katie M. et al., 2013).

Occurrence of seismicity: The first noted seismic event, with M_w 4.1, was recorded near the oilfield in 2010, some 17 years after the start of the injection activities. It is unknown whether any earlier events occurred in the area, mainly due to the lack of nearby seismic stations prior to 2010. On 5, 6 and 8 November 2011, three earthquakes with magnitudes of M_w 5.0, 5.7 and 5.0 occurred (Figure B-4). The M_w 5.7 seismic event is the largest recorded earthquake in Oklahoma to date, whereas the nearest-known Quaternary active fault in the region is located at a distance of 180 km (Keranen, 2013). The large earthquakes and aftershocks delineate steeply dipping fault planes within the Wilzetta fault system, both in the sedimentary and underlying basement rocks. Nearest earthquakes occurred within 200m of the injection wells. 83% of the aftershocks took place at depths below 5 km in the basement rocks, whereas approximately 20% of the earthquakes were localized in the sedimentary rocks which were targeted for injection (Keranen, Katie M. et al., 2013).
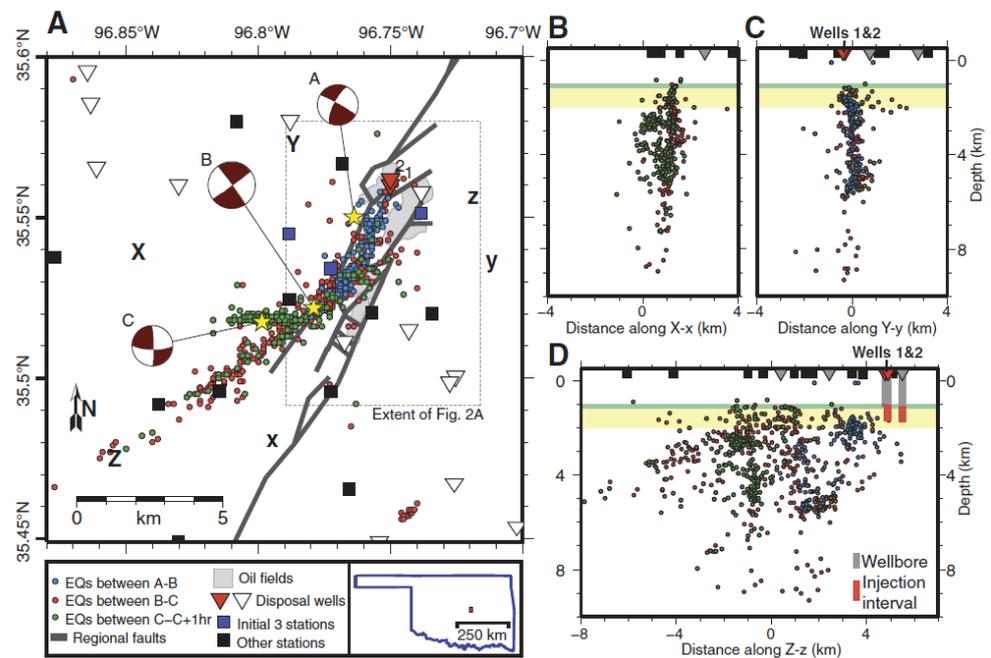
Figure B-4   a) Location of seismicity, seismic stations , injection wells and faults. A,B and C indicate large magnitude events of resp. Mw 5.0, 5.7 and 5.0 which occurred in November 2011. b), c) and d) show location of induced seismic events at depth (From Keranen et al., 2013, Copyright The Geological Society of America, reproduced with permission).

Interpretation: The authors mention that the agreement between the oil volumes produced in earlier years and the volumes of fluids injected supports the hypothesis that critical volumes and pressures were reached in the Wilzetta North reservoir compartment, which led to an increase of pressures in the fault bounding the compartment and the onset of seismicity. The authors associate the first M_w 5.0 earthquake to the injection activities, whereas the two other large events may be a direct consequence of the injection activities or a result of stress transfer and triggering by the earlier M_w 5.0 seismic event (Keranen, Katie M. et al., 2013; Sumy et al., 2014).

B.2.2   Youngstown , Ohio, USA (M 4.0)

Country & place (lat, lon):	Youngstown, Ohio, USA
Activity:	Waste water injection
Start date – End date:	28-12-2010	30-12-2011
Fluid + Fluid balance:	Water	Injection
Activity depth:	2650 m
Activity rocktype:	Sandstone & dolomites, crystalline basement
In-situ T	n.a.
ΔT in-situ – fluid:	n.a.
Cumulative ΔV:	78,798 m^3
Maximum Top Hole Pressure:	17.2 MPa
Maximum flowrate:	3.7 l/s
Monitoring system:	Yes
Maximum magnitude:	4.0
Distance M$_{max}$ – activity:	< 1 km
Intensity [EMS]:	n.a.
Damage:	n.a.
Interpretation	Induced by pore pressure increase

Tectonic setting and geology: Youngstown is located in a stable continental region in North-America. The Northstar-1 well near Youngstown, Ohio, US, is a vertical injection well which is used for the disposal of salt water. The well intersects a 2.7 km thick sequence of near-horizontal Paleozoic sedimentary strata of carbonates, evaporites, shales, sandstones and siltstones, before entering the Precambrian crystalline (igneous and metamorphic) basement rocks (Figure B-5). The depth of the well is 2802 m, with an open hole section of 298 m at the bottom of the well. Most of the open hole section intersects a Cambrian saline aquifer consisting of sandstones and dolomitic layers, characterized by relatively high porosities and permeabilities. The lowermost part of the open hole section intersects some 61 m of the Precambrian basement. Zones of moderately high permeabilities within the basement rocks are present close to the unconformity at the base of the sedimentary sequence (Kim, Won-Young, 2013; Morris et al., 2017). The tectonic regime in this region is strike-slip to reverse faulting, with a predominant ENE-WSW orientation of the maximum horizontal stress (Morris et al., 2017). No faults have been mapped in the sedimentary strata (Kim, Won-Young, 2013).
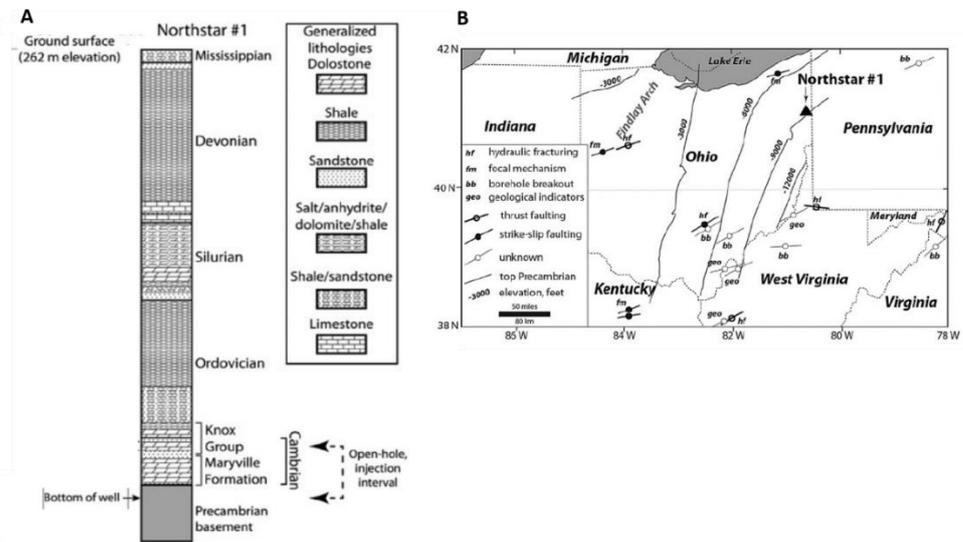
Figure B-5   a) Lithology of the Northstar#1 wastewater injection well, b) location of the Northstar#1 injection well, top of the Precambrian basement rocks and the orientation of the maximum horizontal stress (From Morris et al., 2017, Copyright Elsevier, published under a Creative Commons license).

Activity design: The injection of wastewater in the Northstar#1 well started on 28 December 2010 and continued until 30 December 2011. During this period, a total volume of 78798 m3 of salt water was injected into the subsurface, with maximum wellhead pressures up to 17.2 MPa and maximum injection rates up to 3.7 l/s (Kim, Won-Young, 2013; Morris et al., 2017).
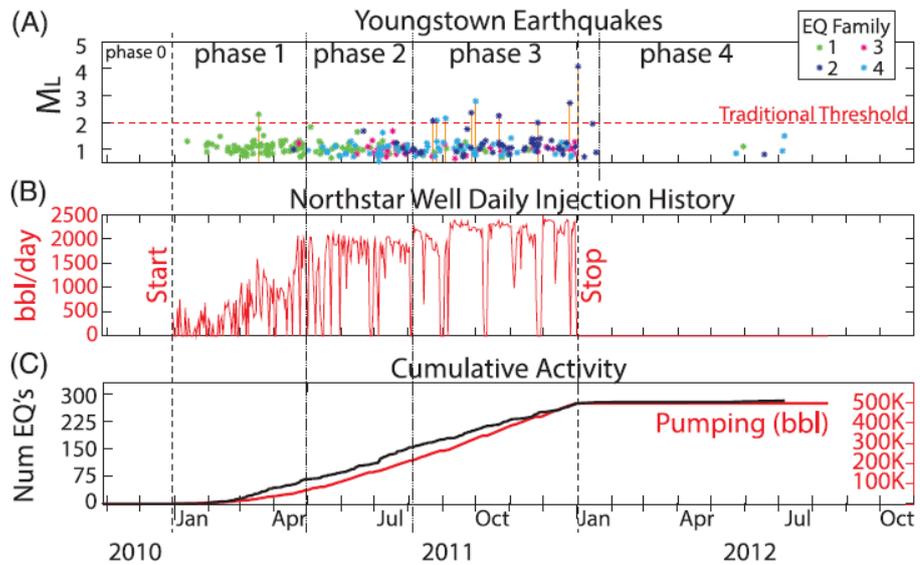

Figure B-6   Rates and magnitudes of induced seismicity versus daily injection volumes (in barrels per day) in the Northstar#1 Injection (From Holtkamp & Brudzinski, 2015, Copyright AAPG, reproduced by permission).

Occurrence of seismicity: First seismicity was recorded 13 days after start of wastewater injection, and increased in frequency and magnitudes (Figure B-6), migrating approximately downward highlighting a fault zone in the basement rocks dipping steeply to the south-southeast. Since 1 December 2011, seismicity is monitored by 4 portable seismograph stations near Youngstown. Around 130 seismic events with magnitudes between M 0.68 and M 4.0 were recorded over a period of 12 months, from January 2011 to January 2012. On December 31st 2011, one day after the end of injection, a maximum magnitude M 4.0 was recorded at a depth of 3.5 to 4 km, characterized by a strike-slip focal mechanism. The locations of the majority of the seismic events were within a vertical and horizontal distance of 1 km of the Northstar#1 injection well. Seismicity was restricted to the Precambrian basement (Kim, Won-Young, 2013; Morris et al., 2017).

Interpretation: Pore pressure perturbations caused by the wastewater injection in the Northstar#1 injection well caused a reactivation of a fault within the fractured Precambrian basement which was favorably oriented for slip. The combination of high permeability fault zones in low-permeability host rocks is thought to amplify the pore pressure perturbation induced by the injection activities. The lack of seismicity in the shallower Cambrian and uppermost Precambrian rocks is attributed to the absence of large favorably oriented fault structures and the high permeabilities of these rocks (Morris et al., 2017).

B.3 Conventional hydrocarbon production

During conventional hydrocarbon production oil or gas are extracted from a permeable reservoir. There are more than 65,000 oil and gas fields worldwide. The extraction of oil and gas can cause induced seismic events. Induced seismicity due to hydrocarbon production has mainly been reported for the Netherlands (>25 fields), Germany, USA, and China. The main mechanism for induced seismicity during depletion is poroelastic stressing (see section 2.4.3). For the extraction of a large amount of mass also unloading can play a role (see appendix B.5).

Comparison to geothermal: Oil and gas fields are usually larger than typical EGS and doublets, but may be of comparable size to volcanic fields. Also, during primary production the pressure in the field decreases. This may be comparable to the initial production stage in a volcanic field, but is not comparable to an EGS or geothermal doublet where fluids are injected and/or circulated. Thermal effects are also smaller than in a geothermal system. In case of gas fields with a long history (~30 years) of induced seismicity including multiple felt events (e.g., more than 200 bar depletion in the Groningen gas field), the inferred mechanisms are poroelastic stressing and differential compaction of reservoir compartments juxtaposed along faults with offset. Although poroelastic stressing also plays a role in geothermal systems, the combination of depletion of large volume of gas, progressive differential compaction and poroelastic stressing is not comparable to geothermal systems. In particular, conventional geothermal systems in the Netherlands are based on fluid circulation and an (approximate) overall balance of fluid volume in the reservoir (cf. section). Accordingly, reservoir compaction is not significant in these conventional geothermal systems. The driving mechanisms of induced seismicity differ between gas production and geothermal systems, and thereby characteristics of induced seismicity (e.g., spatiotemporal distribution, number, frequency and magnitudes) will be different. In case of oil production, pressure maintenance by water injection is usually performed. In that case, driving mechanisms may be more comparable (appendix B.4).

B.3.1   Groningen gas field, the Netherlands (M$_w$ 3.6)

Activity:	Gas production	
Start date:	1963	to date
Fluid + Fluid balance:	Gas	extraction
Activity depth:	3 km	
Activity rocktype:	sandstone	
In-situ T	115 °C	
Cumulative ΔV:	2211.10^9 Nm^3 (2211 BCM)	
Maximum Top Hole Pressure:	35 MPa (initial field pressure)	
Maximum flowrate:	150.10^6 Nm^3/day	
Monitoring system:	from 1990's, increased to > 60 stations to date	
Maximum magnitude + Date:	M$_w$ 3.6	12 – 08 – 2012
Distance M$_{max}$ – activity:	<0.5 km	
Intensity [EMS]:	VI-VII	
Damage:	mostly DSI and DS II damage to infrastructure	
Interpretation	poroelastic stressing, differential compaction	

Tectonic setting and geology: The Groningen field is located in the northeast of the Netherlands. It is one of the largest onshore gas fields. The reservoir formation is the Slochteren sandstone, a 200 m thick porous sandstone formation at 3 km depth. The reservoir is overlain by the Ten Boer claystone and a thick sequence of Zechstein evaporites. It is underlain by Carboniferous silts, sands, and coal layers. Natural seismicity in the region is low, with no events observed prior to gas production. The stress field is a normal faulting regime.

Activity design: The field is 30 x 40 km in dimension, at 3 km depth. Various clusters of production wells are distributed over the field.

Operations and monitoring: Gas production started in 1963. The initial gas in place was 2900 billion m^3 (BCM) and the initial reservoir pressure was 34.6 MPa. In 1991 1240 BCM was produced, and the reservoir pressure had dropped to 20 MPa (NAM, 2013). From 1991 to 2014 between 15 and 53 BCM was produced annually, decreasing the reservoir pressure to 8 MPa. From 2014 onwards the production rate was lowered in the north of the field to mitigate the induced events, and also the field average production was lowered. In 2016 a production cap was imposed of 24 BCM per year for the field, and in 2018 it was decided to phase out the Groningen gas production due to the damage from the induced events.

Since 1995 (4 years after the first earthquake) a monitoring network was installed consisting of 8 borehole stations. This network was extended in 2006 and 2010, so that in 2010 17 shallow borehole stations and 23 accelerometers were installed (Dost 2013). From 2013 the network was again expanded to > 70 shallow borehole sensors, 4 broadband sensors, and 2 deep borehole arrays.

Occurrence of seismicity: The first earthquake was recorded in 1991, almost 30 years after the start of production. Since then the number and magnitude of the earthquakes increased. The largest magnitude was a 3.6 which occurred on the 12th of August 2012, which caused damage to housing. Up to the end of 2018 a total of 1281 earthquakes were recorded including 12 earthquakes with $M_L > 3.0$ were recorded, and 103 earthquakes with $M_L > 2.0$ (www.knmi.nl). The improved locations from the recent network developments showed that hypocenters were located on known faults, and occurred mostly within or very close to the reservoir depth interval (Spetzler & Dost, 2017).
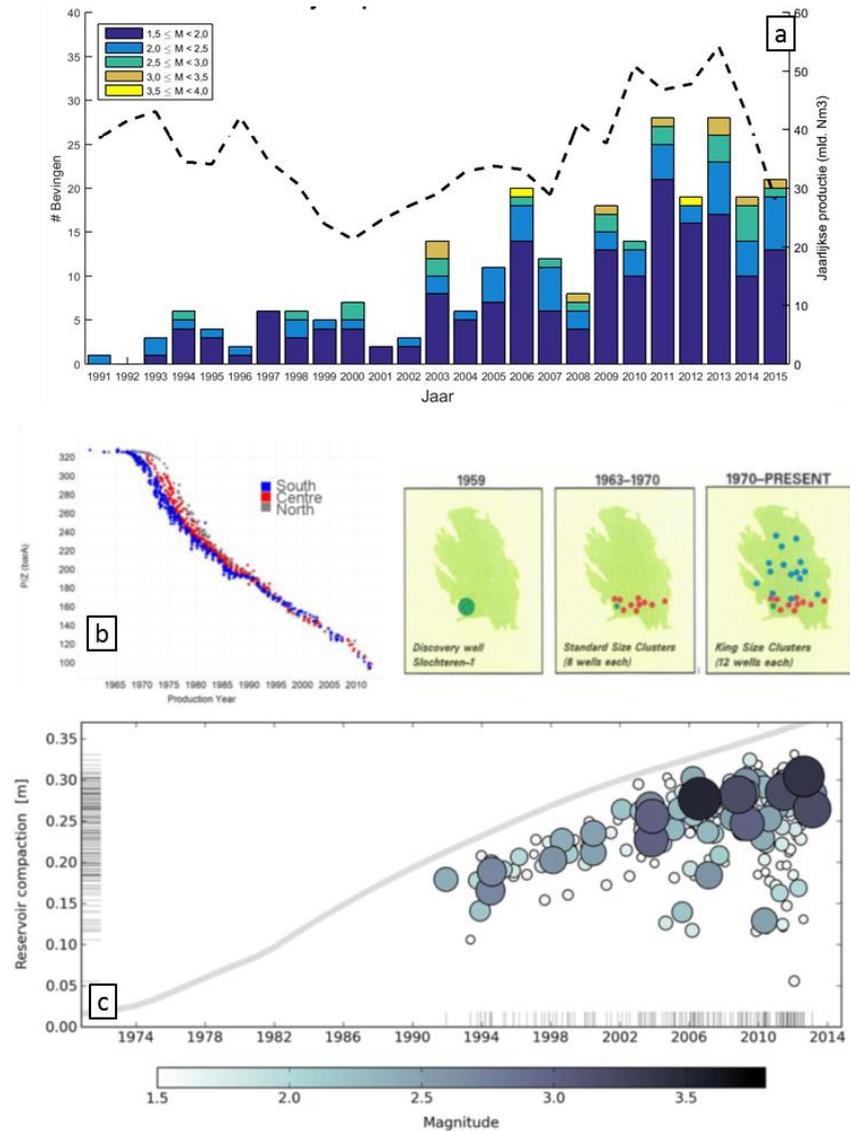

Figure B-7   Gas production and seismicity in the Groningen gas field. a) Annual production from 1991 to 2015 and the number of seismic events recorded (www.nlog.nl). b) Average reservoir pressure with time (FSource: NAM, 2013, Technical addendum to the Winningsplan Groningen 2013: Subsidence, induced earthquakes and seismic hazard analysis in the Groningen field), c) modelled maximum reservoir compaction (grey line) and modelled compaction at the time and location of the earthquake occurrence (From Bourne et al., 2014, Copyright by the authors, published under a Creative Commons license).
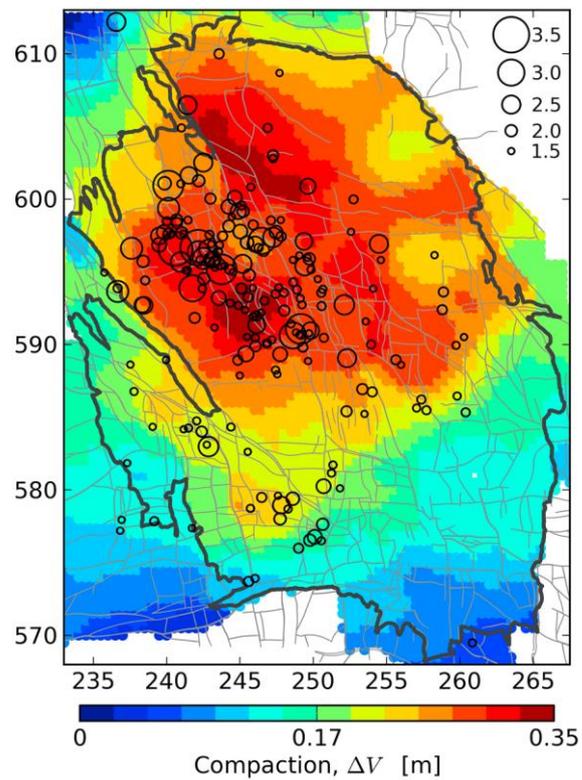
Figure B-8   Modelled compaction the location of induced events. Field outlines are shown by the black lines, and known faults at the reservoir level are shown in light grey (From Bourne et al., 2014, Copyright by the authors, published under a Creative Commons license).

Interpretation: Seismic events of M > 1.5 occurred only in regions which had experienced an inferred reservoir compaction of 0.12 m (Bourne et al., 2014). The inferred mechanisms behind the induced events are poroelastic stressing and differential compaction along faults with offset.

B.4 Secondary and tertiary recovery of oil

Secondary recovery involves the injection of water (waterflooding) to maintain reservoir pressure and to displace the oil to the production wells. The secondary recovery phase follows the initial phase of primary recovery, where the subsurface pressure itself is still sufficient to produce the oil. During the primary phase 5 – 15% of oil is recovered, whereas another 30% may be recovered during secondary recovery. Beyond the secondary recovery stage, another 5 – 15 % of oil may be recovered through tertiary recovery methods (also called Enhanced Oil Recovery). During tertiary recovery the viscosity of oil is lowered, e.g. through the injection of steam or CO_2, or chemical methods.

Secondary recovery was introduced in the 1920's in the USA. Since then, secondary recovery is used in many oil fields worldwide. Tertiary recovery increased in the 1970's and 1980's with up to 500 projects in the USA alone, but decreased in the 1990's and 2000's because of the lower oil price.

Induced seismicity has been recorded in the vicinity of a number of oil fields undergoing secondary recovery, including a number of large events with M>5. These include a M_L 5.3 near Cogdell Oil Field, Texas, and a number of M > 6 events deep below oil fields in California (Coalinga, Kettleman, and Montebello oil fields). Compared to the total number of oil fields the number of induced events is limited. The relevant mechanisms for secondary recovery are poroelastic stressing due to net extraction of hydrocarbons or local reinjection, and (local) pressure increases during injection. For large extracted volumes also mass unloading can play a role. Analyzing the mechanisms for secondary recovery may be challenging, as there are multiple production phases (first production only, then waterflooding which increases the pressure again) and spatially (and temporally) variable injection and production locations.

Comparison to geothermal: The scale and type of operations (production and reinjection) of hydrocarbon fields is comparable to those of geothermal fields, but temperature effects are smaller. The scale and operations are very different compared to EGS and geothermal doublets, which are smaller and involve only injection and or circulation. It should be noted that oil production with pressure maintenance by water injection has been operational for decades in the North Sea without reported seismicity.

B.4.1   Cogdell Oil Field, Texas, USA (M_w 4.6)

Activity:	Oil production, secondary recovery	
Start date:	01-12-1949 01-04-1956 01-01-2002	primary water injection water + CO_2 injection
Fluid + Fluid balance:	Water + oil	extraction
Activity depth:	2.1 km	
Activity rocktype:	carbonate	
In-situ T		
Cumulative ΔV:	67,000,000 m^3 water + 20,000,000 CO_2	
Maximum Top Hole Pressure:	21 MPa	
Maximum flowrate:	190 l/s (field-wide)	
Monitoring system:	1979 – 1983, 2009 – 2011	
Maximum magnitude + Date:	M_w 4.6	16 – 06 – 1978
Distance M_{max} – activity:	unknown	
Intensity [EMS]:	N/A	
Damage:	N/A	
Interpretation	pressure increase, gas injection	

Tectonic setting and geology: The Cogdell Oil Field is located in the northwest of Texas (Davis, Scott D. & Pennington, 1989). Oil is produced from 2.1 km deep from the Canyon Reef limestone, which is part of the Horseshoe atoll, a sinusoidal chain of Paleozoic reefs in the west of Texas. The Horseshoe atoll contains a number of big oil fields, including also Kelly-Snyder and Scurry oil field. The maximum stress is oriented WSW-ENE, and the tectonic regime is transtensional (normal faulting to strike-slip) .

Activity design: The Cogdell oil field was discovered in 1949, and production started in December that year (Davis, Scott D. & Pennington, 1989). The field is ~5 km wide and 20 km long. A total of 119 wells were drilled which were initially all producing, and from 1956 an increasing number of wells was converted to injection wells starting from the peripheries of the field.
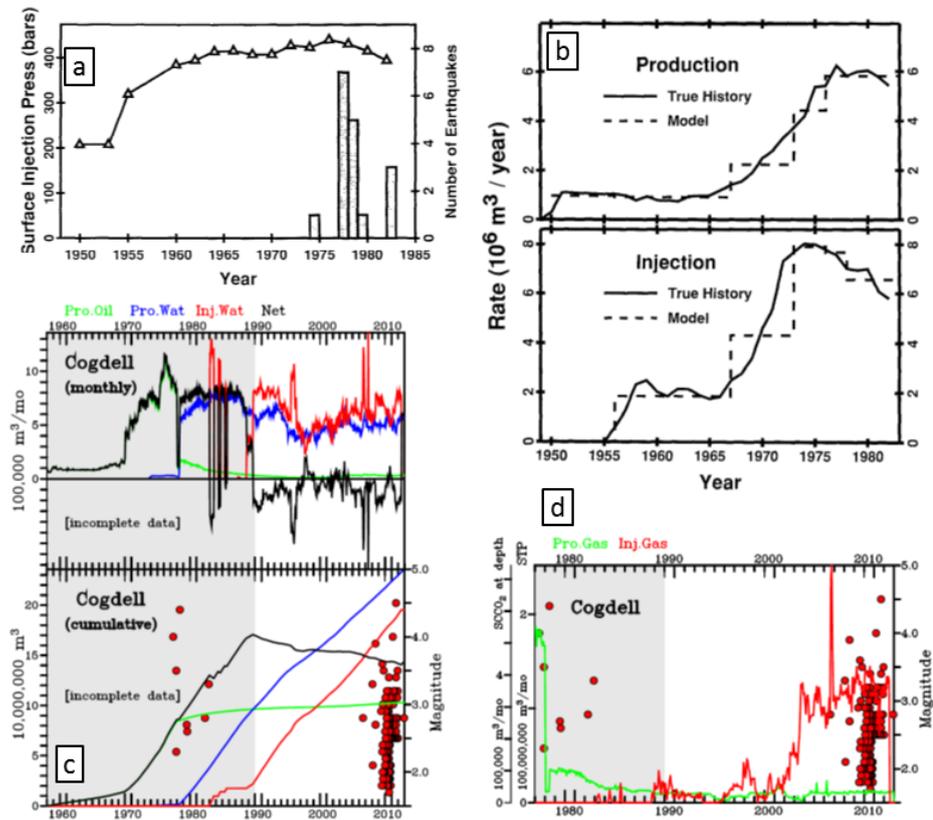
Figure B-9   Production and injection data from Cogdell Oil Field and induced seismicity. a) Bottom-hole injection pressure (bars) and number of earthquakes recorded close to the field. The initial reservoir pressure was 21.5 MPa and b) Net production (water + oil) and injection (water) from 1949 to 1985 (From Davis & Pennington, 1989, Copyright Seismological Society of America, reproduced with permission). c) production and injection data from 1990 to 2010 from Gan & Frohlich., 2013, Copyright National Academy of Sciences of the United States of America, reproduced with permission. Before 1990 the data is incomplete and water injection is not accounted for; according to Davis the volume of water injected was 114,000,000 m^3 in 1985, which corresponds to net volume injected (water injected – oil produced – water produced) of 37,000,000 m^3. d) gas production and injection from 1975 to 2010. The injection rates and production rates are given in volumes at depth and volumes at atmospheric pressure (STP).

Operations and monitoring: Production of oil from the Cogdell field started in December 1949. The initial reservoir pressure of 21.5 MPa dropped rapidly to 7.9 MPa so that saline water injection was started in April 1956 to maintain the pressure and keep up production . The injection pressure increased to ~21 MPa in 1965 and remained constant after that (Figure B-9a). The injection occurred in wells along the peripheries of the field, and with time an increasing number of wells started injecting. In 1985 the net injected volume (water injected – oil produced – water produced) was 37,000,000 m^3 (Davis, S. D. & Frohlich, 1993). Water injection continued after, and after 1990 to 2010 another 30,000,000 m^3 net volume was injected (Figure B-9c). Significant volumes of gas (CO_2 at atmospheric conditions, supercritical at depth) were injected since 2002 with rates of up to 400,000 m^3 per month, totaling 20,000,000 m^3 in 2011 (Figure B-9d). Gas injection started near cluster A (Figure B-10b), then near H in 2003, and near B and C from 2006. After the first earthquake recorded by the National Earthquake Information Center (NEIC) in 1978, an eight-station temporary local network was installed near the field . From 2009 – 2011 the

Earthscope USarray was deployed in Texas, with 6 stations surrounding Cogdell oil field (Gan & Frohlich, 2013).

Occurrence of seismicity: The first earthquake was recorded by the NEIC on 16 June 1978, 29 years after the start of production and 23 years after the start of injection. Its magnitude was m_b 4.9 (M_w 4.6). From 1979 to 1981 20 earthquakes were recorded by the local monitoring network (Harding, 1981), located within or in the vicinity of the oil field (Figure B-10a). The average depth of the events was 1.9 km. From 1983 to 2005 no events were picked up by de NEIC, but from 2006 to 2011 38 events were detected. The Earthscope USarray picked up 105 events near Cogdell between 2009 and 2011 (red dots Figure B-10b). 18 events between 2006 and 2011 had a magnitude larger than 3. The largest event with M_w 4.4 during this time occurred on 9 November 2011. Focal mechanisms showed normal faulting to strike-slip faulting events.
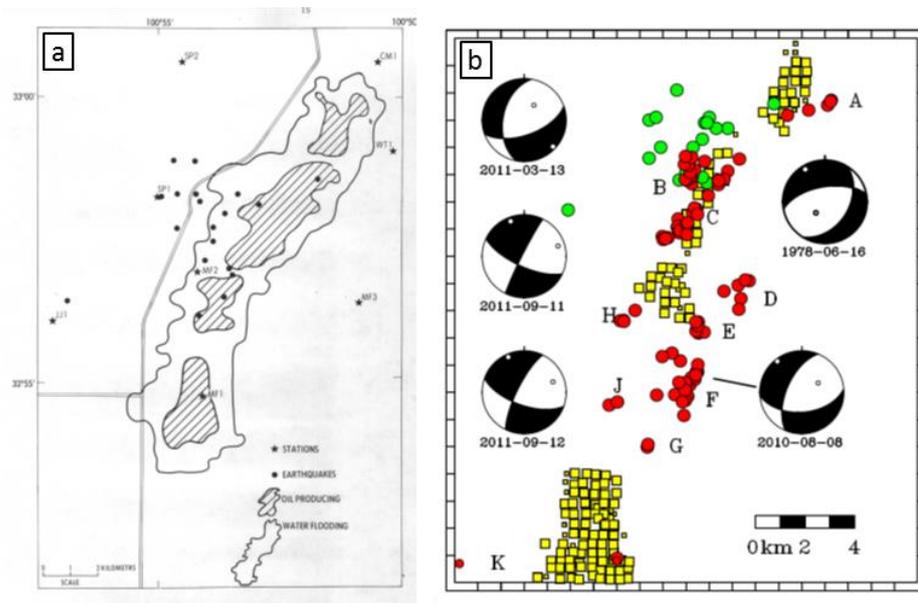

Figure B-10 Locations and focal mechanisms of seismicity near the Cogdell oil field. a) Locations of events recorded from 1979 to 1981 and injection – production zones at the time (Source Harding, 1981, Induced Seismicity Cogdell Canyon Reef Oil Field, USGS Open File Report, Report No. 81-167, Menlo Park, USA). b) events recorded in 2010 and 2011 by the Earthscope US array (red dots) and gas injection wells (yellow squares). The green dots show the events in 1979 – 1981 as in a (From: Gan & Frohlich, 2013, Copyright National Academy of Sciences of the United States of America, reproduced with permission).

Interpretation: The first series of events in 1978–1981 were interpreted to be induced by the increase in fluid pressure. It was postulated that aseismic slip occurred in regions of the highest fluid pressures, increasing the shear stress in regions of lower fluid pressure. This was consistent with the fact that earthquakes did not occur in regions of the highest pressure increase (Davis, Scott D. & Pennington, 1989). However, poroelastic stressing was not considered in this analysis, and also optimally oriented pre-existing faults were not considered. Gas injection was suggested as the main cause for the earthquakes after 2006 (Gan & Frohlich, 2013). The events were located within 2 km of injection wells, and occurred after gas injection started after a period in which no events had been recorded (M > 3 should have been picked up by the NEIC).

B.5 Loading/unloading

The addition or removal of a large fluid or rock mass at or near the earth's surface locally changes the stresses at depth. This may lead to fault reactivation and induced seismicity, depending on the sign and magnitude of the stress changes, the tectonic regime, and the orientation and strength of pre-existing faults. Mass addition (loading) is expected to have a destabilizing effect in normal faulting regimes because it increases the largest (vertical) stress, while unloading may destabilize faults in thrust faulting regimes.

Relevance for geothermal: The removal of mass due to production from geothermal fields has not been proposed as a potential mechanisms for induced seismicity. Net mass changes may be limited as reinjection generally occurs in geothermal fields.
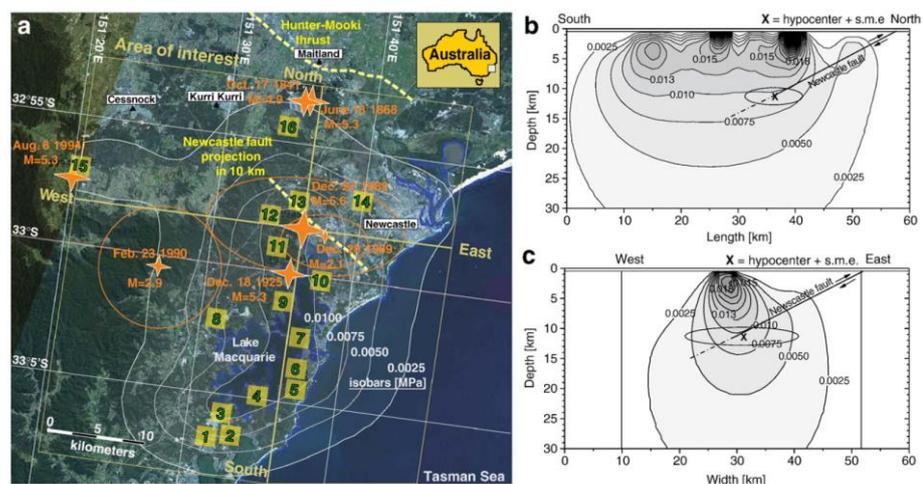

Figure B-11 Seismicity and stress changes at the Newcastle coal field. a) Map view of Newcastle area with 16 collieries of the coal field (numbers), the epicentre of the M 5.7 event on 29 December 1989 (big star) and other earthquakes (smaller stars). b) south-north depth profile with computed shear stress changes due to mass removal, c) west-east profile showing computed shear stress changes due to mass removal. The fault plane on which the Newcastle earthquake occurred is shown for reference. (From Klose, 2007, Copyright Elsevier, reproduced with permission).

Relevancy for other activities: Mass changes play a role below impounded reservoirs, below large mines, and large hydrocarbon fields. For example, loading of the crust has been identified as an important mechanism causing seismicity at the Kariba Dam in Zambia, where magnitudes up to M_b 6 were observed (Gough & Gough, 1970). Interestingly, the reverse effect has also been observed and loading suppressed natural seismicity (Gupta, 2002). Note that not only elastic loading but also pressure diffusion below the reservoir is another important mechanism for reservoir induced seismicity (see section 2.4.1). Unloading due to the removal of >700 Mton kg of coal and > 2000 Mton of water may have triggered the largest seismic event related to mining thus far (Figure B-11); the M 5.6 in Newcastle (Klose, 2007). Unloading has also been proposed as a mechanism for the occurrence of several large earthquakes below large oil and gas fields in California (Segall, Paul, 1985). The earthquakes occurred at large depth (5–20 km), far below the hydrocarbon fields. Stress changes due to loading and unloading at hypocentre depth are usually very small (0.01 MPa at Newcastle), and could only reactivate faults that are critically stressed due to tectonic loading.

B.6 Reservoir impoundment

Reservoir impoundment is also linked to very large (up to M 7.9) seismic events (Foulger et al., 2018). The main mechanism is the increase in pressure in faults and diffusion of pressure to depth. At the base of the reservoirs the hydraulic head increases, as the water level rises several 10's of meters or even up to 160 m (e.g. Gupta, 2002). This can increase pressures at depth as well as laterally as the pressure diffuses through permeable faults and/or lithologies underlying the reservoir, causing faults at depth to fail seismically (Simpson et al., 1988; Talwani & Acree, 1984). In China for example it was observed that in many cases reservoir induced seismicity (with several M >5) was spatially correlated to karstified carbonate formations underlying the reservoir, which provided ample opportunity for pressure diffusion to deeper levels (Chen & Talwani, 1998; Yuliang et al., 1996). For example, the time-dependent nature of the diffusion process was observed at the Açu reservoir, where peaks in seismic activity in the faulted granites underlying the reservoir lagged behind 3 months after peak in rainfall and reservoir level (El Hariri et al., 2010). Hypocenters migrated along a pre-existing fault zone below the reservoir. As for wastewater injection, pressure changes at hypocentre depths are usually small indicating faults are close to the failure stress.

B.7 Mining-induced stresses

The excavation of a rock volume at depth strongly affects the stresses in the subsurface, which causes some special types of mining-induced seismicity. The presence of a void concentrates stresses in the surrounding rock formations, enhancing the stress by up to several 10's of MPa (e.g. Wong, IG, 1985). The stress redistribution may be highly heterogeneous, and depends on the construction of the mine. The increased stresses and presence of a void in the subsurface may cause seismic failure and faulting in a variety of ways (Hasegawa et al., 1989):

(i) Rock falls or roof falls can generate seismic energy (Figure B-12a). They occur when blocks of rock in the mine fall down under their own weight (Cook, 1976), e.g. because blocks break free along pre-existing joints or layer, or after rocks are detached due to fracturing of the mine face (see ii) or fracturing of strata in the roof of the mine (see iv) (Shen et al., 2008).

(ii) Rock bursts: The most abundant seismicity occurs near the advancing front of the mine shaft or mine panel, the so-called stope face (Figure B-12d). Stress concentrations are very high and the confining horizontal stress is locally reduced, which causes intact rock to fracture violently generating non-double couple seismic events. This particular, usual small magnitude, seismicity is correlated in time with the advancing mining activity 0 – 100 m from stope (McGarr and Spottiswood). Also pure shear normal and shear faulting on nearby fractures and joints is observed near the stope face (Bischoff et al., 2010).

(iii) Roof fracture: Stress redistribution may cause the mine roof to fracture, causing dilational events (Figure B-12c).

(iv) Pillar collapse: Closure of excavations under the high stresses loads the mine pillars (columns of the rock formation left behind to support the roof), and may cause them to collapse or fracture seismically (Figure B-12b).

(v) Mine collapse: A sudden extensive breakage of multiple pillars (cascading pillar failure) and/or of the stiffer bridging strata can occur, so that a large part of the mine collapses in a single event. Some of the largest mining-related events are associated with mine collapse, usually in evaporate mines at shallow depths < 1 km. A M_L 5.6 event was recorded in the 900 m deep Merker potash mine when 3200 pillars over an area of 6.5 km^2 collapsed in a matter of 2 seconds, causing damage to houses in the town Völkershausen which was situated right above the mine (Ahorner & Sobisch, 1988; Minkley, 2004). Pillar and roof collapse also caused a M 5.1 event in a trona mine in Wyoming (Pechmann et al., 1995).

(vi) Stress changes at a distance of up to 100's to 1000's of m from the excavated volume can cause shear slip on critically stressed pre-existing faults, with similar signs as in poro-elastic stressing (e and f). Above and below the mine thrust faulting is expected (Figure B-12e), as for example some of the larger $M_L > 4$ events in the Wasatch Plateau mining area (Arabasz & Pechmann, 2001; Wong, Ivan G. et al., 1989).
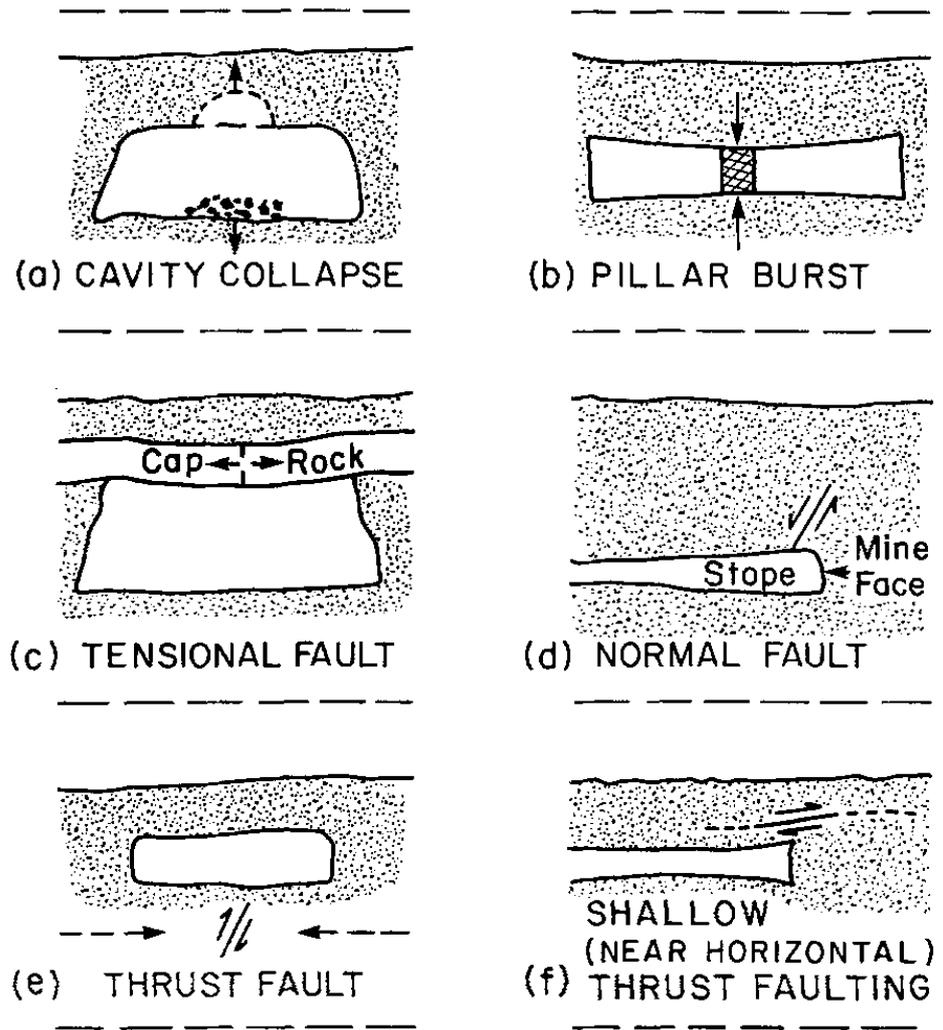
Figure B-12 Different types of mining-induced seismicity. (From Hasegawa et al., 1989, Copyright Springer Nature, reproduced with permission).